



HAL
open science

Molecularly imprinted polymers as selective sorbents for recognition in complex aqueous samples

Sofia Nestora

► **To cite this version:**

Sofia Nestora. Molecularly imprinted polymers as selective sorbents for recognition in complex aqueous samples. Biotechnology. Université de Technologie de Compiègne, 2017. English. NNT : 2017COMP2346 . tel-01587767

HAL Id: tel-01587767

<https://theses.hal.science/tel-01587767>

Submitted on 14 Sep 2017

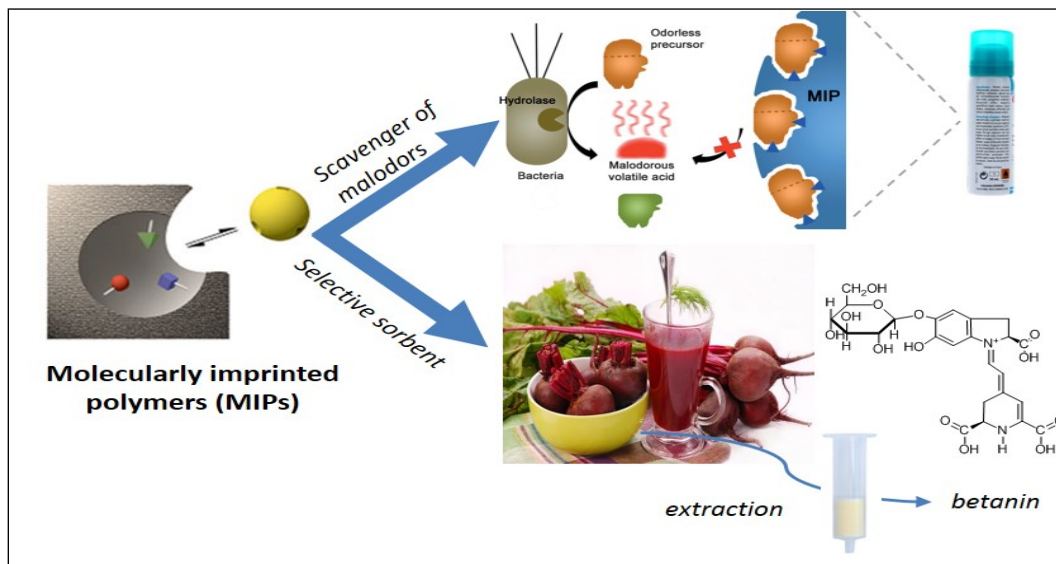
HAL is a multi-disciplinary open access archive for the deposit and dissemination of scientific research documents, whether they are published or not. The documents may come from teaching and research institutions in France or abroad, or from public or private research centers.

L'archive ouverte pluridisciplinaire **HAL**, est destinée au dépôt et à la diffusion de documents scientifiques de niveau recherche, publiés ou non, émanant des établissements d'enseignement et de recherche français ou étrangers, des laboratoires publics ou privés.

Par **Sofia NESTORA**

Molecularly imprinted polymers as selective sorbents for recognition in complex aqueous samples

Thèse présentée
pour l'obtention du grade
de Docteur de l'UTC



Soutenue le 13 avril 2017

Spécialité : Biotechnologie : Unité de recherche Génie
Enzymatique et Cellulaire - GEC (FRE-3580)

D2346

Dissertation

submitted for the obtention of the degree of

DOCTEUR DE L'UNIVERSITÉ DE TECHNOLOGIE DE COMPIÈGNE

Spécialité : Biotechnologie

By

Sofia Nestora

**MOLECULARLY IMPRINTED POLYMERS
AS SELECTIVE SORBENTS
FOR RECOGNITION IN COMPLEX AQUEOUS SAMPLES**

Thesis supervised by Prof. Karsten Haupt, Prof. Claire Rossi and Dr. Bernadette Tse Sum Bui

Disputation on April, 13th 2017, in front of a jury composed of:

Oliver BRÜGGEMANN, Prof.	Johannes Kepler University of Linz, <i>Austria</i>	Reviewer
Dietmar KNOPP, Prof.	Technical University of Munich, <i>Germany</i>	Reviewer
Andrew GREAVES, Dr.	L'Oréal-Paris, <i>France</i>	Examiner
Valerie PICHON, Prof.	École Supérieure de Physique et de Chimie Industrielles, <i>France</i>	Examiner
Karsten HAUPT, Prof.	Université de Technologie de Compiègne, <i>France</i>	Supervisor
Claire ROSSI, Prof.	Université de Technologie de Compiègne, <i>France</i>	Supervisor
Bernadette TSE SUM BUI, Dr.	Université de Technologie de Compiègne, <i>France</i>	Supervisor

Thèse

En vue de l'obtention du grade de

DOCTEUR DE L'UNIVERSITÉ DE TECHNOLOGIE DE COMPIÈGNE

Spécialité: Biotechnologie

Par

Sofia Nestora

POLYMERES A EMPREINTE MOLECULAIRES

EN TANT QU'ADSORBANTS SELECTIFS POUR LA RECONNAISSANCE

DANS DES MILIEUX AQUEUX COMPLEXES

Thèse dirigée par Prof. Karsten Haupt, Prof. Claire Rossi et Dr. Bernadette Tse Sum Bui

Soutenue le Jeudi 13 Avril 2017 devant le jury composé :

Oliver BRÜGGEMANN, Prof.	Johannes Kepler University of Linz, <i>Austria</i>	Rapporteur
Dietmar KNOPP, Prof.	Technical University of Munich, <i>Germany</i>	Rapporteur
Andrew GREAVES, Dr.	L'Oréal-Paris, <i>France</i>	Examineur
Valerie PICHON, Prof.	École Supérieure de Physique et de Chimie Industrielles, <i>France</i>	Examinatrice
Karsten HAUPT, Prof.	Université de Technologie de Compiègne, <i>France</i>	Directeur
Claire ROSSI, Prof.	Université de Technologie de Compiègne, <i>France</i>	Directrice
Bernadette TSE SUM BUI, Dr.	Université de Technologie de Compiègne, <i>France</i>	Directrice

To my parents for all their love and support

Acknowledgements

First, I would like to express my gratitude to Prof. Dr. Oliver Bruggemann and Prof. Dr. Dietmar Knopp for taking the time to review my thesis as well as to Prof. Dr. Valérie Pichon, Dr. Andrew Greaves and for being the examiners of this work.

I am sincerely thankful to my three supervisors Prof. Dr. Karsten Haupt, Dr. Bernadette Tse Sum Bui and Prof. Dr. Claire Rossi for their constant help and advice all these years. Karsten, thank you for giving me the opportunity to join the MIP group, it was a whole new world for me. I am deeply grateful for your ideas and our fruitful discussions. Bernadette, thank you for your guidance, your numerous advices and your persistence to perfection. You were the first to believe in me and taught me so much these three years. It wasn't always easy, but in the end it was a life lesson for me. Claire, warm thanks to you for your positive attitude, your help and your constant availability.

There are so many people that I am grateful, from all these years in Compiègne, old and new, people who left and people that are still here. I sincerely thank all the members of the Enzyme and Cell Engineering Laboratory for their help and nice working environment. Aude, thank you for all your advice, your "chemistry classes" and your delicious tartiflette. Lumi, I am deeply grateful for your help and kindness and for the critical reading of this thesis. Elise, thank you for teaching me a bit of NMR, for improving my French and for your friendship. Franck, thank you for your help and patience with the endless experiments for Chapter 2. Sylvie, I am thankful for your kindness and your support. Special thanks to you Maria, Paulina and Yannick for contributing to this work.

I would like to thank all the people from my first years in Compiègne, Serena, Zeynep, Jacqui, Li Bin, Jean, Doudou, Laetitia, Melody, Paolo, Mira, Xuan-Anh, Selim, Carlo, Yi, Marcelina etc. You each have a place in my heart and I have so many moments to cherish: the crazy party at the old place of Melody in the pool with a watermelon, Paolo smoking and talking NMR, Jacqui dancing, Sere swearing in Italian, Zeynep cooking these delicious salmon rolls. Thank you guys for giving me such happy memories. Doudou, special thanks to you for being always there for me.

What can I say for all the people that we started the PhD life together? My office mates Paulina and Jing Jing and the rest of the gang Maria, Nadie, Frank, Nicolas and Hassan. Jing Jing, you are my Chinese soul mate and sister, I will waini you always. Pau, thank you so much for your friendship, your help and positiveness. Maria, we shared so many things together, our sorrows and our happy moments, life in Compiègne would not be the same without you. Nadie, you know I will always owe you for THAT night, thank you for all the crazy (and unique) memories and for your friendship. Frankie, you left us and went to Bordeaux but I forgive you, because you are the best.

Also thanks to the people that come to our lab for a short time, Martins (crazy Latvian guy), Bilo (crazy surtuk), Leena, Ola, Yolanda and Cecilia, I thank you for all the good moments. Mariano, it was such a pleasure to meet you, I will always remember your nice stories and T-shirts and baby Alexandro.

How can I forget the few Greek people in Compiègne?! My dear friend Maria Gad, we came to France together as Erasmus students and we shared some of the most wonderful experiences and I thank you for being there with me. Maria, Maria M. and Kostas, Chrysanthi and Stelios thank you for being my Greek family in France.

I would like also to thank all the people from every place in the world that I have meet during my thesis. My girls, Marina, Christina, Lauri and Emna as well as Diego, Felipe, Yeli, Alexandra, Heronimo, Florian etc. and my first friends in France, Chiara, Tommaso and Mehdi.

I will also include to my acknowledgements my Greek friends, it was such a warm feeling to see you when back home! Aristeia, Karolina, Vicky, Maria, Georgia, Nena, Natalia and Eleutheria thank you for making my life full of nice moments, for your support and compassion.

Finally, I would like to thank my parents for their endless love, support and patience and for their constant encouragement. Thank you for all you have given me and for the person that I have become. Colin, I cannot thank you enough being there for me during the last months of my thesis, for your motivation, your care and your love. You kept me going when I had lost hope and I love you so much for that.

Abstract in English: *Molecularly imprinted polymers as selective sorbents for recognition in complex aqueous samples*

Keywords: *molecularly imprinted polymer, synthetic receptor, plastic antibodies, stoichiometric monomer, deodorant, body odor, cosmetics, solid phase extraction, betanin, beetroot*

In this thesis, we have demonstrated the feasibility of preparing highly selective molecularly imprinted polymers (MIPs) for recognition in complex aqueous matrices with applications in cosmetics and food technology.

MIPs are synthetic tailor-made receptors, with binding affinities and specificities comparable to those of natural antibodies. Their molecular recognition properties, combined with their high stability, mechanical robustness, low cost and easy synthesis make them extremely attractive as selective capture materials with applications in analytical and preparative separations, sensing and drug delivery, among others. However, their selective recognition in aqueous samples still remains problematic and is one of the reasons for their so far limited commercial expansion.

In the first part, we developed a water compatible MIP for its application as an active ingredient in a deodorant. Body odors are mainly due to volatile fatty acids generated from their glutamine conjugate precursors by hydrolytic enzymes from bacteria present on the skin. Most currently marketed anti-perspirants and deodorants contain, respectively aluminum salts and unspecific antibacterials. However, the extremely wide use of these products requires alternative solutions with regard to various problems (environmental, respect of skin ecosystem, toxicity, etc.). For this reason, a MIP was developed to capture the glutamine conjugate precursors so that they are no longer available to the bacteria, thus preventing their transformation to malodorous compounds. In order to generate binding selectivity in aqueous environments, an amidinium-based monomer which can form a strong stoichiometric electrostatic interaction with the carboxyl groups on the template, was synthesized. The MIP, blended in a dermo-cosmetic formulation, could capture selectively the glutamine precursors, amidst a multitude of other molecules present in human sweat. Furthermore, the MIP did not affect the skin bacteria, paving the way to an innovative and ‘safer’ future-generation deodorant.

In the second part, we developed a fast and efficient procedure based on molecularly imprinted solid-phase extraction (MISPE) for the selective clean-up of betanin and its stereoisomer isobetanin from red beetroot extracts. Betanin is a natural pigment with significant antioxidant and biological activities currently used as food colorant. Dipicolinic acid was used as template for the MIP synthesis, because of its structural similarity to the chromophore group of betanin. The MISPE procedures were optimized allowing the almost complete removal of carbohydrates and the majority of proteins, resulting in high extraction recovery of betanin/isobetanin in a single step. Moreover, the whole extraction procedure was performed in environmentally friendly solvents with either ethanol or water.

To conclude, we believe that this study paves the way towards the development of a new generation of water compatible MIPs with improved recognition properties in highly complex aqueous environments, and should be applicable to other biotechnological and biomedical areas as well.

Résumé en français : *Polymères à empreinte moléculaires en tant qu'adsorbants sélectifs pour la reconnaissance dans des milieux aqueux complexes*

Mots-Clés : *polymères à empreinte moléculaires, récepteur synthétique, anticorps plastiques, monomer stoechiométrique, déodorant, odeur corporelle, extraction sur phase solide, bétanine, betterave*

Dans cette thèse, nous avons démontré la faisabilité de la préparation de polymères à empreinte moléculaires (MIP) hautement sélectifs pour la reconnaissance dans des matrices aqueuses complexes avec des applications dans les cosmétiques et en technologie alimentaire.

Les MIP (de l'anglais *molecularly imprinted polymers*) sont des récepteurs synthétiques comparables aux anticorps, qui sont synthétisés par co-polymérisation de monomères fonctionnels et réticulants en présence d'un gabarit moléculaire. Leurs propriétés de reconnaissance moléculaire, associées à leur grande stabilité, robustesse mécanique, faible coût et leur synthèse facile les rendent extrêmement intéressants comme matériaux de capture sélective, avec des applications dans les séparations analytiques, la détection et la vectorisation des médicaments. Cependant, leur reconnaissance sélective dans des milieux aqueux reste toujours problématique et c'est l'une des raisons de leur expansion commerciale restreinte.

Dans une première partie, nous avons développé un MIP fonctionnant en milieu aqueux pour son application comme ingrédient actif dans un déodorant. Les odeurs corporelles sont principalement dues à des acides gras volatils générés à partir de leurs précurseurs, des conjugués de glutamine par des enzymes hydrolytiques produites à partir de bactéries présentes sur la peau. La plupart des anti-transpirants et des déodorants actuellement commercialisés contiennent des sels d'aluminium et des agents antibactériens non spécifiques, respectivement. Cependant, l'utilisation extrêmement étendue de ces produits nécessite des solutions alternatives en ce qui concerne divers problèmes (environnement, respect de l'écosystème de la peau, toxicité, etc.). Pour cette raison, un MIP a été synthétisé pour capturer les précurseurs conjugués de glutamine afin qu'ils ne soient plus disponibles aux bactéries, empêchant ainsi leur transformation en composés malodorants. Afin de générer des liaisons sélectifs dans des environnements aqueux, un monomère à base d'amidinium qui peut former une interaction électrostatique stoechiométrique forte avec les groupes carboxyle sur le gabarit moléculaire a été synthétisé. Le MIP, mélangé dans une formulation dermo-cosmétique, pourrait capter sélectivement les précurseurs conjugués de glutamine, au milieu d'une multitude d'autres molécules présentes dans la sueur humaine. En outre, le MIP n'affecte pas les bactéries de la peau, ouvrant la voie à des déodorants innovateurs de nouvelle génération, moins problématiques pour la santé.

Dans une deuxième partie, nous avons développé une procédure rapide et efficace basée sur l'extraction en phase solide à empreinte moléculaire (MISPE) pour la purification sélective de la bétanine et de son stéréoisomère l'isobétanine à partir d'extraits de betterave. La bétanine est un pigment naturel ayant un fort pouvoir antioxydant et dont les propriétés pharmacologiques sont de plus en plus étudiées. Ce pigment est actuellement utilisé comme simple colorant alimentaire. Dans notre étude, l'acide dipicolinique a été utilisé comme gabarit moléculaire pour la synthèse de MIP, en raison de sa similarité structurelle avec le groupe chromophore de la bétanine. Les procédures MISPE ont été optimisées permettant l'élimination presque

complète des glucides issus de la matrice végétale ainsi que la majorité des protéines, ce qui permet d'obtenir un rendement élevé d'extraction de la bétanine/isobétanine en une seule étape. De plus, toute la procédure d'extraction a été réalisée dans des solvants respectueux de l'environnement, tels que l'éthanol ou l'eau.

Pour conclure, nous sommes convaincus que ce travail pave le chemin au développement d'une nouvelle génération des MIP fonctionnant en milieu aqueux avec des propriétés de reconnaissance améliorées dans des environnements complexes, qui pourra s'appliquer également à d'autres domaines biotechnologiques et biomédicaux.

List of abbreviations

AA	acrylic acid	HEMA	2-hydroxyethyl methacrylate
AAm	acrylamide	HEPES	2-[4-(2-hydroxyethyl)piperazin-1-yl]ethanesulfonic acid
AB	(4-acrylamidophenyl) - (amino)methaniminium	HPLC	high performance liquid chromatography
ABDV	azo-bis-dimethylvaleronitrile	IF	imprinting factor
ACN	acetonitrile	ITC	isothermal titration calorimetry
AcOH	acetic acid	LB	Luria-Bertani
AEM	aminoethyl methacrylate	LOD	limit of detection
AIBN	azo-bis-isobutyronitrile	MAA	methacrylic acid
ATRP	atom transfer radical polymerization	MALDI-TOF	matrix-assisted laser desorption ionization-time of flight
APTES	aminopropyltrimethoxysilane	MAm	methacrylamide
BHI	brqin heart infusion	MBAm	<i>N,N'</i> -methylene bis(acrylamide)
BIS	<i>N,N'</i> -methylenebisacrylamide	MMA	methyl methacrylate
CP	control polymer	MeOH	methanol
CRP	controlled radical polymerization	MIP	molecularly imprinted polymer
2,4-D	2,4-dichlorophenoxyacetic acid	MIS	molecularly imprinted sol gel
DMF	dimethylformamide	MISPE	molecular imprinted solid phase extraction
DMSO	dimethyl sulfoxide	MPABA	4-[(4-methacryloyloxy)phenylazo] benzoic acid
DPA	dipicolinic acid	MS	mass spectrometry
DVB	divinyl benzene	MTT	3-(4,5-dimethylthiazol-2-yl)-2,5-diphenyltetrazolium bromide
EBAm	<i>N, N'</i> -ethylenebis(acrylamide)	NIP	non-imprinted polymer
EGDMA	ethylene glycol dimethacrylate	NIPAm	<i>N</i> -isopropylacrylamide
ELISA	enzyme-linked immunosorbent assay	NMR	nuclear magnetic resonance
ELSD	evaporative light scattering detector	NPs	nanoparticles
EtOH	ethanol	PBS	phosphate buffered saline
FBS	fetal bovine serum	PETIA	pentaerythritol triacrylate
FRP	free radical polymerization		
HaCaT	cultured human keratinocytes		

PETMOS	pyridyl ethyl trimethoxysilane	SPE	solid phase extraction
PTMS	phenyltrimethoxysilane	SPR	surface plasmon resonance
PVA	poly(vinyl alcohol)	TEM	transmission electron microscopy
QCM	quartz crystal microbalance	TEMED	tetramethylethylenediamine
QD	quantum dot	TBA_m	<i>N</i> -tert-butylacrylamide
RAFT	reversible addition-fragmentation chain transfer	TEOS	tetraethoxysilane
SEM	scanning electron microscopy	TRIM	trimethylolpropane trimethacrylate
SERS	surface-enhanced Raman spectroscopy	UV	ultraviolet
SPME	solid phase microextraction	4-VP	4-vinylpyridine

Table of Contents

Abstract in English	vii
Résumé en Français.....	viii
List of Abbreviations	x
Table of Contents.....	xiii
Table of Figures	xviii
General Introduction.....	1
Chapter 1: Molecularly Imprinted Polymers as synthetic receptors for selective recognition in complex aqueous environments– <i>A Literature Review</i>	4
I. Molecular imprinted polymers : Tailor-made artificial receptors	5
I.1. The origin of molecular imprinting	5
I.2. Polymerization methods	8
<i>I.2.1. Free radical polymerization</i>	<i>8</i>
<i>I.2.2. Controlled radical polymerization.....</i>	<i>10</i>
<i>I.2.3. Sol-gel polymerization</i>	<i>12</i>
I.3. Preparation and optimization of MIPs.....	13
<i>I.3.1. Template.....</i>	<i>13</i>
<i>I.3.2. Functional monomers</i>	<i>14</i>
<i>I.3.3. Cross-linkers.....</i>	<i>15</i>
<i>I.3.4. Solvents</i>	<i>16</i>
I.4. Physical forms of MIPs	17
I.5. Towards a successful imprint for recognition in complex matrices	18
<i>I.5.1. Tailor-made monomers</i>	<i>19</i>
<i>I.5.2. Hydrophilic monomers and cross-linkers.....</i>	<i>20</i>
<i>I.5.3. Post-surface modifications</i>	<i>20</i>

II. Application of MIPs.....	21
II.1. Separation.....	21
<i>II.1.1. Towards a water compatible MIP sorbent</i>	<i>23</i>
<i>II.1.2. Recent advances in real sample treatment.....</i>	<i>28</i>
II.2. Biomimetic assays	39
<i>II.2.1. MIP-based immunoassays as diagnostic tools</i>	<i>41</i>
<i>II.2.2. Optimized ILA protocols for recognition in complex samples</i>	<i>44</i>
II.3. Sensors	46
<i>II.3.1. Detection of environmental pollutants</i>	<i>47</i>
<i>II.3.2. Detection of explosives.....</i>	<i>49</i>
<i>II.3.3. Detection of additives and contaminants in food samples.....</i>	<i>50</i>
<i>II.3.4. Detection of drugs and biomarkers in biological fluids.....</i>	<i>52</i>
<i>II.3.5. Detection of proteins and whole cells.....</i>	<i>54</i>
II.4. Sustained delivery and release.....	56
<i>II.4.1. Stimuli-responsive targeted delivery and sustained release</i>	<i>57</i>
<i>II.4.2. Vectorization of anticancer drugs</i>	<i>60</i>
<i>II.4.3. Ocular therapeutic applications</i>	<i>61</i>
II.5. New application areas: MIPs for proteomics and imaging.....	64
<i>II.5.1. Proteomics</i>	<i>64</i>
<i>II.5.2. Imaging</i>	<i>68</i>
III. Conclusions	71
IV. References	72

Chapter 2: MIPs in cosmetics: a new active principle for scavenging precursors of malodors in human sweat	90
I. Introduction	91
I.1. Polymers and nanomaterials in cosmetics: Applications of MIPs	91
I.2. The potential of MIPs as active principles in cosmetics.....	93
I.3. Origin and composition of axillary malodor.....	95

I.4. Battle against body malodor: The biological effect of treatment agents	99
I.5. Our strategy: MIPs as scavengers for non-odorous precursors of malodors	101
II. Results and Discussion	103
II.1. First attempts toward recognition in sweat.....	103
II.2. Our strategy: MIPs based on a tailor-made amidine monomer.....	105
II.3. Binding studies in artificial sweat	109
II.4. Capture of undesirable molecules in human sweat by the T2-AB MIP.....	110
II.5. Capture of glutamine precursors by the MIP incorporated in deodorant formulation.....	112
II.6. Assessment of HaCaT cell viability in the presence of MIP.....	115
II.7. Effect of MIP on commensal bacteria's growth.....	117
III. Experimental.....	120
III.1. Materials and methods	120
III.2. Synthesis of templates and functional monomer.....	121
III.3. NMR studies	127
III.4. Preparation of MIPs	130
III.5. Analysis on LC-UV-ELSD of targets in ethanol/water (4/1) and artificial sweat.....	130
III.6. Equilibrium binding studies in ethanol/water and in artificial sweat	130
III.7. Analysis by LC-MS/MS of the conjugates and the odorous acids in human sweat	131
III.8. Analysis by LC-UV-ELSD of conjugates in human sweat-.....	131
Capture of these analytes by MIPs	
III.9. Capture of 3H3MH by MIP in human sweat and quantification by LC-MS/MS.....	132
III.10. Preparation of deodorant formulation.....	132
III.11. Equilibrium binding studies of the polymers in a deodorant formulation	133
III.12. Cell culture and count.....	133
III.13. MTT cytotoxicity test on HaCaT cells.....	134
III.14. Isolation of bacteria from human sweat-identification by MALDI-TOF/MS	135
III.15. Effect of MIP on the growth of skin commensal bacteria	136

IV. Conclusions-Perspectives	136
V. References	137
Annex 1.....	143
Annex 2.....	144

Chapter 3: MIPs in food technology- selective extraction of the antioxidant betanin from beetroot extract 146

I. Introduction	147
I.1. MIPs as selective sorbents in food technology	147
I.2. Betanin: An important bioactive natural pigment	148
I.3. Existing protocols for the extraction and purification of betanin.....	151
I.4. Our strategy	152
II. Results and Discussion.....	153
II.1. Extraction-Purification with commercial resins.....	153
<i>II.1.1. Optimization of the extraction process.....</i>	<i>153</i>
<i>II.1.2. Elaboration of the purification process.....</i>	<i>154</i>
<i>II.1.3. Purification results.....</i>	<i>157</i>
II.2. Purification with MIP sorbents	159
<i>II.2.1. Synthesis and evaluation of the binding characteristics of MIPs in batch mode</i>	<i>159</i>
<i>II.2.2. Solid phase extraction of betanin/isobetanin from crude beetroot extract</i>	<i>166</i>
<i>II.2.3. HPLC/ESI-MS analysis of betanin samples</i>	<i>168</i>
<i>II.2.4. Elimination of impurities</i>	<i>171</i>
<i>II.2.5. Determination of the degree of purity- comparison with commercially available resins</i>	<i>172</i>
III. Experimental.....	173
III.1. Chemicals.....	173
III.2. Extraction of pigments from beetroots	173
III.3. Characterization of beetroot extract	174
III.4. Purification with commercial resins.....	175

<i>III.4.1. Preparation-activation of the resins</i>	175
<i>III.4.2. Purification protocol-Determination of the degree of purity</i>	176
III.5. Purification with MIPs	176
<i>III.5.1. Preparation of the imprinted materials</i>	176
<i>III.5.2. Quantification of dipicolinic acid</i>	177
<i>III.5.3. Equilibrium binding assays</i>	178
<i>III.5.4. Evaluation of imprinted materials by SPE</i>	179
<i>III.5.5. HPLC-ESI-MS/MS analysis</i>	181
<i>III.5.6. Isothermal Titration Calorimetry (ITC)</i>	180
<i>III.5.7. Nuclear Magnetic Resonance (NMR) studies</i>	181
<i>III.5.8. Computational studies</i>	181
IV. Conclusions-Perspectives	182
V. References	183
Annex	189
General Conclusions and Perspectives	191
Annex: Achievements	194

Table of Figures

Chapter 1

- Figure 1.1.** Principle of molecular imprinting via covalent interactions, as shown by Wulff and Sarhan, 1972. Reproduced from Andersson and Nicholls, 2000. 6
- Figure 1.2.** General principle of molecular imprinting by self-assembly. Reproduced from Haupt, 2003a. 7
- Figure 1.3.** Mechanism of free radical polymerization. Reproduced from Beyazit et al., 2016. 9
- Figure 1.4.** Schematic representation of RAFT polymerization process. Reproduced from Beyazit et al., 2016. .. 11
- Figure 1.5.** Schematic representation of ATRP polymerization process. Reproduced from Wang and Matyjaszewski, 1995. 11
- Figure 1.6.** Schematic representation of Iniferter polymerization process. Reproduced from Otsu and Yoshida, 1982. 12
- Figure 1.7.** Schematic representation of the silica sol-gel imprinting by self-assembly approach. Reproduced from Díaz-García and Lainño, 2005. 13
- Figure 1.8.** Common functional monomers used for non-covalent molecular imprinting with A) acidic B) basic and C) neutral charge. 15
- Figure 1.9.** Chemical structures of commonly used cross-linkers. 16
- Figure 1.10.** Physical forms of MIPs obtained by A) bulk (Ye and Mosbach 2001); B) precipitation (Yoshimatsu et al., 2007); C) suspension (Mayes and Mosbach 1996) and D) emulsion polymerization (Vaihinger et al., 2002)... 18
- Figure 1.11.** Chemical structures of stoichiometric monomers. 19
- Figure 1.12.** A) Chemical structures of the naphthalene sulfonates (NSs) used to probe the selectivity of the MIP; B) Chromatogram obtained by MISPE of 500 mL river water (pH 2.3). Reproduced from Caro et al., 2004. 24
- Figure 1.13.** A) Chemical structures of the template enrofloxacin (1) and 1-(4-vinylphenyl)-3-(3,5-bis(trifluoromethyl)phenyl) urea functional monomer (2); B) Retention behaviour of ENRO on the MIP and the NIP for different mobile phase compositions. Reproduced from Benito-Peña et al., 2008. 25
- Figure 1.14.** Chromatograms of the on-line extraction of a human plasma sample spiked with bupivacaine and ropivacaine at 75 mmol and ethycaine at 40 mmol on MIP and the reference polymer REF. Reproduced from Cobb et al., 2007. 26
- Figure 1.15.** A) Binding energies, estimated using the LEAPFROG algorithm, of AD with the monomers contained in the virtual library; B) Binding percentage and ratio of AD in solvents of H₂O–EtOH (1:1) and CHCl₃ on polymers in the NIP library. Reproduced from Muhammad et al., 2012. 27
- Figure 1.16.** (a) Chromatogram corresponding to the direct injection of an aqueous standard solution of AD (1.0 mg/L); Chromatogram obtained (b) after protein precipitation of human serum spiked with AD; (c) after MIP extraction of human serum spiked with AD. Inset: Chemical structure of AD. Reproduced from Muhammad et al., 2012. 27
- Figure 1.17.** Schematic representation of the *in situ* imprinting strategy (Henry et al., 2012). 29
- Figure 1.18.** Chromatograms of soy sauce samples before (I) and after (II) MISPE. Peaks corresponding to FZ (1) and DFZ (2) are observed after MISPE. Reproduced from Henry et al., 2012. 30
- Figure 1.19.** A) Chemical structures of the template gastrodin (GAS) and the hydrophilic functional monomer alkenylglycosides glucose (AGG); B) (a) Chromatogram of *G. elata* root extracts before percolating through SPE column; (b) Chromatogram of washing solutions from MISPE column; (c) Chromatogram of eluting solutions from

NISPE column; (d) Chromatogram of eluting solutions from MISPE column. Reproduced from Jin et al., 2015.....	31
Figure 1.20. Schematic representation of the synthetic route for magnetic molecularly imprinted nanoparticles of chlorogenic acid based on polyethylene imine Reproduced from Hao et al., 2016.....	32
Figure 1.21. Chromatograms of apple juice (red line), and the eluted samples after treatment with the magnetic molecularly imprinted nanoparticles of chlorogenic acid (black line). Adapted from Hao et al., 2016.....	32
Figure 1.22. A) Imprinting procedure used to obtain a riboflavin complementary binding site; B) Percent riboflavin (Rf) depleted from a Stella Artois lager beer sample as a function of added imprinted (filled symbols) or nonimprinted (open symbols) polymer adsorbent with no treatment (circles) or subjected to the hydrolytic treatment (squares). Reproduced from Manesiotis et al., 2009.....	33
Figure 1.23. Steps involved in the solid phase extraction utilizing the ISET platform with the molecularly imprinted polymer (MIPs) sorbent. Reproduced from Jagadeesan et al., 2016.	34
Figure 1.24. Proposed complex formation of the urea monomer with the phosphotyrosine bearing peptide in a 2:1 stoichiometric ratio. Adapted from Helling et al., 2011.	35
Figure 1.25. Chromatographs obtained by MALDI MS. Each row of the ISET is loaded with incubated sample/MIP mixture containing different ratios (1:1, 1:5, 1:10) of β -casein and BSA. Reproduced from Jagadeesan et al., 2016.	36
Figure 1.26. A) Recovery of the C-terminal epitopes of A β in the elution fractions after SPE of peptide-spiked blood serum samples (2.5 μ g/mL) on the two complementary MIPs and the NIP; B) Recoveries estimated from spot intensities of the SDS-PAGE/immunoblot analysis; C) Stained gel from urea-SDS-PAGE/ immunoblot analysis of elution fractions from SPE of a blood serum sample spiked with A β 1-40 (5 ng/mL) and A β 1-42 (1 ng/mL). Reproduced from Urraca et al., 2011.....	37
Figure 1.27. Schematic representation of imprinting of endosulfan in poly(methacrylamide functionalized magnetic composites. Reproduced from Shaikh et al., 2014.	38
Figure 1.28. Chromatogram of synthetic wastewater spiked with 0.3 μ g/L of endosulfan I and II (a) obtained by MISPME fiber (b) obtained by PDMS fiber. Reproduced from Shaikh et al., 2014.....	38
Figure 1.29. Principle of a MIP-based radioimmunoassay. Reproduced from Ye and Haupt, 2004.....	39
Figure 1.30. A) Binding of radioligand relative to polymer concentration for the polymers A-D; B) Radioligand displacement curves with unlabeled 2, 4-D as competitor for the polymers A and B, at 150 μ g polymer/1 mL assay. Reproduced from Haupt et al., 1998.....	40
Figure 1.31. Specificity of binding of the HRP-vancomycin conjugate to immobilized nanoMIPs. Reproduced from Chianella et al., 2013°.....	42
Figure 1.32. Schematic representation of the boronate-affinity sandwich assay of glycoproteins. Reproduced from Ye et al., 2014.....	43
Figure 1.33. A) Dependence of the intensity of the SERS signal on the concentration of the AFP solution (containing 100 mM phosphate buffer, pH 7.4); B) Logistic function fitting for determination of the binding constant; C) SERS spectra for serum samples spiked with different AFP concentrations; D) SERS intensity for serum samples spiked with different AFP concentrations. Reproduced from Ye et al., 2014.	43
Figure 1.34. A) Schematic protocol for the synthesis of narrowly dispersed hydrophilic and magnetic MIP microspheres; B) Specific and C) Non-specific binding of the ungrafted, grafted, and grafted magnetic MIP microspheres in different media Adapted from Zhao et al., 2014.	45
Figure 1.35. Schematic representation of a MIP-based chemical sensor. Reproduced from Fuchs et al., 2012.	46

- Figure 1.36.** A) Schematic representation of preparation of molecularly imprinted QCM sensor for atrazine by surface polymerization; B) The QCM responses of ATR, SIM and PRO (each of 0.50 nM) on ATR imprinted sensor; C) The QCM responses of ATR, SIM, and PRO (each of 0.50 nM) on non-imprinted sensor. Reproduced from Gupta et al., 2015. 48
- Figure 1.37.** A) Schematic illustration for the preparation of MIP@QDs and the sensing mechanism for TNT; B) Quenching amounts of MIP@QDs for TNT and its structural analogues. The quenching amount was defined as $(F_0 - F)/F_0$. Reproduced from Xu et al., 2013. 50
- Figure 1.38.** A) Protocol for the preparation of MIPP films: (a) PS colloids self assembled into colloidal crystals on a glass substrate; (b) infiltration of complex solution into a colloidal crystal template; (c) polymerization of a TCs imprinted photonic polymer; (d) MIPP film after the removal of the PS colloidal crystal template and TCs imprinted molecule template; (e) complex of the monomer and imprinted template molecule; (f) imprinted molecules within the polymer networks and (g) imprinted cavities with complementary shape and binding sites to the template molecule; B) Diffraction response of the MIP sensor in the TC spiked honey (a) and milk (b) sample. Reproduced from Wang et al., 2012b. 51
- Figure 1.39.** Typical SERS spectrum of a dried solution of S-propranolol at 10⁻⁵ M on aggregated gold colloids (red), a MIP nanocomposite particle after incubation in 10⁻⁵ M (blue), a MIP nanocomposite particle after incubation in 10⁻⁶ M (black), NIP nanocomposite particle after incubation in 10⁻⁵ M (green) of propranolol in 20x diluted equine serum. 52
- Figure 1.40.** A) Schematic protocol for the synthesis of hydrophilic and fluorescent MIP nanoparticles for the recognition of tetracycline in real, undiluted biological samples; B) Fluorescence spectra of MIP nanoparticles (0.5 mg/mL) with the addition of different concentrations of tetracycline in bovine serum ($\lambda_{exc}=365$ nm; $\lambda_{em} = 467$ nm); C) Fluorescence quenching of the grafted fluorescent Tc-MIP/Tc-CP nanoparticles (0.5mg/mL) after their incubation with a solution of Tc, chlortetracycline (cTc), chloramphenicol (Chl), cefalexinmonohydrate (Lex), vancomycin hydrochloride (Van), or atenolol (Concentration=10 μ M) in bovine serum at 25 °C for 3h. Adapted from Niu et al., 2015. 53
- Figure 1.41.** A) Affinity-based sensor assays for virus detection; B) Real-time sensorgrams of the (a) continuous and (b) regenerative virus binding assays. MIP surface was regenerated using 0.1 M HCl (R1) and 20 mM NaOH (R2) as regeneration solutions for subsequent virus samples tests. (c) Cross-reactivity test using QB phage as control. Reproduced from Altintas et al., 2015. 55
- Figure 1.42.** A) Outline of the bioimprinting process used to create virus responsive super-aptamer hydrogels. B) The volume-shrinking response for the MIP-GLaDiS in Apple stem pitting virus (ASPV) extract is shown in both parts a and b (boxed) for comparison to non imprinted control Gels 1,2 and 3 (a) and cross-reactivity responses to extracts from healthy leaves not infected with ASPV or leaves infected with different apple viruses (b). Reproduced from Bai and Spivak, 2014. 56
- Figure 1.43.** Stimuli-responsive binding of the grafted MIP microspheres in a propranolol solution (0.05 mM) A) under the photoswitching conditions (i.e. UV light on for 6 h and off for 18 h alternately at 25 °C; B) at different temperatures in water and C) at different pH values at 40 °C in buffer (polymer concentration: 1 mg/mL). Reproduced from Ma et al., 2012. 59
- Figure 1.44.** A) Thermodependent adsorption of MIP and NIP; B) SDS-PAGE analysis of the desorbed fraction from MIP (Lane 3) and NIP (Lane 4); Lane 1, 100 times diluted human plasma; Lane 2, standard protein marker. Reproduced from Li et al., 2016. 60
- Figure 1.45.** A) and B) Cancer cells (human prostate cancer cell line, PC-3) internalization of the Fe₂O₃@DOX-MIP nanoparticles;(A) in blue and PKH26 cell membrane dye (A, B) in red, respectively. Z reconstruction; B) identification of DOX inside the cells; C) Viability of cancer cells labelled with Fe₂O₃@DOX-MIP after exposure to the AMF compared to the control experiment (cancer cells labelled with Fe₂O₃ nanoparticles, at the same cellular iron dose, and exposed to the same conditions of AMF); D) Treatment of the cancer cells with free doxorubicin (DOX) incubated for 2 hours from 0.5 to 50 μ M. Reproduced from Griffete et al., 2015. 61
- Figure 1.46.** A) Timolol release in artificial lachrymal fluid (6.78 g/L NaCl, 2.18 g/L NaHCO₃, 1.38 g/L KCl, 0.084 g/L CaCl₂.2H₂O, pH 8) at 37 °C from reloaded imprinted hydrogels. Reproduced from Alvarez-Lorenzo et al., 2002.

B) Norfloxacin (NRF) release profiles in lachrymal fluid from pHEMA hydrogels using different norfloxacin: acrylic acid molar ratios. Reproduced from Alvarez-Lorenzo et al., 2006.	63
Figure 1.47. <i>In vivo</i> ketotifen fumarate tear fluid concentration profile from contact lenses and topical eye drops in a white New Zealand rabbit. Dynamic ketotifen fumarate release from poly(HEMA-co-AA-co-AaM-co-NVP-co-PEG200DMA) contact lenses. Reproduced from Tieppo et al., 2012.	64
Figure 1.48. A) Schematic representation of MIP preparation and its combination with targeted proteomics for the quantification of sTfR protein; B) Representative standard addition analysis curve of VK13 in clinical samples. C) sTfR levels in breast cancer patients and healthy volunteers. Adapted from Liu et al., 2015.	66
Figure 1.49. Two-dimensional electrophoresis of serum subjected to electrodepletion of albumin (b) and control serum (a). Reproduced from Bossi et al., 2007.	67
Figure 1.50. A) Work flow for phosphoproteomic analysis of harvested HEK 293T cells, mouse brain or CSF using SCX fractionation followed by pS-MIP or TiO ₂ enrichment; B) Mean number of phosphopeptides (bar graph) identified in 10 µg or 100 µg (TiO ₂ *) of a tryptic digest of HEK 293T cell lysate by nanoLC-ESI-MS/MS analysis of a sample (lysate) before or after fractionation by SCX chromatography, pS-MIP SPE, TiO ₂ SPE or SCX followed by pS-MIP or TiO ₂ SPE as indicated. Adapted from Chen et al., 2015b.	68
Figure 1.51. Biodistribution of melittin and NPs; A) Fluorescent images of Cy5-melittin after intravenous injection of Cy5-melittin (1 mg/kg), 27 mg/kg of MIPNPs was injected 20 seconds after the injection of melittin (right); B) Fluorescence histology images of the liver (Cy5-melittin 0.3 mg/kg and 10 mg/kg of MIP NPs). Green; Cy5-melittin, red; fluorescein-MIPNPs. The scale bars; 25 µm. Adapted from Hoshino et al., 2010).	69
Figure 1.52. A) Confocal microscopy image of MIP-stained human keratinocytes (HaCaT). Merge image of three color channels: DAPI blue signal (cell nucleus), 3,3'-diiodoacetylcarboxyanineperchlorate (DiO) green signal (cell membrane), rhodamine red signal (MIPs). Scale bar: 20 µm; B) Human skin specimens stained with MIPs. Scale bar: 100 µm. Adapted from Kunath et al., 2015.	70
Figure 1.53. A) Schematic representation of SERS imaging of cancer cells and tissues via sialic acid-imprinted nanotags. B) SERS imaging of cancer and normal liver tissues. Adapted from Yin et al., 2015.	71
 Chapter 2	
Figure 2.1. Schematic representation of the human axillary skin, indicating the location of sebaceous and sweat glands.	95
Figure 2.2. Formation of malodorous volatile fatty acids, (E)-3-methyl-2-hexenoic acid (3M2H) and 3-hydroxy-3-methyl-hexanoic acid (3H3MH) from their non-odorant glutamine conjugates by <i>Corynebacteria</i> spp in axillary sweat.	99
Figure 2.3. Schematic illustration of a MIP as the active ingredient in a cosmetic product to prevent body odor formation. By scavenging the odorless precursor, the MIP prevents its hydrolysis to a volatile malodorous acid by a bacterial enzyme.	102
Figure 2.4. Structural analogues used as template molecules in this study.	102
Figure 2.5. Equilibrium binding isotherms for 200 nmol of N α -hexanoyl glutamine on T1/4-VP polymers in EtOH: water (4:1). MIP (filled circles) and NIP (empty circles).	103
Figure 2.6. Equilibrium binding isotherms for 200 nmol of N α -hexanoyl glutamine on T2/4-VP polymers in EtOH: water (4:1). Batch T2-4VP 1 (rhombuses), batch T2-4VP 2 (squares), batch T2-4VP 3 (triangles) and NIP (crosses).	104
Figure 2.7. Equilibrium binding isotherms for 200 nmol of N α -hexanoyl glutamine for MIP T2-AEM polymers in A) ethanol and B) artificial sweat MIP (filled circles) and NIP (empty circles).	104

Figure 2.8. Structure of tailor-made amidine monomers.	105
Figure 2.9. Proposed complex formation between the template N α -hexanoyl glutamine and the monomer AB.	106
Figure 2.10. ¹ H NMR analysis of Job and titration experiments of N α -hexanoyl glutamine (A, B, C) with AB in CD ₃ OD/D ₂ O (4/1) at 25 °C.....	106
Figure 2.11. Equilibrium binding isotherms for 200 nmol of N α -hexanoyl glutamine in ethanol/water (4/1) for MIP T1-AB (filled circles) and NIP (empty circles), prepared with N α -hexanoyl glutamine as template. Analysis by LC-UV-ELSD.	107
Figure 2.12. Proposed complex formation between the template N α -hexanoyl glutamic acid and the monomer AB.	107
Figure 2.13. ¹ H NMR analysis of Job and titration experiments of N α -hexanoyl glutamic acid with AB in CD ₃ OD/D ₂ O (4/1) at 25 °C.	108
Figure 2.14. Equilibrium binding isotherms in artificial sweat for A) 200 nmol of N α -hexanoyl glutamine; B) 100 nmol of cj3H3MH and C) 100 nmol of cj3M2H, of MIP (filled circles) and NIP (empty circles), prepared with N α -hexanoyl glutamic acid as template.	109
Figure 2.15. SEM images of MIP T2-AB (left) and NIP (right) prepared in methanol.....	109
Figure 2.16. Analysis by LC-MS/MS of the glutamine conjugate precursors and the odorous acids in artificial and human sweat. Representative chromatograms of (A) cj3H3MH (blue), cj3M2H (violet) and 3H3MH (red) spiked in artificial sweat and (B) cj3H3MH (blue), cj3M2H (violet) and 3H3MH (red) present in human sweat.	110
Figure 2.17. Capture of target molecules by 5 mg/mL of MIP and NIP after incubation in human sweat at 20 °C. ...	111
Figure 2.18. Capture at equilibrium of cj3H3MH (circles) and cj3M2H (rhombus) in human sweat by MIP (filled symbols) and NIP (empty symbols) at 20 °C.	112
Figure 2.19. Equilibrium binding isotherms of MIP (filled circles) and NIP (empty circles) for spiked A) 200 μ M cj3H3MH and B) 100 μ M cj3M2H, in a deodorant formulation.....	113
Figure 2.20. Capture of cj3H3MH (circles) and cj3M2H (rhombus) in human sweat by MIP (filled) and NIP (empty) incorporated in a deodorant formulation, at 37 °C.	113
Figure 2.21. Capture of cj3H3MH or hexanoic acid, spiked at 200 μ M, by 10 mg/mL MIP (black) and NIP (grey) in a 1:1 mixture of artificial sweat.....	114
Figure 2.22. Cell viability as determined by MTT assay for HaCaT cells after incubation for 24h (blue) and 48h (red) with MIP particles. Values represent the mean of 5 repetitions in each case. * P< 0.05 compared with Control (n=5).	116
Figure 2.23. Bacterial growth of 50 μ L of human sweat after incubation at 37 °C, plated on A) LB and B) Blood agar.	117
Figure 2.24. Growth curves obtained after incubation of the following bacteria species for a total of 56 hours A) <i>S. epidermidis</i> ; B) <i>C. striatum</i> and C) <i>M. luteus</i> . MIP: violet rhombus, Control: green triangle and silver nitrate: red circle.	118
Figure 2.25. Blood agar plates inoculated with <i>S. epidermidis</i> A) Control samples; B) Supplemented with MIP at 0.5 mg/mL.	119
Figure 2.26. Synthesis of (4-acrylamidophenyl)(amino)methaniminium chloride (Beyazit et al., 2014).	121
Figure 2.27. A) ¹ NMR; B) ¹³ C NMR in DMSO- <i>d</i> ₆ and C) mass spectrum of (4-acrylamidophenyl)(amino)methaniminium acetate; N α -hexanoyl-L-glutamine.....	122

Figure 2.28. Synthesis of N α -hexanoyl-L-glutamine, according to the protocol of L'Oréal.	123
Figure 2.29. A) ^1H NMR; B) ^{13}C NMR in DMSO- d_6 and C) mass spectrum of N α -hexanoyl-L-glutamine.	124
Figure 2.30. Synthesis of N α -hexanoyl-L-glutamic acid, according to the protocol of L'Oréal.....	125
Figure 2.31. A) ^1H NMR; B) ^{13}C NMR in DMSO- d_6 and C) mass spectrum of N α -hexanoyl-L-glutamic acid....	126
Figure 2.32. ^1H NMR of N α -hexanoyl glutamine (A, B) and N α -hexanoyl glutamic acid (C, D) with AB in DMSO- d_6 at 25 °C.	127
Figure 2.33. MTT, a tetrazolium dye is reduced to purple formazan in living cells.	134
Figure S1. COSY spectra of 5 mM (A) N α -hexanoyl glutamine and (B) N α -hexanoyl glutamic acid, in DMSO- d_6	143

Chapter 3

Figure 3.1. A) Generic structure of betacyanins and betaxanthins; B) Chemical structures of betanin and vulgaxanthin I, highlighted in red the betalamic acid common backbone.	149
Figure 3.2. Effect of betanin /isobetanin concentrate on cell proliferation Relative proliferation index of cancer and non-tumorigenic cells treated with betanin /isobetanin. Reproduced from Nowacki et al., 2015.	150
Figure 3.3. Factors influencing the chemical stability of betalains. Reproduced from Herbach et al., 2006.	151
Figure 3.4. Variations of concentrations related to the percentage of water in the extraction solvent for A) betacyanins and betaxanthines; B) Proteins (based on the protocol of Lowry, 1951) and sugars (based on the protocol of Dubois, 1956).....	154
Figure 3.5. Organogram of extraction and purification processes.	155
Figure 3.6. Profile of pigments' color in the column packed with the resin XAD 16 during rinsing with water.	157
Figure 3.7. Concentration of A) proteins and B) total sugars (right) in the beetroot extract corresponding to each purification step.	158
Figure 3.8. Chemical structures of compounds described in this study.	160
Figure 3.9. A) Equilibrium binding isotherms of MIP (filled circles) and NIP (empty circles) for spiked 25 μM in MeOH/water (4/1); B) Equilibrium binding isotherms of MIP (filled circles) and NIP (empty circles) for spiked 25 μM in water; C) Binding capacity of MIP and NIP (8 mg) in 1 mL of water. The concentration of DPA was varied from 10 μM to 150 μM	162
Figure 3.10. Equilibrium binding isotherms of sol gel MIP (filled circles) and NIP (empty circles) for spiked 25 μM in A) ethanol and B) water. Data are the mean from three independent experiments.....	163
Figure 3.11. ITC data and binding analysis of 4-VP/DPA interaction in methanol/water (4/1) at 25 °C. A) Raw data from the titration of 50 mM of 4-VP added into 3 mM of DPA. Upward peaks indicate an exothermic reaction; B) Integrated areas under each peak is represented against the molar ratio of titrant to titrate and fitted with a non-linear single-site model.....	165
Figure 3.12. Equilibrium binding isotherms of MIP (filled circles) and NIP (empty circles) for 10 $\mu\text{g/mL}$ of betanin/isobetanin in beetroot extract after 2 h incubation at 25 °C. The betanin/isobetanin content was measured spectrophotometrically at 538 and 600 nm, as described in Section III.3.	166

Figure 3.13. A) Evolution of betanin/isobetanin concentration throughout the collection of 0.5 mL fractions during percolation of beetroot extract on the MIP sorbent; B) Corresponding graph with percentage of flow-through of pigment vs loaded pigment. 166

Figure 3.14. Extraction recoveries of A) betanin/isobetanin and B) betaxanthins obtained on 60 mg of polymers. Conditioning with 4 mL of water; loading of 2 mL diluted beetroot extract (betanin/isobetanin and betaxanthins 10 µg/mL); washing with 4 mL water; elution with 4 mL ethanol/acetic acid (1/1). Data represent the mean of five independent experiments, with 2 different batches of polymers. 167

Figure 3.15. Representative chromatograms of diluted beetroot extract (A) before and B) after extraction on MIP and C) commercial betanin in dextrin. Retention times were attributed by mass spectrometry analysis: sugars (mainly saccharose $m/z [M+Na]^+ = 365.1054$, $t_R \sim 1.3$ min); vulgaxanthin I ($m/z [M-NH_3]^+ = 323.08$, $t_R = \sim 4.1$ min); betanin ($m/z [M+H]^+ = 551.1497$, $t_R = 12.3$ min) and isobetanin ($m/z [M+H]^+ = 551.1497$, $t_R = 14.6$ min). 169

Figure 3.16. Positive electrospray tandem mass spectrum of A) betanin or isobetanin and B) vulgaxanthin I. The daughter ion of $m/z 389.09$ corresponding to protonated aglycone is obtained by fragmentation of the parent ion of $m/z 551.1$ of betanin or isobetanin. The daughter ion of $m/z 323.08$ corresponding to $[M-NH_3]^+$ obtained by fragmentation of the parent ion of $m/z 340.12$ of vulgaxanthin I. 170

Figure 3.17. Representative chromatograms of A) Crude beetroot extract before MIP; B) Purified sample after MIP and C) Commercial betanin. The identification of peaks was performed by ESI-MS/MS in positive mode: betanin ($m/z [M+H]^+ = 551.1507$, $t_R = 12.3$), isobetanin ($m/z [M+H]^+ = 551.1507$, $t_R = 14.6$ min). Detection with UV at 538 nm. 171

Figure 3.18. Concentration of sugars and proteins before and after purification by the MIP, indicating the percentage of the matrix materials eliminated by the purification process. 172

Figure 3.19. Calibration curves of A) Glucose as a standard for the quantification of carbohydrates at 492 nm by the Dubois method; B) BSA as a standard for the quantification of proteins at 750 nm by the Lowry method. Data represent the mean of three independent experiments. 175

Figure 3.20. A) Calibration curve of the complex Eu^{3+} -DPA in water ($\lambda_{ex} = 280$ nm, $\lambda_{em} = 615$ nm, slit = 3 nm). $Eu^{3+} = 1$ mM. Data represent the mean of three independent experiments; B) Titration of the complex Eu^{3+} -DPA in water ($\lambda_{exc} = 280$ nm, $\lambda_{em} = 615$ nm, slit = 3 nm). 178

Figure S1. ^{13}C NMR studies in MeOD/D₂O for the carboxyl carbon of DPA. A) Job plot and non-linear regression with 1:1 equilibrium equation for the complex DPA/4-VP; B) Titration data and non-linear regression with 1:1 equation, $K_a = 10^3 M^{-1}$ 189

Figure S2. The minimized equilibrium configuration of DPA/4-VP complex obtained in water by molecular modelling with the semi-empirical method AM1 using the software Spartan. This simulation an equilibrium 1:1 for the complex DPA/4-VP. Red balls correspond to oxygens, dark gray to carbons, gray to hydrogens and blue to nitrogens. The dashed green lines correspond to hydrogen bonds. 189

General Introduction

This PhD thesis was funded by the Ministry of Higher Education and Research, France and is a continuation of scientific activities from two precedent projects: an industrial project funded by L’Oreal, the world leader in cosmetics and the BetOX project, funded by the Regional Council of Picardy and the FEDER (Fonds européen de développement économique régional). The work was performed from October 2013 to September 2016, in the UTC/CNRS Laboratory of Enzyme and Cell Engineering, headed by Prof. Karsten Haupt (co-director: Dr. Alain Friboulet), at the Université de Technologie de Compiègne (UTC). This thesis was conducted under the supervision of Prof. Karsten Haupt, Dr. Bernadette Tse Sum Bui and Prof. Claire Rossi.

The general goal of this work is to explore the potential of molecularly imprinted polymers (MIPs) as synthetic receptors for the selective recognition of target molecules in complex aqueous samples. MIPs are tailor-made antibody mimics, with binding affinities and specificities comparable to those of natural antibodies. Their molecular recognition properties, combined with their high stability, mechanical robustness, low cost and easy synthesis make them extremely attractive as selective capture materials with applications in analytical separations, sensing and drug delivery, among others. However, obtaining specific recognition in aqueous samples still remains a problem due to the predominance of hydrophobic interactions

The objective of this thesis was to design a new generation of water-compatible MIPs with highly selective recognition properties in complex environments, which would be performant for “real world applications”. Thus, we developed two novel MIPs that could potentially penetrate the market of cosmetics and food technology. The first part of this thesis was the follow-up of a project funded by L’Oréal (PhD thesis of Bin Li, June 2013). At that time, the MIP synthesized was not performant in an artificial model of human sweat because its binding capacity, though relatively high, was similar to that of a control polymer without imprinted cavities, thus non-specific. Therefore, a new approach was chosen during this thesis in order to resolve these shortcomings.

The second part of this thesis emanated from a project funded by the region of Picardy, BetOX. Picardy is historically an agricultural region where the cultivation of beetroot is well developed. The three-years BetOX project aimed at studying the potential of betanin as bioactive agents in therapeutics. Since long and tedious purification steps were needed to obtain pure betanin from crude beetroot extracts, using a MIP-based extraction to replace these steps was envisaged. The synthesis and application of the MIP is described in this thesis.

This PhD thesis is organized in three chapters: one bibliographic chapter followed by two results chapters. An experimental section specific for each result chapter is provided at the end of the corresponding chapter. After the presentation of the two experimental chapters, the final conclusions and some perspectives for further studies to implement this work will be proposed.

Chapter 1 provides a literature review on molecular imprinting with emphasis on the strategies to achieve selective recognition in complex aqueous samples. Several interesting examples of MIP applications highlighting their outstanding selective recognition properties in water and complex matrices are described.

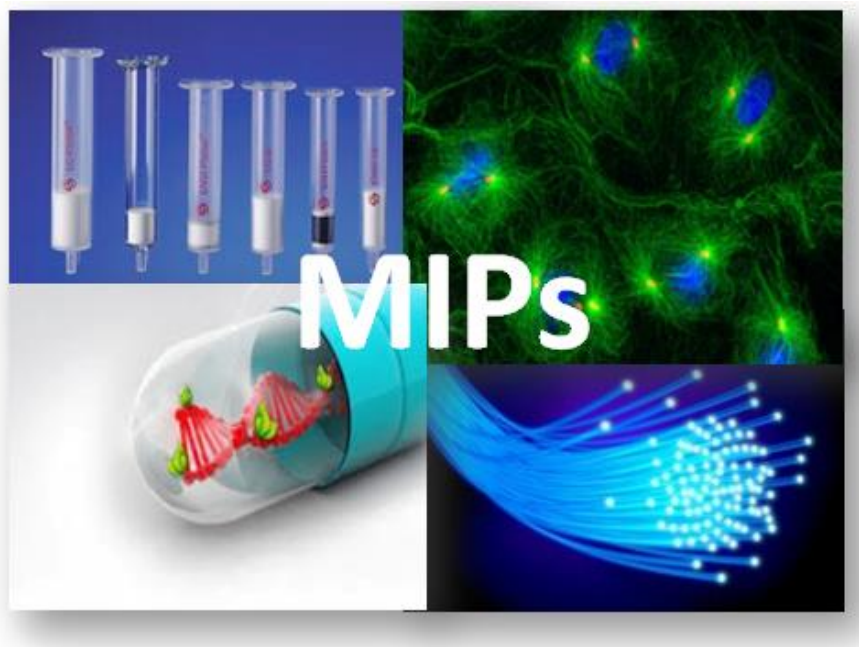
Chapter 2 presents the use of a multi-target, water compatible MIP as an active ingredient of a cosmetic product, for suppressing body malodors. Body odors are mainly due to volatile fatty acids generated from their glutamine precursors by hydrolytic enzymes from bacteria present on the skin. We synthesized a MIP to capture the glutamine conjugate precursors of these volatile acids so that they are no longer available to the bacteria, thus preventing their transformation to malodorous compounds. In this way, the fragile microbial equilibrium of the skin is not perturbed, contrarily to the unspecific antimicrobials used in most deodorants on the market. In order to generate binding selectivity in aqueous environments, an amidinium-based monomer which can form very strong stoichiometric electrostatic interaction with the carboxyl groups on the template, was synthesized. The MIP blended in a dermo-cosmetic formulation, could capture selectively the glutamine precursors, amidst a multitude of other molecules present in human sweat. Preliminary studies on the biological effect of the MIP in terms of epidermal cell viability and effect on the bacteria, commensal to the skin is also discussed in this chapter.

In **Chapter 3** we developed a fast, single-step molecularly imprinted solid-phase extraction (MISPE) procedure for the selective clean-up of betanin and its stereoisomer isobetanin from beetroot extracts. We postulated that the use of MIPs as selective sorbents could be an interesting alternative to traditional purification protocols, since their specific recognition properties could improve the performance of the purification method. In this context, a water compatible MIP imprinted with dipicolinic acid, a dummy template which was chosen because of its structural similarity to the chromophore group of betanin. The MISPE procedures were fully optimized allowing the almost complete removal of carbohydrates and most of the proteins, resulting in a high extraction recovery of betanin/isobetanin in one single step. Moreover, the whole extraction procedure was performed in environmentally friendly solvents, either ethanol or water.

Chapter 1

Molecularly imprinted polymers as synthetic receptors for selective recognition in complex aqueous environments

A literature review



I. Molecularly Imprinted Polymers: Tailor-made artificial receptors

I.1 The origin of molecular imprinting

Nature provides a plethora of materials, structures and functions which feature inspiring properties such as hierarchical organization, miniaturization, adaptability and resistance (Sanchez et al., 2005). Following the example of nature, scientists from multidisciplinary fields search for efficient ways to mimic these properties by designing bioinspired materials that could reproduce natural principles or structures offering a wide range of applications.

Antibodies are excellent examples of natural materials (proteins) with unique properties in terms of functionalities and targeted recognition towards their antigen. These biomacromolecules have a lead role in the regulation of the immune system, participating in several diverse processes, from B cell survival to atherosclerosis, as well as in autoimmunity and protection against infection (Ehrenstein and Notley, 2010). Other examples include enzymes and hormone receptors. The design of synthetic materials that could mimic natural receptors in terms of functionalities and affinities is of great interest, since their large-scale application is limited by their instability, low abundance and expensive production.

One efficient approach for the development of bioinspired synthetic materials is the synthesis of tailor-made receptors by a technique named "molecular imprinting". In this process, a molecular memory is introduced into a synthetic polymer, which can recognize a specific ligand, in a way that resembles the unique fitting of a key to its corresponding lock. Molecularly imprinted polymers (MIPs) are prepared by co-polymerizing functional and cross-linking monomers in the presence of a molecular template (Wulff and Sarhan, 1972; Arshady and Mosbach, 1981; Haupt, 2003). The template can be the target molecule or a derivative thereof. Subsequent removal of the template leaves binding sites cavities complementary in shape, size and functional groups orientation in the polymer network which are able to rebind the template molecule with both high affinity and selectivity that are comparable to those of natural antibodies. The complex between monomers and template molecule can be formed *via* reversible covalent bonds and/or *via* non covalent interactions, which will be presented below (Haupt, 2001).

The idea of molecular imprinting dates from the early 1930s, attributed to the work of Polyakov on silica matrices for chromatographic applications (Polyakov, 1931). He observed that when an additive (benzene, toluene or xylene) is introduced during polymerization of silica, the polymerized matrix is able to rebind this additive with a higher absorption rate. This first observation of the molecular effect generated an increased interest for synthetic imprinting materials and several studies followed, illustrating imprinting on silica.

The feasibility of imprinting on organic materials was demonstrated by the pioneering works of Wulff and Mosbach, who employed two different approaches based on covalent and non-covalent bonding, respectively. First, Wulff described the synthesis of MIPs based on covalent bonds between the template and the functional monomer (Wulff and Sarhan, 1972). He co-polymerized a template molecule functionalized with polymerizable vinyl groups with divinylbenzene (DVB), so as to form a non-swelling macroporous polymer. To illustrate his idea, he chose as a model template the 2,3-*O*-*p*-vinylphenylboronic ester of D-glyceric acid *p*-vinylanilide that was co-polymerized with DVB in acetonitrile (ACN). After polymerization, at most 50% of the D-glyceric acid could be removed by hydrolysis, leaving binding cavities with asymmetrically arranged functional groups, due to the chirality of the template (Figure 1.1). The polymer had the capacity to rebind the quantity of D-glyceric acid that was removed. Moreover, upon interaction a racemic mixture of D, L-glyceric acid, it showed selective binding towards the D-enantiomer over the L-enantiomer, thus demonstrating enantiospecificity. Wulff observed finally that the polymer lost its binding properties when swollen, underlining the importance of the shape of the binding cavities in the molecular recognition process.

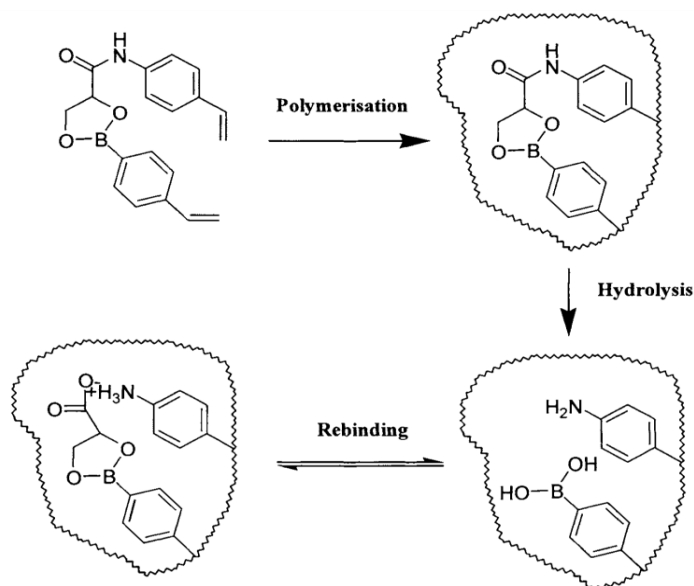


Figure 1.1. Principle of molecular imprinting via covalent interactions, as shown by Wulff and Sarhan, 1972. Reproduced from Andersson and Nicholls, 2000.

Later, Mosbach and co-workers showed the feasibility of molecular imprinting by self-assembly, exploiting weak interactions between the template and the monomers. They called it the “host-guest polymerization”, and in this approach, the interactions between the template and the functional monomers are only based on non-covalent interactions, such as hydrogen bonds, ionic, hydrophobic or π - π stacking interactions and van der Waals forces. The complex between template and functional monomers is formed by self-assembly, and the polymerization is carried out with an excess of cross-linkers, in order to give

rigidity to the polymer matrix and preserve the shape of the binding cavities formed (Arshady and Mosbach, 1981) (Figure 1.2).

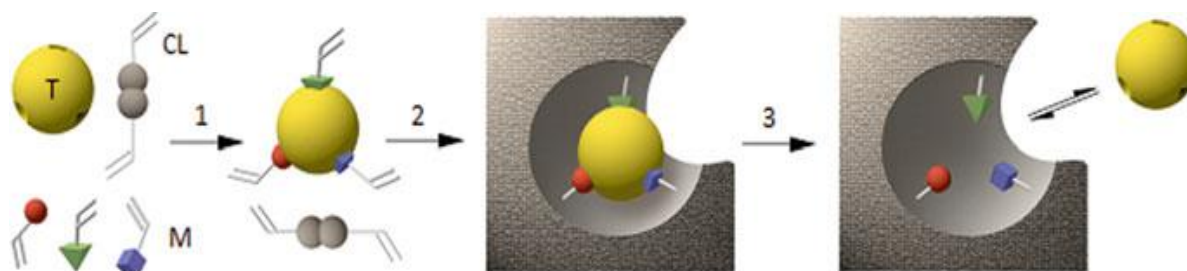


Figure 1.2. General principle of molecular imprinting by self-assembly. A molecular template (*T*) is mixed with functional monomers (*M*) and a cross-linker (*CL*) resulting in the formation of a self-assembled complex (1). The polymerization of the resulting system produces a rigid structure bearing imprinted sites (2). Finally, removal of the template liberates cavities that can specifically recognize and bind the target molecule (3). Reproduced from Haupt, 2003a.

Both covalent and non-covalent imprinting have their advantages but the choice between them can depend on each particular case and application. The main advantage of the covalent approach is the homogeneity of binding sites, which can enhance the specificity of recognition towards the target molecule and thus the imprinting efficiency. However, this method is less versatile, since it requires derivatization of the template to enable chemical reactions with the functional monomers, while is often associated with slow binding kinetics. On the other hand, non-covalent bonding is easily applicable, and rather versatile since a large number of monomers bearing different functional groups are commercially available to interact with almost any kind of target molecule. This justifies the extensive use of non-covalent imprinting, commonly adopted for various applications. Despite its popularity, several hurdles should be tackled for the successful synthesis of a performant MIP. More specifically, the excess of functional monomers utilized (4-fold or 8-fold as reported by Cormack and Elorza, 2004) results in uncomplexed functional groups randomly distributed in the polymeric matrix. Moreover, the yield of imprinted sites is typically quite low as a large percentage of the binding sites is destroyed before the polymeric network rigidifies, owing to the stress-induced relaxation of the polymeric chains (Wulff and Knorr, 2002).

Taking into account the unique advantages of each approach, first Sellergren and later Whitcombe combined these two methods to produce the semi-covalent approach. In their work, Sellergren and Andersson, 1990 synthesized *via* covalent bonding a complex template-monomer using a derivative of propranolol as template which was co-polymerized with DVB. Conversely to the imprint formation which was carried out using covalent bonds, the binding effect was achieved *via* non covalent interactions and in particular hydrogen bonds and electrostatic interactions. The issue observed by employing this protocol is

that non-covalent interactions occur at a longer distance than covalent interactions, which can result in a possible distortion of the binding site geometry. To solve this problem, Whitcombe and co-workers introduced a sacrificial spacer when they imprinted a covalent template–functional monomer complex, cholesteryl (4-vinyl) phenyl carbonate ester. The carbonate group was then eliminated by chemical cleavage, creating some space in the binding site and leaving behind a phenolic hydroxyl group, to which cholesterol could bind *via* a hydrogen bond (Whitcombe et al., 1995). After removal of the template by hydrolysis, re-binding takes place only *via* non covalent interactions.

In earlier years, MIPs were successfully applied as affinity materials for separation applications, for example for the separation of enantiomers from a racemic mixture (Wulff and Sarhan, 1972; Andersson et al, 1984). Later, a revolutionary work from Mosbach and co-workers demonstrated that MIPs could be used as antibody mimics in immunoassays. He demonstrated this idea on the example of a MIP immunosorbent for the determination of drugs (theophylline and diazepam) with high affinity (e.g. for theophylline, $K_d = 65 \mu\text{M}$) and selectivity in human serum, similar to those of antibodies (Vlatakis et al., 1993). This study highlighted the great potential of MIPs as recognition materials and pave the way to a wide range of applications such as immunoassays (Chianella et al., 2013), catalysis (Resmini, 2012), affinity separation (Tse Sum and Haupt, 2010; Martin-Esteban et al., 2016), biosensors (Ton et al., 2013; Uzun and Turner, 2016) and even medical care (Hoshino et al., 2010). Nowadays, commercial products based on MIPs are available, mainly for separation applications. Indeed, MIPs have been successfully applied as solid-phase extraction matrices for sample preparation and analyte pre-concentration, mainly for biomedical and food analyses, commercialized by the companies *Biotage* (<http://www.biotage.com/product-page/mips---molecularly-imprinted-polymers>) and *PolyIntell* (<http://www.affinisep.com>).

I.2 Polymerization methods

1.2.1. Free radical polymerization

In its simplest form, a typical MIP synthesis protocol contains the template, one or more functional monomers, a cross-linker, a polymerization initiator, and a solvent. The imprinting polymer and a control polymer are typically synthesized by free radical polymerization. Free radical polymerization (FRP) is the most commonly used polymerization method because of its simplicity and its compatibility with a large variety of monomers, solvent systems and reaction conditions. FRP proceeds in the following steps (Figure 1.3) (Haupt et al., 2012):

- The polymerization is initiated (1) by generating free radicals I^\bullet using an initiator, a molecule that decomposes under heating or under UV or visible irradiation. A radical attacks the double bond of a monomer, resulting in the formation of an intermediate radical. This is the rate-limiting step of the process.
- The propagation (2) is the main step of radical polymerization. Here, the macromolecular chain is formed by successive additions of monomers on the growing macroradical Pn^\bullet . The result is a mixture of polymer chains with high molecular weights.
- The chain transfer (3) results in the formation of a $Pn-X$ species and a new radical A^\bullet .
- The termination of the reaction (4), which takes place in two ways: (a) disproportionation, yielding a stable species Pn and a Pn alkene with a double bond or (b) recombination of two propagating radicals resulting in a polymer chain with the double molecular weight.

Despite these important advantages, FRP hardly offers any degree of control (in terms of size and architecture) mainly because of some ‘side’ reactions preventing further growth of the chain and resulting in shorter polymer chains (Odian, 2004). Such reactions, i.e. bimolecular termination and chain transfer reactions, strongly compete with the propagation and result in dead polymer chains of very different molecular weights. Thus, the molecular weight of the polymer cannot be controlled or predicted, and block copolymers and other polymers of complex architecture are totally inaccessible. To achieve control over the growing and/or the termination steps of the reaction, controlled radical polymerization methods are employed, which will be mentioned briefly in section I.2.2

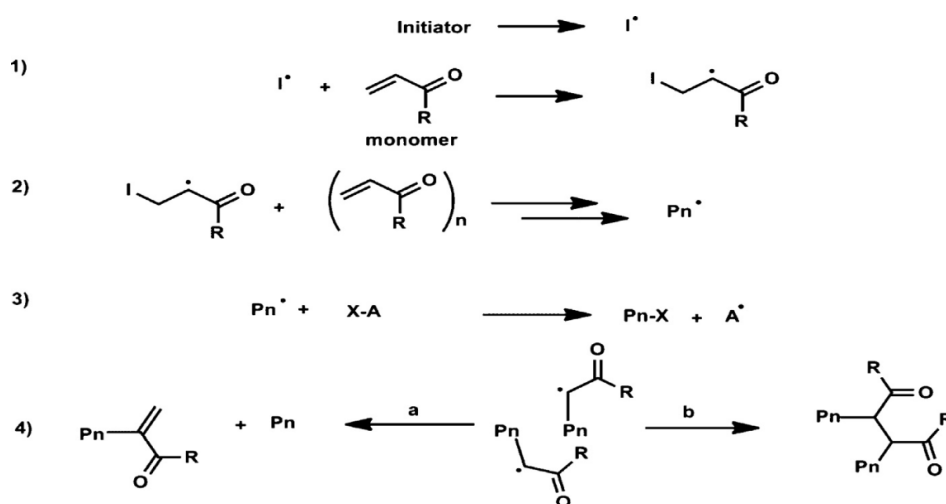


Figure 1.3. Mechanism of free radical polymerization: (1) initiation, (2) propagation, (3) chain transfer, (4) termination via (a) disproportionation and (b) combination. Reproduced from Beyazit et al., 2016.

1.2.2. Controlled radical polymerization

FRP is largely used for the preparation of MIPs despite the related drawbacks such as certain heterogeneity of binding site affinities, and a heterogeneous inner morphology and porosity (Beyazit et al., 2016). Some of these problems can be overcome by using controlled radical polymerization (CRP). The term controlled/living polymerization was introduced by Michael Szwarc as the polymerization process which “does not involve a termination step”, and where in the macromolecular “growth is” just “interrupted if the supply of monomer is exhausted, although the living ends are potentially able to grow further if any additional amount of monomer is available (Szwarc, 1956).

A number of controlled/living radical polymerization methods include: Iniferter (initiator-transfer agent-terminator) polymerization, Reversible addition-fragmentation chain transfer polymerization (RAFT), Atom transfer radical polymerization (ATRP) and Nitroxide mediated polymerization (NMP) (Beyazit et al., 2016).

Lately, there has been an increase of studies for the synthesis of MIPs by employing CRP techniques (Wang et al., 2012a; Zhang et al., 2013), some of them were done in our group (Bompart and Haupt, 2009; Gonzato et al., 2011; Cakir et al., 2013; Adali-Kaya et al., 2015). For instance, our group has recently published a very interesting review paper, where the contribution of CRP to molecular imprinting is discussed (Beyazit et al., 2016). For the experiments performed throughout this thesis, only FRP was used. Nevertheless, it is important to highlight the main advantages of CRP such as easy grafting for the production of various nanocomposites as well as control and fine tuning of the polymer's thickness. These aspects can be proved beneficial for the binding performance and the structural homogeneity of the imprinted materials. In addition, water compatibility can be enhanced by post-surface modifications carried out by CPR (Zhang, 2014). Some of the examples of imprinted polymers for diverse applications that will be described in section II are performed by RAFT, ATRP or Iniferter polymerization.

RAFT is the most suitable CRP technique for synthesizing MIPs: the setup is identical to that of FRP, it is applicable to a wide variety of monomers and can provide good control over polymerization (Barner-Kowollik and Perrier, 2008). This method involves reversible addition-fragmentation sequences in which the transfer of a dithioester moiety between active and dormant chains serves to maintain the living character of the polymerization. Initiation of polymerization is by a classical FRP initiator. Growing chains ($P_n\bullet$ or $P_m\bullet$) are added up successively to the chain transfer agent (CTA). Addition of this macroradical on CTA gives rise to an unstable radical which fragments into either a new radical $R\bullet$ which can polymerize a new polymer chain or $P_n\bullet$ (or $P_m\bullet$) that will propagate until they encounter another CTA, as illustrated in Figure 1.4.

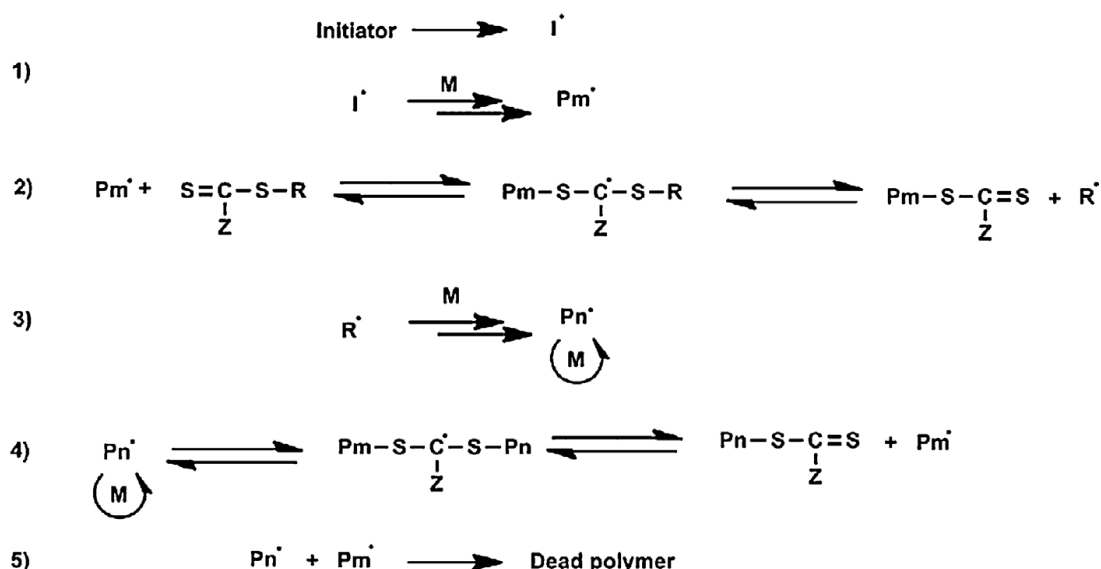


Figure 1.4. Schematic representation of RAFT polymerization process. Reproduced from Beyazit et al., 2016.

Another popular CRP method is ATRP, in which controlled conditions are actually achieved through a redox process involving a transition metal complex (M_t^n) and an organic halide (R-X), as demonstrated in Figure 1.5. More specifically, active species are produced by a reversible redox reaction, catalyzed by a transition metal/ligand complex ($\text{M}_t^{n+1}-\text{Y}/\text{L}_x$). This catalyst is oxidized via the halogen atom transfer from the dormant species (Pn-X) to form an active species (Pn^\bullet) and then complex at a higher oxidation state ($\text{X-M}_t^{n+1}-\text{Y}/\text{L}_x$).

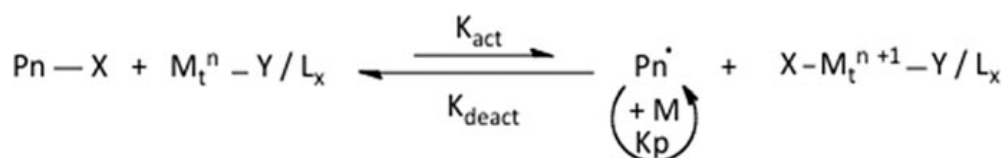


Figure 1.5. Schematic representation of ATRP polymerization process. Reproduced from Wang and Matyjaszewski, 1995.

Iniferter polymerization, introduced by Otsu and Yoshida 1982 consists in the dissociation of dithiocarbamates into an initiating alkyl radical and a second radical species that is stabilized and not capable of initiating a new polymer chain (Figure 1.6). When the energy supply to the reaction in form of heat or UV irradiation ceases, the two radicals recombine and the chain growth stops. The system can later be reinitiated with the same or other monomers, thus providing some degree of living character.

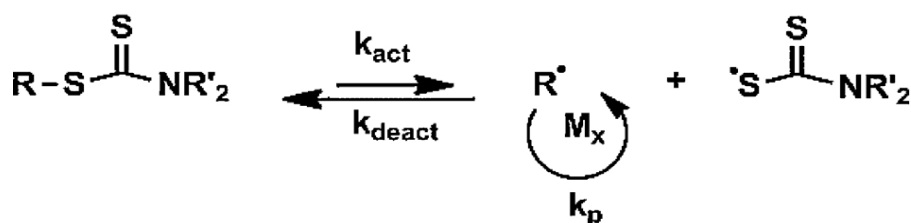


Figure 1.6. Schematic representation of Iniferter polymerization process. Reproduced from Otsu and Yoshida, 1982.

1.2.3. Sol-gel polymerization

Another way to obtain MIPs is by the sol-gel process, which uses metal alkoxide molecular precursors to produce a metal oxide in aqueous media. Sol-gel imprinting has several advantages such as robustness, porosity, thermal and chemical stability (Lofgreen and Ozin, 2014). Most importantly, sol-gel MIPs are *a priori* water compatible, since polymerization is carried out principally in water. Thus, sol-gel imprinting constitutes an attractive strategy to achieve recognition in complex aqueous samples.

Much effort concerning the sol-gel polymerization has been focused on silica, metallosilicates and titanium, zirconium and aluminium oxides (Díaz-García and Laíño, 2005). Generally, the formation of a sol-gel network involves two steps: hydrolysis and condensation. Hydrolysis occurs when silicate or a metal alkoxide precursor and water are mixed in a solvent, usually in ethanol. Then, the hydrated silanes interact in a condensation reaction. After poly-condensation, a highly cross-linked sol-gel network with pores is formed and the solvents are retained inside the pores. The small molecules like water and alcohol generated during the process can be removed through evaporation.

The sol-gel technique offers a wide range of processing approaches that can produce three-dimensional matrices in different configurations (thin films, porous materials, bulk structures) for use as sorbent and separation materials, catalysts and sensors. In the sol-gel imprinting *via* the self-assembly approach, the functional monomer (an organoalkoxysilane such as 3-aminopropyltriethoxysilane (APTES)) is combined with the cross-linker, a tetrafunctional alkoxysilane such as tetramethoxysilane (TMOS) or tetraethoxysilane (TEOS), a catalyst (such as hydrochloric acid or ammonia), and the template molecule. The template is subsequently removed from the polymer matrix by extreme acidic or basic washing. The general principle of sol-gel imprinting by self-assembly is shown in Figure 1.7.

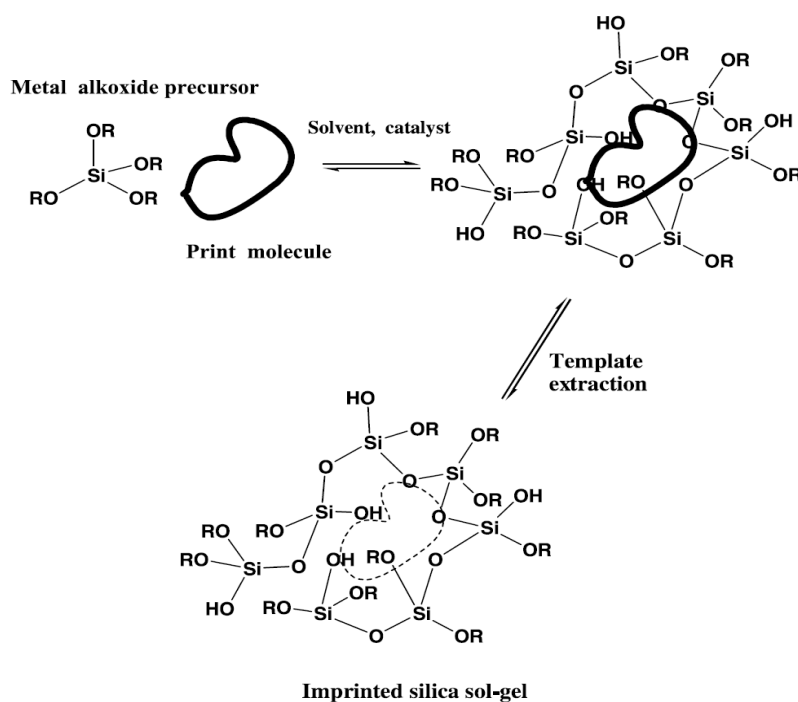


Figure 1.7. Schematic representation of the silica sol-gel imprinting by self-assembly approach (Reproduced from Díaz-García and Lainño, 2005).

Advances in sol-gel imprinting allowed their application as recognition elements in biosensors, as stationary phase materials for chromatographic separation and as solid phase extraction sorbents (Mujahid et al., 2010; Lofgreen and Ozin, 2014). Importantly, several studies highlight their use for recognition in complex aqueous samples (Lordel et al., 2010; Fang et al., 2016).

1.3 Preparation and optimization of MIPs

Regardless of the polymerization method, the synthesis of MIP requires the template, one or more functional monomers, a cross-linker and polymerization solvent. Usually, MIPs are synthesized in apolar and aprotic solvents to preserve the hydrogen and electrostatic interactions between template and monomer (Pichon and Haupt, 2006). In the following section, the major elements of MIP synthesis will be discussed.

1.3.1. Template

The template is the central element for the preparation of an imprinted polymer, since it directs the organization of the functional groups present on the functional monomers. Traditionally, templates are small organic molecules which should be chemically inert and stable during polymerization (Cormack and Elorza, 2004). If the target analyte is not compatible under these conditions, a dummy template can be utilized, bearing structural similarities with the target analyte.

In real-world applications, MIPs are targeting compounds such as biomarkers which are present (and often exclusively soluble) in complex aqueous samples. In that case, the synthesized MIP, templated with the target analyte or a structural analogue, should be performant in aqueous environments. The strategies to achieve better water compatibility are discussed in section I.6.

Apart from small molecules, MIPs are also employed for the imprinting of large biomacromolecules, such as proteins. The design of MIPs for proteins can be challenging due to their large molecular size, complexity, conformational flexibility, and solubility in aqueous media (Turner et al., 2006). Moreover, the conditions of biomacromolecular imprinting need to be close to their natural environment (for instance biological fluids) to ensure that their conformational integrities and binding activities are maintained (Bossi et al., 2007a).

Usually, the conventional protocol of the synthesis of a MIP is not adapted for the imprinting of proteins, mainly due to the limited access of the protein to the binding sites owing to its large size (Ge and Turner, 2008). To design MIPs for proteins, three different approaches are currently employed: surface imprinting using immobilized protein template, the particle based imprinting in the form of hydrogels, and the imprinting of a structural epitope (a peptide sequence accessible at the surface of the protein) (Kryscio and Peppas, 2012; Haupt et al., 2012). In our group, successful imprinting of serine proteases was carried out *via* immobilization on solid support (Xu et al., 2016) or with MIP hydrogels based on a specific anchoring monomer (Cutivet et al., 2009). A milestone study on epitope imprinting of proteins was reported by Nishino et al., 2006, who prepared MIPs for bovine serum albumin (BSA), cytochrome C and alcohol hydrogenase using C-terminus peptide sequences as the epitope domain.

1.3.2. Functional monomers

A wide range of commercially available monomers can be utilized for the synthesis of MIPs. The choice of monomers is based on the type and complementarity of interactions between the functional groups of the template. Importantly, the nature of the template and monomers and the polymerization reaction itself determine the quality and quantity of the recognition sites (Karim et al., 2005).

Common acidic, basic and neutral functional monomers are displayed in Figure 1.8 This type of monomers interact weakly with the molecular template through hydrogen bonding, electrostatic, or π - π stacking interactions. They are normally used in excess relative to the number of moles of template to favor the formation of template and functional monomer(s) complex (template to functional monomer ratios of 1:4 or higher are rather common for non-covalent imprinting) (Cormack and Elorza, 2004).

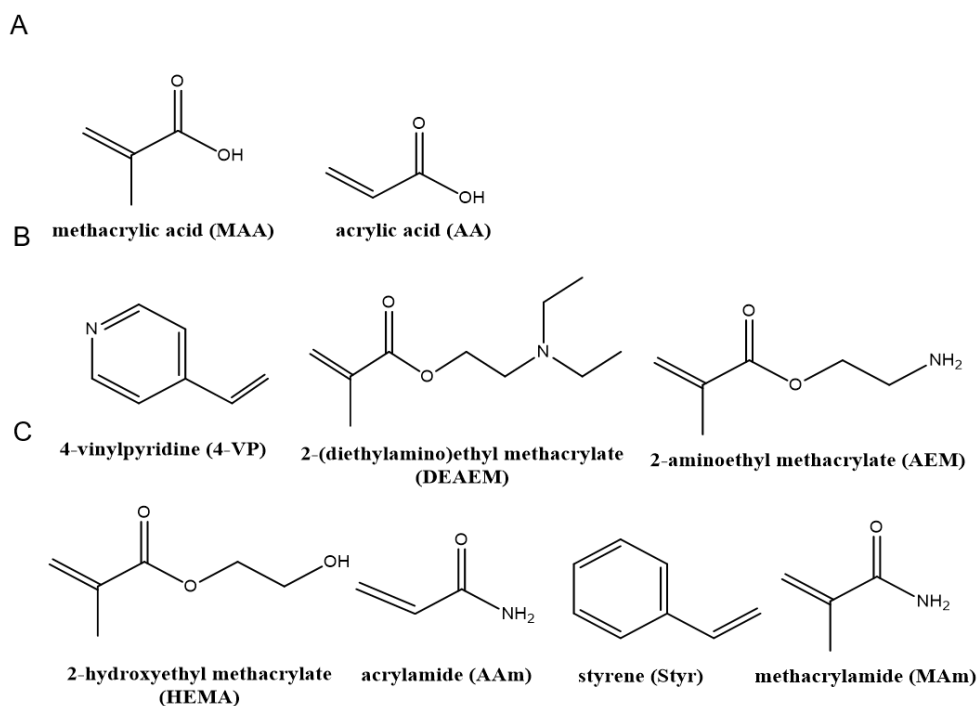


Figure 1.8. Common functional monomers used for non-covalent molecular imprinting with A) acidic B) basic and C) neutral charge.

To obtain MIPs with the best recognition properties, combinatorial synthesis and molecular modeling approaches have been developed (Tse Sum Bui and Haupt, 2010). The combinatorial MIP optimization is based on the preparation of a library of different MIPs, from which the best is selected for strong and selective target binding and low non-specific binding (Takeuchi et al., 1999). It is important to note that the constitution of a combinatorial library on multi-component systems based on experimental data can be time-consuming. A potential solution to this problem is to perform thermodynamic calculations by molecular modeling and to screen a virtual library of monomers for a given template (Chianella et al., 2002; Liu et al., 2007).

Evidence of the formation of monomer-template interactions can be provided by titration techniques like Nuclear Magnetic Resonance (NMR) (O'Mahony et al., 2005), or Isothermal Titration Calorimetry (ITC) (Kirchner et al., 2002). In many NMR studies, it is possible as well to determine the exact composition and the stoichiometry of the complex template-monomer (Svenson et al., 2004).

1.3.3. Cross-linkers

Essentially, organic MIPs are polyacrylates or polymethacrylates, due to the high quantity of cross-linking monomers (acrylates or methacrylates) that they contain. The role of the cross-linker in the polymeric network is to impart enough rigidity so as to maintain the structure of the polymer and the spatial conformation of the functional groups (Muhammad et al., 2012a). Usually, an 80% cross-linking degree is applied for the preparation of imprinted polymers (Cormack and Elorza, 2004).

The recognition properties of the MIP as well as its mechanical properties are strongly dependent on the degree of cross-linking and on the nature of the cross-linker. Highly cross-linked systems demonstrate lower template release, as reported by Salian and Byrne, 2013. On the other hand, low cross-linked structures present enhanced loading capacity due to the flexibility of the polymeric network (da Silva et al., 2011). This signifies that the MIP synthesis can be optimized for a certain application by adapting the amount of the cross-linker utilized. The choice of the cross-linker is important for recognition in biological systems, since some cross-linkers can render the MIP more water compatible (refer to section I.6.).

The chemical structures of several well-known bifunctional and trifunctional cross-linking monomers are presented in Figure 1.9. EGDMA is a very common bifunctional cross-linker, as it combines both the flexibility of its chain structure and rigidity (attributed to the prochiral methacrylate groups) (Alexander et al., 2006) and thus is employed in many examples presented in section II.

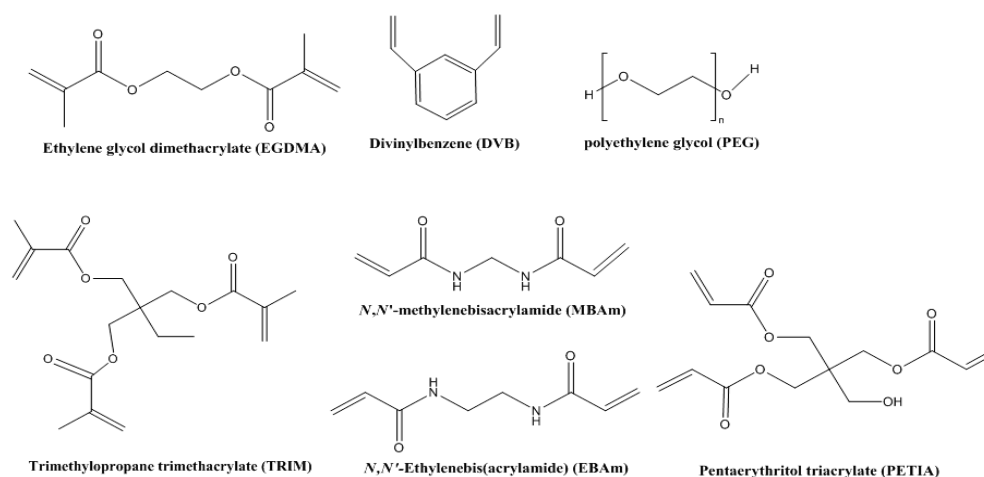


Figure 1.9. Chemical structures of commonly used cross-linkers.

1.3.4. Solvents

The choice of polymerization solvent is very crucial for a successful MIP, since the solvent system used can either favor or suppress specific interactions between the template and the monomers. Moreover, the mechanical properties and the porosity can be tuned by the type and volume of solvent. Indeed, the amount of solvent used results to highly solvated systems (precipitation polymerization) or low solvated systems (bulk polymerization).

Generally, MIPs show the best recognition properties in the solvent in which they are synthesized (Andersson, 1996). MIPs are conventionally prepared with apolar and aprotic solvents such as toluene and chloroform, which favor hydrogen bonding. However, for many applications and for solubility reasons, polar solvents or mixtures with water are also employed. In such cases, the imprinting effect is based on electrostatic and π - π stacking interactions, favored in polar media. The use of a mixture of methanol/water was first applied by Haupt et al., 1998a and 1998b) for the recognition of the herbicide 2,4-dichlorophenoxyacetic acid (2,4-D) in phosphate buffer.

I.4 Physical forms of MIPs

Traditionally, MIPs have been prepared by bulk polymerization, resulting in monolithic micrometer-sized particles. Nowadays, there is a growing interest for the design of MIPs with optimized physical properties, adaptable to a wide range of applications, from biosensors to drug delivery.

Bulk polymerization is still used for a number of applications such as SPE, where larger particles are required to avoid elution through the SPE cartridge. A small volume of solvent is required for the polymerization, while a tedious and time-consuming grinding and sieving procedure is applied to obtain irregularly shaped microparticles. The main drawback of this method comes from the partial destruction of the imprinted cavities during the grinding process, which in turn decreases the binding capacity of the MIP (Biffis et al., 2012).

For more advanced applications the synthesis of spherical, nanosized particles are required. These can be obtained by precipitation or emulsion polymerization. Precipitation polymerization is widely used because of its simplicity and absence of stabilizers. In this approach, the monomers are soluble in the porogen, and the resulting polymeric network precipitates. This method was first adopted by Ye et al., 1999 for the imprinting of estradiol and theophylline. Compared to bulk polymerization, the small regular size of the particles prepared by precipitation polymerization have a positive impact on the binding performance and the accessibility of binding sites (Poma et al., 2010). A number of interesting MIPs were prepared by precipitation polymerization and used in binding assays performed in real samples (Ma et al., 2013), for sensing in biological fluids (Prasad et al., 2016) and for separation as selective sorbents (Barahona et al., 2011).

Other synthetic procedures are suspension and emulsion polymerization. Both methods take place in a biphasic system where the monomers or the resulting polymers are dispersed. In the case of suspension MIPs, polymerization occurs entirely within monomer droplets that are dispersed inside a monomer immiscible phase. On the other hand, in emulsion polymerization the monomers are emulsified in the porogen by the use of surfactants, which form micelles around the monomer droplets. The presence of the surfactant allows to reach much smaller particle sizes, in the range of tens to hundreds of nanometers. Finally, polymerization of a MIP can be performed also *in situ* inside a chromatography column or on optical fibers (Ton et al., 2015). Microscopy images of typical MIP formats are illustrated in Figure 1.10.

MIPs can be also synthesized by immobilization to a solid support, such as glass beads. This approach, dubbed as solid phase synthesis, allows the orientation of binding sites, located at the surface of the MIP particle, which can be of great importance for protein imprinting, as described in section I.2.4. For instance, Piletsky and co-workers reported for the first time the synthesis of MIP NPs *via* a solid-phase template approach which was compatible with automated UV photochemical reactor (Poma et al., 2013).

Later, in our group the solid-phase synthesis approach was further extended for the imprinting of proteins (Ambrosini et al., 2013; Xu et al., 2016).

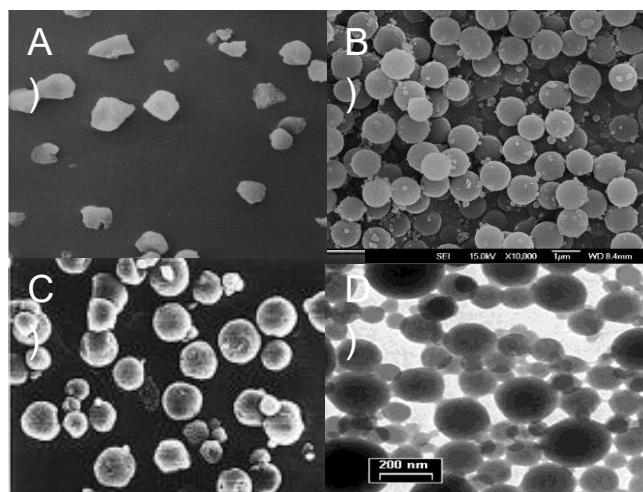


Figure 1.10. Physical forms of MIPs obtained by A) bulk (Ye and Mosbach 2001); B) precipitation (Yoshimatsu et al., 2007); C) suspension (Mayes and Mosbach 1996) and D) emulsion polymerization (Vaihinger et al., 2002).

I.5 Tow ards a successful imprint for recognition in complex matrices

As mentioned before, MIPs are traditionally synthesized in apolar and aprotic solvents and therefore their recognition properties are typically evaluated in the same medium. However, for real-life applications, MIPs should be performant in complex aqueous matrices such as biological fluids, environmental or food samples. This necessitates the development of water compatible MIPs which can be directly applicable in aqueous conditions and consequently in complex samples. The synthesis of water compatible MIPs can be a challenging task since the molecular recognition process can be compromised by the presence of water. In fact, hydrogen bonding and electrostatic interactions between the template and the binding cavities of the MIP are seriously affected in aqueous conditions (Nicholls et al., 1995). Moreover, non specific binding is enhanced in water compared to organic solvents, due to hydrophobic interactions which are usually favored in aqueous conditions. To render MIPs more water compatible different strategies are employed, focusing on the optimization of the MIP synthesis, as described in the following section (Zhang et al., 2014a). Moreover, to enhance the performance of MIPs in complex environments, issues related to their selectivity and the influence of matrix materials to their binding properties should be taken into account.

1.5.1. Use of tailor-made monomers

One approach to address the issue of MIP poor performance in water is by favoring interactions with high association constants. To this end, rationally designed monomers can be synthesized, able to form stable complexes with the respective template in polar aqueous solvents through stoichiometric interactions. The structure of the most commonly used stoichiometric monomers is presented in Figure 1.11.

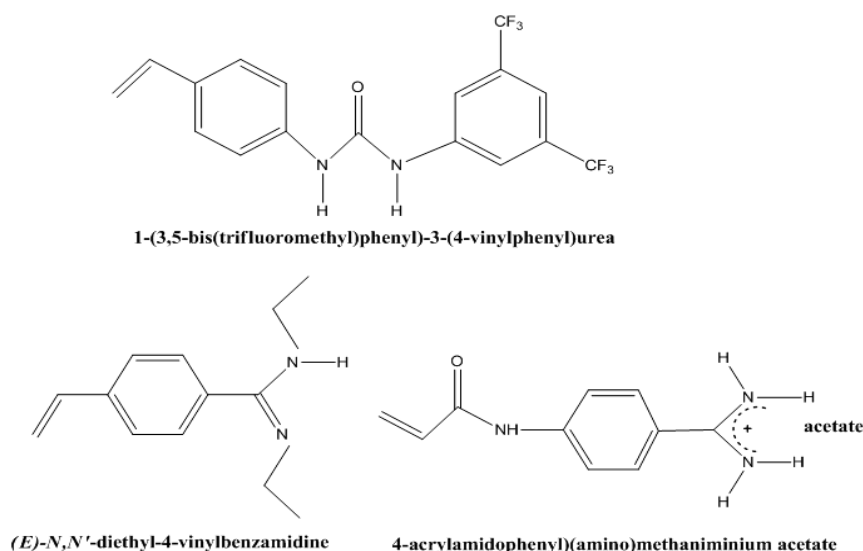


Figure 1.11. Chemical structures of stoichiometric monomers.

Wulff and co-workers have synthesized an amidine-based monomer, (E)-N,N'-diethyl-4-vinylbenzamidine (Figure 1.11) which can form stoichiometric non-covalent complexes with a high association constant of $K_a > 10^3 \text{ M}^{-1}$ with various oxyanions like carboxylates, phosphonates and phosphates, in CD_3CN or CD_3Cl (Wulff and Knorr, 2002). Similarly, our group recently synthesized an unsubstituted amidine-based monomer, (4-acrylamidophenyl)-(amino)methaniminium acetate (AB) to form a soluble complex with carboxylates in polar solvents (Nestora et al., 2016a; Panagiotopoulou et al., 2016). This monomer and its excellent recognition properties in complex aqueous matrices will be thoroughly described in chapter 2.

Another example of stoichiometric monomers which can be applied in aqueous conditions are 1,3-disubstituted ureas (Figure 1.11), developed by Hall and co-workers (Hall et al., 2005). For instance, urea-based monomers were employed stoichiometrically for the preparation of MIPs to extract penicillin (Urraca et al., 2006) and fluoroquinolones (Benito-Peña et al., 2008) directly from aqueous samples. More recently, these monomers were utilized in more elaborated imprinting protocols targeting peptides and protein fragments in biological samples as exemplified by Urraca et al., 2011 for discrimination of β -amyloid isoforms in blood serum or Helling et al., 2011 and Shinde et al., 2012 for the targeting of phosphorylated and sulfated peptides respectively (for more details on these examples refer to section II.1).

1.5.2. Hydrophilic monomers and cross-linkers

Another way to enhance the water compatibility of MIPs is by increasing their surface hydrophilicity. This can be achieved either by using hydrophilic functional and/or cross-linking monomers or by surface modifications (see section I.6.3). In the first case, hydrophilic monomers or co-monomers such as acrylamide (AAm) or hydroxyethyl methacrylate (HEMA) can be employed for the synthesis of hydrophilic MIPs, with specific recognition properties in aqueous environments. To improve surface hydrophilicity, HEMA is a very common option, used as monomer or co-monomer in both FRP (Ton et al., 2012; Gupta et al., 2015) and CRP (Niu et al., 2015) formats. Furthermore, hydrogel MIPs for drug delivery applications are often synthesized by co-polymerizing HEMA (Tieppo et al., 2012) or with AAm (Griffete et al., 2015). The aforementioned studies showcasing the use of hydrophilic monomers will be discussed in section II.

An issue often encountered when recognition takes place in aqueous conditions, is the important amount of non specific interactions, resulting in increased cross-reactivity of the MIP towards structurally relevant molecules. An example illustrating this problematic point is reported by Meng et al., 2005, who used AAm for the synthesis of MIPs targeting α -estradiol in acetonitrile. Although the resulting MIPs showed high affinity ($K_d=38 \mu\text{M}$) towards the template in water, low selectivity was observed for analogue molecules. To minimize the non specific interactions in water, careful optimization of the amount of hydrophilic monomer used for the polymerization is required.

Furthermore, choosing the right cross-linker can also enhance the water compatibility of MIPs. For example, pentaerythritol triacrylate (PETIA), an hydrophilic cross-linker, is often used to improve the hydrophilicity of the MIPS (Manesiotis et al., 2009; Ambrosini et al., 2012). Other examples of hydrophilic cross-linkers applied are polyethylene glycol (PEG) and derivatives (Pan et al., 2011; Henry et al., 2012). Hydrophilic MIPs can be also synthesized in the form of hydrogels using the water soluble bisacrylamide (BIS) as cross-linker (Zhang et al., 2015).

1.5.3. Post-Surface modifications

The grafting of hydrophilic polymer layers onto the MIP surface is a versatile approach for the preparation of hydrophilic MIPs, which can find a broad spectrum of applications such as SPE, proteomics and drug delivery (Zhang et al., 2014a). The introduction of hydrophilic functional groups can be performed either *via* FRP (Hoshina et al., 2009), CRP (Xu et al., 2010; Ma et al., 2013, Zhao et al., 2014), or chemical modification (Manesiotis et al., 2009). This technique enhances the surface hydrophilicity of MIPs and accounts for their unique recognition properties in complex aqueous samples such as waste waters, serum and milk. Some interesting examples of post surface modifications will be discussed more thoroughly in section II.

II. Applications of MIPs

In this section, we present some of the most interesting applications of MIPs, with focus on recognition in complex aqueous environments. The most recurrent approaches to improve water compatibility will be discussed, based on the strategies mentioned in section I.5, as well as new formats of MIPs with improved recognition properties, that should be applicable to a wide range of biotechnological areas.

II.1 Separation

As mentioned earlier in this chapter, one of the first successful applications of MIPs was in the field of affinity separation and more specifically for solid phase extraction (SPE). As early as 1994, Sellergren developed a MIP for the extraction of pentamidine, a drug used for the treatment of AIDS-related pneumonia, directly from urine samples (Sellergren, 1994). The MIP was synthesized using MAA and EGDMA as functional monomer and cross-linker respectively, using 2-propanol as porogen. Loaded on SPE columns the MIP sorbent could selectively enrich pentamidine from spiked urine samples diluted in ACN. The method was highly efficient and selective in this complex sample, rendering unnecessary further analytical procedures such as mass spectrometry.

Since then, several studies reported the use of MIPs for the extraction of organic compounds from aqueous complex samples. SPE is the ideal separation technique in which MIPs can outplay their advantages particularly well (so-called as molecularly imprinted solid phase extraction-MISPE). MIPs are an attractive alternative to immunosorbents because of their superior stability, robustness and ease of use. However, an important issue that should be addressed for a successful MISPE is their performance in aqueous environments. In most cases, MIPs are conventionally synthesized in aprotic organic solvents with low or intermediate polarity such as toluene, dichloromethane, chloroform and acetonitrile, as mentioned in section I. Hence, the molecular recognition between the template and functional monomer is mostly based on hydrogen bonds which are strongly favored in apolar and aprotic media (Pichon, 2007; Tse Sum Bui and Haupt, 2010). Thus, the direct application of such MIP-based extraction systems in aqueous conditions still remains a challenge, since their molecular recognition properties can be compromised in aqueous media and all the more in complex matrices. The water compatibility of MIPs is of utmost importance for SPE applications, since most target analytes are present in aqueous media such as biological fluids and environmental samples.

Hence, many approaches were developed during these past few years to improve MIPs efficiency in complex aqueous samples (refer also to section I.6). Due to their high selectivity, MIPs have been extensively used for the extraction of compounds from a large variety of matrices including food, biofluids,

environmental samples and plants. Advantageously, their application as selective treatment sample materials allows not only the successful clean-up of target analytes, but also the elimination of matrix components in complex aqueous samples (Tse Sum Bui and Haupt, 2010; Turiel and Martin-Esteban, 2010). A summary of MIPs applied as selective sorbents in complex samples and the strategies followed to render them more water compatible are illustrated in Table 1.1. It is important to note that several MIPs are already commercially available, for the clean-up and trace analysis of various analytes of interest such as the drug clenbuterol from calf urine, available from *Biotage*. In addition, *Polyintell* has developed sample preparation methods in complex samples for a broad range of target molecules such as mycotoxins (patulin, zearalenone, ochratoxin A, fumonisins), drugs (amphetamines), endocrine disrupting compounds on food matrices (cereals, milk, coffee, wine etc.) such as bisphenol A, estrogens (estradiol).

Table 1.1. A summary of MIP-based SPE applied in complex samples.

Target analytes	Matrices	Strategies	References
Riboflavin	Beverages	Chemically modified MIPs bearing hydrophilic functional groups	Manesiotis et al., 2009
Nitroaromatics	Soil samples	Sol gel imprinting	Lordel et al., 2010
β-amyloid isoforms	Blood serum	Highly selective MIPs based on urea stoichiometric monomer	Urraca et al., 2011
Fructosamine	Soy samples	<i>In situ</i> templating in pure water	Henry et al., 2012
Endosulfan	River waters	Core-shell MIP-coated silica fibers	Shaikh et al., 2014
Gastrodin	Plant extracts	Water soluble monomer	Ji et al., 2015
Cannabinoids	Oral and urine fluids	Water-compatible imprinted pills	Cela-Pérez et al., 2016
Chrologenic acid	Fruit juice	Hydrophilic magnetic MIPs based on a hydrophilic imine monomer	Hao et al., 2016

In the following section, some interesting examples showing the efforts toward a successfully water compatible MIP, will be discussed. This part does not pretend to perform an exhaustive description of all MIP-based separation applications reported in the literature, since several review papers exist which cover thoroughly this subject (Pichon, 2007; Hu et al., 2013, Martin-Esteban, 2016). Instead, emphasis is given on a few selective cases which demonstrate efficient approaches to overcome the water compatibility issue

and lead to improved protocols for the treatment of complex samples. In this respect, very recent advances on sample preparation and high performance in real complex environments will be also illustrated.

II.1.1. Towards a water compatible MIP sorbent

i) Imprinting in protic solvents

As already mentioned, MIPs are conventionally synthesized in apolar and aprotic solvents. However, the direct application of these MIPs for selective recognition in aqueous environments is problematic and requires extensive optimization. In some cases, screening of different solvent systems could be effective and SPE can be performed directly in complex aqueous samples (Chapuis, 2006; Sun et al., 2008a). Nevertheless, it is a general consensus that the presence of water or protic solvents can disrupt the formation of selective interactions between the analyte and the MIP sorbent. Moreover, the presence of matrix components at high concentrations can be detrimental to the analyte-specific interactions leading to a substantial decrease in extraction recoveries (Maier et al., 2004). Often, a drying step is necessary after the loading of the aqueous sample for the improvement of the binding selectivity of the MIP, however residual water may still affect the selective retention of the analyte during the subsequent clean-up step (Berezki et al., 2001; Pap et al., 2002).

Although most of the MIPs are traditionally synthesized in organic solvents, there is a growing interest towards the direct synthesis of MIPs in polar and protic solvents which would facilitate complex sample treatment. Imprinting in mixtures of alcohols and water or in buffered media can be performed for solubility reasons or to enhance interactions which are favored in polar environments. In this case, the driving forces allowing complex formation between the template and the monomers are based on hydrophobic, ionic and π - π stacking interactions (O' Mahony et al., 2006). This protocol of synthesis was first adopted by Haupt et al., 1998, who demonstrated the feasibility of the imprinting of the herbicide 2,4-D with 4-VP as functional monomer in the presence of polar protic solvents, based on a combination of hydrophobic effect and ionic interactions. One of the first SPE applications based on this principle was reported by Caro and co-workers for the extraction of naphthalene sulphonates (Figure 1.12A) from river water (Caro et al., 2004). This water compatible MIP, prepared with 4-VP as functional monomer and EGDMA as cross-linker was able to extract selectively the naphthalene sulfonates from river waters, amongst a multitude of other polar compounds, such as phenols and other pesticides (Figure 1.12B).

Another polymerization protocol where methanol/water was employed as the progen system was developed by Sun and co-workers. They prepared a water compatible MIP using MAA as functional monomer for the determination of nine quinolones in urine, achieving a LOD of 0.036-0.10 $\mu\text{g/mL}$ (Sun et al., 2008b). In the same context, we recently reported the synthesis of water compatible MIP sorbent prepared also in methanol/water, for the selective clean-up of betanin from beetroots (Nestora et al., 2016b).

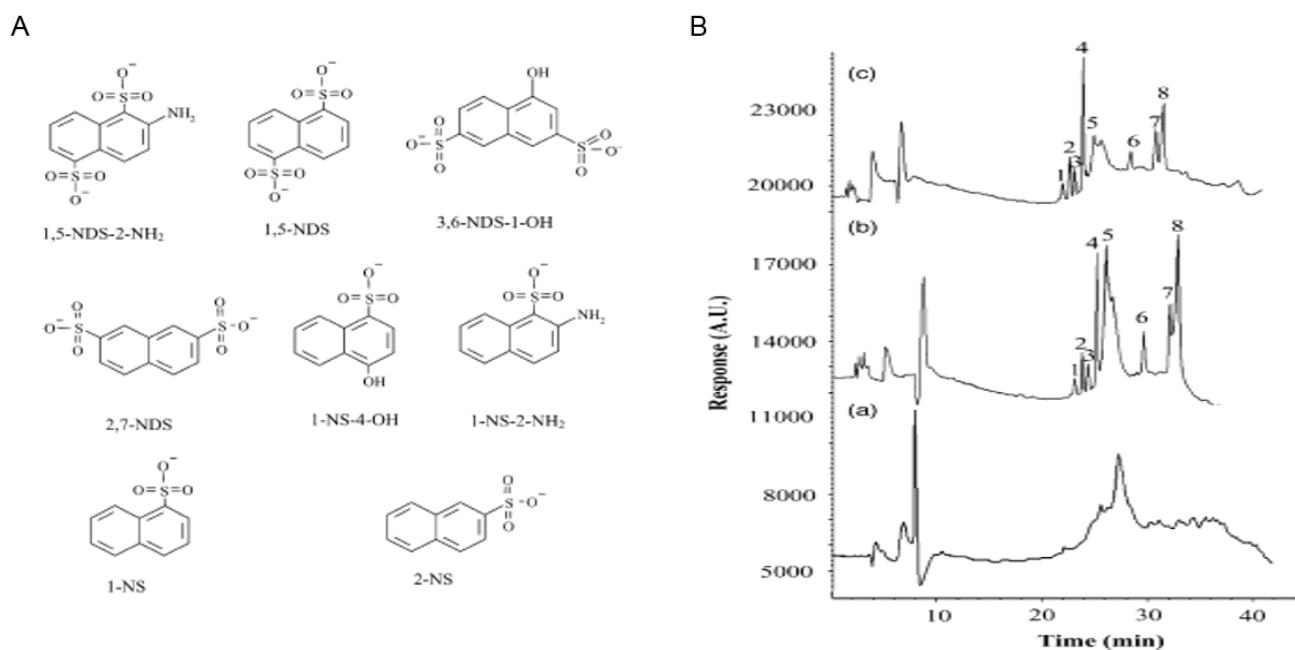


Figure 1.12. A) Chemical structures of the naphthalene sulfonates (NSs) used to probe the selectivity of the MIP; B) Chromatogram obtained by MISPE of 500 mL river water (pH 2.3). (a) Blank of river water, (b) river water spiked at 10 μg/L with each NS compound, and (c) River water spiked at 10 μg/L with each NS compound and a washing step using 20 ml of MeOH. Peak designation: (1) 1,5-NDS-2-NH₂, (2) 1,5-NDS, (3) 3,6-NDS-1-OH, (4) 2,7-NDS, (5) 1-NS-4-OH, (6) 1-NS-2-NH₂, (7) 1-NS, (8) 2-NS. Reproduced from Caro et al., 2004.

ii) Choosing the right monomers

-Stoichiometric monomers

Importantly, one approach solving the problem of water compatibility is the stoichiometric imprinting (refer also to section I.5.1). Interactions involving high affinity constants ($K_a > 10^3 \text{ M}^{-1}$) can lead to an enhanced stability of the monomer-template complex allowing effective binding even in water rich media (Wulff and Knorr, 2002). An example of stoichiometric monomer application was demonstrated by Moreno-Bondi and co-workers, where a urea-based MIP was utilized for the preconcentration of fluoroquinolones in environmental water samples (Benito-Peña et al., 2008). The optimized MISPE/HPLC with fluorescence detection method allows the class extraction of the antibiotics (enrofloxacin, danofloxacin, oxolinic acid and flumequine) from the aqueous samples using a selective washing with ACN/HEPES buffer, pH 7.5 (10/90, v/v) and elution with 2% trifluoroacetic acid in methanol. The pH of HEPES buffer was selected to ensure deprotonation of the carboxylic acid groups of the analytes, which promotes the formation of quadruple hydrogen bonds between the urea groups and the template carboxylate group. The effect of the mobile phase composition was evaluated, showing that the increase of the buffer percentage favors the ionic interactions between the polymer and the antibiotic, as shown in Figure 1.13B.

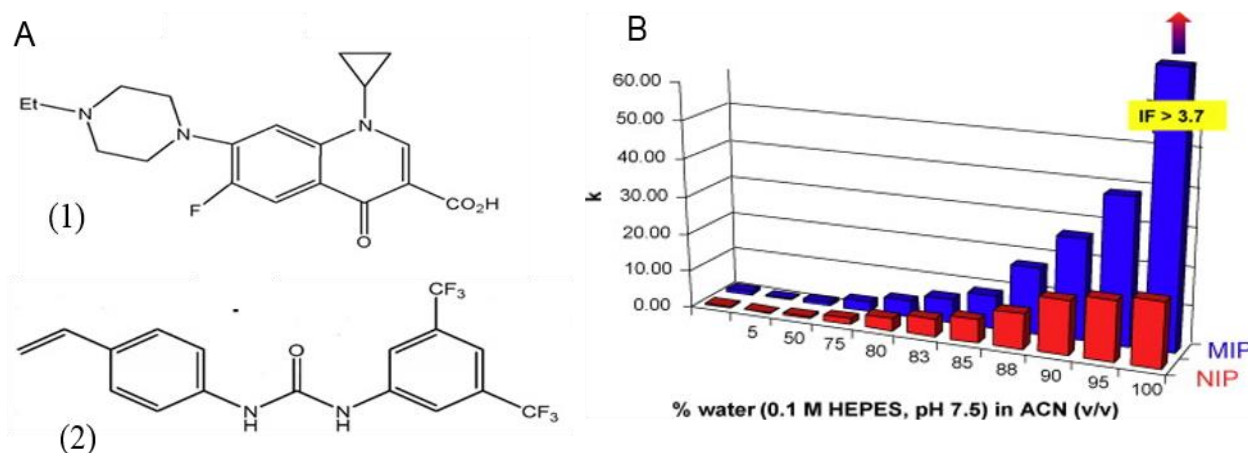


Figure 1.13. A) Chemical structures of the template enrofloxacin (1) and 1-(4-vinylphenyl)-3-(3,5-bis(trifluoromethyl)phenyl) urea functional monomer (2); B) Retention behaviour of ENRO on the MIP and the NIP for different mobile phase compositions. The retention factor (k) for each analyte was calculated as $k = (t - t_0)/t_0$, where t and t_0 are the retention times of the analyte and the void marker (methanol), respectively. Sample volume, 20 μ L; analyte concentration, 3mM (ENRO in ACN/0.1 M HEPES, pH 7.5 (10:90, v/v)); flow rate, 1 mL/mL; $\lambda = 270$ nm. Reproduced from Benito-Peña et al., 2008.

- Hydrophilic functional monomers or co-monomers and cross-linkers

The improvement of the water compatibility of MIPs can also be performed by adding a hydrophilic monomer to the polymerization mixture e.g. HEMA, PETIA etc, as mentioned in section I.6.2. This was ideally exemplified on an on-line format by Cobb et al., 2007, who prepared partially hydrophobic MIPs containing HEMA as a co-monomer for selective solid-phase extraction of local anesthetics including bupivacaine and ropivacaine from human plasma. Two MIPs were synthesized using the apolar organic solvents toluene and 1,1,1-trichloroethane. In order to obtain binding in aqueous media, the existence of strong hydrophobic interactions are essential, which is often correlated with an important amount of non-specific binding. In such systems, selectivity and specificity can be enhanced using additives, such as ethanol and surfactants, or by switching solvent systems (Haupt et al.; 1998; Karlsson et al., 2001). Interestingly, the incorporation of the hydrophilic monomer improved the water compatibility of the MIPs and at the same time promoted the selective imprint-template interactions. In this respect, the synthesized MIPs required less additives when performing direct SPE of buffered plasma samples with selective extraction achieved without the use of a solvent switch step using organic solvents. This method allows high recovery, efficient extraction of the analytes and very clean extracts in less than 15 min (Figure 1.14). Another example illustrating the use of HEMA for imparting water compatibility, is reported by Dzygiel et al., 2007, for the extraction of sildenafil (drug used as active principle in *Viagra*) from plasma samples.

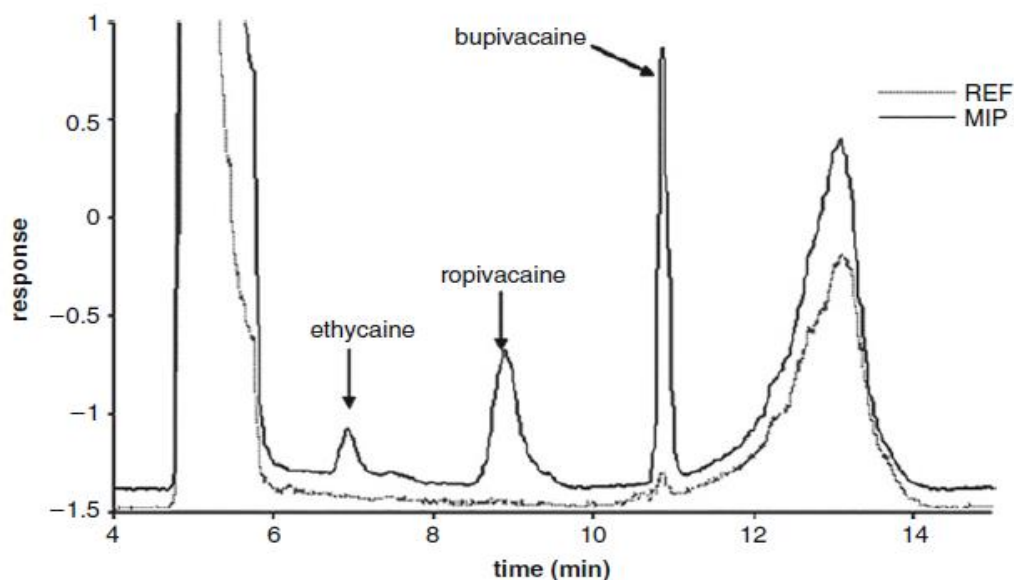


Figure 1.14. Chromatograms of the on-line extraction of a human plasma sample spiked with bupivacaine and ropivacaine at 75 mmol and ethycaine at 40 mmol on MIP and the reference polymer REF both prepared using 1,1,1-trichloroethane as the porogen, using the extraction method without using a solvent switch wash step. Reproduced from Cobb et al., 2007.

iii) Rational design of MIPs

An alternative approach for the identification of the right monomers suitable for water compatible MIPs is reported by Muhammad et al., 2012b. They have used molecular modeling for the rational design of MIPs targeting the drug amiodarone (AD). A virtual library containing 24 of the most commonly used monomers in molecular imprinting was created and was screened for possible interaction with AD, using the LEAPFROGTM algorithm (Figure 1.15A). In parallel and for comparison, a non-imprinted polymer library consisting of cross-linked co-polymers was synthesized in DMF from 18 monomers commonly used in molecular imprinting. The NIP library in the form of SPE cartridges was tested for adsorption of 1.0 g/L AD in two solvents, water–ethanol (1/1, v/v) and chloroform. The verification of polymer binding properties in an organic apolar solvent and in aqueous environment is performed so as to assess the relative contribution in the molecular recognition of specific (ionic interactions, hydrogen bonds) in chloroform, and non-specific interactions (hydrophobic interactions) in water (Figure 1.15B). The affinity and specificity in both solvent systems was evaluated and it was demonstrated that 4-VP, ethylene glycol methacrylate phosphate and AAm could be good candidates for the preparation of a MIP against AD. These results obtained from the NIP library were in good agreement with those obtained by the computational approach. Thus, 4-VP was selected as the best monomer for developing a MIP for AD. The MIP sorbent, prepared by bulk polymerization in chloroform, was employed for the SPE of AD in phosphate buffer as well as in spiked human serum. High recoveries ($82 \pm 6\%$) were obtained in spiked serum (pretreated with ACN for protein precipitation), while low cross-reactivity towards structural analogues of AD was

observed. Importantly, the MIP could selectively recognize and enrich AD amongst the multitude of interferents present in human serum, as deduced from the Figures I.16b and I.16c. The specificity of the MIP in aqueous environments was attributed to the π - π stacking interactions due to aromatic nature of the template and monomer, as reported elsewhere (Haupt et al., 1998).

Monomer	Binding energy (kcal mol ⁻¹)	Monomer used																
		Binding recovery%		Binding ratio														
		H ₂ O-EtOH	CHCl ₃															
Acrylamide	-25.91	Acrylamido-2-methyl-1-propanesulfonic acid (B3) ^a	92.71	81.06	0.87													
Ethyleneglycol methacrylate phosphate (EGMP) deprotonated	-20.68		4-Vinylpyridine (B5)	40.79	19.39	0.48												
Ethyleneglycol methacrylate phosphate (EGMP)	-20.59			Ethyleneglycol methacrylate phosphate (B17)	99.81	44.86	0.45											
Itaconic acid	-18.04				Acrylamide (B7)	38.20	16.53	0.43										
4-Vinylpyridine protonated	-17.94					1-Vinylimidazole (B1)	56.24	21.30	0.38									
Uracanic acid	-17.64						Lauryl methacrylate (B9)	50.87	15.57	0.31								
Uracanic acid ethyl ester	-17.20							Uracanic acid (B10)	62.55	19.11	0.31							
1-Vinylimidazole protonated	-17.01								Acrolein (B6)	49.44	14.78	0.30						
2-Vinylpyridine protonated	-16.82									Ethyleneglycol dimethacrylate (B11)	39.12	10.74	0.27					
Acrylamido-2-methyl-1-propanesulfonic acid deprotonated	-16.79										2-(Trifluoromethyl)acrylic acid (B16)	98.89	26.19	0.26				
Itaconic acid deprotonated	-16.03											Itaconic acid (B12)	90.98	23.66	0.26			
N,N'-Methylenebis(acrylamide)	-14.59												N,N-Diethylamino ethylmethacrylate (B18)	75.22	16.64	0.22		
2-(Trifluoromethyl)acrylic acid deprotonated	-13.49													2-Vinylpyridine (B2)	39.12	7.76	0.20	
Ethyleneglycol dimethacrylate (EGDMA)	-11.02														Acrylic acid (B8)	78.49	13.55	0.17
Methacrylic acid deprotonated	-10.51															Bisacrylamide (B13)	25.22	4.05
2-Hydroxyethyl methacrylate	-10.15	Styrene (B15)															42.15	5.85
1-Vinylimidazole	-9.19		2-Hydroxyethyl methacrylate (B4)														29.67	2.08
p-Divinylbenzene	-9.00			Methacrylic acid (B14)													47.71	0.39
N,N-Diethylamino ethylmethacrylate (DEAEM)	-8.61																	
Styrene	-7.63																	
m-Divinylbenzene	-7.60																	

^a B3: Symbol character and serial number of each copolymer in the library.

Figure 1.15. A) Binding energies, estimated using the LEAPFROG algorithm, of AD with the monomers contained in the virtual library; B) Binding percentage and ratio of AD in solvents of H₂O-EtOH (1:1) and CHCl₃ on polymers in the NIP library. Reproduced from Muhammad et al., 2012.

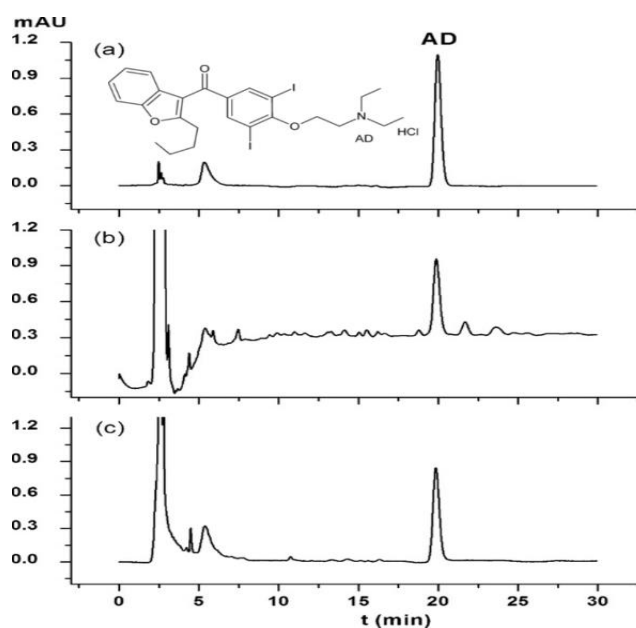


Figure 1.16. (a) Chromatogram corresponding to the direct injection of an aqueous standard solution of AD (1.0 mg/L); Chromatogram obtained (b) after protein precipitation of human serum spiked with AD; (c) after MIP extraction of human serum spiked with AD. Inset: Chemical structure of AD. Reproduced from Muhammad et al., 2012.

iv) **Sol-gel imprinting**

A more generic method, where the imprinting effect *de facto* takes place in aqueous conditions is the sol-gel process. In the latter, hydrophobic and electrostatic interactions are predominant, as illustrated in section I.2.3. Sol-gel based MISPE was exemplified by Pichon's group, who has synthesized a MIP *via* the sol gel process for the simultaneous selective extraction of nitroaromatics from aqueous samples (Lordel et al., 2010). The sol-gel MIP was prepared with phenyltrimethoxysilane (PTMS) as monomer, TEOS as cross-linker and 2,4-dinitrotoluene (2,4-DNT) as template in basic aqueous media. The authors reported the first application of sol-gel MIPs for the selective retention of four nitroaromatic compounds, with high selectivity and specificity. It is important to note that careful optimization is required in order to control the particles size of a sol-gel MIP as well as to have reproducible results. A recent example showcasing this method for the treatment of food samples will be discussed in the next section.

II.1.2. Recent advances in real sample treatment

The use of compound-specific and class-specific sorbents may be essential to address the problems related to the isolation of highly polar species or macromolecules from aqueous samples and for complex samples containing large amounts of interfering species. Thus, there is considerable interest in novel selective SPE materials that could be successfully applied to wider range of matrixes and analytes (Augusto et al., 2013). In the following section, very recent examples of MIPs applied for the extraction of analytes from environmental, food and biological samples will be discussed, focusing on novel formats that facilitate miniaturization and deal efficiently with the treatment of complex samples.

i) Agrifood applications

The development of fast, cost-effective and selective pre-treatment methods in the agrifood area is necessary to meet the requirements of industrial scale applications related with food safety and nutrition. Sample treatment protocols entail the extraction of bioactive compounds from their natural sources, or the purification of food constituents as well contaminants from complex food matrices. Extensive research has been done towards the design of MIP sorbents with selective recognition properties in foodstuffs,

The direct extraction from food samples suffer from the matrix effect, which compromises the MIP selectivity and reduces the extraction recoveries (Maier et al., 2004). To circumvent the problem of matrix effect, careful optimization of the MIP synthesis is required, aiming to enhance affinity in water and consequently in complex samples. Towards this direction, two remarkable examples of organic MIPs synthesized directly in pure water have been reported for the sample pretreatment in food. These MIPs could be applied directly in complex samples featuring high recoveries and selectivities. The first one makes use of covalent imprinting while in the second the self-assembly approach is employed.

In the first study, Henry et al., 2012 focused on the selective extraction of two flavoring agents, fructozamine (FZ) and 2, 5-deoxyfructosamine (DFZ). A water compatible MIP was prepared *via* covalent imprinting with 2 boronate esters as functional monomers and a hydrophilic cross-linker, polyethylene glycol diacrylate. The templates FZ and DFZ were formed *in situ* from the condensation of vinylphenyl boronic acid with glucosamine. Conversely to most bulk MIP preparation protocols where the presence of water can be detrimental to the molecular recognition, herein water readily contributes to the successful imprinting process, since it provides stable ester bonds and high solubility of glucosamine (Figure 1.17). The authors report that this is the first time that a highly cross-linked and at the same time polar imprinted polymer for FX and DFZ is obtained as a solid material and not a hydrogel. To simulate the conditions as in a real food application, extraction was carried out in soy sauce, diluted in ammonium phosphate buffer. Two elution steps were performed allowing for the selective extraction of the two flavor agents from soy sauce; the majority (89%) of FZ(1) was extracted in the first elution step carried out in water, while DFZ (2) was recovered at 60% in the second fraction eluted with ethanol/ammonium phosphate buffer (80/20, v/v), as shown in Figure 1.18.

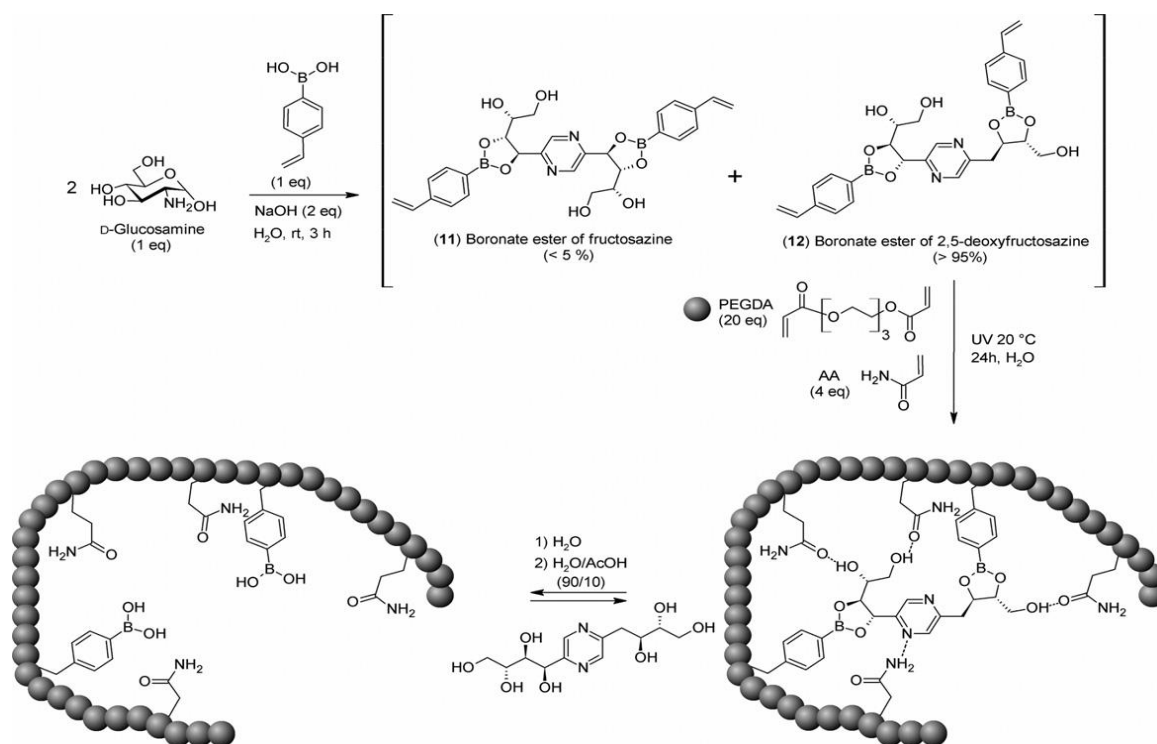


Figure 1.17. Schematic representation of the *in situ* imprinting strategy (Henry et al., 2012).

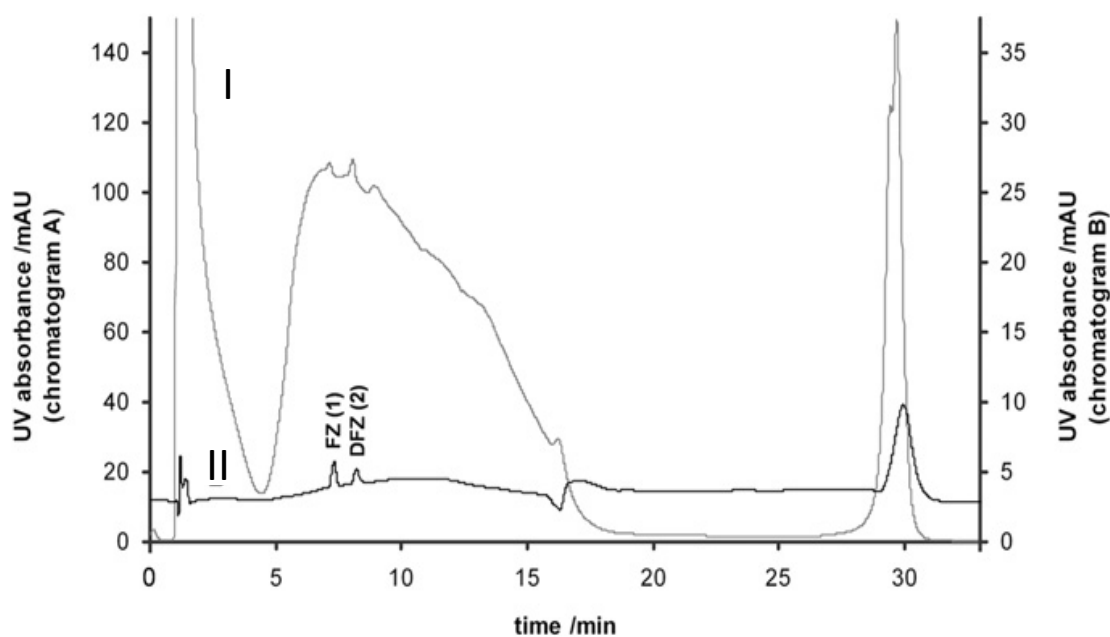


Figure 1.18. Chromatograms of soy sauce samples before (I) and after (II) MISPE. Peaks corresponding to FZ (1) and DFZ (2) are observed after MISPE. Reproduced from Henry et al., 2012.

The second example of a direct MIP synthesis in water is reported by Ji et al., 2015 who synthesized a water-soluble monomer to prepare MIPs for the extraction of gastrodin from aqueous plant extracts. Gastrodin (GAS) is one of the water-soluble bioactive constituent isolated from *Gastrodia elata Blume* and it is known for its anti-convulsing properties. Super hydrophilic MIPs were prepared by bulk free radical polymerization directly in water using the tailor-made water soluble monomer, alkenylglycoside glucose (AGG) as the functional monomer and MBAm as a cross-linker. Selective extraction of gastrodin was carried out in plant extracts, resulting in highly enriched purified samples, while most of the interferents present in the plant extracts were eliminated, as shown in Figure 1.19B. Moreover, the MIP has highly selective for GAS when applied for the extraction of structurally related interferents, namely 4-hydroxybenzaldehyde (PHBA), 4-hydroxybenzyl alcohol (PHA), 4-hydroxy-3-methoxybenzyl alcohol (PHMA), 4-hydroxy-3-methoxybenzaldehyde (PMA) and d-(+)-glucose.

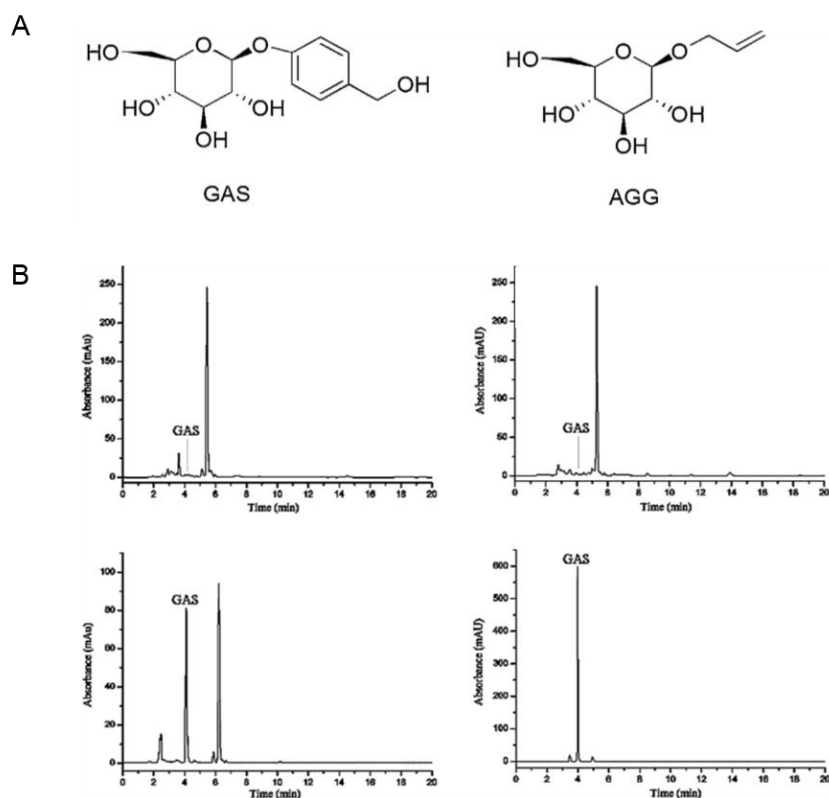


Figure 1.19. A) Chemical structures of the template gastrodin (GAS) and the hydrophilic functional monomer alkenylglycosides glucose (AGG); B) (a) Chromatogram of *G. elata* root extracts before percolating through SPE column; (b) Chromatogram of washing solutions from MISPE column; (c) Chromatogram of eluting solutions from NISPE column; (d) Chromatogram of eluting solutions from MISPE column. Reproduced from Jin et al., 2015.

Other examples report the use of tailor-made monomers that improve the hydrophilicity of MIPs sorbents. A recent study illustrates the design of hydrophilic magnetic MIP based on a dendritic monomer for selective extraction of chlorogenic acid (CGA) in fruit juices (Hao et al., 2016). CGA is a bioactive phenolic acid, possessing several biological properties, including antibacterial and cancer inhibitory effects amongst others. In this application, magnetic composite nanoparticles were employed for their good biocompatibility and low toxicity as well as for their easy handling related to their fast separation. The dendritic polycation polyethylene imine (PEI) (Figure 1.20, in green) was chosen as a functional monomer for three reasons: due to its interaction with the template through multiple hydrogen bonds and electrostatic interactions, the enhancement of the density of the imprinted cavities, and the improvement of the MIP hydrophilicity. The protocol of the synthetic procedure is presented in Figure 1.20 and includes the immobilization of the CGA onto $\text{Fe}_3\text{O}_4@\text{NH}_2$ through hydrogen bond and electrostatic interactions and the subsequent reaction with PEI which resulted in the formation of a thin and adherent imprinting shell. The obtained $\text{Fe}_3\text{O}_4@\text{CGA}$ -MIPs were used as SPE sorbents coupled with HPLC and were applied in the specific isolation and determination of CGA in fruit juices. For instance, treatment of apple juice with the

designed MIP resulted in total or partial elimination of interferences present in abundance in the sample matrix, while preconcentrating the CGA found originally in apple juice (amount quantified 0.92 $\mu\text{g/mL}$) (Figure 1.21). It is important to note that the unique dendritic structure of PEI, which provides multiple anchoring points for the formation of imprinted cavities, renders this water compatible monomer a very promising choice for the improvement of the binding capacity and hydrophilicity of MIPs.

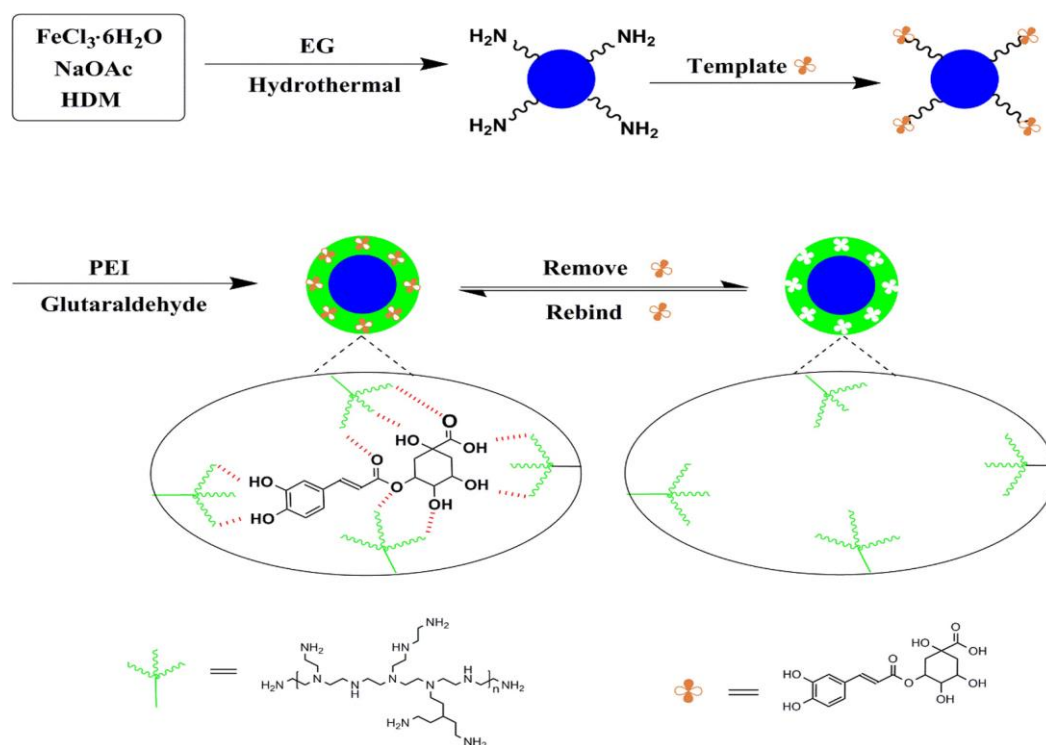


Figure 1.20. Schematic representation of the synthetic route for magnetic molecularly imprinted nanoparticles of chlorogenic acid based on polyethylene imine (Hao et al., 2016).

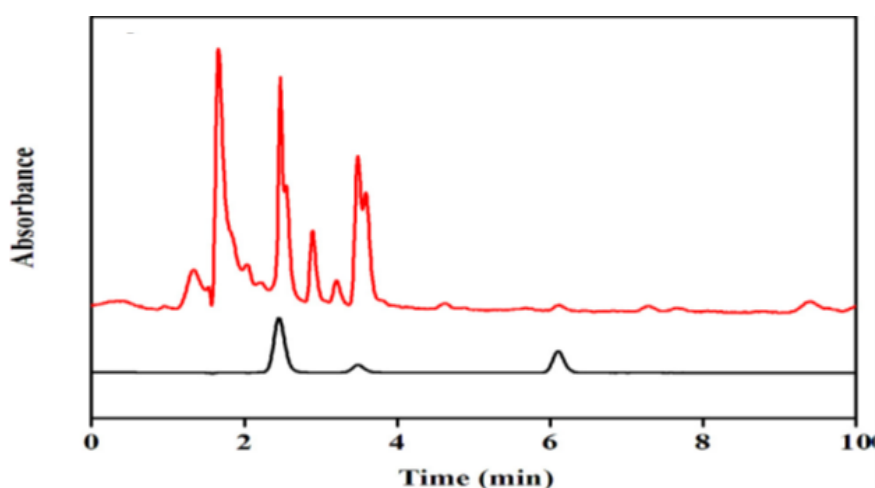


Figure 1.21. Chromatograms of apple juice (red line), and the eluted samples after treatment with the magnetic molecularly imprinted nanoparticles of chlorogenic acid (black line). Adapted from Hao et al., 2016.

As discussed in the previous section, surface post-modification approach is also adopted for the synthesis of highly specific water compatible MIPs for SPE applications in complex food samples. This was exemplified by Manesiotis et al., 2009, who prepared water compatible MIPs for the selective extraction of the vitamin riboflavin from beverages. Firstly, a MIP was prepared in chloroform using the hydrogen-bond donor–acceptor–donor functional monomer (2,6-bis(acrylamido)pyridine), complementary to the imide motif of the template and PETIA as a hydrophilic cross-linking monomer (Figure 1.22A). Unfortunately, high non specific binding was observed upon application of this MIP for the extraction of riboflavin from milk and an artificial vitamin mixture. In order to suppress non specific interactions, an alkaline post-treatment was applied, to hydrolyze unreacted acrylate groups, acting as anchoring points for non specific riboflavin binding. This chemical modification resulted in effectively inhibit the hydrophobically driven nonspecific binding based imprinted materials while simultaneously maintaining the integrity of the binding sites. The increase of imprinting factor was demonstrated on the example of riboflavin depletion from beer samples, as illustrated in Figure 1.22B.

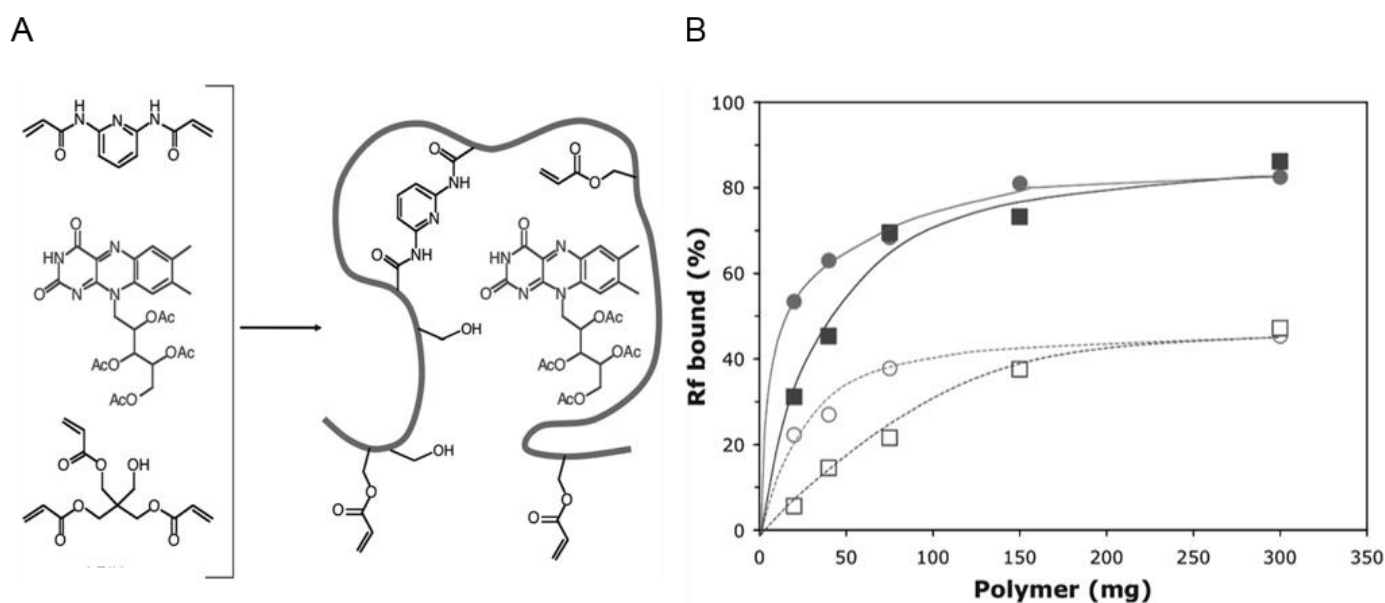


Figure 1.22. A) Imprinting procedure used to obtain a riboflavin complementary binding site; B) Percent riboflavin (Rf) depleted from a Stella Artois lager beer sample as a function of added imprinted (filled symbols) or nonimprinted (open symbols) polymer adsorbent with no treatment (circles) or subjected to the hydrolytic treatment (squares). Reproduced from Manesiotis et al., 2009.

ii) Proteomics and Diagnostics

Efficient sample preparation is of utmost importance for applications such as proteomics, where a selective enrichment in specific proteins or peptides is required (Helling et al., 2011). The ability to develop advanced SPE protocols that maximize the selectivity of MIPs is a key aspect for successful applications using real clinical samples. To that end, Sellergren and co-workers have very recently demonstrated the

feasibility of optimizing a MIP-based SPE for the selective enrichment of phosphoserine (pS) containing peptides (Jagadeesan et al., 2016) from complex biological samples. They have fabricated an Integrated Selective Enrichment Target (ISET) platform system interfaced with MALDI mass spectrometry, able to provide an efficient, economic and generic screening process for the screening of the ideal SPE conditions required for the effective treatment of complex samples. Figure 1.23 illustrates the different steps of the miniaturized SPE procedure, performed in a rapid and parallel fashion, with a processing time of only 2 hours per ISET with 96 samples. Under these conditions, different loading, washing and elution systems were evaluated in a cost and time-efficient way since a minute amount of solvent (for instance the MIP material corresponding to an SPE volume of 500–600 nL was added to each well prior analysis) is required for the screening of the experimental conditions.

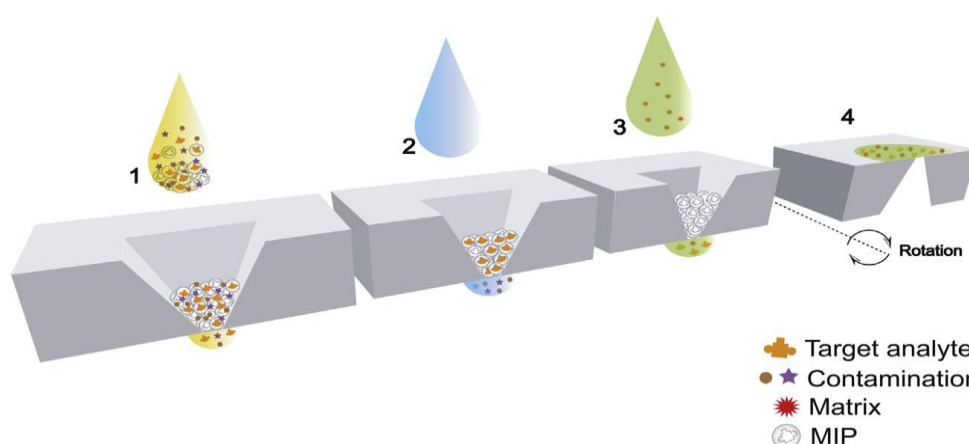


Figure 1.23. Steps involved in the solid phase extraction utilizing the ISET platform with the molecularly imprinted polymer (MIPs) sorbent. In the ISET SPE, sample preparation incubated with MIP material were transferred to ISET nanowells (1) followed by a wash step to remove undesired components (2). The captured analytes were then displaced by the elution step (3) and addition of MALDI matrix on the backside at low vacuum. Subsequently the ISET was turned over (4) and inserted into mass spectrometry for analysis. Reproduced from Jagadeesan et al., 2016.

From previous work, the authors have developed specific MIPs toward the phosphotyrosine (Helling et al., 2011) and sulfotyrosine group (Shinde et al., 2012), which allow for the affinity-based enrichment of tyrosine phosphorylated or sulfated peptides. These MIPs were synthesized using 1,3-disubstituted urea monomers specially designed for stoichiometric oxyanions targeting ($K_{a(\text{DMSO-}d_6)} 9 \times 10^3 \text{ M}^{-1}$) and were successfully employed on an SPE protocol for the selective fractionation of sulfopeptides and phosphopeptides in aqueous conditions (Figure 1.24). However, when challenged with a more complex sample a triply tyrosine-phosphorylated peptide was out-competing a singly phosphorylated, and some non-specific binding of serine and threonine, as well as unphosphorylated peptides was also observed.

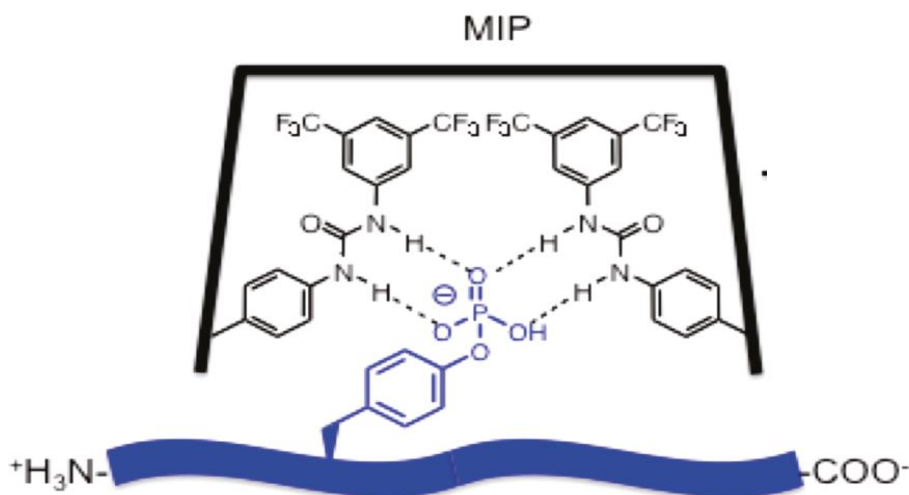


Figure 1.24. Proposed complex formation of the urea monomer with the phosphotyrosine bearing peptide in a 2:1 stoichiometric ratio. Adapted from Helling et al., 2011.

To circumvent this problem, Sellergren and co-workers employed the ISET platform to quickly screen and optimize the SPE conditions for a selective enrichment of peptides in complex biological samples. Amongst other applications, this protocol was tested using samples of high complexity containing different ratios of β -casein and BSA (1:10, 1:5, 1:1). The different samples of trypsin digested β -casein and BSA were incubated with the pS-MIP for 90 min in a loading buffer with 100 % ACN, 100 mM NaCl. The incubated sample-MIP mixture was then transferred to the ISET and subjected to a SPE protocol followed by elution and MALDI-MS analysis. As demonstrated by the MALDI TOF chromatographs (Figure 1.25) this optimized SPE protocol allowed for pS-MIP selective capture of one phosphopeptide (2062.5 m/z) even when the ratio of β -casein and BSA was 1:10. The authors postulated that this platform allows for a systematic study of the MIPs performance in terms of binding specificity and results in an improved protocol for the enrichment of the phosphopeptides in real clinical samples, which can find utility in mapping of post-translational modifications of proteins.

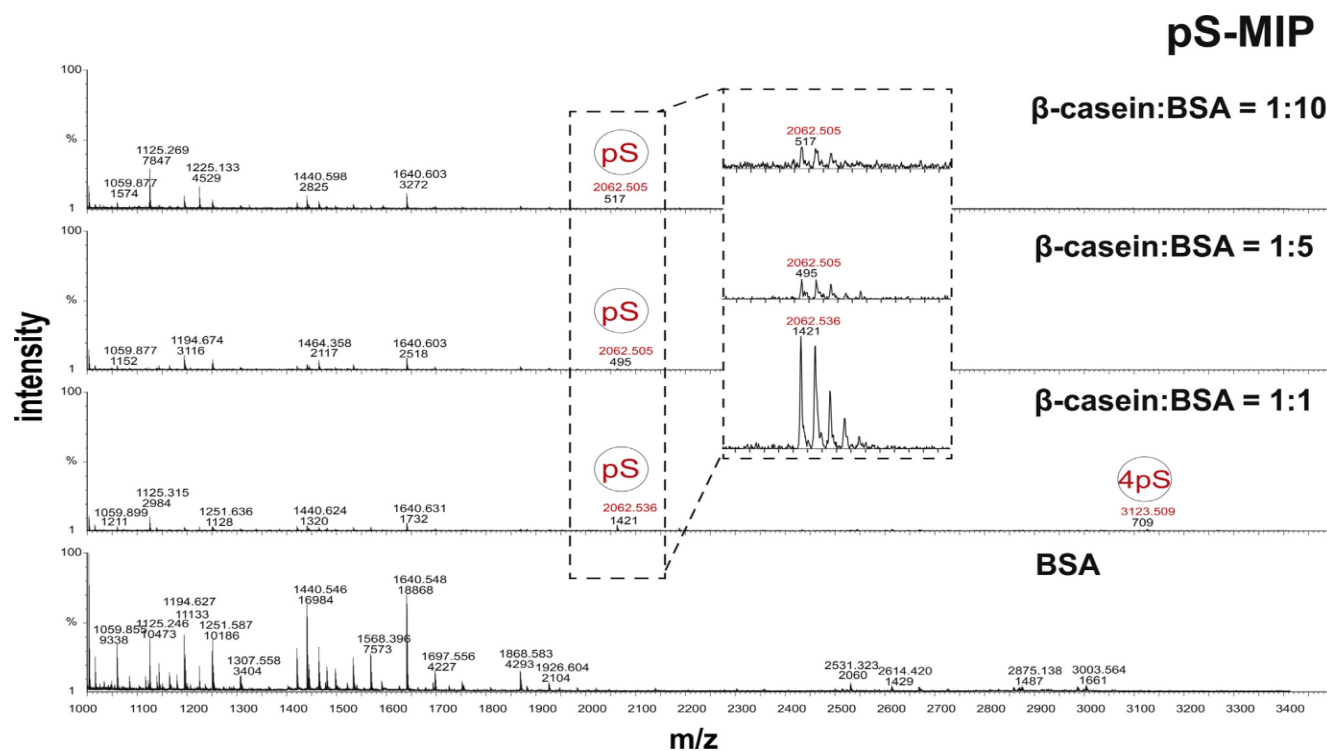


Figure 1.25. Chromatographs obtained by MALDI MS. Each row of the ISET is loaded with incubated sample/MIP mixture containing different ratios (1:1, 1:5, 1:10) of β -casein and BSA. The observed MALDI spectra of pS-MIP enriched β -casein spiked in BSA at different ratios (1:1, 1:5, 1:10). Reproduced from Jagadeesan et al., 2016.

In addition to proteomics, selective extraction of proteins or peptides is of great importance for the diagnostics and treatment of various diseases. This was exemplified by Urraca et al., 2011, who prepared highly selective MIPs capable of discriminating the two β -amyloid isoforms, $A\beta$ 1-40 and $A\beta$ 1-42, important biomarkers of Alzheimer's disease. To that end, a combinatorial library of stoichiometric urea-based MIPs was prepared in DMSO targeting both the C-terminus epitope and the full peptide sequence of each isoform. Two MIPs, namely MIP $A\beta$ 1-40 and MIP $A\beta$ 1-42 were synthesized using as templates the C-terminal epitopes of each isoform respectively, which correspond to the sequences $A\beta$ 33-40 and $A\beta$ 33-42. A solid-phase extraction method was developed for the treatment of denatured blood serum spiked with the C-terminus epitopes as well as the full-length β -amyloid peptides at concentrations relative to those found in patient samples. Higher recoveries were obtained on each MIP sorbent for their respective C-terminus epitopes compared to the NIP (Figure 1.26A). Furthermore, to assess whether the binding cavities formed by the epitope can be accessed by the full-length β -amyloid peptide, fortified serum samples with synthetic $A\beta$ 1-40 (5 ng/mL) and $A\beta$ 1-42 (1 ng/mL) were tested using the same SPE protocol. The corresponding elution fractions were analyzed for the presence of the peptides by SDS-PAGE immunoblot analysis (Figure 1.26C). Remarkably, the MIP $A\beta$ 1-42 could selectively enrich the amyloid isoform $A\beta$ 1-42 over $A\beta$ 1-40, conversely to the MIP $A\beta$ 1-40, which was less selective (Figure 1.26B). In conclusion,

these important results showed the unique potential of MIPs for enrichment and discrimination of both the C-terminal end and the full-length sequence of the β -amyloid isoforms $A\beta$ 1-40 $A\beta$ 1-42, and pave the way for applications in diagnostics of Alzheimer's disease.

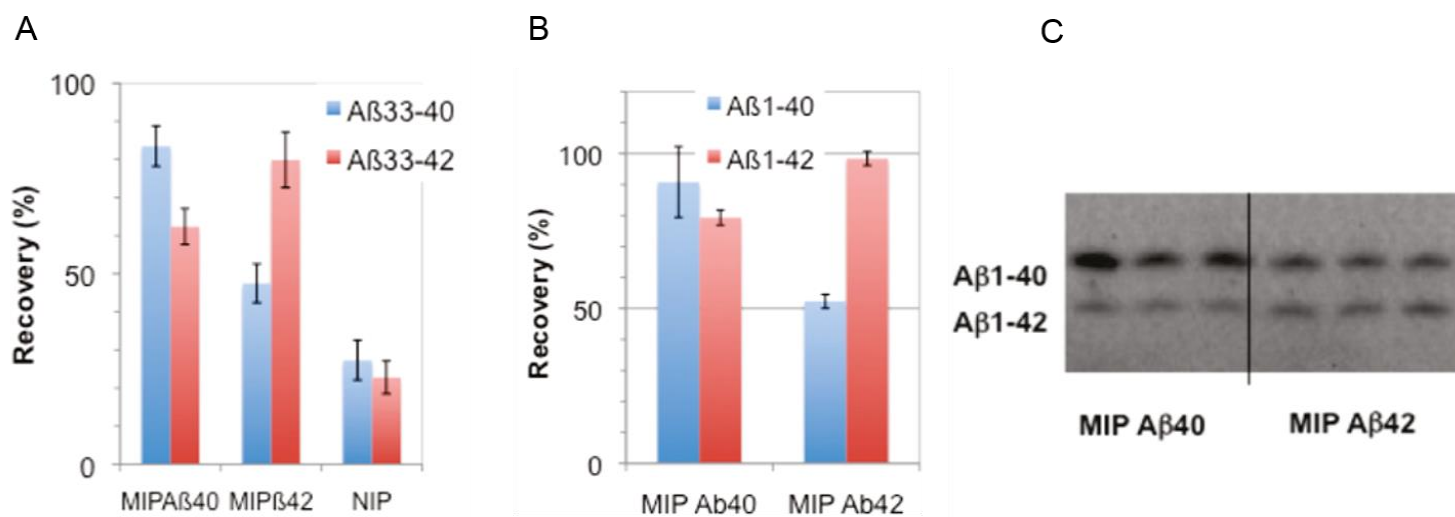


Figure 1.26. A) Recovery of the C-terminal epitopes of $A\beta$ in the elution fractions after SPE of peptide-spiked blood serum samples (2.5 $\mu\text{g}/\text{mL}$) on the two complementary MIPs and the NIP; B) Recoveries estimated from spot intensities of the SDS-PAGE/immunoblot analysis; C) Stained gel from urea-SDS-PAGE/immunoblot analysis of elution fractions from SPE of a blood serum sample spiked with $A\beta$ 1-40 (5 ng/mL) and $A\beta$ 1-42 (1 ng/mL). Reproduced from Urraca et al., 2011.

iii) Environmental analysis

The utility of MIP-based SPE protocols for environmental analysis is well documented in the literature. A very recent review summarized the extraction approaches utilized for treatment of complex environmental samples, such as wastewaters (Martin-Esteban, 2016). As an example, Denizli and co-workers reported the synthesis of core-shell MIP-coated silica fibers for the trace analysis of the pesticides endosulfan I and II in river water and wastewater samples (Shaikh et al., 2014). Endosulfan is an endocrine disruptor which is classified as a highly toxic chemical, requiring careful monitoring in environmental waters. To enhance the performance of the MIP in highly complex aqueous samples hybrid organic-inorganic MIPs based on silica was employed (for more details on sol-gel imprinting refer to section I.2.3). Briefly, Fe_3O_4 particles were functionalized with APTES and further modified with methacrylamide. Then, the imprinted polymers of $\text{Fe}_3\text{O}_4@SiO_2$ -methacrylamide composites and *N,N'*-methylene-bis-acrylamide (MBam) were prepared by means of water in oil suspension polymerization, as illustrated in Figure 1.27. The synthesized MIP was implemented on a solid phase microextraction system (SPME) and the efficiency of the MIP-coated silica fiber was investigated in a synthetic waste water sample and compared to a polydimethylsiloxane (PDMS) fiber. Figure 1.28 shows that the absorption performance in this medium

was not compromised due to the presence of interferents proving the presence of high fidelity binding sites. In fact, the intensity of endosulfan I and II is 4 times more important compared to the non specific PDMS fiber. Importantly, the MISPE optimized method allowed the selective extraction of endosulfan I and II from river waters with a limit of detection of 2 ng/L and 3 ng/L respectively, far below the limit imposed for pesticides by European Union (1 $\mu\text{g/L}$ in surface water and 0.1 $\mu\text{g/mL}$ in drinking water). It is important to note that in this work, problems related to the adaptation of MIPs for SPME were resolved such as low capacity, slow kinetics of adsorption, uncontrolled shape and fragility of the MIP shell.

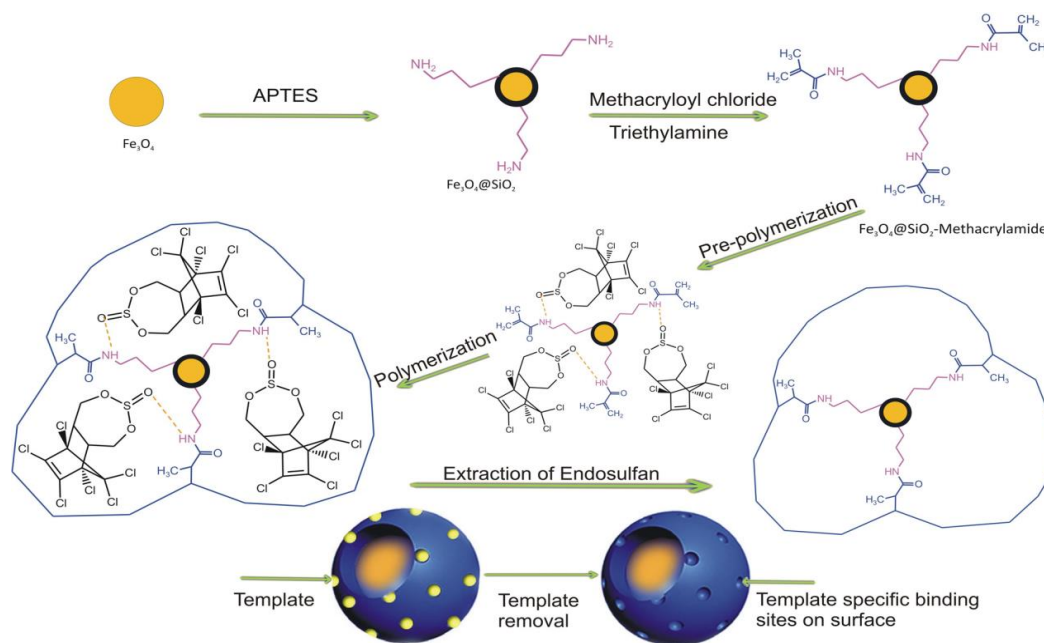


Figure 1.27. Schematic representation of imprinting of endosulfan in poly(methacrylamide functionalized magnetic composites). Reproduced from Shaikh et al., 2014.

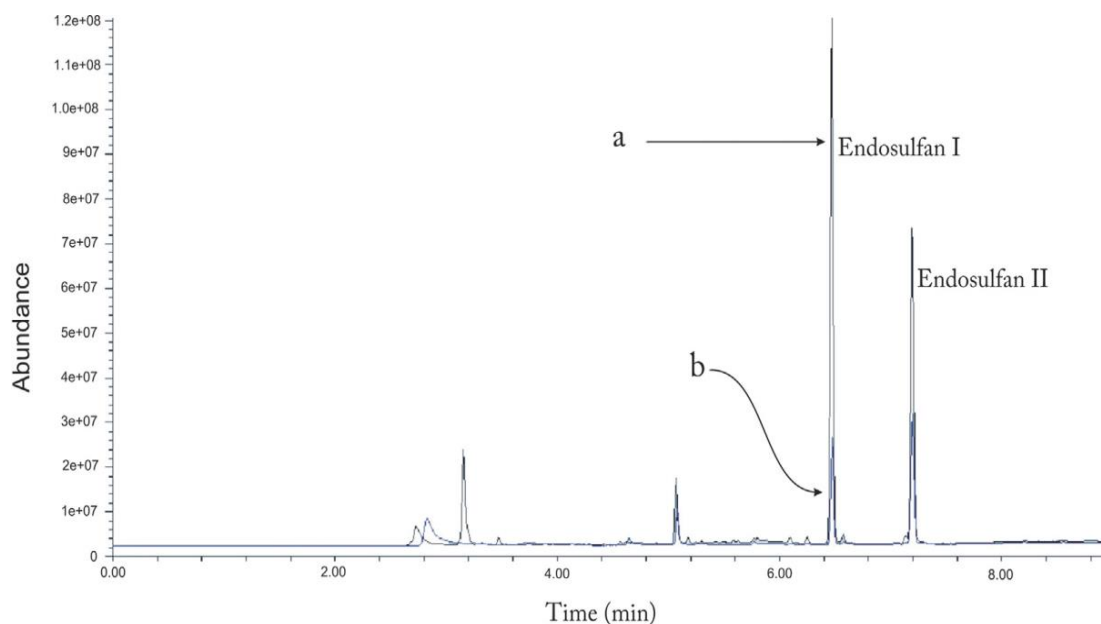


Figure 1.28. Chromatogram of synthetic wastewater spiked with 0.3 $\mu\text{g/L}$ of endosulfan I and II (a) obtained by MISPE fiber (b) obtained by PDMS fiber. Reproduced from Shaikh et al., 2014.

II.2 Biomimetic assays

In their traditional format, immunoassays feature the use of antibodies to form an antibody-antigen complex which can generate a measurable signal that allows the quantification of the targeted antigen. MIPs, as selective recognition materials can mimic the action of antibodies in immunoassays, with similar affinities and selectivities (Ye and Haupt, 2004). Moreover, they are more stable, robust and less expensive compared to their natural counterparts. The use of MIPs can be an attractive alternative in immunodiagnosics for the direct analysis in complex samples (Moreno-Bondi et al., 2012). Assays based on MIPs have received the name of Molecular Imprinting Sorbent Assays (MIAs) or MIP immuno-like assays (MIP-ILAs).

MIP-ILAs are developed using a wide range of techniques such as radioactivity, fluorescence, optical density as detection method. The selection of labeling agent (radioactive tracers, luminescent labels, or enzymes) will also affect sensitivity and, sometimes, selectivity (Piletsky et al., 2001). High sensitivity can be obtained by employing radioligand immunoassays, usually performed in a competitive format between the non-labeled target analyte and a radioisotope-labeled tracer (Figure 1.29). On the other hand, optical methods can prove to be very advantageous since they can be combined with the sensing of target analytes in real situations. For instance, MIP-based fluorescence binding assays are widely adopted because they offer numerous advantages such as the stability and freedom from hazards of fluorescent labels compared to radioactive tracers, the moderate cost of analysis, the wide availability of the equipment needed, and the potential high sensitivity. In general, the sensitivity of fluorescence measurements is 10- to 1000-fold higher than the absorption counterparts (Moreno-Bondi et al., 2012).

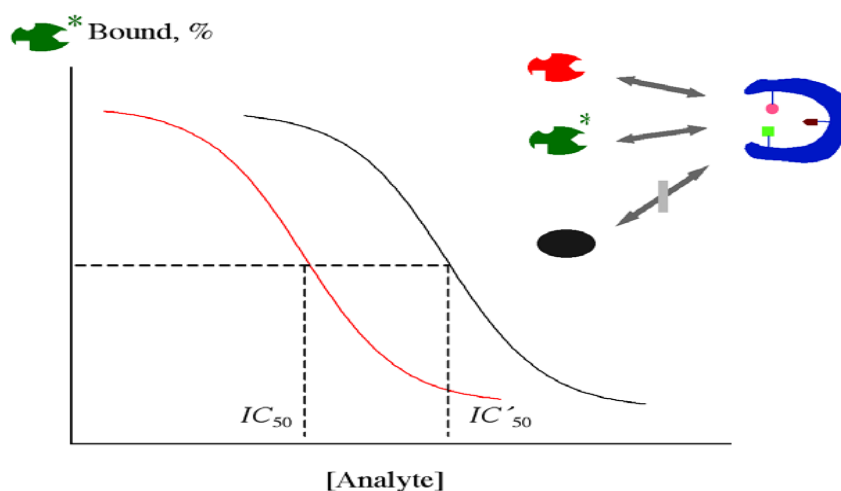


Figure 1.29. Principle of a MIP-based radioimmunoassay. The non-labeled template (in red) inhibits binding of the radioisotope-labeled template (in green, marked with *) to a limited number of sites on the MIP, whereas a compound with a slightly different structure (in black) has much less effect. Reproduced from Ye and Haupt, 2004.

The first example of a MIP-ILA was reported in the pioneering work of Vlatakis et al., 1993. They developed for the first time a MIP-based competitive radioligand immunoassay for the determination of the drugs theophylline and diazepam in blood serum. The MIP was prepared in chloroform using MAA as functional monomer and EGDMA as cross-linker. Competitive radiolabeled immunoassay showed that the MIP could recognize theophylline with high affinity ($K_d = 65 \mu\text{M}$) and selectivity (<1% cross-reactivity), comparable to those obtained by the standard ELISA immunoassay. A milestone study featuring the use of MIP as immunosorbent for the detection of the herbicide 2,4-D in phosphate buffer was developed by Haupt et al., 1998. To achieve recognition in aqueous environment, imprinting was performed in MeOH/H₂O, using 4-VP and EGDMA as functional and cross-linking monomers, respectively. Ionic and hydrophobic interactions contributed to high and specific binding in phosphate buffer, as demonstrated by equilibrium radioligand assays (Figure 1.30).

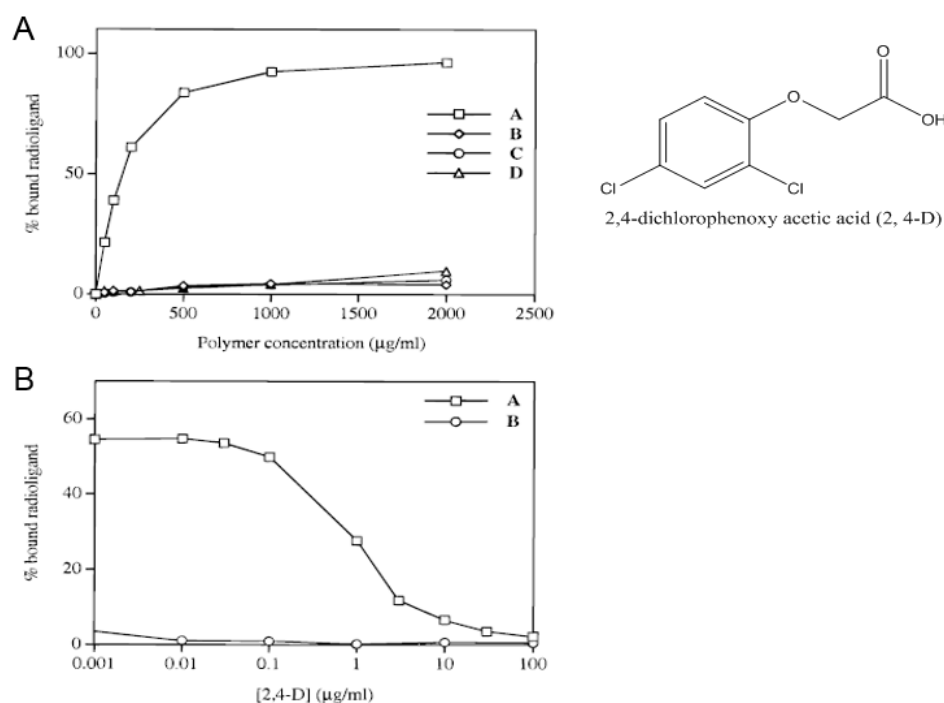


Figure 1.30. A) Binding of radioligand relative to polymer concentration for the polymers A-D; B) Radioligand displacement curves with unlabeled 2,4-D as competitor for the polymers A and B, at 150 µg polymer/1 mL assay. Conditions: 20 mM sodium phosphate buffer pH 7; 0.1% Triton X-100. The polymers are prepared as follows: A: the imprinted polymer, B: the non-imprinted polymer, C: control polymer containing toluene and acetic acid and D: control polymer containing phenoxyethanol instead of the 2,4-D. Reproduced from Haupt et al., 1998.

The aforementioned pioneering studies open new possibilities for the implementation of MIPs in binding assays for recognition of a wide range of analytes. Herein, some recent examples of MIP-ILAs will be illustrated, with emphasis on MIP ILAs as diagnostic tools and on direct real-time methods for recognition in complex aqueous matrices. Various strategies were employed to impart water compatibility and achieve better performance in complex samples (refer also to section I.5).

II.2.1. MIP based immunoassays as diagnostic tools

Complex biological matrices constitute recurrent samples for immunoassays carried out for real-life applications, such as in diagnostics and biomedicine. One important problem that should be overcome for the efficient recognition in such media is the sensitivity, which can be compromised by the presence of matrix material and the aggregation of proteins. Thus, there is a need to develop novel imprinting methods, to render MIPs immunosorbents highly performant for the recognition of biomarkers and target proteins in complex biological samples.

The enzyme-linked immunoassay (ELISA) is one of the most common diagnostic test, which is carried out mainly in clinical and forensic laboratories for the analysis of proteins, hormones and microorganisms in complex biological samples. In its direct format, either the antibody or the antigen is immobilized on microplate wells and the direct binding of antigen or antibody produces the analytical signal. In the indirect format, the antigen is immobilized on the microplate wells, followed by the binding of the antibody, which is subsequently bound by an anti-species antibody labeled with an enzyme to produce the analytical signal. In the competitive format, the antibody is immobilized on the microplate wells and competition for the binding to the antibody is between the free analyte and the analyte conjugated with an enzyme, which gives the analytical signal. In the sandwich format, an antibody (capture) is immobilized on the microplate wells and after the binding of the antigen, a detection antibody, often labeled with an enzyme and capable to bind a different epitope of the antigen, is used to get the analytical signal (Caceres et al., 2016).

An interesting example of an ELISA immunoassay that addresses the issue of sensitivity of MIP immunoassays in biological samples, has been described by Piletsky and co-workers for the recognition of vancomycin in blood plasma, an antibiotic used for the treatment of various serious gram-positive infections (Chianella et al., 2013). A pseudo-ELISA immunoassay was developed using vancomycin-imprinted nanoparticles, synthesized based on an automated solid-phase synthesis approach (Poma et al., 2013). Briefly, vancomycin was immobilized through its amino group by glutaraldehyde coupling to the surface of amine-derivatized glass beads. The polymerization mixture consisting of NIPAm, MBAm, TBAm and AA dissolved in water, was loaded on the reactor and polymerization was carried out at ambient temperature. Unreacted monomers and low-affinity polymers were washed away at ambient temperature and high-affinity MIP nanoparticles, sized 200-300 nm, were then eluted at 60 °C. The synthesized MIPs were subsequently fixed on microplate wells, by evaporation to dryness. Competitive binding experiments using vancomycin-horseradish peroxidase (HRP) as the enzyme conjugate for colorimetric detection were carried out and vancomycin was measured in buffer and in blood plasma within the dynamic range 0.001-70 nM with a low LOD of 0.0025 nM (Figure 1.31). Very low cross-reactivity of the assay was observed by assessing the response to other commonly used antibiotics: amoxicillin, gentamicin and bleomycin. In

conclusion, the novel MIP-based ELISA assay features enhanced sensitivity in plasma at clinically relevant concentrations and high stability compared to antibodies-based ELISA.

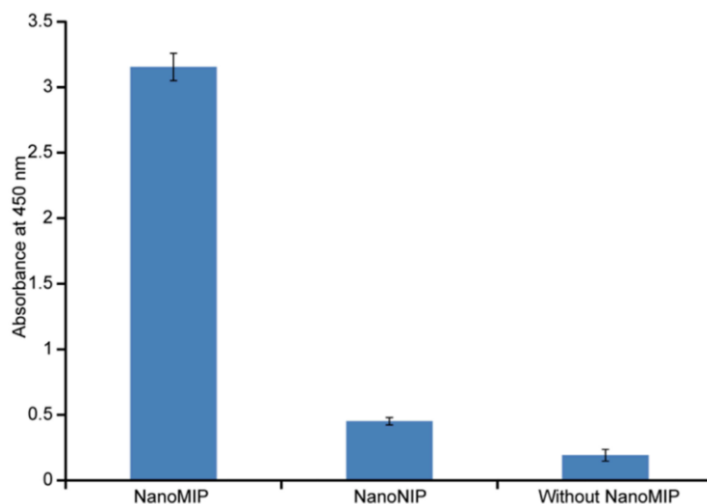


Figure 1.31. Testing the specificity of binding of the HRP-vancomycin conjugate to immobilized nanoMIPs. Binding of HRP-V to microplate wells coated with nanoMIPs, nanoNIPs or to bare wells, as revealed by color development with TMB reagent (100 μ L) for 10 min. Error bars represent ± 1 standard deviation for experiments performed in triplicate. Reproduced from Chianella et al., 2013°.

A different approach of a successful immunoassay in biological samples is reported by Ye et al., 2014 who developed a boronate-affinity sandwich assay (BASA) for the specific and sensitive determination of trace glycoproteins in serum, *via* Surface enhanced Raman Spectroscopy (SERS) (Ye et al., 2014). BASA relies on the combination of a boronate-affinity MIP that functions similarly to a capture antibody, as well as boronate-affinity-functionalized silver nanoparticles (AgNPs) that function as SERS probes. The MIP arrays were prepared using the photolithographic boronate-affinity molecular imprinting approach, while the boronate-affinity SERS probe was prepared by modification of gold NPs with 4-mercaptophenylboronicacid (MPBA) (Figure 1.32). To examine the performance of the BASA, horseradish peroxidase (HRP) was first employed as a model glycoprotein. As inferred by SEM images, the formation of MIP-glycoprotein-AgNPs was carried out by boronate-affinity binding between the MIP and the glycoprotein HRP as well as between HRP and the SERS probes. SERS binding experiments showed high affinity and specificity for HRP in phosphate buffer, 100 mM at pH=7.4 ($K_d=3.0$ nM). The cross-reactivity of the HRP-imprinted MIP towards different proteins (RNase B, transferrin, ovalbumin and bovine serum albumin) was negligible (except in the case of ovalbumin), which highlights the selectivity of the MIP. Furthermore, the feasibility of the BASA approach for real-world applications was demonstrated by an assay of the glycoprotein α -fetoprotein (AFP) in human serum, a biomarker in clinical screening for liver cancer. The AFP-imprinted array exhibited a linear response toward AFP within the range of 1 ng/mL to 10 μ g/mL (Figure 1.33A), featuring a K_d value of 0.7 nM (Figure 1.33B). To control the influence of the

matrix effect, serum samples spiked with known AFP concentrations were tested and the amount determined was in agreement with the result reported in the literature (Figures 1.30C and 1.30D). In conclusion, this study illustrates the great potential of MIPs in immunoassays and all the more for macromolecular recognition in complex biological samples.

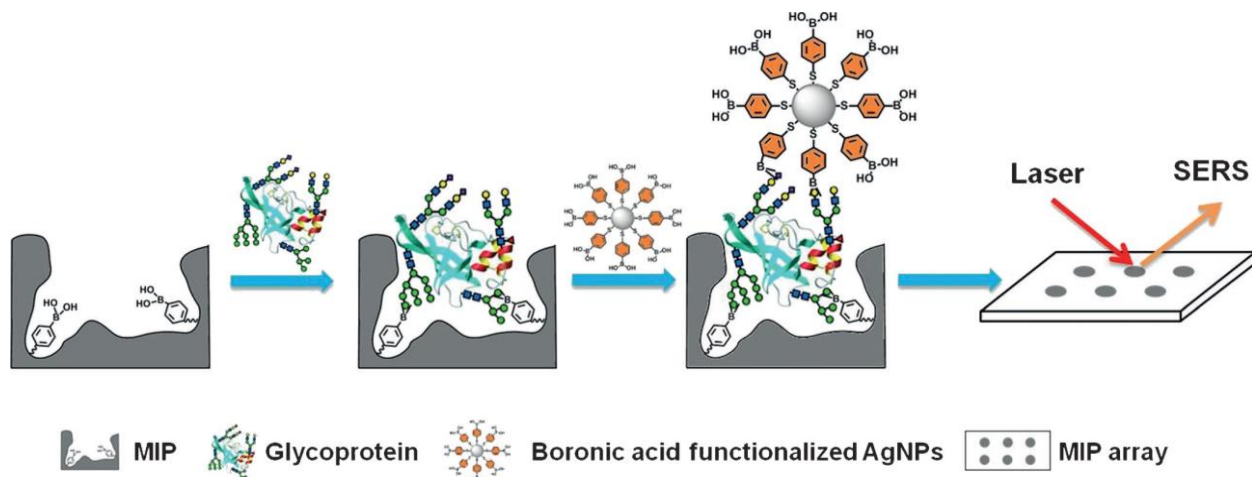


Figure 1.32. Schematic representation of the boronate-affinity sandwich assay of glycoproteins. Reproduced from Ye et al., 2014.

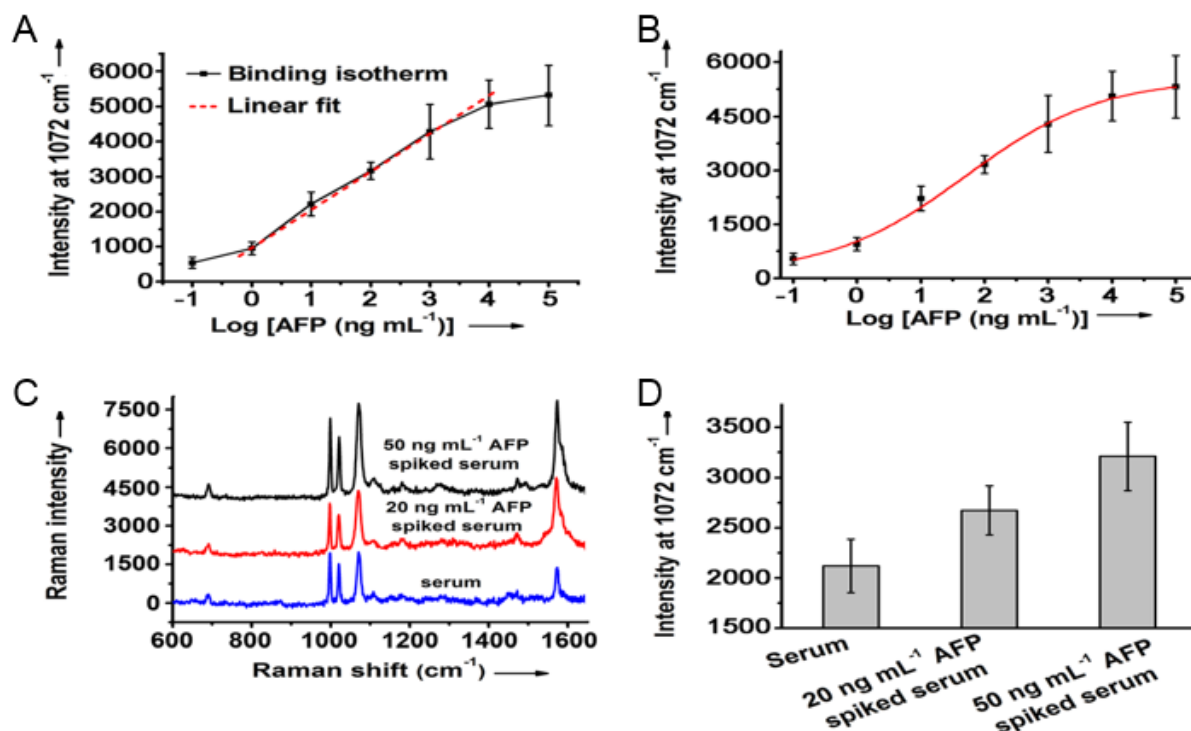


Figure 1.33. A) Dependence of the intensity of the SERS signal on the concentration of the AFP solution (containing 100 mM phosphate buffer, pH 7.4); B) Logistic function fitting for determination of the binding constant; C) SERS spectra for serum samples spiked with different AFP concentrations; D) SERS intensity for serum samples spiked with different AFP concentrations. Reproduced from Ye et al., 2014.

II.2.2. Optimized ILA protocols for recognition in complex samples

In Haupt's approach for the imprinting of 2,4-D and its successful recognition in phosphate buffer, a traditional free radical polymerization protocol was employed. In some applications, the improvement of MIP hydrophilicity and consequently the performance in more complicated matrices requires surface modifications such as the grafting of hydrophilic layers, performed *via* Controlled Radical Polymerization (CRP-section I.2.2.). This approach was exemplified by Ma et al., 2013, who synthesized 2,4-D imprinted nanoparticles (NPs) with surface -grafted hydrophilic brushes by Reversible addition-fragmentation chain-transfer (RAFT) precipitation polymerization. These MIP NPs were fully compatible with various real samples (including river water, diluted and undiluted milk and bovine serum), while the hydrophilic HEMA brushes also acted as a protective layer to prevent the proteins from blocking the imprinting cavities. Fluorescence equilibrium binding studies in undiluted milk and bovine serum samples were performed and the MIP could bind more of the target analyte compared to the control polymer (IF=2).

Another example of 2,4-D imprinted immunosorbent was reported by Zhang and co-workers, featuring the design of RAFT synthesized hydrophilic and magnetic MIPs with more pronounced specificity in undiluted bovine serum (Zhao et al., 2014). Briefly, MIP microspheres were synthesized with surface-grafted hydrophilic poly(glyceryl monomethacrylate) (poly(GMMA) or PGMMA) brushes by the combined use of RAFT precipitation polymerization (RAFTPP) and surface-initiated RAFT polymerization and the subsequent attachment of magnetic Fe₃O₄ nanoparticles *via* a simple co-precipitation process (Figure 1.34A). The performance of the grafted and grafted magnetic MIPs was compared and it was demonstrated that both MIP formats could exhibit specific binding for 2,4-D in pure water and bovine serum, comparable to that obtained in methanol/water (Figure 1.34B). The non specific binding of the ungrafted MIP particles in pure water and in bovine serum were apparently higher than that obtained in methanol–water, as determined by fluorescence binding studies (Figure 1.34C). Surprisingly, the non specific binding of the grafted magnetic MIP particles in such aqueous media proved to be essentially the same as that obtained in methanol/water (Figure 1.34C). The authors postulated that the enhanced surface hydrophilicity of magnetic MIP particles due the attachment of very hydrophilic Fe₃O₄ nanoparticles in comparison with the grafted MIP particles is responsible for the suppression of non specific binding.

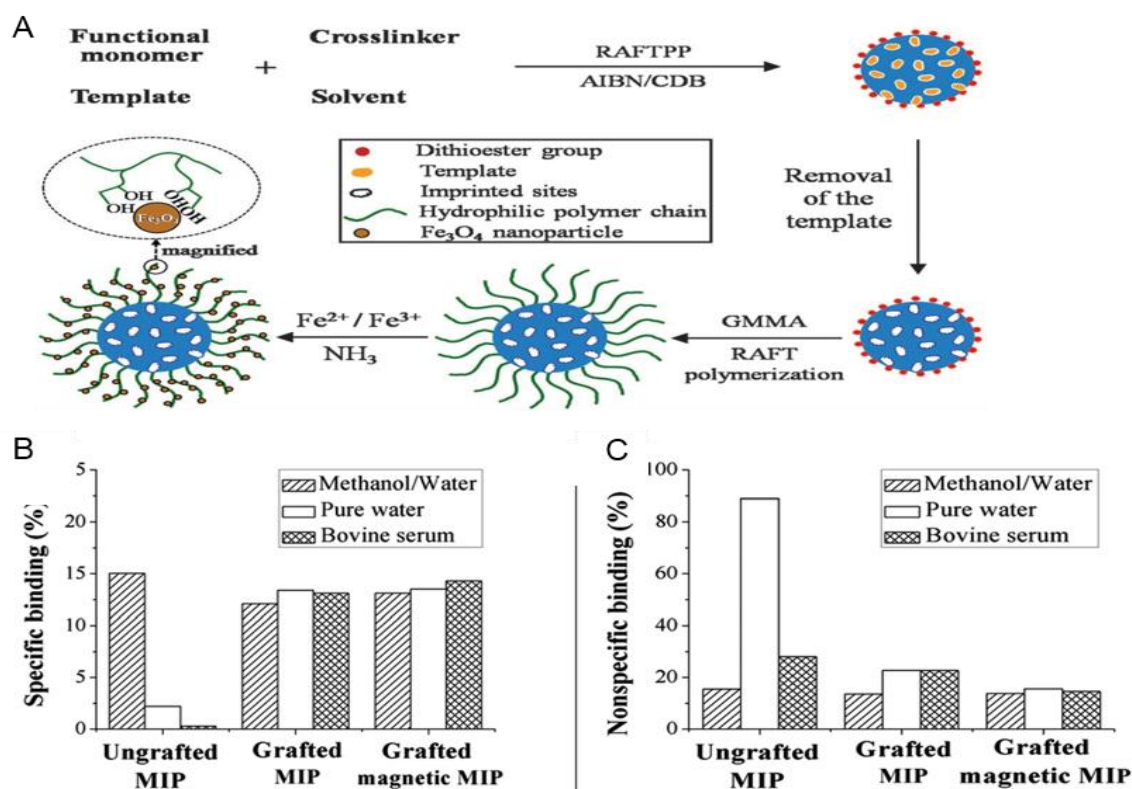


Figure 1.34. A) Schematic protocol for the synthesis of narrowly dispersed hydrophilic and magnetic MIP microspheres; B) Specific and C) Non-specific binding of the ungrafted, grafted, and grafted magnetic MIP microspheres in different media (0.02 mM of 2,4-D, polymer concentration: 12 mg/mL). Adapted from Zhao et al., 2014.

Other options to enhance the water compatibility of MIPS are the use of hydrophilic or stoichiometric monomers. For instance, Urraca et al., 2007 have prepared penicillin-imprinted polymers using an urea-based functional monomer to target the single oxyanionic groups in the template molecule (refer also to section I.5.1) This polymer has shown excellent recognition in aqueous samples and has been applied to the development of the first automated molecularly imprinted sorbent based assay for the analysis of penicillin type β -lactam antibiotics, performed on a reactor. After application of a desorbing solution, the fluorescence of the labeled derivative eluted from the sorbent was measured and related to the analyte concentration in the sample. The automatic assay has been successfully applied to the direct analysis of penicillin in spiked urine samples with excellent recoveries (mean value 92%).

Alternatively, careful optimization of the porogen system for the polymerization can render the resulting MIP polymer more water compatible. This was demonstrated on the example of an ELISA-based competitive immunoassay for the determination of the pesticide trichlorfon in vegetable samples (Meng et al., 2012). The assay was based on a trichlorfon-imprinted hydrophilic MIP membrane which was prepared in a mixture of water and ACN using MAA and EGDMA as functional and cross-linking monomers respectively and was directly polymerized on the surface of the ELISA well-plates. Both solvents were necessary for the preparation of the MIP membrane; the addition of water as porogen is important for the

good sensitivity of the resulting MIP in aqueous environments, while ACN improves the mechanical properties of the membrane and allows its attachment to the ELISA microwell plates. Competitive binding experiments using hapten as enzyme conjugate for colorimetric detection showed a good linearity of 3.2 to 50000 $\mu\text{g/L}$ for trichlorfon was observed in PBS, while the LOD was similar to the one reported for monoclonal antibodies (4.8 ng/mL). This method was also applied for the determination of trichlorfon in cucumber samples and high recoveries ranging from 106 to 110 % were achieved. Still, some optimization is required for the quantitative determination of the pesticide residues in spiked leek samples, since the amount quantified is 14-fold higher than the trichlorfon maximum residue level reported in the literature.

II.3 Sensors

A sensor is a device which produces a measurable detection signal in response to a physical or chemical stimulus. Two functional units constitute a sensing device: the receptor or recognition element and the transducer. Upon binding of the analyte molecule to the recognition element, a chemical or physical signal is generated. The transducer, which is in close contact with the recognition element, will then transform this signal into a measurable output signal that can be correlated with the analyte concentration (Figure I.35). The signal transduction can be based on optical, electrochemical or a mass sensitive device. Biosensors are a subclass of chemosensors based on biological receptors (e.g. enzymes, DNA, antibodies) that are in most cases immobilized on the surface of the transducer. The biological receptors used as recognition elements exhibit high affinity for the ligand, however their use is limited because of their high fabrication costs and limited stability (pH, temperature, ionic strength, organic solvents and other additives).

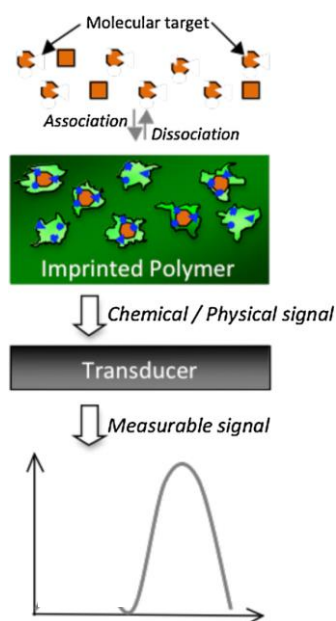


Figure 1.35. Schematic representation of a MIP-based chemical sensor. Reproduced from Fuchs et al., 2012.

MIPs have been implemented as selective recognition elements in different types of biomimetic sensors, since they feature mechanical stability and robustness combined with excellent recognition properties. For instance, optical sensors employing techniques such as optical absorption, photoluminescence, Surface Plasmon Resonance (SPR) and Surface Enhanced Raman Spectroscopy (SERS) were successfully combined with MIPs for selectivity enhancement (Suriyanarayanan et al., 2012). Another popular example is mass-sensitive sensors based on a quartz crystal-microbalance (QCM) transducer using MIPs as receptors (Haupt et al., 1999). Over the years, several applications of MIP-based sensors have been extensively reviewed for the detection of pesticides, chemical warfare reagents, environmental pollutants and antibiotics (Wulff, 1995; Haupt and Mosbach, 2000).

The main issues that should be addressed for real time applications of biosensors is the complexity of the samples in combination with the low concentrations of the target analytes (Mustafa et al., 2013). To avoid the interference of matrix materials, separation methods such as chromatography or electrophoresis were often applied for the clean-up of highly complex samples. In order to avoid the time-consuming separation steps, high selectivity towards the target analyte is required (Suriyanarayanan et al., 2012). In this respect, MIPs as recognition elements can outplay their advantages particularly well in the development of highly selective sensing devices for the detection of small molecules such as contaminants in environmental samples and food, biomarkers and drugs in biological fluids and even whole proteins and cells (Uzun and Turner, 2016). In this section, a few examples of MIP-based sensors for the selective detection of a wide range of analytes in complex samples will be discussed.

II.3.1. Detection of environmental pollutants

The sensing of pollutants such as pesticides in environmental samples is of great interest since these contaminants are raising public health issues related to their toxicity and to their environmental impact. An important number of MIP-based sensors has been developed for the detection of environmental pollutants (Pichon and Chapuis-Hugon, 2008; Warwick et al., 2013) in complex samples. One of the first attempts is the design of a conductometric sensor for the detection of the herbicide atrazine (ATR) in aqueous solutions using a highly selective MIP membrane (Sergeyeva et al., 1999), prepared by photopolymerization of MAA as the functional monomer and tri(ethylene glycol) dimethacrylate as the cross-linker. High selectivity was exhibited towards ATR, while the LOD in aqueous conditions was at 5 nM. Interestingly, the sensor response is not affected by environmental parameters such as the pH and the salt content, highly suitable for real life applications.

Since then substantial efforts have been made for the fabrication of MIP-based sensors of pollutants in real samples, such as wastewater samples. Wastewaters constitute a complex matrix, containing significant amount of solids (total solid 350-1200 mg/mL), microorganisms (up to 10^9 number/mL),

nutrients, heavy metals and micro-pollutants (Warwick et al., 2013). Very recently, Gupta and co-workers were the first to report a MIP for the detection of ATR directly in wastewaters (Gupta et al., 2015). They fabricated a MIP based sensor as follows: the QCM chip was modified by allylmercaptan, then an atrazine-imprinted poly(HEMA-phenol) film was co-polymerized *in situ* with EGDMA on the QCM chip gold surface (Figure 1.36A). Detection of atrazine directly in wastewaters was performed by QCM, with a low LOD of 0.028 nM, while negligible signal was obtained for the non-imprinted polymer. Selectivity studies were carried out in wastewater sample using the structurally similar triazines, simazine (SIM) and prometryn (PRO). The results show that ATR-imprinted QCM sensor was approximately 31 and 29 times more selective for ATR compared to SIM and PRO respectively (Figure 1.36B and I.36C). Importantly, this sensing method was compared with a traditional but time-consuming LC-MS/MS method and no significant difference of ATR determination in wastewater samples was observed.

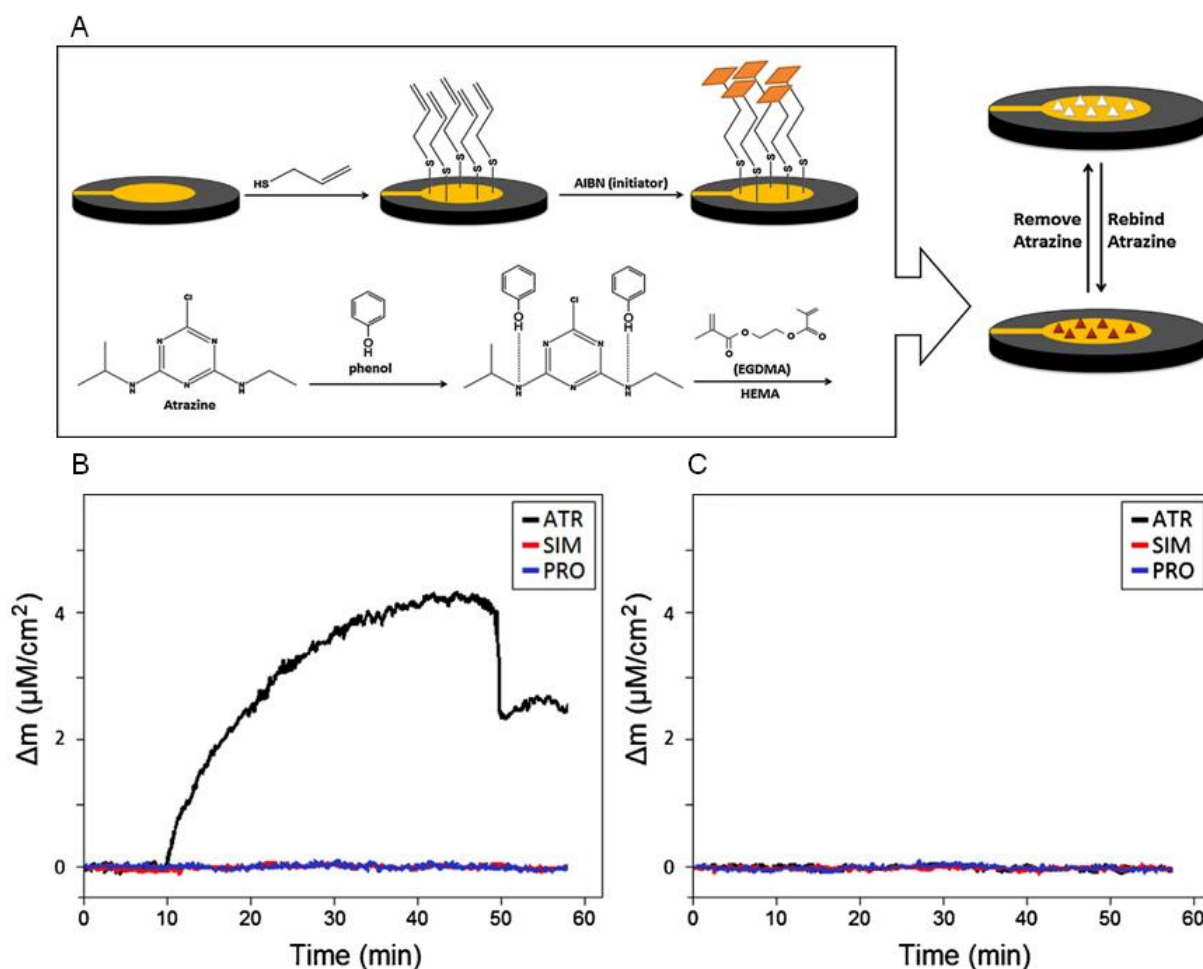


Figure 1.36. A) Schematic representation of preparation of molecularly imprinted QCM sensor for atrazine by surface polymerization; B) The QCM responses of ATR, SIM and PRO (each of 0.50 nM) on ATR imprinted sensor; C) The QCM responses of ATR, SIM, and PRO (each of 0.50 nM) on non-imprinted sensor. Reproduced from Gupta et al., 2015.

II.3.2. Detection of explosives

The design of sensors for explosives using MIPs as recognition elements is rather recent, maybe due to safety considerations. In 2001, Murray and co-workers filed a patent for a MIP sensor containing a porphyrin ring which undergoes a detectable change in absorption and/or emission of electromagnetic radiation when the polymer is exposed to explosives, namely 2,4,6-trinitrotoluene (TNT) and 1,3,5-trinitrobenzene (TNB). In fact, vapors or particulate emissions of an explosive or a liquid containing an explosive, if present, bind to the molecularly imprinted polymer are causing light absorbance in the rear-IR region. As an example, in one of the patented formats, a surface acoustic wave sensor was fabricated which is comprised of a MIP film containing a porphyrin disposed on a substrate, wherein a lanthanide-complex is capable of chemically binding with vapors of an explosive.

Since the work of Murray, the studies reported in the literature focused on the elaboration of new sensing systems for the sensing of explosives but in most cases the application is not extended to complex samples. Recently, some efforts are made towards the optimization of the MIP-based sensing devices, capable of rapid and selective detection of explosives in complex environmental samples. Still, for solid samples such as soil, direct sensing is not feasible and an extraction step is required prior to the determination of the spiked target analyte.

As an example of explosives sensing in soil, Xu et al., 2013 designed an optical sensor for the detection of TNT, based on MIP-capped quantum dots. MIP silica nanospheres were prepared in ethanol by the seed-growth method using APTES and TEOS as functional and cross-linking monomers while trinitrophenol (TNP) was employed as dummy template (Figure 1.37A). Fluorescence quenching was observed upon binding of TNT and the LOD was determined to be 0.28 μM . This water compatible sol-gel MIP sensor exhibited distinguished selectivity and a high binding affinity to TNT over the applied competitors 2,4-dinitrophenol (DNP), 4-nitrophenol (4-NP), phenol, and dinitrotoluene (DNT) (Figure 1.37B). The feasibility of sensing in soil samples was demonstrated, after an acetone-based extraction step, and high extraction recoveries were observed, ranging from 90.3 to 97.8%.

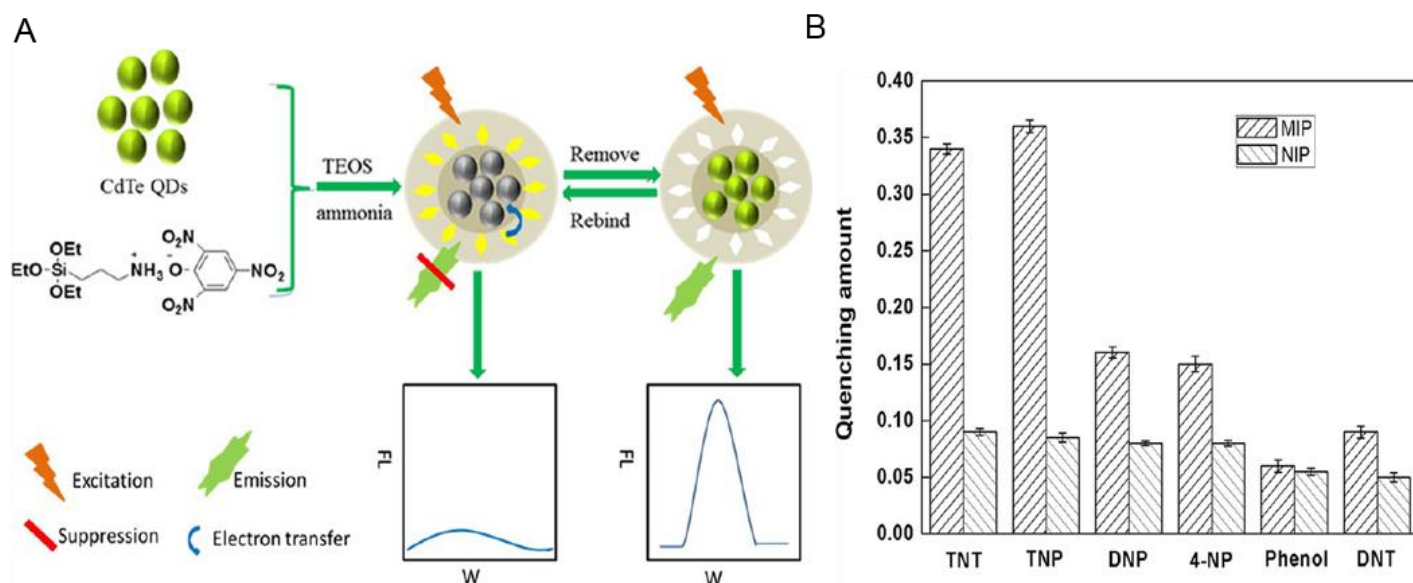


Figure 1.37. A) Schematic illustration for the preparation of MIP@QDs and the sensing mechanism for TNT; B) Quenching amounts of MIP@QDs for TNT and its structural analogues. The quenching amount was defined as $(F_0 - F)/F_0$. Reproduced from Xu et al., 2013.

II.3.3 Detection of additives and contaminants in food samples

The detection of contaminants in food is very important with regards to food safety issues and requires the development of effective sensing methods in complex matrices. Besides, the determination of trace contaminants in food, often involves extensive sample extraction and preparation regimes prior to instrumental analysis (see section II.1 for more details) (Ridgway et al., 2007). A few examples of MIP-based sensors for detection of contaminants in food samples have been reported in the literature, but still optimization of the existing methods is necessary. For instance, it is interesting to point out that the solid food samples require a multistep sample preparation, as exemplified by Yang et al., 2013, which hampers the facile and time-efficient application of the proposed MIP sensors.

An interesting study reports a MIP electrochemical sensor based on the combination of a water compatible sol-gel MIP film with the unique electrochemical properties of multi-walled carbon tubes (MWCT) for the trace analysis of the feed additive quinoxaline-2 carboxylic acid (QCA) from pork samples (Yang et al., 2013). The composite material was synthesized on a glassy carbon electrode coated with chitosan -modified MWCT. Chitosan is often employed as a coating layer on electrodes to impart water compatibility and provide high mechanical strength and film adhesion. A MIP sol-gel film was subsequently grafted on the MWCT modified electrode, using APTES and TEOS as functional and cross-linking monomers respectively. The MIP sensor showed a linear current response to the target QCA concentration in the wide range from 2×10^{-6} to 1×10^{-3} mol/L with a LOD of 4.4×10^{-7} mol/L in PBS buffer, while very low response was obtained from the NIP. Furthermore, the sensitivity of the sensor was

verified on treated pork samples with high recoveries, ranging from 93.5 to 98.6%, with SDs of 1.7–3.3%, while very low cross reactivity was observed for QCA structural analogues. In conclusion, this MIP sensor constitutes an representative example of sensing in treated solid food samples, in terms of selectivity and sensitivity. It should be noted, though, that the sensing of QCA in pork samples required a tedious multistep treatment, involving centrifugation, extraction in 20% ACN, drying and re-suspension in MeOH.

Conversely, the direct sensing of contaminants in liquid food samples is feasible, as exemplified by Wang et al., 2012b. Molecularly imprinted photonic sensors was prepared for the detection of the antibiotics tetracycline, oxytetracycline and chlortetracycline (TCs) in milk and honey samples. The development of the sensors was based on the combination of a colloidal crystal templating method, prepared from monodisperse polystyrene colloids and a MIP synthesized in water with AA and AAm as functional monomers and BIS as a cross-linker. After removal of the colloidal crystal template and the molecular template, a water compatible macroporous structure was obtained, with a thin hydrogel wall bearing nanocavities complementary to the template (Figure 1.38A). The response of the synthesized MIPPs to their respective template antibiotics in aqueous conditions is assessed through a readable Bragg diffraction red-shift, which is attributed to the lattice change of MIP structure upon binding of the target analyte. Moreover, the MIPP sensor showed enhanced selectivity and was able to differentiate among the three tetracyclines, employed for the purpose of this study. The sensitivity of the MIP sensor was not disrupted, when applied in spiked whole milk and honey samples (after dilution with PBS); the diffraction response shifted considerably upon binding of 0.08 mM and 0.12 mM tetracycline in milk and honey respectively (Figure 1.38B). The authors postulate that the enhanced sensitivity and selectivity of the MIPP sensor in aqueous conditions is due to the presence of high fidelity binding sites and to the hydrogen bonding formed between the AA and the template.

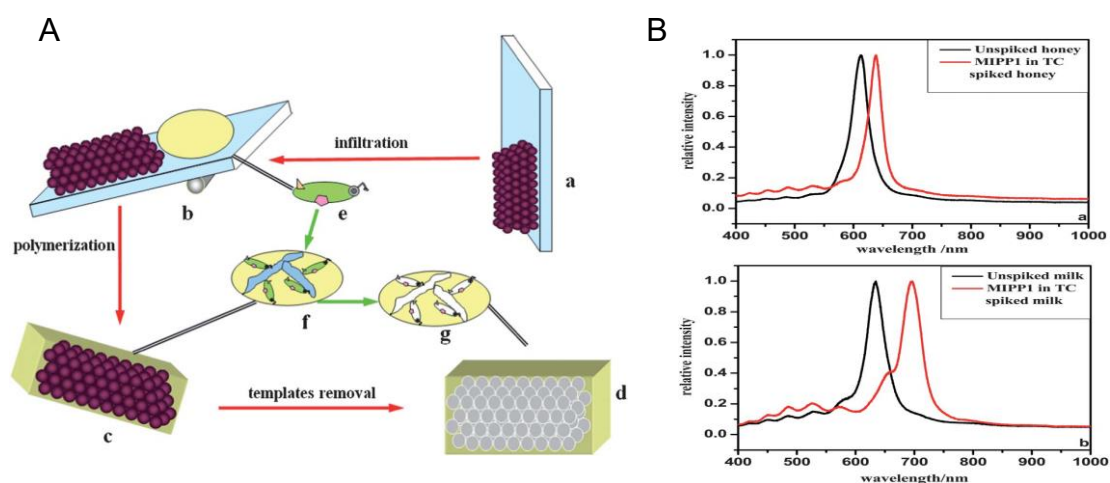


Figure 1.38. A) Protocol for the preparation of MIPP films: (a) PS colloids self assembled into colloidal crystals on a glass substrate; (b) infiltration of complex solution into a colloidal crystal template; (c) polymerization of a TCs imprinted photonic polymer; (d) MIPP film after the removal of the PS colloidal

crystal template and TCs imprinted molecule template; (e) complex of the monomer and imprinted template molecule; (f) imprinted molecules within the polymer networks and (g) imprinted cavities with complementary shape and binding sites to the template molecule; B) Diffraction response of the MIP sensor in the TC spiked honey (a) and milk (b) sample. Reproduced from Wang et al., 2012b.

II.3.4. Detection of drugs and biomarkers in biological fluids

Efficient monitoring of biomarkers and trace analysis of drugs is an area of great importance in clinical diagnostics and biomedical analysis. An optimized biosensor should be able to selectively detect low concentrations of target molecules in very small sample volumes. In this respect, an interesting work was reported by our group, who proposed the combination of MIPs with gold nanocomposites for signal amplification in a single-particle chemical nanosensor for the detection of the drug (*S*)-propranolol (Bompart et al., 2010). The (*S*)-propranolol templated MIP shell prevents interfering molecules from coming into contact with the gold colloids, and thus hinders enhancement of the matrix signal. The designed nanosensor was tested in 20 times diluted equine serum spiked with propranolol, achieving a LOD of 10^{-6} M, while no drug was detectable in the case of non imprinted control particles (Figure 1.39). Unfortunately, no difference could be obtained by this sensing method between the two enantiomers of propranolol at the low concentrations tested since they give the same SERS spectra, conversely to the traditional radioligand competitive assay.

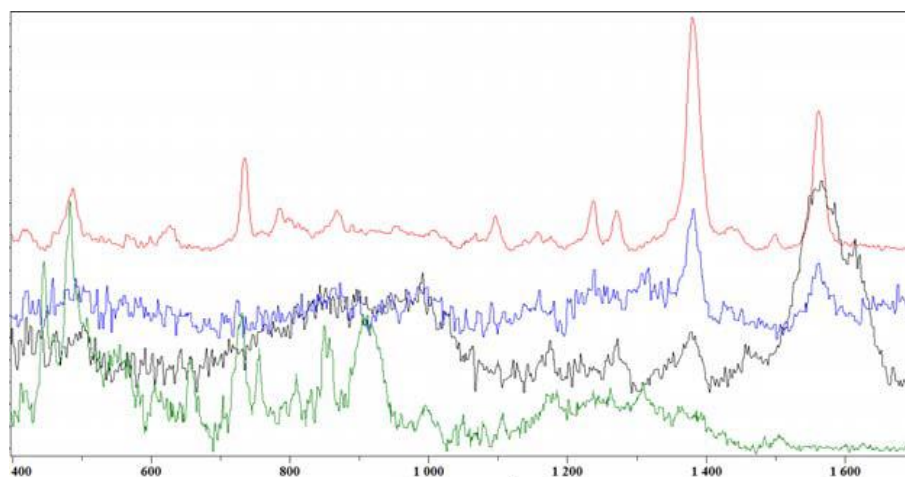


Figure 1.39. Typical SERS spectrum of a dried solution of *S*-propranolol at 10^{-5} M on aggregated gold colloids (red), a MIP nanocomposite particle after incubation in 10^{-5} M (blue), a MIP nanocomposite particle after incubation in 10^{-6} M (black), NIP nanocomposite particle after incubation in 10^{-5} M (green) of propranolol in 20x diluted equine serum.

Among other drugs, the detection of antibiotics is crucial not only for clinical analysis but also for toxicity evaluation, since strains of antibody-resistant bacteria have appeared with unknown health impact (Benito-Peña et al., 2009). Very recently, Zhang and co-workers described a sensing method for the direct

quantification of tetracycline (Tc) in undiluted biological samples (Niu et al., 2015). The general principle is presented in Figure 1.40A and involves the one-pot synthesis of fluorescent polymer nanoparticles bearing hydrophilic polymer brushes *via* poly(HEMA) macromolecular RAFT precipitation polymerization in the presence of a fluorescent monomer (anHEMA), where Tc, MAA, EGDMA, CDB, AIBN, and a mixture of ACN and DMF (4:1 v/v) were used as the template, functional monomer, cross-linker, RAFT agent, free radical initiator, and porogen, respectively. The fluorescent monomer anHEMA (HEMA modified with anthracene) plays a double role: it enhances the surface hydrophilicity and it also imparts to the MIP with fluorescent properties. The sensitivity of the MIP opto-sensor towards tetracycline was tested in undiluted bovine serum; fluorescent quenching was observed upon binding to increased concentrations of Tc, with a reported LOD of 0.26 μM (Figure 1.40B). Furthermore, the MIP was highly selective towards Tc, since negligible interference to its fluorescence response for Tc (10 μM) in undiluted bovine serum was observed in the presence of 10-fold concentrations of competitor drugs (including chloramphenicol (Chl), cefalexin monohydrate (Lex), and vancomycin hydrochloride (Van) and a selective β_1 receptor antagonist atenolol) except for the structurally related analog chlortetracycline Figure 1.40C).

Later, the same group focused on the improvement of the issues related to the use of organic dyes such as photobleaching which hinders the application of fluorescent MIP-based sensors in continuous sensing. In this respect, they prepared with ATRP Tc-imprinted microparticles with QD labeling and hydrophilic brushes which showed template-binding-induced fluorescence quenching and could be applied directly in biological samples (Yang et al., 2016). By applying this method, an LOD of 0.14 μM was obtained in milk and bovine serum, lower compared to their previous study.

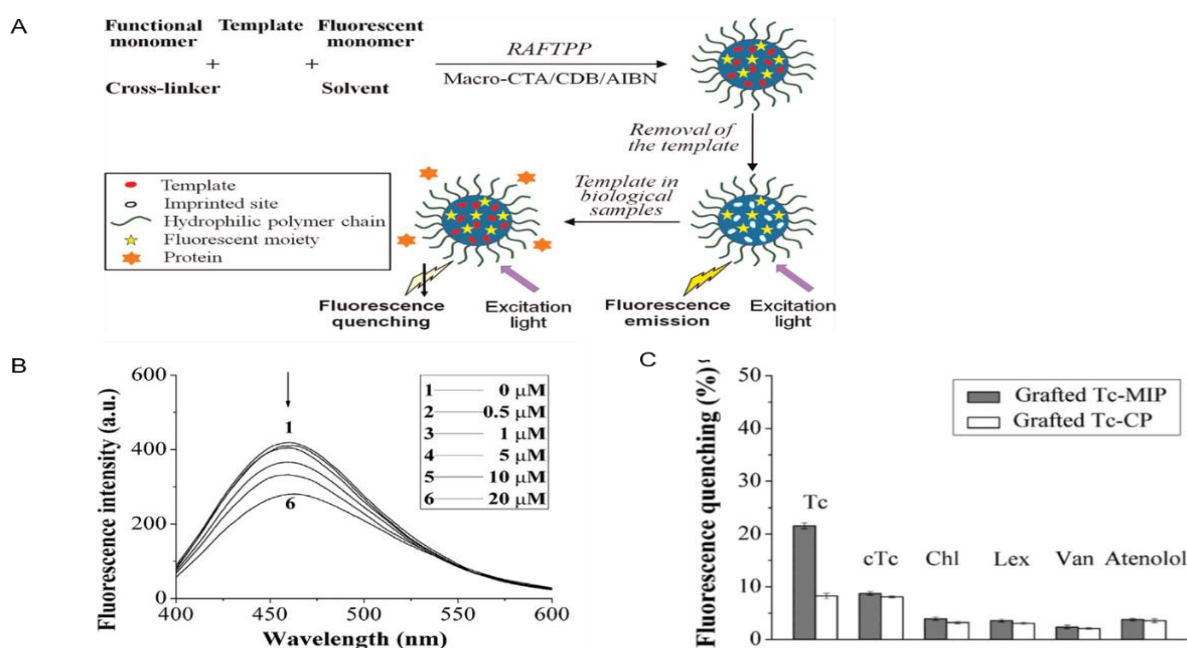


Figure 1.40. A) Schematic protocol for the synthesis of hydrophilic and fluorescent MIP nanoparticles for the recognition of tetracycline in real, undiluted biological samples; B) Fluorescence spectra of MIP

nanoparticles (0.5 mg/mL) with the addition of different concentrations of tetracycline in bovine serum ($\lambda_{exc}=365$ nm; $\lambda_{em} = 467$ nm); C) Fluorescence quenching of the grafted fluorescent Tc-MIP/Tc-CP nanoparticles (0.5mg/mL) after their incubation with a solution of Tc, chlortetracycline (cTc), chloramphenicol (Chl), cefalexinmonohydrate (Lex), vancomycin hydrochloride (Van), or atenolol (Concentration=10 μ M) in bovine serum at 25 °C for 3h. Adapted from Niu et al., 2015.

II.3.5. Detection of proteins and whole cells

A few recent studies demonstrated the feasibility of using MIPs for the detection of macromolecules (such as proteins) or even entire cells (e.g erythrocytes) or bacteria. The efficiency of MIPs towards macromolecules paved the way for their implementation as recognition elements for sensing *in vivo*, with potential applications in diagnostics and clinical treatments (Ge et al., 2013).

As an example of proteins sensing, a potentiometric sensor for the detection of myoglobin or hemoglobin in complex protein mixtures at a low μ g/mL range was developed by Wang et al., 2008. They fabricated thiol self monolayers by surface imprinting on a gold-coated silica chip, imprinted either with myoglobin or hemoglobin. Binding test was performed in PBS buffer, pH 7.15, resulting in charged or neutral proteins which are trapped within the insulating layer of the corresponding MIP over the electrode of the potentiometric sensor. This interaction alters the surface potential on the electrode, allowing potentiometric monitoring of the binding effect based on hydrogen bonding between the protein and the hydroxyl groups of the thiol. The selectivity of the sensor for either hemoglobin or myoglobin was verified using hemoglobin, myoglobin and ovalbumin mixtures, proving selective recognition of the target protein in the presence of other competing proteins. Similarly, a disposable sensing device based on a myoglobin-imprinted polyvinyl chloride-COOH film cast on a gold surface of a screen printed electrode was designed by Moreira et al., 2013. This matrix had non-charged amide groups, polymerized in aqueous environment and was biocompatible to the target protein. By employing this method the LOD of myoglobin in synthetic serum samples was 2.25 μ g/mL, however the authors mention that careful optimization and control of the MIP film thickness is required.

An interesting study, illustrating the sensing of waterborne viruses based on MIPs was reported by Altintas et al., 2015. They synthesized a MIP *via* solid phase approach, for the sensing and removal of the *E. coli* bacteriophage MS2 from water sources. According to their protocol, the bacteriophage was attached to silica microbeads and was used as the template for MIP synthesis, as demonstrated in Figure 1.41A. Affinity analysis performed by the SPR sensor functionalized with the nanoMIPs using amine coupling chemistry with a serial dilution of virus solutions in PBS (0.33 pmol–27 pmol) resulted in virus capture and detection in real-time (Figure 1.41B). Very high affinity between nanoMIP and bacteriophage MS2 was found to be 3×10^{-9} M and no cross reactivity was obtained with other virus or analyte (QB phage, vancomycin) (Figure 1.41B, c). The authors postulated that this method could be generalized for the

efficient sensing and removal of any kind of virus from complex water samples. To that end, a regenerative MIP surface has been developed for the first time to enable the use of the MIP NPs for an extended period, applied for viruses capture and analysis.

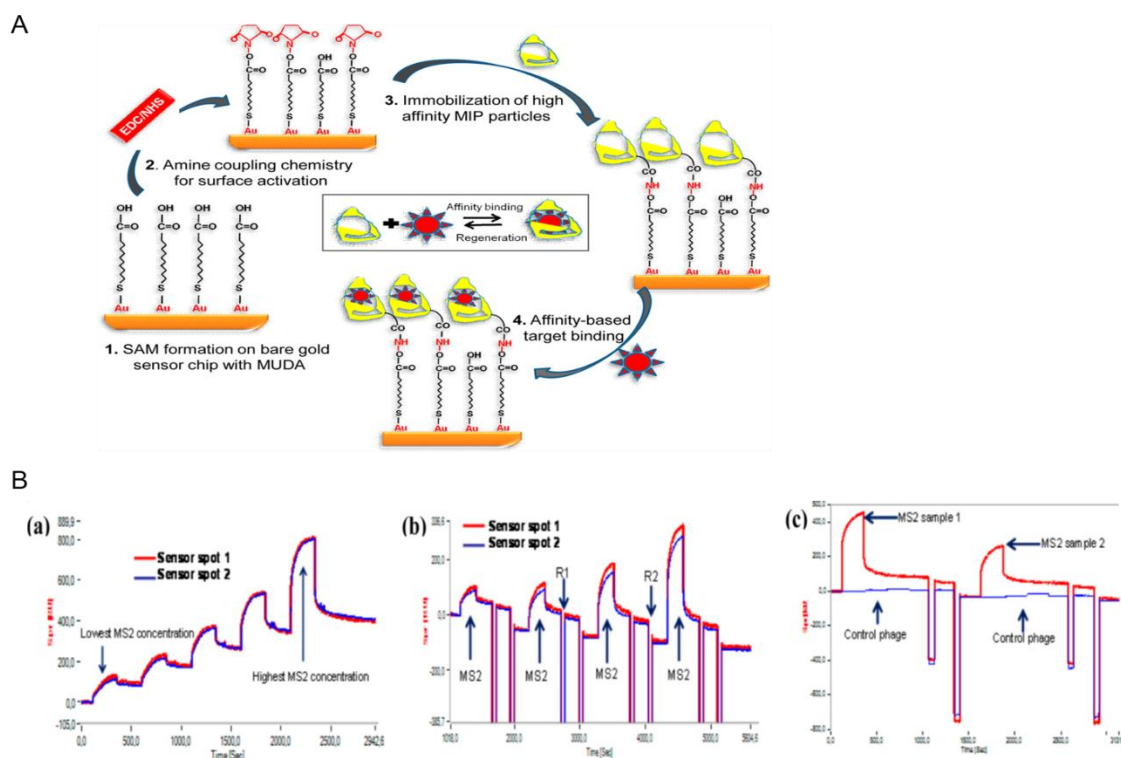


Figure 1.41. A) Affinity-based sensor assays for virus detection. The sensor chips were initially coated with mercaptoundeconoic acid (MUDA) to obtain self-assembled monolayer (SAM) on the surface to protect the immobilized compound from degradation and control signal decrease during the assays. The surface was then activated using the mixture of EDC/NHS prior to immobilization of MIP nanoparticles to the activated surface. EDC: 1-ethyl-3-(3-(dimethylamino)propyl) carbodiimide, NHS: N-hydroxysuccinimide; B) Real-time sensorgrams of the (a) continuous and (b) regenerative virus binding assays. MIP surface was regenerated using 0.1 M HCl (R1) and 20 mM NaOH (R2) as regeneration solutions for subsequent virus samples tests. (c) Cross-reactivity test using QB phage as control; blue line shows QB-phage binding on MS2-MIP whereas red line represents the MS2-phage binding on MS2-MIP. Reproduced from Altintas et al., 2015.

A novel approach for Apple stem pitting virus (ASPV) imprinting, combining MIPs and aptamers was reported by Bai and Spivak, 2014. They developed a new “double imprinting” method whereby a virus-bioimprinted hydrogel is further micromolded into a diffraction-grating sensor to give a “Molecularly Imprinted Polymer Gel Laser Diffraction Sensor” (MIP-GLaDiS), as described in Figure 1.37A. Briefly, MIP-GLaDiS were synthesized in two steps; in the first one the synthesis of the prehydrogel solution is carried out by incubation of the polymerizable ASPV-specific aptamers with an impure ASPV extract. Then, the remaining components (presented in Figure 1.42A). were added to the prehydrogel solution, which was subsequently cast onto the elastomer grating micromolds and allowed to polymerize. Once the hydrogel is formed, the film is delaminated from the elastomeric grating template and the virus template

removed by immersing the hydrogel film several times in an ethanol/NaOH regenerating solution. A laser transmission apparatus was used to measure the change in the diffraction of the MIP GLaDiS in response to virus samples, with a LOD of 10 ng/mL comparable to that of antibodies applied for ELISA test. To verify that the MIP-GLaDiS shrinking response is due to the bioimprinted virus, the response of three similarly formulated control gels were also verified (Figure 1.42B); one without the ASPV extract or the aptamer monomer (Grating Gel 1), a second without the aptamer monomer (Grating Gel 2), and a third without the virus extract (Grating Gel 3). The results showed clearly that both the aptamer preorganisation step and the presence of specific imprinting sites are essential for an accountable response of the biosensor. In conclusion, this study illustrated perfectly the great potential of MIPs as recognition elements in biosensors, which should be applicable in many biotechnological areas and could be combined with other new generation receptors such as the aptamers.

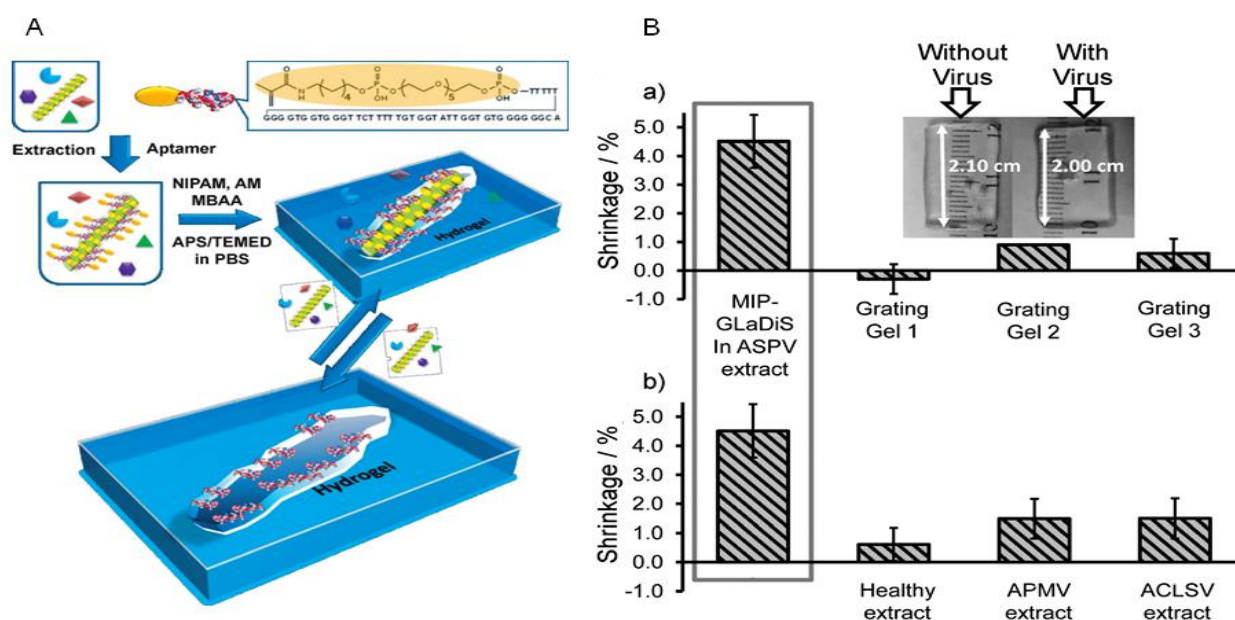


Figure 1.42. A) Outline of the bioimprinting process used to create virus responsive super-aptamer hydrogels. NIPAM: *N*-isopropylacrylamide, AM: acrylamide, MBAA: *N,N'*-methylene bisacrylamide, APS: ammonium persulfate, TEMED: *N,N,N',N'*-tetramethylethylenediamine, PBS: phosphate-buffered saline; B) The volume-shrinking response for the MIP-GLaDiS in Apple stem pitting virus (ASPV) extract is shown in both parts a and b (boxed) for comparison to non imprinted control Gels 1,2 and 3 (a) and cross-reactivity responses to extracts from healthy leaves not infected with ASPV or leaves infected with different apple viruses (b). Reproduced from Bai and Spivak, 2014.

II.4 Sustained delivery and release

Generally, nanomaterials have mediated marked advances in drug delivery (Farokhzad and Langer, 2009). In particular, MIP nanoparticles implemented in drug delivery systems can facilitate controlled drug loading and release as well as promote specific disease targeting. A controlled drug delivery system would enable a maximized drug efficacy and safety and provide a suitable rate of delivery of the therapeutic dose,

at the most appropriate site in the body. This would prolong the duration of the drug's pharmacological activity, reduce side effects, and minimize administration frequency, thus enhancing patient compliance (Wang and von Recum, 2011).

MIPs can be utilized for drug delivery in different concepts: as simple drug excipients or as vectors for targeted drug delivery release (Selligren and Allender, 2005). Several issues must be addressed for the successful design of MIPs for drug delivery systems. First, a compromise between the optimal rigidity and flexibility of the polymeric network is necessary. The MIP should maintain its conformation after the removal of the template and at the same time, be flexible enough to facilitate a sustained drug release. Moreover, MIPs should be chemically stable to resist enzymatic and chemical attack under mechanical stress. Last but not least, the biocompatibility of the MIP materials is of outmost importance for drug delivery applications, since the MIPs implemented in these systems will be in direct contact with sensitive tissues. Thus, cytotoxicity studies both *in vitro* and *in vivo* are necessary so as to ensure the non-toxicity of MIPs for applications in real situations (Alvarez-Lorenzo et al., 2004).

The first report of MIPs in drug delivery was reported by Norell et al., 1998 for the controlled release of theophylline, based on the protocol developed originally by Mosbach and co-workers (Vlatakis et al. 1993). Theophylline is a drug with a narrow therapeutic index, used for the treatment of asthma. In the study of Norell, theophylline loaded microparticles were able to prevent drug release in phosphate buffer, pH 7, especially for low concentrations of theophylline (<2 mg drug/ g of polymer). However, at higher drug loading concentrations, the release profile was similar to the control polymer, which suggests that the capture of the drug is partially attributed to non specific interactions.

Since the pioneering work of Norell, the format of drug delivery devices has evolved considerably. Nowadays, cross-linked hydrogels are typically utilized as matrices for the encapsulation and controlled release of bioactive molecules in aqueous conditions (Hennink and van Nostrum, 2002). Obviously, the design of appropriate MIPs for drug delivery applications, requires their outstanding performance in complex samples, such as tissues and biological fluids. This is in fact a limitation factor for the vast commercialization of MIPs as drugs delivery systems. However, several approaches can enhance the biocompatibility of MIPs, such as the use of hydrophilic monomers and cross-linkers or even bio-conjugates such as dextrin and gelatin. In the following section, the main contributions of MIPs in drug delivery systems will be discussed with emphasis on applications in real situations, for example the *in vivo* treatment of cancer tissues or in ocular therapeutics.

II.4.1. Stimuli-responsive targeted delivery and sustained release

It is a general consensus that biological receptors such as enzymes and antibodies demonstrate high responsivity towards external stimuli. To be competitive over their natural counterparts, MIPs as artificial receptors should respond to a single or more stimuli, such as the combination of heat and pH. Thus, the

development of stimuli-responsive, biocompatible MIPs is of great importance for applications such as intelligent delivery.

The successful design of stimuli-responsive MIPs requires the effective combination of the molecular recognition properties of a MIP with stimuli-responsive properties (Chen et al., 2015a). To provide switchable capacity during binding and release processes, optimization of the polymerization protocol is necessary. More specifically, it must be taken into account that the high amount of cross-linker typically used to stabilize the binding sites, prevents any response of the MIPs towards physical or even chemical stimuli (Ma et al., 2012). Nevertheless, an important progress was made in recent years and some interesting examples illustrate the applicability of stimuli-responsive MIPs for tunable drug delivery/controlled release systems. Their huge potential could bring about intelligent drug release in a predictable way, of therapeutic agents in response to specific environmental stimuli (the presence of another molecule, pH changes, temperature, etc.) (Puoci et al., 2008b).

Currently, the use of stimuli-responsive MIPs for drug delivery applications is investigated in aqueous or buffered conditions. For instance, the design of pH-responsive MIPs for controlled release in water was reported, *via* sol gel process (Güney and Serin, 2015) or metal coordination (Zhang et al., 2014b). An example of water compatible MIP microspheres with photo-, thermo- and pH-responsive properties for the delivery of propranolol was reported by Ma et al., 2012. More specifically, a polymer core was prepared with 4-VP and EGDMA, followed by the formation of the shell by surface initiated RAFT polymerization of 4-[(4-methacryloyloxy)phenylazo]benzoic acid (MPABA) and EGDMA in the presence of the template propranolol. Finally, the thermoresponsive monomer NIPAm was co-polymerized by RAFT polymerization with the monomer DEAEM, producing grafted core-shell microspheres with size around 2-3 μm . The photo-responsivity of the synthesized MIP microspheres was demonstrated by photoregulated release and uptake of propranolol in water. Photoswitching cycles performed at different temperatures and different pH values at 40 °C showed the reversibility of the binding site configuration, which allows for a tunable drug delivery upon external stimulus in aqueous environments (Figure 1.43). This delivery application of stimuli-responsive MIPs, though not in complex samples, is quite interesting, since it features the synthesis of a water compatible MIP, which is performant in aqueous conditions.

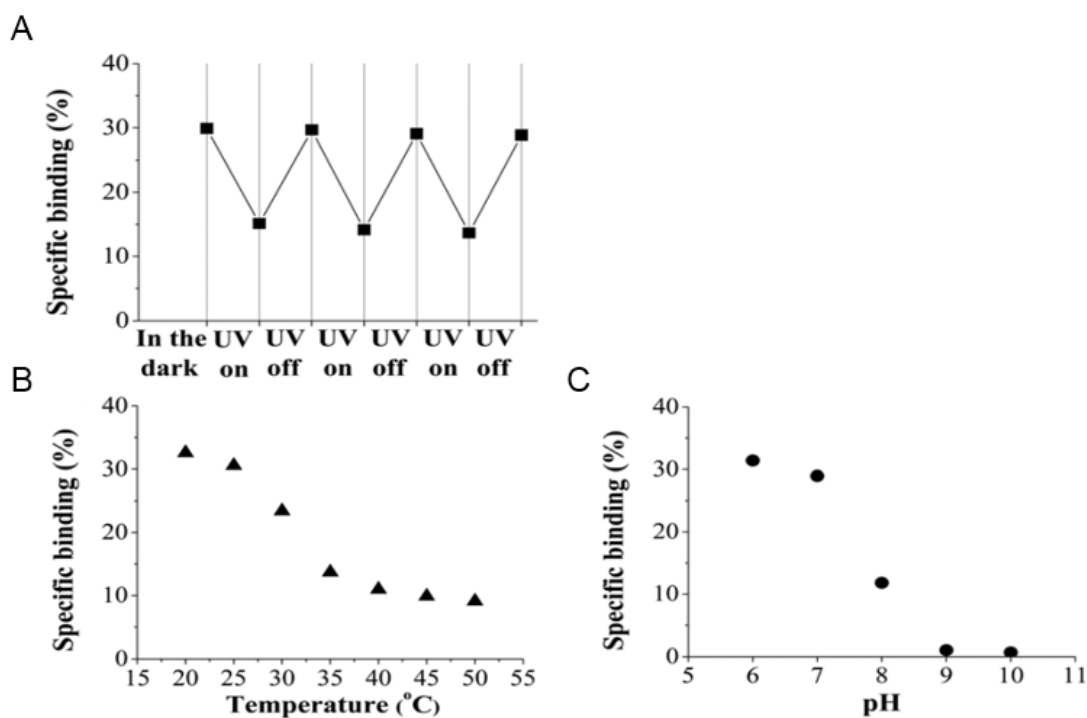


Figure 1.43. Stimuli-responsive binding of the grafted MIP microspheres in a propranolol solution (0.05 mM) A) under the photoswitching conditions (i.e. UV light on for 6 h and off for 18 h alternately at 25 °); B) at different temperatures in water and C) at different pH values at 40 °C in buffer (polymer concentration: 1 mg/mL). Reproduced from Ma et al., 2012.

To date, stimuli-responsive MIPs for drug delivery applications directly in biological samples or *in vivo* have not been reported. Conversely, some studies illustrated the use of stimuli-responsive MIPs for the recognition and the sustained release of biomacromolecules. For instance, the selective capture and release of human serum albumin in real biological samples based on stimuli responsive properties of MIPs was reported very recently by Li et al., 2016. They fabricated thermoresponsive MIP hydrogels for the selective capture and release of human serum protein by epitope imprinting. Briefly, immobilization was conducted on modified SiO₂, *via* the His tag epitope of the protein and polymerization was carried out using NIPAm as thermoresponsive monomer. NIPAm has an LCST of 32 °C, which signifies that above that point it is in the collapsed state, while below it is soluble. To evaluate the thermo-responsivity, the synthesized MIP and the control polymer (NIP) were incubated with the target protein, at different temperatures ranging from 15 to 55 °C (Figure 1.44A). Increased absorption capacity was observed as the temperature reaches 45 °C, suggesting enhanced affinity while the polymeric network is collapsed around the epitope binding site. However, at 55 °C, important non specific binding was observed, attributed to the dominant hydrophobic interactions. Capture and release studies were performed in 100-fold diluted serum. It can be observed from the result of SDS-PAGE analysis (Figure 1.44B) that the diluted plasma (lane 1) shows numerous fractions from large Mw to small Mw, but after the capture and temperature dependent release of MIP (lane 3), only two major fractions are observed, the target HSA at ca. 69 kDa and a

nonspecific binding fraction at ca. 55 kDa, related to interaction with the complex matrix of serum. In conclusion, this interesting study highlights the use of MIPs as intelligent capture and release materials which can be successfully applied in complex matrices.

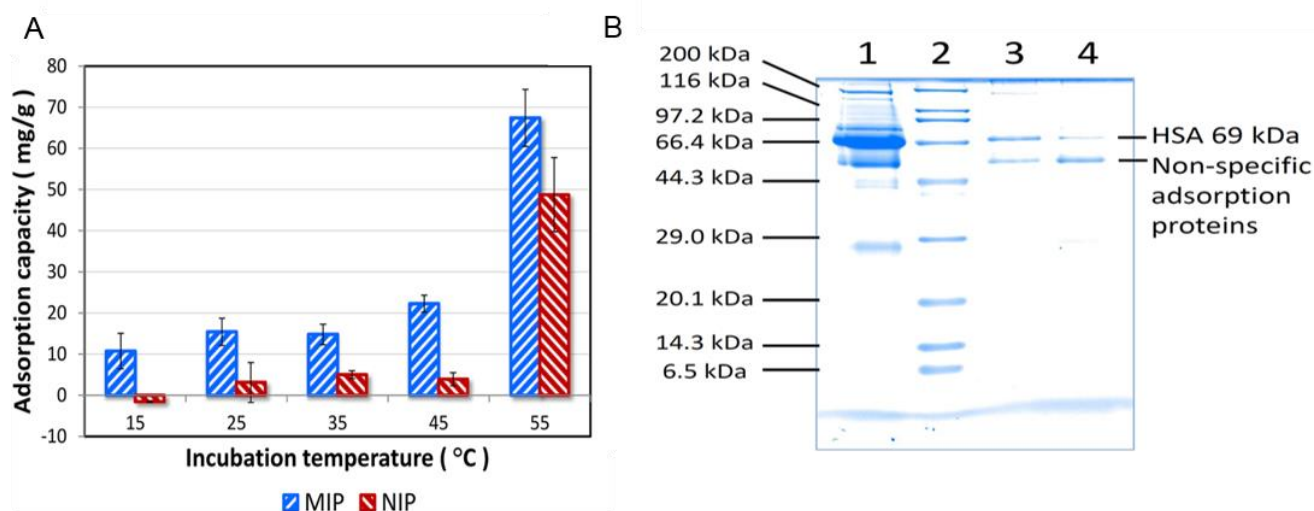


Figure 1.44. A) Thermodependent adsorption of MIP and NIP. Amount of MIP and NIP, 0.8 mg; incubation volume, 0.4 mL; incubation media, Tris-HCl buffer (10 mM, pH 7.0); incubation time, 3 h; initial concentration, 0.5 mg/mL. The data represents the mean values of three parallel incubations. The error bars represent the standard error; B) SDS-PAGE analysis of the desorbed fraction from MIP (Lane 3) and NIP (Lane 4); Lane 1, 100 times diluted human plasma; Lane 2, standard protein marker. Reproduced from Li et al., 2016.

II.4.2 Vectorization of anticancer drugs

Targeted therapy is very important for cancer treatment, so as to minimize side effects to healthy tissue and organs. A very interesting example of triggered drug release from a MIP carrier is reported by Griffete et al., 2015, using as a model the anti-cancer drug doxorubicin. They designed a new magnetic doxorubicin (DOX) delivery system ($\text{Fe}_2\text{O}_3@DOX\text{-MIP}$) by growing molecularly imprinted polymers from an individual iron oxide nanoparticle surface *via* acrylic acid as the polymerization initiator anchored on the surface of Fe_2O_3 nanoparticles and DOX as the template. Polymerization was performed at 70 °C using AAm and EGDMA as functional and cross-linking monomers respectively and resulted in MIP particles with size around 50 nm, as inferred by TEM images. The drug release was investigated in cancer cells under alternative magnetic field excitation (AMF). As illustrated by the confocal images in Figure 1.45A and 1.45B, DOX loaded nanoparticles were successfully internalized by the cells, however DOX did not induce cancer since it was bound by the MIP (Figure 1.45C, No AMF). After AMF application, cancer cell viability was reduced to 60% after 90 min treatment (Figure 1.41C). Similar toxicity was obtained when free doxorubicin was incubated with the cancer cells for 2 hours at a concentration in the range of 0.5–2 μM (Figure D), corresponding to the concentration which could be AMF released by the $\text{Fe}_2\text{O}_3@DOX\text{-MIP}$

incubated with the cells. It is important to note that the drug release is induced by the application of the magnetic field while the temperature was maintained at physiological levels throughout the experiments. This approach of magnetic MIPs under AMF can find many applications in targeted drug delivery since no temperature increase or irradiation is required for the drug release which limits the side effects of chemotherapy on bystander tissues. Moreover, the great advantage of MIPs as carriers for sustained delivery and release was clearly highlighted.

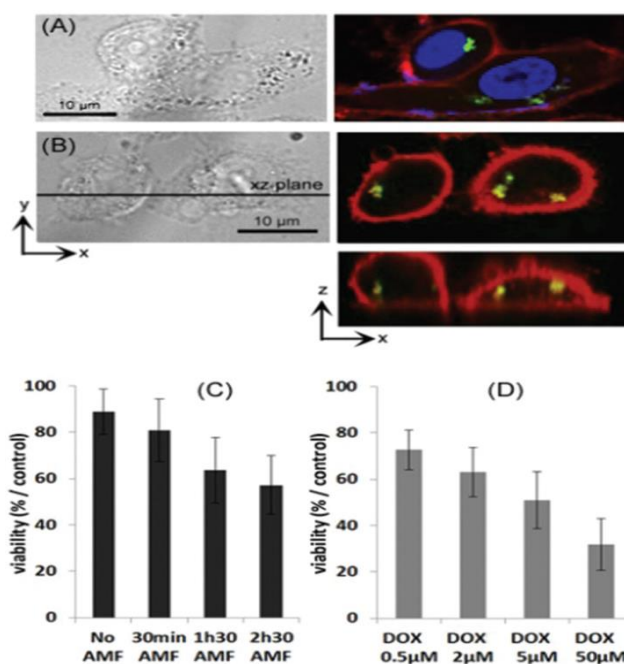


Figure 1.45. A) and B) Cancer cells (human prostate cancer cell line, PC-3) internalization of the $Fe_2O_3@DOX$ -MIP nanoparticles. DOX is detected in the green channel (excitation at 488 nm, emission at 561 nm). Nuclei and cell membranes are stained with DAPI (A) in blue and PKH26 cell membrane dye (A, B) in red, respectively. Z reconstruction; B) identification of DOX inside the cells; C) Viability of cancer cells labelled with $Fe_2O_3@DOX$ -MIP after exposure to the AMF compared to the control experiment (cancer cells labelled with Fe_2O_3 nanoparticles, at the same cellular iron dose, and exposed to the same conditions of AMF); D) Treatment of the cancer cells with free doxorubicin (DOX) incubated for 2 hours from 0.5 to 50 μM . Cell viability (normalized by control cells) was measured 24 hours after the incubation. Reproduced from Griffete et al., 2015.

II.4.3. Ocular therapeutic applications

Applications involving the treatment of ocular diseases are the most active area research involving MIPs, as drug delivery vehicles (Wang and von Recum, 2011). Several studies reported the utility of MIPs as effective vehicles for ocular delivery of bioactive compounds (Hiratani et al., 2002; Alvarez-Lorenzo et al., 2006; Ali and Byrne., 2009; Tieppo et al., 2012). The design of MIPs for this purpose should address the challenges of commercial design for a clinically effective drug delivery system. Conventional ophthalmic formulations for treating ocular diseases have limited bioavailability of 1-10%, owing to ocular

mechanisms such as blinking and lachrymal fluid removal. In addition, the mechanical and optical properties of delivery systems such as contact lenses requires extensive optimization, so as to achieve clear, flexible and oxygen permeable materials that do not cause irritations and discomfort (Alvarez-Lorenzo and Concheiro, 2004).

Due to the excellent comfortable feeling and biocompatibility, a soft contact lens is an ideal option for an ophthalmic drug vehicle, which could be used as an alternative of topical drop therapy for the slow release of a drug. However, drug loading capacity of conventional lenses can be insufficient, so the implementation of drug-loaded MIPs can provide an efficient solution to that problem. Due to the requirements of optical clarity, flexibility and oxygen permeability, only a selective amount of materials can be utilized for the synthesis of MIPs, usually in the form of hydrogels.

Alvarez-Lorenzo and co-workers have extensively studied the application of MIPs for ocular therapeutics (Alvarez-Lorenzo et al., 2002; 2006; Hiratani et al., 2002; 2004). More specifically they proposed the synthesis of timolol-imprinted hydrogels for the treatment of glaucoma (Alvarez Lorenzo et al., 2002). A series of hydrogels were prepared by self assembly of prepolymerization solution composed of varying concentrations of MAA and HEMA, subsequently polymerized in a mold. The resulting hydrogels, after boiling (for sterilization) and drying were optically clear and poreless. The timolol loading capacity of non imprinted and imprinted hydrogels (the latter after total release of imprinting timolol), was studied in a timolol solution with a concentration of 0.5 mg/mL and it was observed that loading was completed in 8 hours. Amongst the experimental conditions applied, best loading capacity was obtained for the MAA hydrogel at pH 5.5 (12 mg of timolol/g of dry gel), significantly exceeding the uptake by the non imprinted hydrogel (4 mg/g). The pH is a regulatory factor of the loading and release mechanisms, since at pH 7.5, significant hydrogel swelling occurs, resulting in the same loading capacity for imprinted and non-imprinted materials. Total release of the loaded timolol in an 8 hours' time frame was achieved in artificial lachrymal fluid (6.78 g/L NaCl, 2.18 g/L NaHCO₃, 1.38 g/L KCl, 0.084 g/L CaCl₂.2H₂O, pH 8) (Figure 1.46A). The authors concluded that the imprinting effect (using MAA as co-monomer) resulted in an increased timolol loading capacity to therapeutically useful levels compared to non imprinted poly(HEMA) hydrogels. Careful optimization was needed to obtain the HEMA/MAA hydrogel which shows the slowest release rate in lacrimal fluid.

Later, the same group designed soft contact lenses based on poly(HEMA) MIPs for the controlled release of the antibiotic norfloxacin (NRF) (Alvarez-Lorenzo et al., 2006). The poly(HEMA) imprinted hydrogels were prepared using AA and EGDMA in different concentrations, based on the protocol described above. When reloaded in NRF solutions of low concentration range, imprinted hydrogels were able to uptake significantly greater amounts than the non-imprinted ones. Importantly, NRF-loaded hydrogels did not release the drug when immersed in water (only 4% after 24 h), which confirms the strength of the interactions and opens also the possibility of storing the drug-loaded lenses in aqueous

medium. The synthetic protocol providing hydrogels with NRF:AA 1:3 or 1:4 molar ratios showed the greatest ability to control the release of the drug, sustaining the process for 2 to 5 days (Figure 1.46B). An evidence that the sustained release mechanism is controlled by the imprinting effect is the fact that the release rate is unaffected by the thickness of the hydrogel, which signifies that the loading and release mechanisms are dependent on the affinity and not simply on diffusion phenomena.

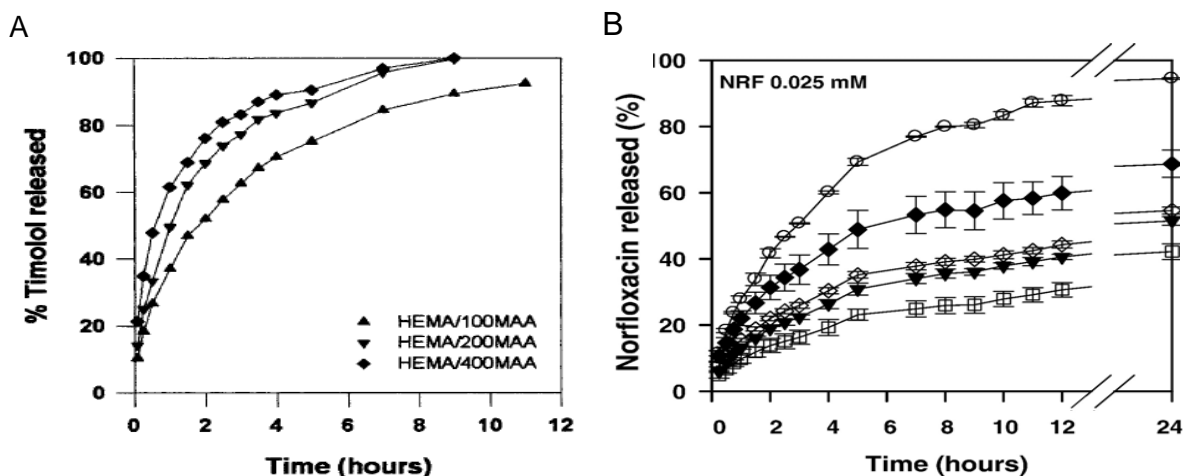


Figure 1.46. A) Timolol release in artificial lachrymal fluid (6.78 g/L NaCl, 2.18 g/L NaHCO₃, 1.38 g/L KCl, 0.084 g/L CaCl₂·2H₂O, pH 8) at 37 °C from reloaded imprinted hydrogels. Reproduced from Alvarez-Lorenzo et al., 2002. B) Norfloxacin (NRF) release profiles in lachrymal fluid from pHEMA hydrogels using different norfloxacin: acrylic acid molar ratios; zero, i.e. non-imprinted hydrogels (empty circles), 1:16 (filled rhombus), 1:10 (empty rhombus), 1:6 (filled triangle), and 1:4 (empty squares). The hydrogels (thickness 0.4 mm) were previously loaded by immersion in 0.025 mM, of NRF solutions (n=3). Reproduced from Alvarez-Lorenzo et al., 2006.

Another example of therapeutic contact lenses is reported by Ali and Byrne, 2009 who synthesized hydrogel contact lenses for the controlled release of hyaluronic acid (HA), used for the treatment of ocular discomfort and dryness. Delayed release characteristics were significantly improved by the MIP, providing a delivery rate of HA from a daily disposed contact lenses of 6 µg/hour, for 24 hours. More recently, Byrne and co-workers proposed imprinted soft contact lenses for the controlled delivery of ketotifen fumarate *in vivo* (Tieppo et al., 2012). Poly(HEMA) hydrogels were synthesized using AA, AAm and N-vinyl 2-pyrrolidone (NVP) as co-monomers and polyethylene glycol (200) dimethacrylate as cross-linker. The imprinted hydrogels had a much greater loading (4 times more) and a considerably slower transport (19 times slower) than non-imprinted materials. When applied *in vivo* on rabbits, a dramatic increase in ketotifen mean residence time (MRT) and bioavailability was observed for the fabricated hydrogels compared to topical drop therapy and drug soaked lenses (Figure 1.47). Remarkably, the concentration of ketotifen fumarate in the tear fluid was still high at a value of 160 µg/mL (clinically effect amount), after

24 hours of contact lenses application, as opposed to the tear drop therapy, where the drug was totally eliminated after 45 min.

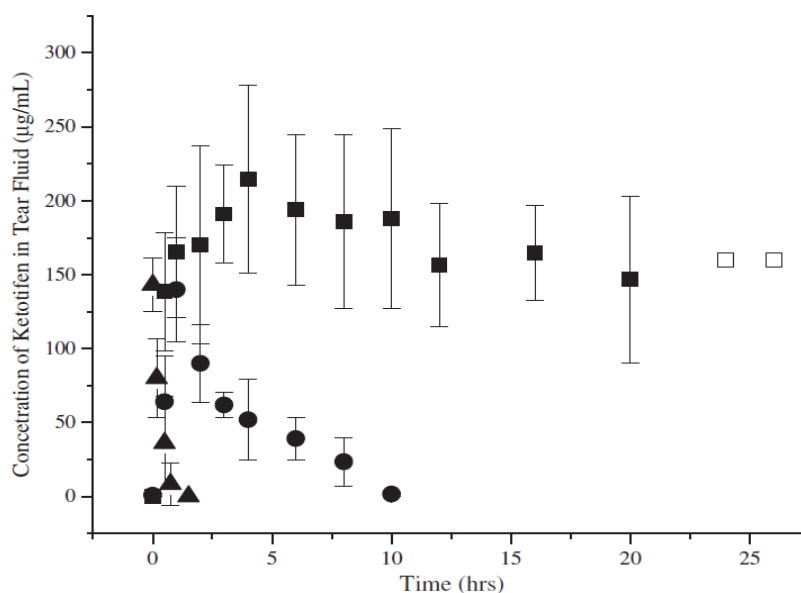


Figure 1.47. *In vivo* ketotifen fumarate tear fluid concentration profile from contact lenses and topical eye drops in a white New Zealand rabbit. Dynamic ketotifen fumarate release from poly(HEMA-co-AA-co-AaM-co-NVP-co-PEG200DMA) contact lenses, Imprinted (■, □) and non-imprinted (●) (lens details: 100 ± 5 μm thickness, diameter 11.8 mm, loaded at 0.3 mg/mL ketotifen). Release from one eye drop (0.035% solution Zaditor® Novartis) (▲). Reproduced from Tieppo et al., 2012.

As a general conclusion, the implementation of imprinted hydrogel for ocular disease treatment has a huge potential in terms of controlled released and increased bioavailability. Careful optimization of the preparation methods could improve the loading capacity of the imprinted materials, an aspect which still remains a challenge for the real-time application of MIPs in drug delivery and therapeutics.

II.5 New application areas: MIPs for proteomics and imaging

Nowadays, several new applications areas for MIP have been identified such as in proteomics and imaging. MIPs labeled with various fluorophores such as organic dyes and quantum dots could selectively target cells and tissues, allowing their bioimaging. MIPs for proteomics should be extremely competitive over the typically applied antibodies concerning performance, simplicity and cost-efficiency.

II.5.1. Proteomics

Targeted proteomics has recently become increasingly popular because of its ability to quantify selected proteins in a complex biological medium (Doerr, 2010). The primary advantage of targeted proteomics is the ability to quantify proteins in a more accurate manner with high sensitivity, high selectivity and wide dynamic ranges. Proteomics can be an important diagnostic tool for *in vitro* clinical

diagnostics and as such, it should provide reliable results and meet the performance criteria in terms of accuracy and sensitivity (Vitzhum et al., 2005).

Several methods can be applied for the quantification of proteome, such as Western blot analysis and ELISA. However, poor specificity and reproducibility is observed. In this respect, liquid chromatography coupled with tandem mass spectrometry (LC-MS/MS)-based targeted proteomics proved to be an alternative option. Importantly, an enrichment step is required to prior analysis, and to that end MIPs can be an interesting approach. However, the application of MIPs for the imprinting of large macromolecules such as proteins is not an easy task and several issues must be tackled. The major obstacles to protein imprinting include the acquisition of pure protein templates, the sensitivity of the three-dimensional structures of proteins to harsh conditions, the restricted transfer of proteins, and the insolubility of proteins in the typical polymerization mixtures used for imprinting (Liu et al., 2014). For the imprinting of proteins the "epitope approach" is often applied (refer also to section 1.3.1).

An interesting application of MIPs in targeted proteomics was reported by Liu et al., 2015, who developed an LC-MS/MS targeted proteomics assay coupled with MIPs for the enrichment and quantification of the soluble transferrin receptor protein (sTfR) in human serum samples. sTfR, an important biomarker in cancer diagnosis and treatment, is a transmembrane protein consisting of two 760-amino acid glycoprotein monomers linked by two disulfide bridges to form a dimer of approximately 190 kDa. The amount of this protein in the serum is at low $\mu\text{g/mL}$ range, thus an enrichment step is required prior to proteomic analysis. To that end, a modified molecular imprinting strategy that recognizes the proteolytic peptides of the protein instead of the whole protein is adopted. This method features the selection of a surrogate peptide VK13 (with the amino acid sequence VEYHFLSPYVSPK), the most abundant sTfR peptide, based on the response in LC-MS/MS analysis (Figure 1.48A). For the MIP synthesis and to prevent potential template bleeding, a corresponding dummy peptide that mimics the structure of the VK13 peptide was synthesized having a leucine substitution for valine at position 1 of VK13. Different functional monomers and cross-linkers were tested and the best results in terms of adsorption capacity were obtained using MAA and EGDMA in methanol with a molar ratio of 1:8:40 (template/monomer/crosslinker). The designed MIP, coupled with LC-MS/MS-based targeted proteomics was successfully used for quantification of sTfR in breast cancer patients and healthy volunteers. By employing standard addition analysis, serum samples (depleted of 14 highly abundant proteins using IgY spin columns with 95 % accuracy) were spiked with five different amounts of surrogate peptide in the range of 0–80 ng/mL providing calibration curves with a good linearity (Figure 1.48B). Based on these calibration curves, the levels of sTfR were determined, namely $1.59 \pm 0.36 \mu\text{g/mL}$ (range: 0.96–2.34 $\mu\text{g/mL}$) in the volunteers and $1.82 \pm 0.42 \mu\text{g/mL}$ (range: 0.95–2.47 $\mu\text{g/mL}$) in breast cancer patients, lower than those reported by ELISA (Figure 1.48C). Importantly, the MIP enrichment step rendered feasible the detection and quantification of

the low concentration levels of sTfR in breast cancer patients after chemotherapy (LOD around 0.95 $\mu\text{g}/\text{mL}$).

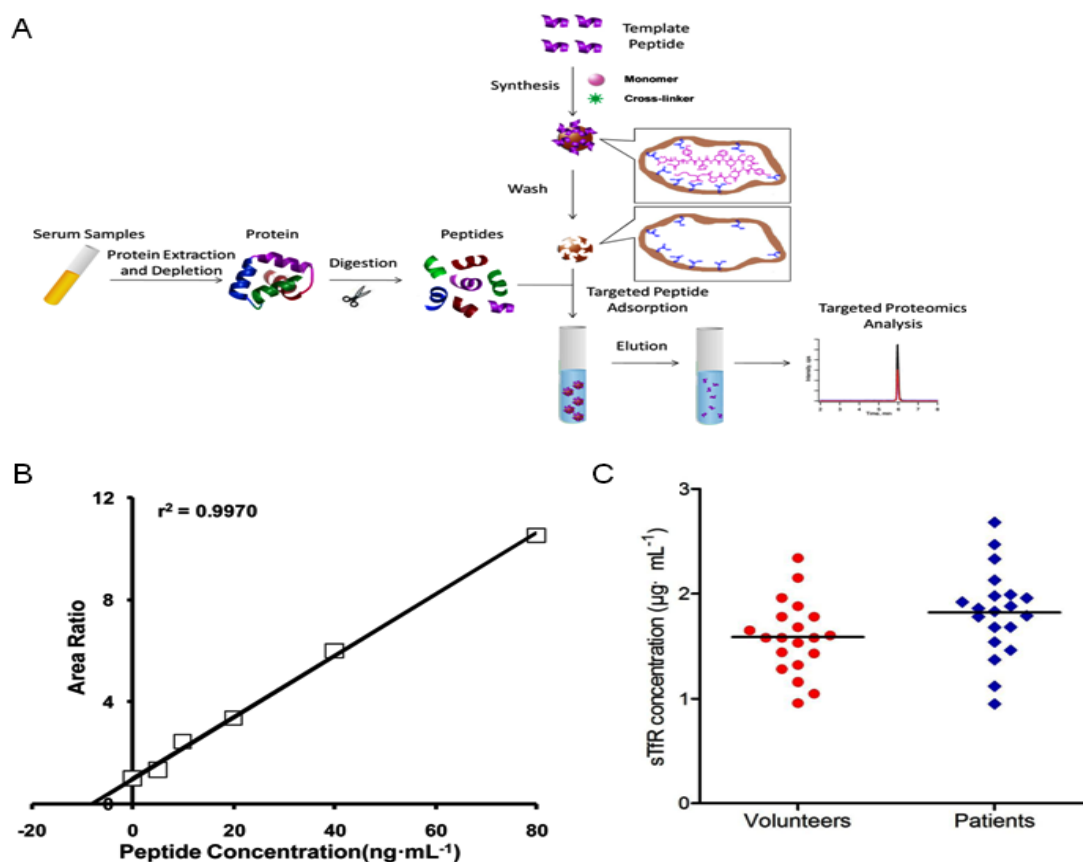


Figure 1.48. A) Schematic representation of MIP preparation and its combination with targeted proteomics for the quantification of sTfR protein. The prepared MIPs could recognize and enrich the peptide VK13, followed by LC-MS/MS-based targeted proteomics analysis; B) Representative standard addition analysis curve of VK13 in clinical samples. C) sTfR levels in breast cancer patients and healthy volunteers. Adapted from Liu et al., 2015.

In another example of MIPs utilized in proteomics, Piletsky and co-workers prepared imprinted hydrophilic polyacrylamide (PAA) membranes templated with bovine serum albumin (BSA) to remove albumin from human serum (Bossi et al., 2007). The PAA gels were prepared with AAm as functional monomer and BIS as cross-linker in supporting films for electrophoresis using ammonium persulfate and TEMED for 2 h at ambient temperature. The template, BSA, was subsequently added at concentrations of 0.5, 1, 3, and 10 mg/mL to the monomer and was removed by washing with water. The structural properties and recognition abilities of the materials formed were evaluated by studying the electrically driven transport of various proteins through these membranes. Interestingly, it was observed that BSA and proteins with structural properties similar to those of the template are always transported through the template membrane faster than other proteins. This preferential migration was referred to as ‘gate effect’ and is dependent on the size of the proteins and pore distribution of the membrane. The unique permeation properties of the

templated PAA membranes were further exploited for the selective removal of albumin, which is predominant (50-70% of total proteins) from human serum. Thus, two-dimensional electrophoresis of albumin serum showed a significant reduction of the albumin spot upon PAA membrane treatment of the sample (Figure 1.49). In conclusion, the removal of albumin by the MIP PAA membranes allows to increase the resolution of proteomic analysis and can potentially improve the detection of low-expressed proteins.

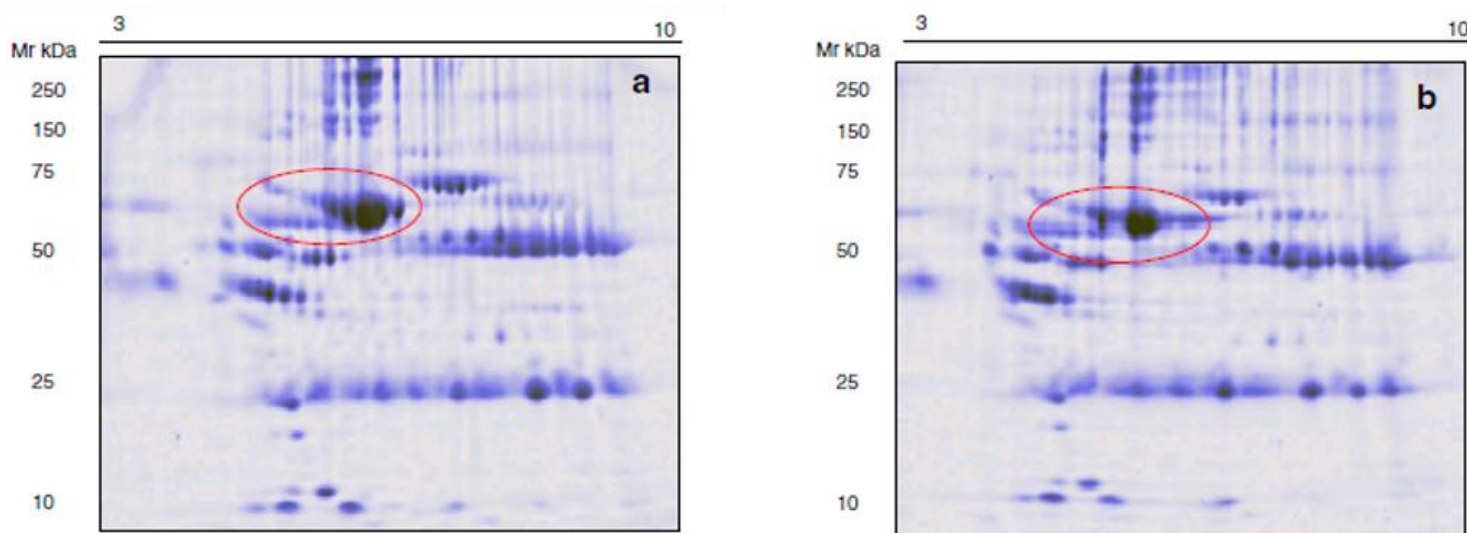


Figure 1.49. Two-dimensional electrophoresis of serum subjected to electrodepletion of albumin (b) and control serum (a). Reproduced from Bossi et al., 2007.

Proteomics applications not only include the analysis and quantification of proteins but also peptide sequences. MIP based proteomic analysis of peptides was exemplified by Chen et al., 2015b, who reported a fast and simple approach for selective phosphopeptide capture and enrichment (Figure 1.50). A phosphotyrosine imprinted polymer (pY-MIP) was used to selectively enrich tyrosine-phosphorylated peptides spiked at low levels into proteolytic digests with only minor cross-reaction with pS peptides. The synthesis of pY-MIP was based on the urea monomer capable of strong stoichiometric interactions with oxyanions such as phospho groups (refer also to section I.5.1). By employing the aforementioned pY MIP as sorbent on a SPE column, several phosphopeptides could be identified by nanoLC-ESI-MS/MS from clinical relevant samples, such as whole-cell lysate from human embryonic kidney (HEK) 293T cells, human neuroblastoma SH-SY5Y cells, mouse brain or human cerebrospinal fluid (CSF) (Figure 1.46B) Remarkably, the combined application of pY MIPs SPE column after pre-fractionation of trypsinized proteins by strong cation exchange (SCX) column, resulted in the increase of the identified phosphopeptides by 4-fold compared to the TiO_2 in HEK cell lysate and by 2-fold in human CFS tryptic digests.

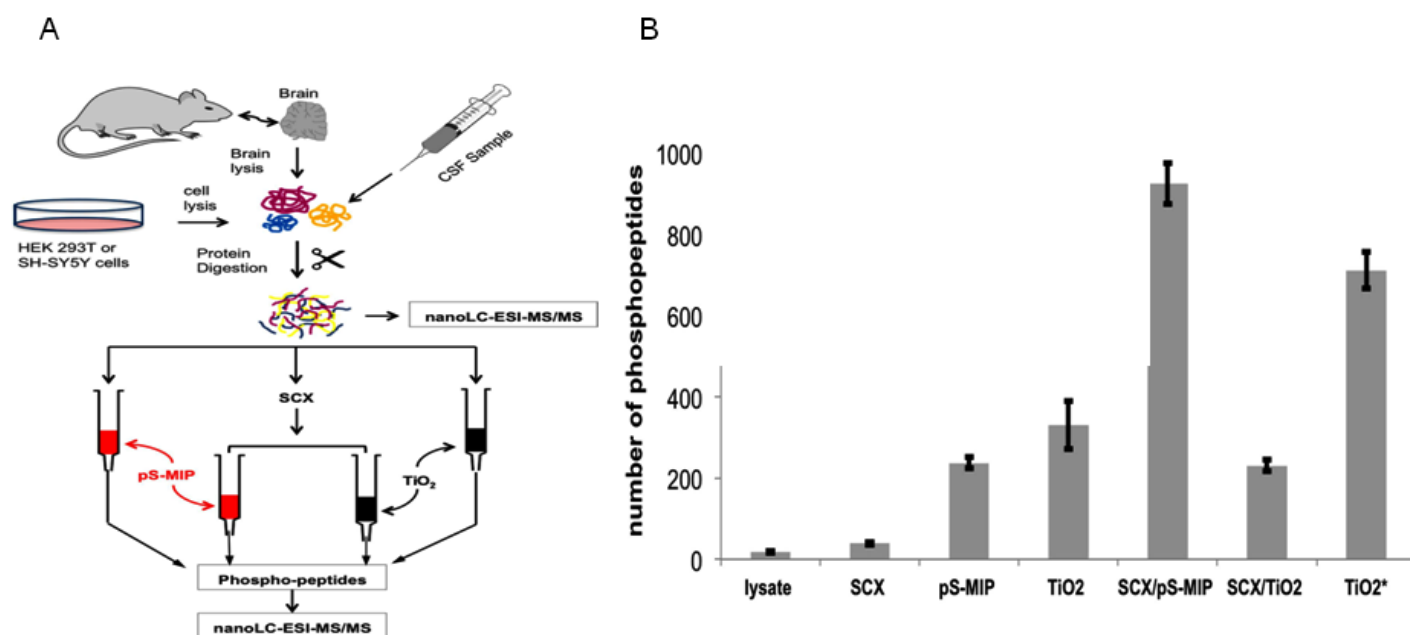


Figure 1.50. A) Work flow for phosphoproteomic analysis of harvested HEK 293T cells, mouse brain or CSF using SCX fractionation followed by pS-MIP or TiO₂ enrichment. Samples of cell lysate or CSF tryptic digests were loaded before or after pre-fractionation with SCX onto pS-MIP or TiO₂ columns for phosphospecific enrichment; B) Mean number of phosphopeptides (bar graph) identified in 10 μ g or 100 μ g (TiO₂*) of a tryptic digest of HEK 293T cell lysate by nanoLC-ESI-MS/MS analysis of a sample (lysate) before or after fractionation by SCX chromatography, pS-MIP SPE, TiO₂ SPE or SCX followed by pS-MIP or TiO₂ SPE as indicated. Adapted from Chen et al., 2015b.

II.5.2. Imaging

Advances in clinical diagnostics require the development of efficient bioimaging techniques, that can facilitate the early prognosis and treatment of diseases such as cancer (Van Dam et al., 2011). Much effort has been devoted in optimizing the imaging modalities, so as to achieve targeted localization of specific biomarkers expressed on cells and tumors. The implication of nanomaterials for improving the existing diagnostic and therapeutic techniques can be very promising (Janib et al., 2010; Lee et al., 2012), nevertheless it is essential to consider the potential cytotoxic effect of such materials, especially at nanosized range (Choi et al., 2010). Recently, interest is raised for applications of MIPs as selective receptors for targeted cell and tissue imaging. MIPs, as imaging probes, present a number of advantages such as easy functionalization with fluorescent dyes and quantum dots and tailored size (Kunath et al., 2015). As with any material used in biological applications, issues related to biocompatibility and toxicity should be thoroughly addressed.

Early applications of MIPs combined with imaging techniques concerned only the detection of small molecules and proteins in batch mode. However, recent advances in molecular imprinting potential expanded the MIP application areas, which now feature MIP-based imaging in cancer cell and tissues. This indicates an extensive effort to design efficient MIPs as selective receptors of biomarkers expressed on cells

and tissues, which requires their outstanding recognition in complex matrices. Lately, a few interesting studies prove the feasibility of MIPs as imaging tools for *in vivo* applications.

The first *in vivo* application of MIPs for imaging was reported by Shea and co-workers (Hoshino et al., 2010) for the recognition of the toxic peptide melittin from the blood stream of leaving mice. They synthesized a water compatible MIP using NIPAm, TBAAm and AA as functional monomers and BIS as cross-linker. Successful recognition in such complex matrix was achieved based on a synergistic effect of ionic and hydrophobic interactions. To observe distribution of melittin and MIP NPs in mice tissues and organs, melittin was labeled with the fluorescent dye (Cy-5) at the ϵ amine of an additional lysine on the *N*-terminal and MIP NPs were labeled with radioisotope (^{14}C) or the fluorescent dye (fluorescein) by copolymerization MIP NPs with ^{14}C -enriched acrylamide (5 mol%) or fluorescein *o*-acrylate (1 mol%). *In vivo* fluorescent imaging on live mice demonstrated that the MIP NPs significantly altered the biodistribution of melittin, as deduced by the decrease of the fluorescent intensity of Cy5-melittin immediately after administration of MIPNPs (Figure 1.51A). Furthermore, confocal microscopy was performed to study the distribution of MIP NPs and melittin along the *z*-axis, showing that both MIP NPs (labeled by fluorescein) and Cy5-melittin were captured together in the same cells (macrophages) 10 min after injection of melittin and the NPs (Figure 1.51B). Put together, these results demonstrate the great potential of MIPs as tools for bioimaging in complex biological samples and tissues and pave the way for further applications in clinical diagnostics and theranostics.

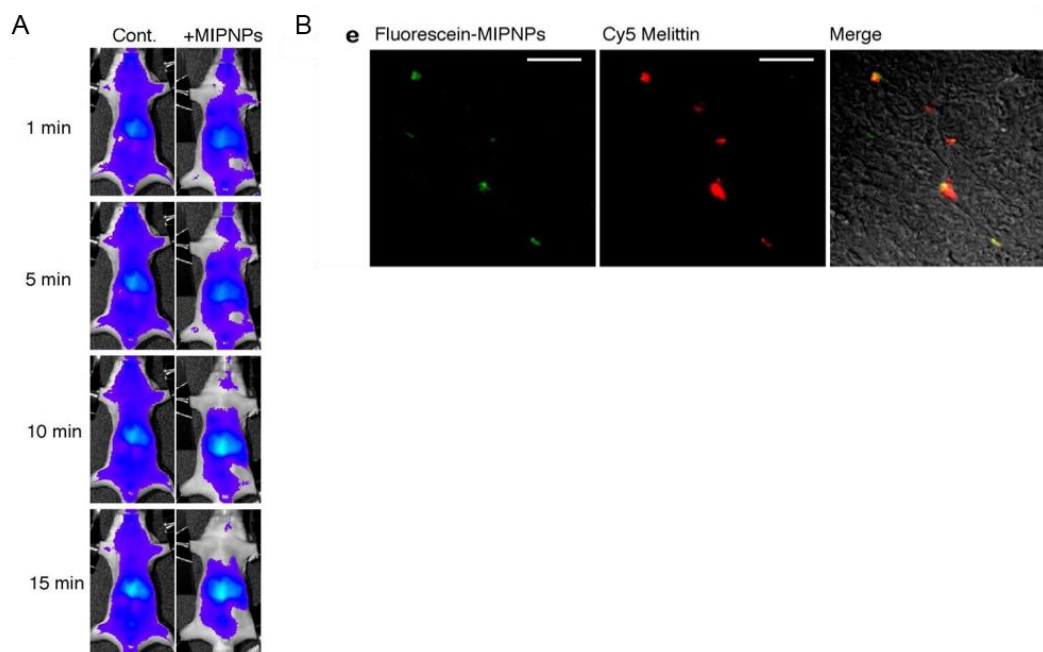


Figure 1.51. Biodistribution of melittin and NPs; A) Fluorescent images of Cy5-melittin after intravenous injection of Cy5-melittin (1 mg/kg), 27 mg/kg of MIPNPs was injected 20 seconds after the injection of melittin (right); B) Fluorescence histology images of the liver (Cy5-melittin 0.3 mg/kg and 10 mg/kg of MIP NPs). Green; Cy5-melittin, red; fluorescein-MIPNPs. The scale bars; 25 μm . Adapted from Hoshino et al., 2010).

More recently, our group has reported for the first time the use of fluorescently labeled MIPs for the localization and quantification of glycosylations on fixed and living cells as well as on skin tissue (Kunath et al., 2015). In this study, hyaluronan was employed as a model to prove that MIPs can be applied as a specific staining material for glycosylations. The target molecule of these glycosylations, glucuronic acid, is abundant on the surface of cells such as keratinocytes in the form of hyaluronan as part of the glycocalix. The measurement of hyaluronan levels in blood is clinically relevant for the assessment of the degree of liver fibrosis and cirrhosis in chronic liver disease. Thus, polymers imprinted with glucuronic acid (GA) were synthesized in DMSO using AB and MAM and to impart fluorescence a polymerizable rhodamine derivative was added in the prepolymerization mixture. The resulting fluorescently-labelled MIPs could specifically bind at the terminal glucuronic acid of hyaluronan, localized on the keratinocyte cells (HaCaT) and skin tissue. More specifically, confocal images performed on HaCaT cells (sample prepared in PBS) showed that the red fluorescent MIP particles are localized only on the cell surface due to specific binding to hyaluronan (Figure 1.52A). Moreover, it was demonstrated that the MIP particles are mainly localized on the basal lane of papillary dermis on skin tissues, in agreement with the reports in the literature concerning hyaluronan localization (Figure 1.52B).

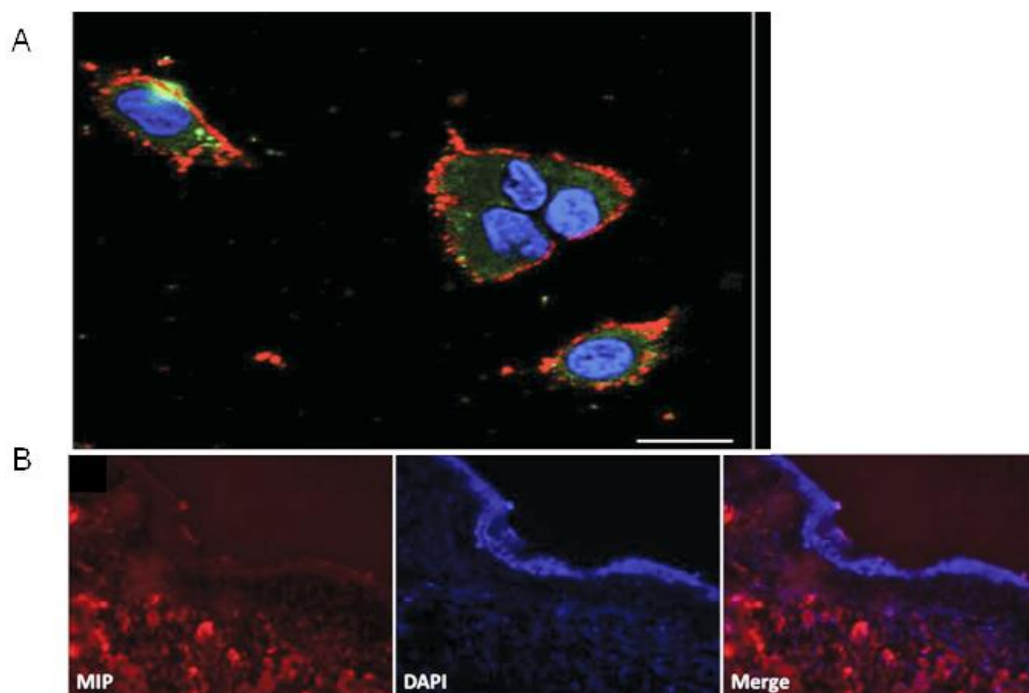


Figure 1.52. A) Confocal microscopy image of MIP-stained human keratinocytes (HaCaT). Merge image of three color channels: DAPI blue signal (cell nucleus), 3,3'-dioctadecyloxycarbocyanineperchlorate (DiO) green signal (cell membrane), rhodamine red signal (MIPs). Scale bar: 20 μm ; B) Human skin specimens stained with MIPs. Scale bar: 100 μm . Adapted from Kunath et al., 2015.

Another example which describes the targeting of glycosylation sites, was reported by Yin et al., 2015, who prepared sialic acid-imprinted MIP nanoparticles for the selective imaging of cancer cells and

tissues, based on SERS spectroscopy. Briefly, Raman-active silver nanoparticles were first prepared as a signal reporting core and the template sialic acid was imprinted into a thin shell using boronic acid functionalities via surface imprinting (Figure 1.53A.) The sialic acid-imprinted SERS nanotags were able to differentiate cancer cells and tissues from normal cells and tissues (Figure 1.53B). In a very recent study, Wang and co-workers prepared fluorescent silica NPs with a monosaccharide-imprinted shell for the specific targeting and imaging of cancer cells (Wang et al., 2016), while in our group multiplexed imaging of glycosylations in keratinocytes was achieved, by MIP-coated quantum dots imprinted with glucuronic acid and *N*-acetylneuraminic acid (sialic acid) (Panagiotopoulou et al., 2016).

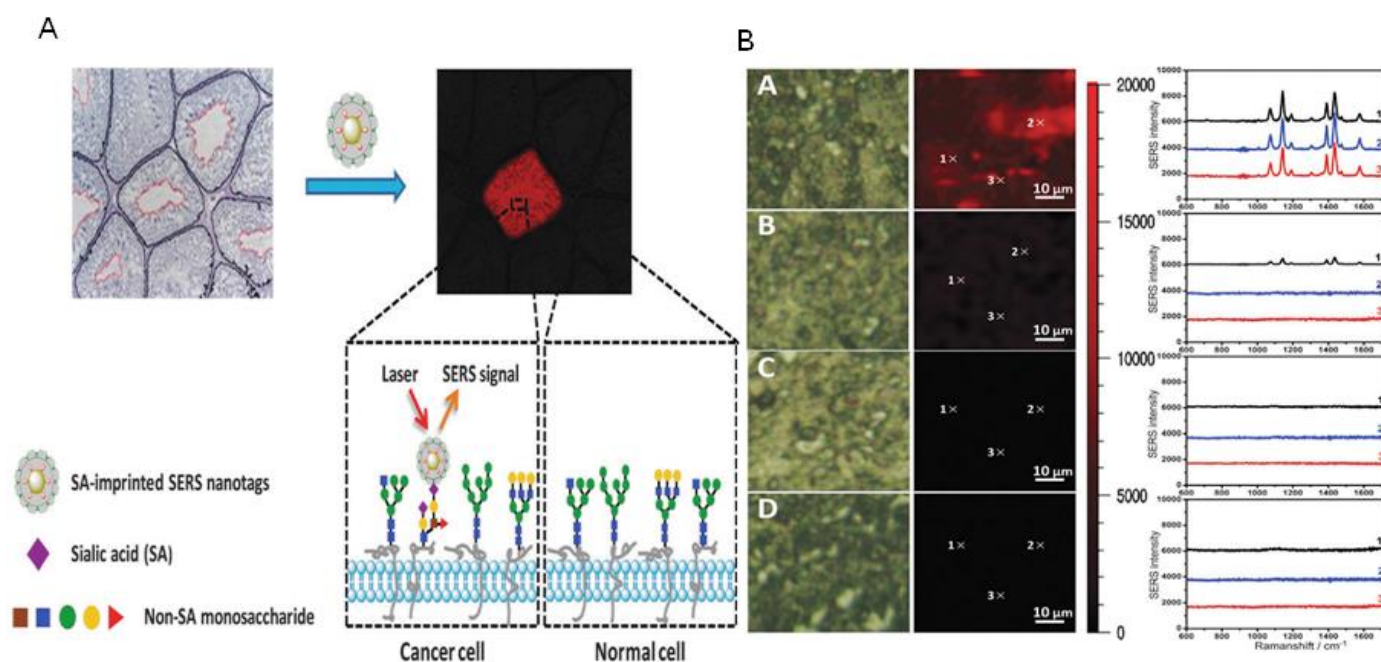


Figure 1.53. A) Schematic representation of SERS imaging of cancer cells and tissues via sialic acid-imprinted nanotags. B) SERS imaging of cancer and normal liver tissues (A) cancer liver tissue after incubation with sialic acid-imprinted SERS nanotags; (B) normal liver tissue after incubation with sialic acid-imprinted SERS nanotags; (C) cancer liver tissue after incubation with non-imprinted SERS nanotags; and (D) normal liver tissue after incubation with non-imprinted SERS nanotags. Columns from left to right: bright field, SERS image and representative SERS spectra at three locations on tissue surfaces as indicated by the symbol *x*. Adapted from Yin et al., 2015.

III. Conclusions

In this chapter, the history and diverse applications of molecularly imprinted polymers were presented with emphasis on their recognition properties in complex aqueous samples, which is the subject of this thesis. Recent advances concerning the use of MIPs as selective receptors in many application areas such as separation, biosensing, proteomics and drug delivery were discussed through numerous examples. Special importance was given on the current approaches to improve the water compatibility of MIPs,

although it must be noted that this field is the focus of constant efforts of optimization. Still, an important progress is achieved in the last years and several studies highlight the use of MIPs as promising synthetic substitutes for biological receptors in complex samples with real-world applications such as food safety, environmental analysis, clinical diagnostics and theranostics.

In the following chapters, the development of water compatible MIPs for cosmetic and food applications will be presented. In these experimental chapters, we aimed to design a novel generation of MIPs with improved selectivities in highly complex aqueous environments, which should be applicable to food, cosmetic and biotechnological areas.

IV. References

[A]

Adali-Kaya, Z.; Tse Sum Bui, B.; Falcimaigne-Cordin, A.; Haupt, K., Molecularly imprinted polymer nanomaterials and nanocomposites: Atom-transfer radical polymerization with acidic monomers. *Angewandte Chemie International Edition* **2015**, *54*, 5192-5195.

Augusto, F., Hantao, L. W. Mogollón, N. G. S., Braga, S. C. G. N., New materials and trends in sorbents for solid-phase extraction. *TrAC Trends in Analytical Chemistry* **2013**, *43*, 14623.

Alexander, C.; Andersson, H. S.; Andersson, L. I.; Ansell, R. J.; Kirsch, N.; Nicholls, I. A.; O'Mahony, J.; Whitcombe, M. J. Molecular imprinting science and technology: a survey of the literature for the years up to and including 2003. *Journal of Molecular Recognition* **2006**, *19*, 106.

Ali, W. H.; Derrien, D.; Alix, F.; Pérollier, C.; Lépine, O.; Bayouhd, S.; Chapuis-Hugon, F.; Pichon, V., Solid-phase extraction using molecularly imprinted polymers for selective extraction of a mycotoxin in cereals. *Journal of Chromatography A* **2010**, *1217* (43), 6668-6673.

Allender, C. J.; Richardson, C.; Woodhouse, B.; Heard, C. M.; Brain, K. R., Pharmaceutical applications for molecularly imprinted polymers. *International Journal of Pharmaceutics* **2000**, *195* (1-2), 39-43.

Altintas, Z.; Gittens, M.; Guerreiro, A.; Thompson, K.-A.; Walker, J.; Piletsky, S.; Tothill, I. E., Detection of waterborne viruses using high affinity molecularly imprinted polymers. *Analytical Chemistry* **2015**, *87* (13), 6801-6807.

Alvarez-Lorenzo, C.; Hiratani, H.; Gómez-Amoza, J. L.; Martínez-Pacheco, R.; Souto, C.; Concheiro, A., Soft contact lenses capable of sustained delivery of timolol. *Journal of Pharmaceutical Sciences* **2002**, *91* (10), 2182-2192.

Alvarez-Lorenzo, C.; Concheiro, A., Molecularly imprinted polymers for drug delivery. *Journal of Chromatography B* **2004**, *804* (1), 231-245.

Alvarez-Lorenzo, C.; Yañez, F.; Barreiro-Iglesias, R.; Concheiro, A., Imprinted soft contact lenses as norfloxacin delivery systems. *Journal of Controlled Release* **2006**, *113* (3), 236-244.

Ambrosini, S.; Shinde, S.; De Lorenzi, E.; Sellergren, B., Glucuronide directed molecularly imprinted solid-phase extraction: isolation of testosterone glucuronide from its parent drug in urine. *Analyst* **2012**, *137* (1), 249-254.

Ambrosini, S.; Beyazit, S.; Haupt, K.; Tse Sum Bui, B., Solid-phase synthesis of molecularly imprinted nanoparticles for protein recognition. *Chemical Communications* **2013**, *49* (60), 6746-6748.

Andersson, L.; Sellergren, B.; Mosbach, K. Imprinting of amino acid derivatives in macroporous polymers. *Tetrahedron letters* **1984**, *25*, 5211.

Andersson, L. I. Application of molecular imprinting to the development of aqueous buffer and organic solvent based radioligand binding assays for (S)-propranolol. *Analytical Chemistry* **1996**, *68*, 111.

Andersson, H. S.; Nicholls, I. A. A historical perspective of the development of molecular imprinting. *Techniques and Instrumentation in Analytical Chemistry* **2000**, *23*, 1.

Ansell, R. J., Molecularly imprinted polymers in pseudoimmunoassay. *Journal of Chromatography B* **2004**, *804* (1), 151-165.

Arshady, R.; Mosbach, K., Synthesis of substrate-selective polymers by host-guest polymerization. *Die Makromolekulare Chemie* **1981**, *182* (2), 687-692.

[B]

Bai, W.; Spivak, D. A., A double-imprinted diffraction-grating sensor based on a virus-responsive superaptamer hydrogel derived from an impure extract. *Angewandte Chemie International Edition* **2014**, *53* (8), 2095-2098.

Barahona, F.; Turiel, E.; Cormack, P. A. G.; Martín-Esteban, A., Synthesis of core-shell molecularly imprinted polymer microspheres by precipitation polymerization for the inline molecularly imprinted solid-phase extraction of thiabendazole from citrus fruits and orange juice samples. *Journal of Separation Science* **2011**, *34* (2), 217-224.

Barner-Kowollik, C.; Perrier, S., The future of reversible addition fragmentation chain transfer polymerization. *Journal of Polymer Science Part A: Polymer Chemistry* **2008**, *46* (17), 5715-5723.

Benito-Peña, E.; Urraca, J. L.; Sellergren, B.; Moreno-Bondi, M. C., Solid-phase extraction of fluoroquinolones from aqueous samples using a water-compatible stoichiometrically imprinted polymer. *Journal of Chromatography A* **2008**, *1208* (1-2), 62-70.

Benito-Peña, E.; Martins, S.; Orellana, G.; Moreno-Bondi, M. C., Water-compatible molecularly imprinted polymer for the selective recognition of fluoroquinolone antibiotics in biological samples. *Analytical and Bioanalytical Chemistry* **2009**, *393* (1), 235-245.

Benito-Peña, E.; González-Vallejo, V.; Rico-Yuste, A.; Barbosa-Pereira, L.; Cruz, J. M.; Bilbao, A.; Alvarez-Lorenzo, C.; Moreno-Bondi, M. C., Molecularly imprinted hydrogels as functional active packaging materials. *Food Chemistry* **2016**, *190*, 487-494.

Berczki, A.; Tolokán, A.; Horvai, G.; Horváth, V.; Lanza, F.; Hall, A. J.; Sellergren, B., Determination of phenytoin in plasma by molecularly imprinted solid-phase extraction. *Journal of Chromatography A* **2001**, *930* (1-2), 31-38.

Beyazit, S.; Tse Sum Bui, B.; Haupt, K.; Gonzato, C., Molecularly imprinted polymer nanomaterials and nanocomposites by controlled/living radical polymerization. *Progress in Polymer Science* **2016**, *62*, 1-21.

Biffis, A.; Dvorakova, G.; Falcimaigne-Cordin, A., Physical Forms of MIPs. In *Molecular Imprinting*, Haupt, K., Ed. Springer Berlin Heidelberg: Berlin, Heidelberg, **2012**; pp 29-82.

Bompart, M.; Haupt, K., Molecularly imprinted polymers and controlled/living radical polymerization. *Australian Journal of Chemistry* **2009**, *62* (8), 751-761.

Bompart, M.; De Wilde, Y.; Haupt, K., Chemical nanosensors based on composite molecularly imprinted polymer particles and surface-enhanced raman scattering. *Advanced Materials* **2010**, *22* (21), 2343-2348.

Bossi, A.; Bonini, F.; Turner, A. P. F.; Piletsky, S. A., Molecularly imprinted polymers for the recognition of proteins: The state of the art. *Biosensors and Bioelectronics* **2007a**, *22* (6), 1131-1137.

Bossi, A.; Andreoli, M.; Bonini, F.; Piletsky, S., 'Gate effect' in templated polyacrylamide membranes influences the electrotransport of proteins and finds applications in proteome analysis. *Analytical and Bioanalytical Chemistry* **2007b**, *389* (2), 447-454.

Brüggemann, O.; Haupt, K.; Ye, L.; Yilmaz, E.; Mosbach, K., New configurations and applications of molecularly imprinted polymers. *Journal of Chromatography A* **2000**, *889* (1-2), 15-24.

[C]

Caceres, C.; Canfarotta, F.; Chianella, I.; Pereira, E.; Moczko, E.; Esen, C.; Guerreiro, A.; Piletska, E.; Whitcombe, M. J.; Piletsky, S. A., Does size matter? Study of performance of pseudo-ELISAs based on molecularly imprinted polymer nanoparticles prepared for analytes of different sizes. *Analyst* **2016**, *141* (4), 1405-1412.

Çakir, P.; Cutivet, A.; Resmini, M.; Tse Sum Bui, B.; Haupt, K., Protein-size molecularly imprinted polymer nanogels as synthetic antibodies, by localized polymerization with multi-initiators. *Advanced Materials* **2013**, *25* (7), 1048-1051.

Caro, E.; Marcé, R. M.; Cormack, P. A. G.; Sherrington, D. C.; Borrull, F., Molecularly imprinted solid-phase extraction of naphthalene sulfonates from water. *Journal of Chromatography A* **2004**, *1047* (2), 175-180.

Castell, O. K.; Allender, C. J.; Barrow, D. A., Novel biphasic separations utilising highly selective molecularly imprinted polymers as biorecognition solvent extraction agents. *Biosensors and Bioelectronics* **2006**, *22* (4), 526-533.

Castro López, M. d. M.; Cela Pérez, M. C.; Dopico García, M. S.; López Vilariño, J. M.; González Rodríguez, M. V.; Barral Losada, L. F., Preparation, evaluation and characterization of quercetin-molecularly imprinted polymer for preconcentration and clean-up of catechins. *Analytica Chimica Acta* **2012**, *721* (0), 68-78.

Cela-Pérez, M. C.; Bates, F.; Jiménez-Morigosa, C.; Lendoiro, E.; de Castro, A.; Cruz, A.; López-Rivadulla, M.; López-Vilariño, J. M.; González-Rodríguez, M. V., Water-compatible imprinted pills for sensitive determination of cannabinoids in urine and oral fluid. *Journal of Chromatography A* **2016**, *1429*, 53-64.

Cenci, L.; Anesi, A.; Busato, M.; Guella, G.; Bossi, A. M., Molecularly imprinted polymers coupled to matrix assisted laser desorption ionization mass spectrometry for femtomoles detection of cardiac troponin I peptides. *Journal of Molecular Recognition* **2016**, 29 (1), 41-50.

Chapuis, F.; Mullet, J.-U.; Pichon, V.; Tuffal, G.; Hennion, M.-C., Molecularly imprinted polymers for the clean-up of a basic drug from environmental and biological samples. *Journal of Chromatography A* **2006**, 1135 (2), 127-134.

Chen, H.; Yuan, D.; Li, Y.; Dong, M.; Chai, Z.; Kong, J.; Fu, G., Silica nanoparticle supported molecularly imprinted polymer layers with varied degrees of crosslinking for lysozyme recognition. *Analytica Chimica Acta* **2013**, 779, 82-89.

Chen, W.; Ma, Y.; Pan, J.; Meng, Z.; Pan, G.; Sellergren, B., Molecularly imprinted polymers with stimuli-responsive affinity: Progress and perspectives. *Polymers* **2015a**, 7 (9), 1478.

Chen, J.; Shinde, S.; Koch, M.-H.; Eisenacher, M.; Galozzi, S.; Lerari, T.; Barkovits, K.; Subedi, P.; Krüger, R.; Kuhlmann, K.; Sellergren, B.; Helling, S.; Marcus, K., Low-bias phosphopeptide enrichment from scarce samples using plastic antibodies. *Scientific Reports* **2015b**, 5, 11438.

Chianella, I.; Lotierzo, M.; Piletsky, S. A.; Tothill, I. E.; Chen, B.; Karim, K.; Turner, A. P. F., Rational design of a polymer specific for microcystin-LR using a computational approach. *Analytical Chemistry* **2002**, 74 (6), 1288-1293.

Chianella, I.; Guerreiro, A.; Moczko, E.; Caygill, J. S.; Piletska, E. V.; De Vargas Sansalvador, I. M. P.; Whitcombe, M. J.; Piletsky, S. A., Direct replacement of antibodies with molecularly imprinted polymer nanoparticles in ELISA—Development of a novel assay for vancomycin. *Analytical Chemistry* **2013**, 85 (17), 8462-8468.

Choi, H. S.; Liu, W.; Liu, F.; Nasr, K.; Misra, P.; Bawendi, M. G.; Frangioni, J. V., Design considerations for tumour-targeted nanoparticles. *Nature Nanotechnology* **2010**, 5 (1), 42-47.

Cobb, Z.; Sellergren, B.; Andersson, L. I., Water-compatible molecularly imprinted polymers for efficient direct injection on-line solid-phase extraction of ropivacaine and bupivacaine from human plasma. *Analyst* **2007**, 132 (12), 1262-1271.

Cormack, P. A. G.; Elorza, A. Z., Molecularly imprinted polymers: synthesis and characterization. *Journal of Chromatography B* **2004**, 804 (1), 173-182.

Cutivet, A.; Schembri, C.; Kovensky, J.; Haupt, K., Molecularly imprinted microgels as enzyme inhibitors. *Journal of the American Chemical Society* **2009**, 131 (41), 14699-14702.

[D]

da Silva, M. S.; Nobrega, F. L.; Aguiar-Ricardo, A.; Cabrita, E. J.; Casimiro, T., Development of molecularly imprinted co-polymeric devices for controlled delivery of flufenamic acid using supercritical fluid technology. *The Journal of Supercritical Fluids* **2011**, 58 (1), 150-157.

Doerr, A., Targeted proteomics. *Nature Methods* **2010**, 7 (1), 34-34.

Díaz-García, E. M.; Laínño, B. R., Molecular imprinting in sol-gel materials: Recent developments and applications. *Microchimica Acta* **2005**, 149 (1), 19-36.

Dzygiel, P.; O'Donnell, E.; Fraier, D.; Chassaing, C.; Cormack, P. A. G., Evaluation of water-compatible molecularly imprinted polymers as solid-phase extraction sorbents for the selective extraction of sildenafil and its desmethyl metabolite from plasma samples. *Journal of Chromatography B* **2007**, *853* (1–2), 346-353.

[E]

Emgenbroich, M.; Borrelli, C.; Shinde, S.; Lazraq, I.; Vilela, F.; Hall, A. J.; Oxelbark, J.; DeLorenzi, E.; Courtois, J.; Simanova, A.; Verhage, J.; Irgum, K.; Karim, K.; Sellergren, B., A phosphotyrosine-imprinted polymer receptor for the recognition of tyrosine phosphorylated peptides. *Chemistry – A European Journal* **2008**, *14* (31), 9516-9529.

Ehrenstein, M. R.; Notley, C. A., The importance of natural IgM: scavenger, protector and regulator. *Nature Reviews Immunology* **2010**, *10* (11), 778-786.

[F]

Fang, G.; Wang, H.; Yang, Y.; Liu, G.; Wang, S., Development and application of a quartz crystal microbalance sensor based on molecularly imprinted sol-gel polymer for rapid detection of patulin in foods. *Sensors and Actuators B: Chemical* **2016**, *237*, 239-246.

Farokhzad, O. C.; Langer, R., Impact of nanotechnology on drug delivery. *ACS Nano* **2009**, *3* (1), 16-20.

Figueiredo, L.; Erny, G. L.; Santos, L.; Alves, A., Applications of molecularly imprinted polymers to the analysis and removal of personal care products: A review. *Talanta* **2016**, *146*, 754-765.

Fuchs, Y.; Soppera, O.; Haupt, K., Photopolymerization and photostructuring of molecularly imprinted polymers for sensor applications—A review. *Analytica Chimica Acta* **2012**, *717*, 7-20.

[G]

Ge, Y.; Turner, A. P. F., Too large to fit? Recent developments in macromolecular imprinting. *Trends in Biotechnology* **2008**, *26* (4), 218-224.

Ge, Y.; Akhtar, S.; Mirza, F.; Piletsky, S.; Wang, S.; Fei, D., Molecularly Imprinted Polymers: Promising Advanced Materials for In Vivo Sensing. In *Microelectrode Biosensors*, Marinesco, S.; Dale, N., Eds. Humana Press: Totowa, NJ, **2013**; pp 369-384.

Griffete, N.; Fresnais, J.; Espinosa, A.; Wilhelm, C.; Bee, A.; Menager, C., Design of magnetic molecularly imprinted polymer nanoparticles for controlled release of doxorubicin under an alternative magnetic field in athermal conditions. *Nanoscale* **2015**, *7* (45), 18891-18896.

Gomez-Caballero, A.; Diaz-Diaz, G.; Bengoetxea, O.; Quintela, A.; Unceta, N.; Goicolea, M. A.; Barrio, R. J., Water compatible stir-bar devices imprinted with underivatized glyphosate for selective sample clean-up. *Journal of Chromatography A* **2016**, *1451*, 23-32.

Gonzato, C.; Courty, M.; Pasetto, P.; Haupt, K., Magnetic molecularly imprinted polymer nanocomposites via surface-initiated RAFT polymerization. *Advanced Functional Materials* **2011**, *21* (20), 3947-3953.

Guerreiro, J. R. L.; Bochenkov, V. E.; Runager, K.; Aslan, H.; Dong, M.; Enghild, J. J.; De Freitas, V.; Ferreira Sales, M. G.; Sutherland, D. S., Molecular imprinting of complex matrices at localized surface

plasmon resonance biosensors for screening of global interactions of polyphenols and proteins. *ACS Sensors* **2016**, *1* (3), 258-264.

Güney, O.; Serin, E., Stimuli-responsive molecularly imprinted hybrid polymer gel as a potential system for controlled release. *Journal of Applied Polymer Science* **2016**, *133* (4), 42913-42921

Gupta, V. K.; Yola, M. L.; Eren, T.; Atar, N., Selective QCM sensor based on atrazine imprinted polymer: Its application to wastewater sample. *Sensors and Actuators B: Chemical* **2015**, *218*, 215-221.

[H]

Hall, A. J.; Manesiotis, P.; Emgenbroich, M.; Quaglia, M.; De Lorenzi, E.; Sellergren, B., Urea host monomers for stoichiometric molecular imprinting of oxyanions. *The Journal of Organic Chemistry* **2005**, *70* (5), 1732-1736.

Hao, Y.; Gao, R.; Liu, D.; He, G.; Tang, Y.; Guo, Z., Selective extraction and determination of chlorogenic acid in fruit juices using hydrophilic magnetic imprinted nanoparticles. *Food Chemistry* **2016**, *200*, 215-222.

Haupt, K.; Dzgoev, A.; Mosbach, K., Assay system for the herbicide 2, 4-dichlorophenoxyacetic acid using a molecularly imprinted polymer as an artificial recognition element. *Analytical Chemistry* **1998a**, *70* (3), 628-631.

Haupt, K.; Mayes, A. G.; Mosbach, K., Herbicide assay using an imprinted polymer-based system analogous to competitive fluoroimmunoassays. *Analytical Chemistry* **1998b**, *70* (18), 3936-3939.

Haupt, K.; Noworyta, K.; Kutner, W. Imprinted polymer-based enantioselective acoustic sensor using a quartz crystal microbalance. *Analytical Communications* **1999**, *36*, 391.

Haupt, K.; Mosbach, K., Molecularly imprinted polymers and their use in biomimetic sensors. *Chemical Reviews* **2000**, *100* (7), 2495-2504.

Haupt, K., Molecularly imprinted polymers in analytical chemistry. *Analyst* **2001**, *126* (6), 747-756.

Haupt, K., Peer Reviewed: Molecularly imprinted polymers: The Next Generation. *Analytical Chemistry* **2003a**, *75* (17), 376 A-383 A.

Haupt, K., Imprinted polymers-Tailor-made mimics of antibodies and receptors. *Chemical Communications* **2003b**, (2), 171-178.

Haupt, K.; Linares, A. V.; Bompert, M.; Tse Sum Bui, B., Molecularly Imprinted Polymers. In *Molecular Imprinting*, Haupt, K., Ed. Springer Berlin Heidelberg: Berlin, Heidelberg, **2012**; pp 1-28.

Helling, S.; Shinde, S.; Brosseron, F.; Schnabel, A.; Müller, T.; Meyer, H. E.; Marcus, K.; Sellergren, B., Ultratrace enrichment of tyrosine phosphorylated peptides on an imprinted polymer. *Analytical Chemistry* **2011**, *83* (5), 1862-1865.

Hennink, W. E.; van Nostrum, C. F., Novel crosslinking methods to design hydrogels. *Advanced Drug Delivery Reviews* **2002**, *54* (1), 13-36.

Henry, N.; Delépée, R.; Seigneuret, J.-M.; Agrofoglio, L. A., Synthesis of water-compatible imprinted polymers of in situ produced fructosazine and 2,5-deoxyfructosazine. *Talanta* **2012**, *99*, 816-823.

Hiratani, H.; Alvarez-Lorenzo, C., Timolol uptake and release by imprinted soft contact lenses made of N,N-diethylacrylamide and methacrylic acid. *Journal of Controlled Release* **2002**, 83 (2), 223-230.

Hiratani, H.; Alvarez-Lorenzo, C., The nature of backbone monomers determines the performance of imprinted soft contact lenses as timolol drug delivery systems. *Biomaterials* **2004**, 25 (6), 1105-1113.

Horemans, F.; Weustenraed, A.; Spivak, D.; Cleij, T. J., Towards water compatible MIPs for sensing in aqueous media. *Journal of Molecular Recognition* **2012**, 25 (6), 344-351.

Hoshina, K.; Horiyama, S.; Matsunaga, H.; Haginaka, J., Molecularly imprinted polymers for simultaneous determination of antiepileptics in river water samples by liquid chromatography–tandem mass spectrometry. *Journal of Chromatography A* **2009**, 1216 (25), 4957-4962.

Hoshino, Y.; Koide, H.; Urakami, T.; Kanazawa, H.; Kodama, T.; Oku, N.; Shea, K. J., Recognition, neutralization, and clearance of target peptides in the bloodstream of living mice by molecularly imprinted polymer nanoparticles: a plastic antibody. *Journal of the American Chemical Society* **2010**, 132 (19), 6644-6645.

Hu, Y.; Pan, J.; Zhang, K.; Lian, H.; Li, G., Novel applications of molecularly-imprinted polymers in sample preparation. *TrAC Trends in Analytical Chemistry* **2013**, 43, 37-52.

[J]

Janib, S. M.; Moses, A. S.; MacKay, J. A., Imaging and drug delivery using theranostic nanoparticles. *Advanced Drug Delivery Reviews* **2010**, 62 (11), 1052-1063.

Jagadeesan, K. K.; Wierzbicka, C.; Laurell, T.; Sellergren, B.; Shinde, S.; Ekström, S., Multiplexed MALDI-MS arrays for screening of MIP solid phase extraction materials. *Journal of Chromatography B* **2016**, 1021, 213-220.

Ji, W.; Zhang, M.; Wang, D.; Wang, X.; Liu, J.; Huang, L., Superhydrophilic molecularly imprinted polymers based on a water-soluble functional monomer for the recognition of gastrodin in water media. *Journal of Chromatography A* **2015**, 1425, 88-96.

[K]

Karim, K.; Breton, F.; Rouillon, R.; Piletska, E. V.; Guerreiro, A.; Chianella, I.; Piletsky, S. A., How to find effective functional monomers for effective molecularly imprinted polymers? *Advanced Drug Delivery Reviews* **2005**, 57 (12), 1795-1808.

Karlsson, J. G.; Andersson, L. I.; Nicholls, I. A., Probing the molecular basis for ligand-selective recognition in molecularly imprinted polymers selective for the local anaesthetic bupivacaine. *Analytica Chimica Acta* **2001**, 435 (1), 57-64.

Kirchner, R.; Seidel, J.; Wolf, G.; Wulff, G., Calorimetric investigation of chiral recognition processes in a molecularly imprinted polymer. *Journal of Inclusion Phenomena and Macrocyclic Chemistry* **2002**, 43 (3), 279-283.

Kryscio, D. R.; Peppas, N. A., Critical review and perspective of macro-molecularly imprinted polymers. *Acta Biomaterialia* **2012**, 8 (2), 461-473.

Kunath, S.; Panagiotopoulou, M.; Maximilien, J.; Marchyk, N.; Sanger, J.; Haupt, K., Cell and tissue imaging with molecularly imprinted polymers as plastic antibody mimics. *Advanced Healthcare Materials* **2015**, *4* (9), 1322-1326.

[L]

Lee, D.-E.; Koo, H.; Sun, I.-C.; Ryu, J. H.; Kim, K.; Kwon, I. C., Multifunctional nanoparticles for multimodal imaging and theragnosis. *Chemical Society Reviews* **2012**, *41* (7), 2656-2672.

Li, B.; Xu, J.; Hall, A. J.; Haupt, K.; Tse Sum Bui, B., Water-compatible silica sol-gel molecularly imprinted polymer as a potential delivery system for the controlled release of salicylic acid. *Journal of Molecular Recognition* **2014**, *27* (9), 559-565.

Li, S.; Yang, K.; Deng, N.; Min, Y.; Liu, L.; Zhang, L.; Zhang, Y., Thermoresponsive epitope surface-imprinted nanoparticles for specific capture and release of target protein from human plasma. *ACS Applied Materials & Interfaces* **2016**, *8* (9), 5747-5751.

Liu, Y.; Wang, F.; Tan, T.; Lei, M., Study of the properties of molecularly imprinted polymers by computational and conformational analysis. *Analytica Chimica Acta* **2007**, *581* (1), 137-146.

Liu, J.; Deng, Q.; Tao, D.; Yang, K.; Zhang, L.; Liang, Z.; Zhang, Y., Preparation of protein imprinted materials by hierarchical imprinting techniques and application in selective depletion of albumin from human serum. *Scientific Reports* **2014**, *4*, 5487.

Liu, L.; Zhong, T.; Xu, Q.; Chen, Y., Efficient molecular imprinting strategy for quantitative targeted proteomics of human transferrin receptor in depleted human serum. *Analytical Chemistry* **2015**, *87* (21), 10910-10919.

Lofgreen, J. E.; Ozin, G. A., Controlling morphology and porosity to improve performance of molecularly imprinted sol-gel silica. *Chemical Society Reviews* **2014**, *43* (3), 911-933.

Lordel, S.; Chapuis-Hugon, F.; Eudes, V.; Pichon, V., Development of imprinted materials for the selective extraction of nitroaromatic explosives. *Journal of Chromatography A* **2010**, *1217* (43), 6674-6680.

Lordel-Madeleine, S.; Eudes, V.; Pichon, V., Identification of the nitroaromatic explosives in post-blast samples by online solid phase extraction using molecularly imprinted silica sorbent coupled with reversed-phase chromatography. *Analytical and Bioanalytical Chemistry* **2013**, *405* (15), 5237-5247.

[M]

Ma, Y.; Zhang, Y.; Zhao, M.; Guo, X.; Zhang, H., Efficient synthesis of narrowly dispersed molecularly imprinted polymer microspheres with multiple stimuli-responsive template binding properties in aqueous media. *Chemical Communications* **2012**, *48* (50), 6217-6219.

Ma, Y.; Pan, G.; Zhang, Y.; Guo, X.; Zhang, H., Narrowly dispersed hydrophilic molecularly imprinted polymer nanoparticles for efficient molecular recognition in real aqueous samples including river water, milk, and bovine serum. *Angewandte Chemie International Edition* **2013**, *52* (5), 1511-1514.

Maier, N. M.; Buttinger, G.; Welhartizki, S.; Gavioli, E.; Lindner, W., Molecularly imprinted polymer-assisted sample clean-up of ochratoxin A from red wine: merits and limitations. *Journal of Chromatography B* **2004**, *804* (1), 103-111.

Manesiotis, P.; Hall, A. J.; Courtois, J.; Irgum, K.; Sellergren, B., An artificial riboflavin receptor prepared by a template analogue imprinting strategy. *Angewandte Chemie International Edition* **2005**, *44* (25), 3902-3906.

Manesiotis, P.; Borrelli, C.; Aureliano, C. S. A.; Svensson, C.; Sellergren, B., Water-compatible imprinted polymers for selective depletion of riboflavine from beverages. *Journal of Materials Chemistry* **2009**, *19* (34), 6185-6193.

Martín-Esteban, A., Recent molecularly imprinted polymer-based sample preparation techniques in environmental analysis. *Trends in Environmental Analytical Chemistry* **2016**, *9*, 8-14.

Masqué, N.; Marcé, R. M.; Borrull, F.; Cormack, P. A. G.; Sherrington, D. C., Synthesis and evaluation of a molecularly imprinted polymer for selective on-line solid-phase extraction of 4-nitrophenol from environmental water. *Analytical Chemistry* **2000**, *72* (17), 4122-4126.

Mayes, A. G.; Mosbach, K., Molecularly imprinted polymer beads: suspension polymerization using a liquid perfluorocarbon as the dispersing phase. *Analytical Chemistry* **1996**, *68* (21), 3769-3774.

Meng, Z.; Chen, W.; Mulchandani, A., Removal of estrogenic pollutants from contaminated water using molecularly imprinted polymers. *Environmental Science & Technology* **2005**, *39* (22), 8958-8962.

Meng, L.; Qiao, X.; Xu, Z.; Xin, J.; Wang, L., Development of a direct competitive biomimetic enzyme-linked immunosorbent assay based on a hydrophilic molecularly imprinted membrane for the determination of trichlorfon residues in vegetables. *Food Analytical Methods* **2012**, *5* (5), 1229-1236.

Molinelli, A.; O'Mahony, J.; Nolan, K.; Smyth, M. R.; Jakusch, M.; Mizaikoff, B., Analyzing the mechanisms of selectivity in biomimetic self-assemblies via IR and NMR spectroscopy of prepolymerization solutions and molecular dynamics simulations. *Analytical Chemistry* **2005**, *77* (16), 5196-5204.

Moreira, F. T. C.; Dutra, R. A. F.; Noronha, J. P. C.; Sales, M. G. F., Electrochemical biosensor based on biomimetic material for myoglobin detection. *Electrochimica Acta* **2013**, *107*, 481-487.

Moreno-Bondi, M. C.; Benito-Peña, M. E.; Urraca, J. L.; Orellana, G., Immuno-like assays and biomimetic microchips. In *Molecular Imprinting*, Haupt, K., Ed. Springer Berlin Heidelberg: Berlin, Heidelberg, **2012**; pp 111-164.

Moreno-Bondi, M., Songjun Li, Yi Ge, Sergey A. Piletsky, Joseph Lunec (Eds.): Molecularly imprinted sensors: overview and applications. *Analytical and Bioanalytical Chemistry* **2013**, *405* (20), 6385-6386.

Muhammad, T.; Nur, Z.; Piletska, E. V.; Yimit, O.; Piletsky, S. A., Rational design of molecularly imprinted polymer: the choice of cross-linker. *Analyst* **2012a**, *137* (11), 2623-2628.

Muhammad, T.; Cui, L.; Jide, W.; Piletska, E. V.; Guerreiro, A. R.; Piletsky, S. A., Rational design and synthesis of water-compatible molecularly imprinted polymers for selective solid phase extraction of amiodarone. *Analytica Chimica Acta* **2012b**, *709*, 98-104.

Mujahid, A.; Lieberzeit, P. A.; Dickert, F. L., Chemical sensors based on molecularly imprinted sol-gel materials. *Materials* **2010**, *3* (4), 2196-2217.

Murray, G. M.; Arnold, B. M.; Lawrence, D. S., Molecularly imprinted polymeric sensor for the detection of explosives. WO2001077664 A2, **2001**.

Mustafa, G.; Lieberzeit, P. A., MIP Sensors on the Way to Real-World Applications. In *Designing Receptors for the Next Generation of Biosensors*, Piletsky, A. S.; Whitcombe, J. M., Eds. Springer Berlin Heidelberg: Berlin, Heidelberg, **2013**; pp 167-187.

[N]

Nestora, S.; Merlier, F.; Beyazit, S.; Prost, E.; Duma, L.; Baril, B.; Greaves, A.; Haupt, K.; Tse Sum Bui, B., Plastic antibodies for cosmetics: Molecularly imprinted polymers scavenge precursors of malodors. *Angewandte Chemie International Edition* **2016a**, *55*, 6252-6256.

Nestora, S.; Merlier, F.; Prost, E.; Haupt, K.; Rossi, C.; Tse Sum Bui, B., Solid-phase extraction of betanin and isobetanin from beetroot extracts using a dipicolinic acid molecularly imprinted polymer. *Journal of Chromatography A* **2016b**, *1465*, 47-54.

Nicholls, I. A.; Ramström, O.; Mosbach, K., Insights into the role of the hydrogen bond and hydrophobic effect on recognition in molecularly imprinted polymer synthetic peptide receptor mimics. *Journal of Chromatography A* **1995**, *691* (1), 349-353.

Nishino, H.; Huang, C.-S.; Shea, K. J., Selective protein capture by epitope imprinting. *Angewandte Chemie International Edition* **2006**, *45* (15), 2392-2396.

Niu, H.; Yang, Y.; Zhang, H., Efficient one-pot synthesis of hydrophilic and fluorescent molecularly imprinted polymer nanoparticles for direct drug quantification in real biological samples. *Biosensors and Bioelectronics* **2015**, *74*, 440-446.

Norell, M. C.; Andersson, H. S.; Nicholls, I. A., Theophylline molecularly imprinted polymer dissociation kinetics: a novel sustained release drug dosage mechanism. *Journal of Molecular Recognition* **1998**, *11* (16), 98-102.

[O]

Odian, G., Radical Chain Polymerization. In *Principles of Polymerization*, John Wiley & Sons, Inc.: **2004**; pp 198-349.

O'Mahony, J.; Molinelli, A.; Nolan, K.; Smyth, M. R.; Mizaikoff, B., Towards the rational development of molecularly imprinted polymers: ¹H NMR studies on hydrophobicity and ion-pair interactions as driving forces for selectivity. *Biosensors and Bioelectronics* **2005**, *20* (9), 1884-1893.

Otsu, T.; Yoshida, M., Role of initiator-transfer agent-terminator (iniferter) in radical polymerizations: Polymer design by organic disulfides as iniferters. *Die Makromolekulare Chemie, Rapid Communications* **1982**, *3* (2), 127-132.

[P]

Panagiotopoulou, M.; Salinas, Y.; Beyazit, S.; Kunath, S.; Duma, L.; Prost, E.; Mayes, A. G.; Resmini, M.; Tse Sum Bui, B.; Haupt, K., Molecularly imprinted polymer coated quantum dots for multiplexed cell targeting and imaging. *Angewandte Chemie International Edition* **2016**, *55*, 8244-8248.

Pan, G.; Zhang, Y.; Ma, Y.; Li, C.; Zhang, H., Efficient one-pot synthesis of water-compatible molecularly imprinted polymer microspheres by facile RAFT precipitation polymerization. *Angewandte Chemie International Edition* **2011**, *50* (49), 11731-11734.

Pap, T.; Horváth, V.; Tolokán, A.; Horvai, G.; Sellergren, B., Effect of solvents on the selectivity of terbutylazine imprinted polymer sorbents used in solid-phase extraction. *Journal of Chromatography A* **2002**, *973* (1–2), 1-12.

Parker, C. E.; Pearson, T. W.; Anderson, N. L.; Borchers, C. H., Mass-spectrometry-based clinical proteomics - a review and prospective. *Analyst* **2010**, *135* (8), 1830-1838.

Pichon, V.; Bouzige, M.; Miège, C.; Hennion, M.-C., Immunosorbents: natural molecular recognition materials for sample preparation of complex environmental matrices. *TrAC Trends in Analytical Chemistry* **1999**, *18* (3), 219-235.

Pichon, V.; Haupt, K., Affinity separations on molecularly imprinted polymers with special emphasis on solid-phase extraction. *Journal of Liquid Chromatography & Related Technologies* **2006**, *29* (7-8), 989-1023.

Pichon, V., Selective sample treatment using molecularly imprinted polymers. *Journal of Chromatography A* **2007**, *1152* (1–2), 41-53.

Pichon, V.; Chapuis-Hugon, F., Role of molecularly imprinted polymers for selective determination of environmental pollutants—A review. *Analytica Chimica Acta* **2008**, *622* (1–2), 48-61.

Pichon, V.; Combès, A., Selective tools for the solid-phase extraction of ochratoxin A from various complex samples: immunosorbents, oligosorbents, and molecularly imprinted polymers. *Analytical and Bioanalytical Chemistry* **2016**, *25*, 6983-6999.

Piletsky, S. A.; Piletska, E. V.; Bossi, A.; Karim, K.; Lowe, P.; Turner, A. P. F., Substitution of antibodies and receptors with molecularly imprinted polymers in enzyme-linked and fluorescent assays. *Biosensors and Bioelectronics* **2001**, *16* (9–12), 701-707.

Polyakov, M. V. Adsorption properties and structure of silica gel. *Zhurnal Fizieskoj Khimii/Akademiya SSSR*, **1931**, *2*, 799-805.

Poma, A.; Turner, A. P. F.; Piletsky, S. A., Advances in the manufacture of MIP nanoparticles. *Trends in Biotechnology* **2010**, *28* (12), 629-637.

Poma, A.; Guerreiro, A.; Whitcombe, M. J.; Piletska, E. V.; Turner, A. P. F.; Piletsky, S. A., Solid-phase synthesis of molecularly imprinted polymer nanoparticles with a reusable template—“Plastic antibodies”. *Advanced Functional Materials* **2013**, *23* (22), 2821-2827.

Prasad, B. B.; Kumar, A.; Singh, R., Development of water compatible imprinted polymer beads for piezoelectric sensing of ultra-trace 5,6-dihydrouracil in biological fluids. *Sensors and Actuators B: Chemical* **2016**, *235*, 94-102.

Puoci, F.; Cirillo, G.; Curcio, M.; Iemma, F.; Parisi, O. I.; Castiglione, M.; Picci, N., Molecularly imprinted polymers for α -tocopherol delivery. *Drug Delivery* **2008a**, *15* (4), 253-258.

Puoci, F.; Iemma, F.; Picci, N., Stimuli-responsive molecularly imprinted polymers for drug delivery: A review. *Current Drug Delivery* **2008b**, *5* (2), 85-96.

Puoci, F.; Hampel, S.; Parisi, O. i.; Hassan, A.; Cirillo, G.; Picci, N., Imprinted microspheres doped with carbon nanotubes as novel electroresponsive drug-delivery systems. *Journal of Applied Polymer Science* **2013**, *130* (2), 829-834.

[R]

Ramström, O.; Skudar, K.; Haines, J.; Patel, P.; Brüggemann, O., Food analyses using molecularly imprinted polymers. *Journal of Agricultural and Food Chemistry* 2001, 49 (5), 2105-2114.

Resmini, M., Molecularly imprinted polymers as biomimetic catalysts. *Analytical and Bioanalytical Chemistry* 2012, 402 (10), 3021-3026.

Ridgway, K.; Lalljie, S. P. D.; Smith, R. M., Sample preparation techniques for the determination of trace residues and contaminants in foods. *Journal of Chromatography A* 2007, 1153 (1–2), 36-53.

[S]

Salian, V. D.; Byrne, M. E., Crosslinking diversity on network morphology, template binding, and template transport of molecularly imprinted polymers prepared via living radical polymerization. *Journal of Applied Polymer Science* 2013, 130 (5), 3588-3599.

Sanchez, C.; Arribart, H.; Giraud Guille, M. M., Biomimetism and bioinspiration as tools for the design of innovative materials and systems. *Nature Materials* 2005, 4 (4), 277-288.

Sellergren, B.; Andersson, L. Molecular recognition in macroporous polymers prepared by a substrate analog imprinting strategy. *Journal of Organic Chemistry* 1990, 55, 3381.

Sellergren, B., Direct drug determination by selective sample enrichment on an imprinted polymer. *Analytical Chemistry* 1994, 66 (9), 1578-1582.

Sellergren, B.; Wieschemeyer, J.; Boos, K.-S.; Seidel, D., Imprinted polymers for selective adsorption of cholesterol from gastrointestinal fluids. *Chemistry of Materials* 1998, 10 (12), 4037-4046.

Sellergren, B.; Allender, C. J., Molecularly imprinted polymers: A bridge to advanced drug delivery. *Advanced Drug Delivery Reviews* 2005, 57 (12), 1733-1741.

Sergeyeva, T. A.; Piletsky, S. A.; Brovko, A. A.; Slinchenko, E. A.; Sergeeva, L. M.; El'skaya, A. V., Selective recognition of atrazine by molecularly imprinted polymer membranes. Development of conductometric sensor for herbicides detection. *Analytica Chimica Acta* 1999, 392 (2–3), 105-111.

Shaikh, H.; Memon, N.; Bhangar, M. I.; Nizamani, S. M.; Denizli, A., Core-shell molecularly imprinted polymer-based solid-phase microextraction fiber for ultra trace analysis of endosulfan I and II in real aqueous matrix through gas chromatography-micro electron capture detector. *Journal of Chromatography A* 2014, 1337, 179-187.

Shea, K. J.; Thompson, E., Template synthesis of macromolecules. Selective functionalization of an organic polymer. *The Journal of Organic Chemistry* 1978, 43 (21), 4253-4255.

Shen, X.; Xu, C.; Ye, L., Imprinted polymer beads enabling direct and selective molecular separation in water. *Soft Matter* 2012, 8 (27), 7169-7176.

Shinde, S.; Bunschoten, A.; Kruijtzter, J. A. W.; Liskamp, R. M. J.; Sellergren, B., Imprinted polymers displaying high affinity for sulfated protein fragments. *Angewandte Chemie International Edition* 2012, 51 (33), 8326-8329.

Spivak, D.; Gilmore, M. A.; Shea, K. J., Evaluation of binding and origins of specificity of 9-ethyladenine imprinted polymers. *Journal of the American Chemical Society* **1997**, *119* (19), 4388-4393.

Spivak, D. A., Optimization, evaluation, and characterization of molecularly imprinted polymers. *Advanced Drug Delivery Reviews* **2005**, *57* (12), 1779-1794.

Sun, Z., Schüssler, W., Sengl, M., Niessner, R., Knopp, D., Selective trace analysis of diclofenac in surface and wastewater samples using solid-phase extraction with a new molecularly imprinted polymer. *Analytica Chimica Acta*, **2008a**, *620*, 73–81.

Sun, H.-W.; Qiao, F.-X., Recognition mechanism of water-compatible molecularly imprinted solid-phase extraction and determination of nine quinolones in urine by high performance liquid chromatography. *Journal of Chromatography A* **2008b**, *1212* (1–2), 1-9.

Sun, H.; Lai, J.-P.; Chen, F.; Zhu, D.-R., Molecularly imprinted microspheres synthesized by a simple, fast, and universal suspension polymerization for selective extraction of the topical anesthetic benzocaine in human serum and fish tissues. *Analytical and Bioanalytical Chemistry* **2015**, *407* (6), 1745-1752.

Suriyanarayanan, S.; Cywinski, P. J.; Moro, A. J.; Mohr, G. J.; Kutner, W., Chemosensors based on molecularly imprinted polymers. In *Molecular Imprinting*, Haupt, K., Ed. Springer Berlin Heidelberg: Berlin, Heidelberg, **2012**; pp 165-265.

Surugiu, I.; Danielsson, B.; Ye, L.; Mosbach, K.; Haupt, K., Chemiluminescence imaging ELISA using an imprinted polymer as the recognition element instead of an antibody. *Analytical Chemistry* **2001**, *73* (3), 487-491.

Svenson, J.; Karlsson, J. G.; Nicholls, I. A., ¹H Nuclear magnetic resonance study of the molecular imprinting of (–)-nicotine: template self-association, a molecular basis for cooperative ligand binding. *Journal of Chromatography A* **2004**, *1024* (1–2), 39-44.

Szwarc M., ‘Living’ polymers. *Nature* **1956**, *178*, 1168–1169.

[T]

Takeuchi T, Matsui J. Molecular imprinting: An approach to “tailor-made” synthetic polymers with biomimetic functions, *Acta Polymerica* **1996**, *47*,471–480.

Takeuchi, T.; Fukuma, D.; Matsui, J., Combinatorial molecular imprinting: An approach to synthetic polymer receptors. *Analytical Chemistry* **1999**, *71* (2), 285-290.

Tieppo, A.; White, C. J.; Paine, A. C.; Voyles, M. L.; McBride, M. K.; Byrne, M. E., Sustained in vivo release from imprinted therapeutic contact lenses. *Journal of Controlled Release* **2012**, *157* (3), 391-397.

Ton, X.-A.; Acha, V.; Haupt, K.; Tse Sum Bui, B., Direct fluorimetric sensing of UV-excited analytes in biological and environmental samples using molecularly imprinted polymer nanoparticles and fluorescence polarization. *Biosensors and Bioelectronics* **2012**, *36* (1), 22-28.

Ton, X.-A.; Tse Sum Bui, B.; Resmini, M.; Bonomi, P.; Dika, I.; Soppera, O.; Haupt, K., A versatile fiber-optic fluorescence sensor based on molecularly imprinted microstructures polymerized in situ. *Angewandte Chemie International Edition* **2013**, *52* (32), 8317-8321.

Ton, X.-A.; Acha, V.; Bonomi, P.; Tse Sum Bui, B.; Haupt, K., A disposable evanescent wave fiber optic sensor coated with a molecularly imprinted polymer as a selective fluorescence probe. *Biosensors and Bioelectronics* **2015**, *64*, 359-366.

Tóth, B.; Horvai, G., Chromatography, Solid-Phase Extraction, and Capillary Electrochromatography with MIPs. In *Molecular Imprinting*, Haupt, K., Ed. Springer Berlin Heidelberg: Berlin, Heidelberg, **2012**; pp 267-306.

Tse Sum Bui, B.; Haupt, K., Molecularly imprinted polymers: synthetic receptors in bioanalysis. *Analytical and Bioanalytical Chemistry* **2010**, *398* (6), 2481-2492.

Tse Sum Bui, B.; Merlier, F.; Haupt, K., Toward the use of a molecularly imprinted polymer in doping analysis: selective preconcentration and analysis of testosterone and epitestosterone in human urine. *Analytical Chemistry* **2010**, *82* (11), 4420-4427.

Turiel, E.; Martín-Esteban, A., Molecularly imprinted polymers for sample preparation: A review. *Analytica Chimica Acta* **2010**, *668* (2), 87-99.

Turner, N. W.; Jeans, C. W.; Brain, K. R.; Allender, C. J.; Hlady, V.; Britt, D. W., From 3D to 2D: A review of the molecular imprinting of proteins. *Biotechnology Progress* **2006**, *22* (6), 1474-1489.

[U]

Urraca, J. L.; Hall, A. J.; Moreno-Bondi, M. C.; Sellergren, B., A stoichiometric molecularly imprinted polymer for the class-selective recognition of antibiotics in aqueous media. *Angewandte Chemie International Edition* **2006**, *45* (31), 5158-5161.

Urraca, J. L.; Moreno-Bondi, M. C.; Orellana, G.; Sellergren, B.; Hall, A. J., Molecularly imprinted polymers as antibody mimics in automated on-line fluorescent competitive assays. *Analytical Chemistry* **2007**, *79* (13), 4915-4923.

Urraca, J. L.; Aureliano, C. S. A.; Schillinger, E.; Esselmann, H.; Wiltfang, J.; Sellergren, B., Polymeric complements to the Alzheimer's disease biomarker β -Amyloid Isoforms A β 1-40 and A β 1-42 for blood serum analysis under denaturing conditions. *Journal of the American Chemical Society* **2011**, *133* (24), 9220-9223.

Urraca, J. L.; Huertas-Pérez, J. F.; Cazorla, G. A.; Gracia-Mora, J.; García-Campaña, A. M.; Moreno-Bondi, M. C. Development of magnetic molecularly imprinted polymers for selective extraction: determination of citrinin in rice samples by liquid chromatography with UV diode array detection. *Analytical and Bioanalytical Chemistry* **2016**, *408*(11), 3033-3042.

Uzun, L., Turner, A. P. F., Molecularly-imprinted polymer sensors: realizing their potential. *Biosensors and Bioelectronics* **2016**, *76*, 131-144.

[V]

Vaihinger, D.; Landfester, K.; Kräuter, I.; Brunner, H.; Tovar, G. E. M., Molecularly imprinted polymer nanospheres as synthetic affinity receptors obtained by miniemulsion polymerisation. *Macromolecular Chemistry and Physics* **2002**, *203* (13), 1965-1973.

van Dam, G. M.; Themelis, G.; Crane, L. M. A.; Harlaar, N. J.; Pleijhuis, R. G.; Kelder, W.; Sarantopoulos, A.; de Jong, J. S.; Arts, H. J. G.; van der Zee, A. G. J.; Bart, J.; Low, P. S.; Ntziachristos, V., Intraoperative

tumor-specific fluorescence imaging in ovarian cancer by folate receptor-[alpha] targeting: first in-human results. *Nature Medicine* **2011**, *17* (10), 1315-1319.

Velázquez-Campoy, A.; Ohtaka, H.; Nezami, A.; Muzammil, S.; Freire, E., Isothermal Titration Calorimetry. In *Current Protocols in Cell Biology*, John Wiley & Sons, Inc.: 2001.

Vitzthum, F.; Behrens, F.; Anderson, N. L.; Shaw, J. H., Proteomics: from basic research to diagnostic application. A review of requirements and needs. *Journal of Proteome Research* **2005**, *4* (4), 1086-1097.

Vlatakis, G.; Andersson, L. I.; Muller, R.; Mosbach, K., Drug assay using antibody mimics made by molecular imprinting. *Nature* **1993**, *361*, 645-647.

[W]

Wang, J.-S.; Matyjaszewski, K., Controlled/"living" radical polymerization. atom transfer radical polymerization in the presence of transition-metal complexes. *Journal of the American Chemical Society* **1995**, *117* (20), 5614-5615.

Wang, Y.; Zhou, Y.; Sokolov, J.; Rigas, B.; Levon, K.; Rafailovich, M., A potentiometric protein sensor built with surface molecular imprinting method. *Biosensors and Bioelectronics* **2008**, *24* (1), 162-166.

Wang, N. X.; von Recum, H. A., Affinity-based drug delivery. *Macromolecular Bioscience* **2011**, *11* (3), 321-332.

Wang, H.; Dong, X.; Yang, M., Development of separation materials using controlled/living radical polymerization. *TrAC Trends in Analytical Chemistry* **2012a**, *31*, 96-108.

Wang, L.-Q.; Lin, F.-Y.; Yu, L.-P., A molecularly imprinted photonic polymer sensor with high selectivity for tetracyclines analysis in food. *Analyst* **2012b**, *137* (15), 3502-3509.

Wang, S.; Yin, D.; Wang, W.; Shen, X.; Zhu, J.-J.; Chen, H.-Y.; Liu, Z., Targeting and imaging of cancer cells via monosaccharide-imprinted fluorescent nanoparticles. *Scientific Reports* **2016**, *6*, 1-10.

Warwick, C.; Guerreiro, A.; Soares, A., Sensing and analysis of soluble phosphates in environmental samples: A review. *Biosensors and Bioelectronics* **2013**, *41*, 1-11.

Whitcombe, M. J.; Rodriguez, M. E.; Villar, P.; Vulfson, E. N. A new method for the introduction of recognition site functionality into polymers prepared by molecular imprinting: synthesis and characterization of polymeric receptors for cholesterol. *Journal of the American Chemical Society* **1995**, *117*, 7105-7111.

Whitcombe, M. J.; Chianella, I.; Larcombe, L.; Piletsky, S. A.; Noble, J.; Porter, R.; Horgan, A., The rational development of molecularly imprinted polymer-based sensors for protein detection. *Chemical Society Reviews* **2011**, *40* (3), 1547-1571.

Wu, X.; Wang, X.; Lu, W.; Wang, X.; Li, J.; You, H.; Xiong, H.; Chen, L., Water-compatible temperature and magnetic dual-responsive molecularly imprinted polymers for recognition and extraction of bisphenol A. *Journal of Chromatography A* **2016**, *1435*, 30-38.

Wulff, G.; Sarhan, A. The use of polymers with enzyme-analogous structures for resolution of racemates, *Angewandte Chemie International Edition* **1972**, *11*, 341.

Wulff, G., Molecular imprinting in cross-Linked materials with the aid of molecular templates— A way towards artificial antibodies. *Angewandte Chemie International Edition in English* **1995**, *34* (17), 1812-1832.

Wulff, G.; Knorr, K., Stoichiometric noncovalent interaction in molecular imprinting. *Bioseparation* **2002**, *10* (6), 257-276.

[X]

Xu, W.; Su, S.; Jiang, P.; Wang, H.; Dong, X.; Zhang, M., Determination of sulfonamides in bovine milk with column-switching high performance liquid chromatography using surface imprinted silica with hydrophilic external layer as restricted access and selective extraction material. *Journal of Chromatography A* **2010**, *1217* (46), 7198-7207.

Xu, Z. X.; Gao, H. J.; Zhang, L. M.; Chen, X. Q.; Qiao, X. G., The Biomimetic immunoassay based on molecularly imprinted polymer: A comprehensive review of recent progress and future prospects. *Journal of Food Science* **2011**, *76* (2), R69-R75.

Xu, S.; Lu, H.; Li, J.; Song, X.; Wang, A.; Chen, L.; Han, S., Dummy molecularly imprinted polymers-capped CdTe quantum dots for the fluorescent sensing of 2,4,6-trinitrotoluene. *ACS Applied Materials & Interfaces* **2013**, *5* (16), 8146-8154.

Xu, J.; Ambrosini, S.; Tamahkar, E.; Rossi, C.; Haupt, K.; Tse Sum Bui, B., Towards a universal method for preparing molecularly imprinted polymer nanoparticles with antibody-like affinity for proteins. *Biomacromolecules* **2016**, *17* (1), 345-353.

[Y]

Yang, Y.; Fang, G.; Liu, G.; Pan, M.; Wang, X.; Kong, L.; He, X.; Wang, S., Electrochemical sensor based on molecularly imprinted polymer film via sol-gel technology and multi-walled carbon nanotubes-chitosan functional layer for sensitive determination of quinoxaline-2-carboxylic acid. *Biosensors and Bioelectronics* **2013**, *47*, 475-481.

Yang, Y.; Niu, H.; Zhang, H., Direct and highly selective drug optosensing in real, undiluted biological samples with quantum-dot-labeled hydrophilic molecularly imprinted polymer microparticles. *ACS Applied Materials & Interfaces* **2016**, *8* (24), 15741-15749.

Ye, L.; Cormack, P.; Mosbach, K., Molecularly imprinted monodisperse microspheres for competitive radioassay. *Analytical Communications* **1999**, *36* (2), 35-38.

Ye, L.; Mosbach, K., Molecularly imprinted microspheres as antibody binding mimics. *Reactive and Functional Polymers* **2001**, *48* (1-3), 149-157.

Ye, L.; Haupt, K., Molecularly imprinted polymers as antibody and receptor mimics for assays, sensors and drug discovery. *Analytical and Bioanalytical Chemistry* **2004**, *378* (8), 1887-1897.

Ye, J.; Chen, Y.; Liu, Z., A Boronate Affinity Sandwich Assay: An appealing alternative to immunoassays for the determination of glycoproteins. *Angewandte Chemie International Edition* **2014**, *53* (39), 10386-10389.

Yin, D.; Wang, S.; He, Y.; Liu, J.; Zhou, M.; Ouyang, J.; Liu, B.; Chen, H.-Y.; Liu, Z., Surface-enhanced Raman scattering imaging of cancer cells and tissues via sialic acid-imprinted nanotags. *Chemical Communications* **2015**, *51* (100), 17696-17699.

Yoshimatsu, K.; Reimhult, K.; Krozer, A.; Mosbach, K.; Sode, K.; Ye, L., Uniform molecularly imprinted microspheres and nanoparticles prepared by precipitation polymerization: The control of particle size suitable for different analytical applications. *Analytica Chimica Acta* **2007**, *584* (1), 112-121.

[Z]

Zhang, Z.; Tan, W.; Hu, Y.; Li, G., Simultaneous determination of trace sterols in complicated biological samples by gas chromatography–mass spectrometry coupled with extraction using β -sitosterol magnetic molecularly imprinted polymer beads. *Journal of Chromatography A* **2011**, *1218* (28), 4275-4283.

Zhang, H., Controlled/“living” radical precipitation polymerization: A versatile polymerization technique for advanced functional polymers. *European Polymer Journal* **2013**, *49* (3), 579-600.

Zhang, H., Water-compatible molecularly imprinted polymers: Promising synthetic substitutes for biological receptors. *Polymer* **2014a**, *55* (3), 699-714.

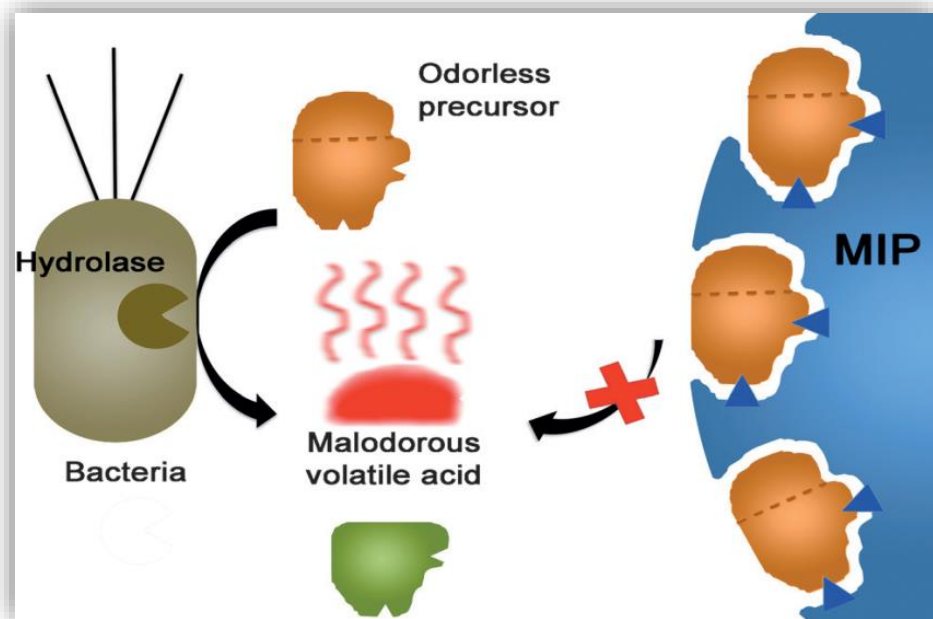
Zhang, Q.; Zhang, L.; Wang, P.; Du, S., Coordinate bonding strategy for molecularly imprinted hydrogels: Toward pH-responsive doxorubicin delivery. *Journal of Pharmaceutical Sciences* **2014b**, *103* (2), 643-651.

Zhang, Y.; Deng, C.; Liu, S.; Wu, J.; Chen, Z.; Li, C.; Lu, W., Active targeting of tumors through conformational epitope imprinting. *Angewandte Chemie International Edition* **2015**, *54* (17), 5157-5160.

Zhao, M.; Chen, X.; Zhang, H.; Yan, H.; Zhang, H., Well-defined hydrophilic molecularly imprinted polymer microspheres for efficient molecular recognition in real biological samples by Facile RAFT coupling chemistry. *Biomacromolecules* **2014**, *15* (5), 1663-1675.

Chapter 2

MIPs in cosmetics: a new active principle for scavenging precursors of malodors in human sweat



I. Introduction

I.1 Polymers and nanomaterials in cosmetics: Application of MIPs

Nowadays, consumers around the world are increasingly focused on health and beauty. Cosmetics is a dynamic market which is promoted by our current lifestyle and is expected to garner \$429.8 billion by 2022 (<https://www.alliedmarketresearch.com/cosmetics-market>, accessed January 27, 2017). Sun care, skin care, hair care, deodorants, makeup and color cosmetics, and fragrances are some of the cosmetics products that are predominantly available and used regularly by the consumers. According to the Food and Drug Administration (FDA), cosmetics are “intended to be applied to the human body for cleansing, beautifying, promoting attractiveness, or altering the appearance without affecting the body’s structure or functions” (FDA, 2012). As such, cosmetics can be grouped in seven categories: skin care and maintenance, cleansing, odor improvement by use of fragrances and deodorants, hair care and maintenance, hair removal, care and maintenance of mucous membranes and decorative cosmetics (such as nail care or make-up products) (Rieger, 2000). On the other hand, cosmeceuticals are defined as cosmetic products that exert a pharmaceutical therapeutic benefit (Brody, 2005).

To meet the high demand of consumers for safe and highly performant cosmetics, field manufacturers are constantly improving the formulation of their products. In this respect, the cosmetics field was among the first to implement nanotechnological principles in product development (Mihrianyan et al., 2012). For instance, liposome-based anti-aging topical formulations (creams, lotions, gels and hydrogels) have been formulated for the cosmetic market since 1986 by L’Oréal in the form of niosomes and by Christian Dior in the form of liposomes (Capture™) (Mu and Sprando, 2010).

The safety assessment is an important feature for any ingredient employed in a cosmetic product. According to EU legislation for cosmetics and their ingredients (Regulation 1223/2009), validated *in vitro* methods have been developed mainly for genotoxicity and local toxicity (http://ec.europa.eu/health/scientific_committees/consumer_safety/docs/sccs_o_190.pdf, accessed September. 4, 2016), so as to replace animal testing. Different test models are employed to assess skin irritation *in vitro*, studying parameters such as the concentration, the duration, and frequency of exposure, the exposed skin rate, the rate of penetration and the intrinsic toxic potential of the substance (Welss et al., 2004). To better comprehend the irritant responses towards skin sensitizers, the use of biomarkers, which undergo changes in their viability, morphological characteristics, differential expression of genes following treatment with irritants are employed. Such biomarkers reflect the metabolic activity of the sensitized cells (MTT cytotoxicity test), their membrane integrity (e.g. neutral red-uptake or lactate dehydrogenase release cytotoxicity test) or constitute inflammatory mediators (cytokines). Furthermore, the use of skin equivalent such as *Episkin* for the *in vitro* assessment of skin irritants is an interesting approach, mostly in the case of

reconstituted epidermis formed by fully differentiated keratinocytes. Interestingly, the European Center for the Validation of Alternative Methods (ECVAM) supported a prevalidation study on *in vitro* tests for acute skin irritation triggered by chemicals, performed on *EpiSkin*, which featured good correlation for these measured parameters between skin *in vivo* and *in vitro EpiSkin* model (Netzlaff et al., 2005).

Both natural and synthetic polymer materials are largely employed in the cosmetic and personal care industry. Several applications of polymers have been identified in cosmetics such as film formers, fixatives, rheology modifiers, emulsifiers, conditioners, moisturizers, etc. Another important feature is the encapsulation of active ingredients, for topical and transdermal delivery of cosmeceuticals. For instance, biodegradable polymers can be utilized as carriers of a large variety of biologically active substances, preserving their properties and facilitating their efficacy and bioavailability (Ammala, 2013).

The application of MIPs as selective polymeric materials in cosmetic products can offer significant advantages over the use of polymers without an imprint. Interestingly, the key feature of MIPs is their excellent recognition properties which can be proved necessary for specific analyte targeting. Thus, MIPs have an important potential in cosmetics as selective sorbents for sample preparation, as targeted carriers of active compounds or as capture materials for the removal of pollutants found in cosmetic products from a wide range of matrices. It is, therefore, surprising that the implication of MIPs in cosmetics is limited and only a few reports refer to their applications for extraction/separation during the preparation and/or processing of active compounds (Henry et al., 2015; Liu et al., 2015; Figuierido et al., 2016) and as a delivery system (Wendel et al., 2010).

A very interesting review summarizes the applications of MIPs in cosmetics mainly focused on the extraction and quantification of active ingredients such as antimicrobials, musks and UV-filters (Figuierido et al., 2016). The authors highlighted the complexity of cosmetic samples and other matrices containing these compounds as one of the main challenges for the successful design of MIPs. In most cases, MIPs were applied as selective SPE sorbents for the extraction of active ingredients (mainly parabens) from a large variety of samples including environmental waters, soils and plant extracts. Interestingly, for a period between 2001 and 2014, only 19 papers were published involving the synthesis of imprinted polymers for the analysis or the extraction of personal care products (13 for preservatives such as parabens, 4 for antimicrobials such as triclosan, and 1 for both UV filters and musks). Some interesting examples featured the extraction of triclosan from environmental samples with core-shell imprinted carbon nanotubes prepared *via* surface sol gel imprinting implemented carbon tubes (Gao et al., 2010) or the separation of benzoic acid from aqueous samples by magnetic MIP microspheres (Shi et al., 2014). Apart from SPE, MIP-based sensors are also employed in the field of cosmetics, for instance, Gholivand et al., 2014 prepared imprinted nanoparticles *via* precipitation polymerization on a carbon paste electrode for the detection of propylparaben in cosmetic samples with good recoveries of the target analyte ranging between 97.3 % and 103 %.

The development of novel cosmetic products certainly necessitates more than extraction/separation during the preparation and/or processing of active compounds. For instance, the control of body odor is one of the main actions of cosmetic products, as previously mentioned. Body odor of complex matrix of volatile organic compounds (VOCs) including low molecular weight fatty acids, aldehydes, alcohols, amines, ketones, ethers, hydrocarbons, esters, sulphides, etc. VOCs constitute significant biomarkers in human body odor, thus the development of efficient analytical approaches for their quantitative and qualitative recognition of in body odor is of great importance for the design of deodorants. In this context, Jha et al., 2014 have recently developed a volatile acid- imprinted quartz crystal microbalance (QCM) sensor array has been designed for the selective recognition of organic acids odor. The MIP-based QCM sensor is prepared by spin coating polyacrylic MIP films and its performance has been studied by exposing different concentrations of propenoic acid, hexanoic acid, and octanoic acid in singly and their binary mixtures. The designed sensor featured quick response in vapor contact and high selectivity and sensitivity.

Finally, special mention is to be accorded to the only delivery application of MIPs in cosmetic samples reported until now. In their patent, Wendel et al., 2010 described the development of MIPs prepared by free radical polymerization for encapsulation and protection of antioxidants and vitamins used as active principles in dermocosmetic formulations (prepared in the form of cream, foam, spray, gel, gel spray, lotion, oil, oily gel or mousse). They demonstrated their application on the example of the vitamin α -tocopherol, employed as template for the preparation of a MIP in ACN using MAA and TRIM as functional and cross-linking monomers. The synthesized MIP particles loaded with the active compound were introduced as a solid constituent in various formulations such as shampoo, conditioner, gel cream and sunscreen. The encapsulation of α -tocopherol by the MIP contributed to its sustained pH-responsive release over 12h, which clearly indicates the advantages of MIPs for vectorization/controlled release systems.

I.2 The potential of MIPs as active principles in cosmetics and other biotechnological areas

In dermocosmetics, an active ingredient is defined as any component that has an effect on the skin for the treatment or prevention of a disorder. Inactive ingredients on the other hand are included to help deliver or stabilize the active ingredients, as well as to preserve the product and make it aesthetically pleasing ([https://www.sharecare.com/health/skin-and-beauty/what-are active- ingredient](https://www.sharecare.com/health/skin-and-beauty/what-are-active-ingredient) ([http://www.skininc.com/skinscience/ ingredients/167877195.html](http://www.skininc.com/skinscience/ingredients/167877195.html))).

There is a growing interest in polymer research for the development of active materials possessing unique properties, such as antimicrobial activity (biocidal polymers). In the field of healthcare and hygienic applications, biocidal polymers may be incorporated into fibers, or possibly extruded into fibers themselves, and used for contact disinfectants in many biomedical applications such as sterile bandages and clothing (Kenawy et al., 2007). By attaching bioactive substrates to synthetic or naturally occurring macromolecules, it is expected to increase their therapeutic efficiencies while lowering their potential toxicity. This attachment can be performed following various approaches such as by preparation of a polymerizable monomer-bearing groups with antimicrobial activity, immobilization of antimicrobial agent on synthetic preformed or naturally occurring polymers or by preparation of hydrolysable antimicrobial agents as part of the polymer main chain.

Polymers, in the field of cosmetics and more specifically in deodorants have been applied as inactive ingredients for the improvement of the deodorant release and activity. In their patent, Hu et al., 2005 prepared deodorant polymer fabrics which are capable of releasing deodorant agents at certain temperatures. The smart fabric is made by coating a polymeric hydrogel based on NIPAm on the textile surface. The hydrogel is bonded to the textiles by using a hydrophilic functional monomer such as 2-hydroxypropyl methacrylate, and a cross-linking agent such as BIS. A deodorant compound can be loaded into the hydrogel during or after the bonding reaction. Furthermore, incorporation of the hydrophobic cyclodextrin to the hydrogel formulation can further enhance the controlled release properties of hydrogel modified textiles and thus a variety of hydrophobic guest deodorant molecules can be encapsulated in the polymer's cavity (Liu and Fan, 2002). So far, deodorant polymer fabrics responsive to specified bodily functions have not been commercialized as far as we know (Hu et al., 2012).

As discussed in the previous section, the application of MIPs in cosmetics has been limited to the separation and delivery of active compounds. Taking into account all biotechnological areas, the closest application to that of an active ingredient could be considered the actively targeted therapeutic MIP nanoparticles, surface-functionalized with targeting ligands towards specific cells or tissues. Still, MIPs in drug delivery are employed in the sense of “smart” excipients that enhance the therapeutic effect of the drug administered and not as active ingredients.

In this chapter, we pushed the boundaries of MIP applications a bit further and we report, for the first time, the use of MIPs as the active ingredient in a cosmetic product, for suppressing the axillary body malodor.

I.3 Origin and composition of axillary malodor

The human scent is genetically controlled and systemically influenced by dietary and medicinal intake, as well as the application of fragrance products. Heavy sweating or hyperhidrosis, particularly at axillary sites, leads to unpleasant odors that cause social embarrassment and reduce self-confidence. Body malodor treatment products are part of a multibillion dollar industry and are important for social confidence, improving the quality of life of many people worldwide (Piérard et al., 2003; Preti and Leyden, 2010).

The human axilla (armpit) is one of the predominant anatomical skin sites responsible for the formation of strong and unpleasant body odors (Martin et al., 2010). The axillary region contains sebaceous glands and a large density of eccrine and apocrine sweat glands (Figure 2.1). Apocrine gland secretions include proteins, lipids, sulphur-containing amino acids, volatile short-chain fatty acids and steroids such as dehydroepiandrosterone (DHEA), DHEA sulphates (DHEAS), androsterone and testosterone (Labows, 1982), whereas secretions from the eccrine glands mainly consist of electrolytes (Na^+ , Cl^- , NH_4^+), lactic acid, glycerol and urea (Shirreffs and Maughan, 1997) (Table 2.1). This availability of nutrients combined with the humid and semi-occluded environment of the armpit allows for dense bacterial colonization reaching up to 1 million of cells per cm^2 (Fredrich et al., 2013).

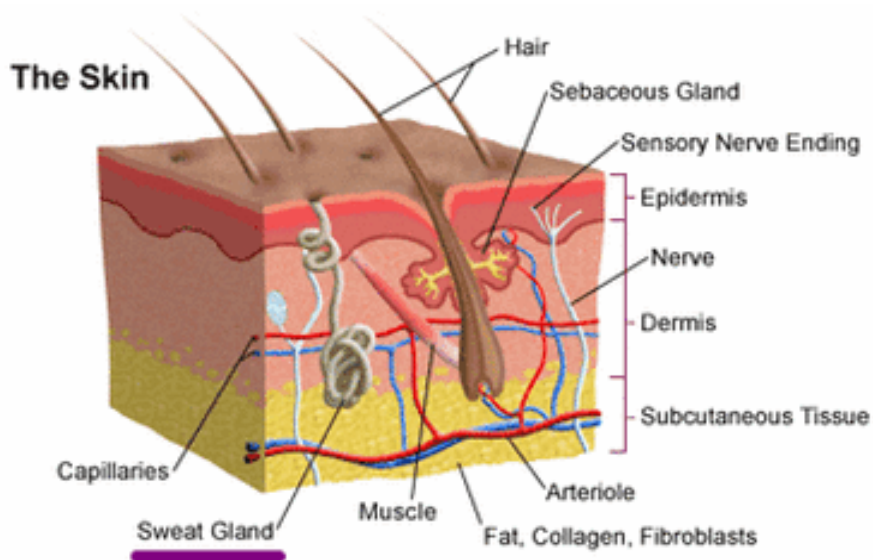


Figure 2.1. Schematic representation of the human axillary skin, indicating the location of sebaceous and sweat glands. (<http://www.naturallyhealthyskin.org/anatomy-of-the-skin/the-epidermis/m>, accessed January 27, 2017).

Table 2.1. Selection of the most abundant molecules present in human sweat

(Extracted from Harvey et al., 2010).

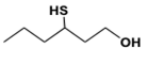
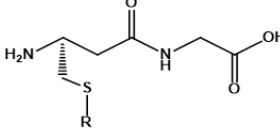
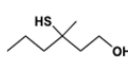
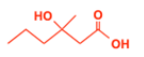
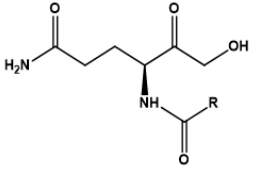
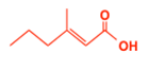
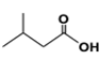
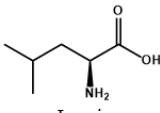

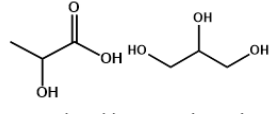
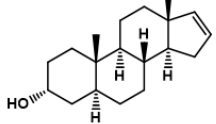
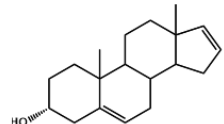
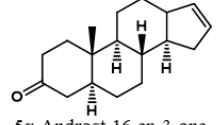
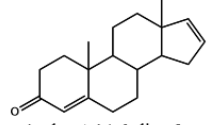
Constituents	Median concentration (mM)	Constituents	Median concentration (mM)
Sodium	31	Pyruvic acid	0.18
Chloride	23	Isoleucine	0.17
Riboflavin	20	Tyrosine	0.17
Lactic acid	14	Lysine	0.15
Urea	10	Ornithine	0.15
Ammonia	5.2	Phenylalanine	0.13
Thiamine	5	Acetic acid	0.13
Nicotinic acid	410	Uric acid	0.059
Pantothenic acid	130	Tryptophan	0.055
Arginine	0.78	Creatine	0.015
Histidine	0.52	Dehydroascorbic acid	0.011
Threonine	0.45	Ascorbic acid	0.01
Citrulline	0.4	Propionic acid	0.0035
Glycine	0.39	Butyric acid	0.0024
Glutamic acid	0.37	Isovaleric acid	0.0011
Alanine	0.36	Hexanoic acid	0.0009
Aspartic acid	0.34	Isobutyric acid	0.0008
Valine	0.25	p-aminobenzoic acid	7.1×10^{-5}
Leucine	0.21	Folic acid	1.6×10^{-5}

The composition of the bacterial community colonizing the axillary glands is quite diverse, presenting significant variations depending on every individual and even slight differences can be observed between the right and left axilla of the same individual (Barzantny et al., 2012; Costelo et al., 2009; Callewaert, 2013). The characterization of the axillary microbiota was traditionally performed by culture-based microbiological and biochemical studies. Nowadays, culture-independent DNA sequencing approaches are employed, which allow a more comprehensive approach regarding the taxonomic composition of the axillary microbiota. The three phyla populating the axillae are *Actinobacteria* (59.7%), *Firmicutes* (23.2%) and *Proteobacteria* (16.7%) (Callewaert et al., 2013), of which *Staphylococcus spp.* (*Firmicutes*) and *Corynebacterium spp.* (*Actinobacteria*) were typified as two of the most important species in the axillary region (Leyden et al., 1981).

The understanding of the nature and biogenesis of axillary odors has been the focus of many scientific studies (Natsch et al., 2003; Troccaz et al., 2009; Martin et al., 2010). It has been evident since the 1950s that malodor generation on axillary skin is due to the biotransformation of odorless gland secretions into volatile odorous molecules, by the bacteria, commensal to the skin (Shelley et al., 1953). The odorous molecules include sulfanylalkanols, steroid derivatives, and volatile short chain fatty acids, whose combination and ratios account for the intensity of human axillary odor (Troccaz et al., 2009). For instance, lactic acid and glycerol are catabolized by *Propionibacteria*, *Staphylococcus* and *Corynebacteria* to short-chain (C2–C3) volatile fatty acids (VFAs) such as acetic, and propionic acids (Kanlayavattanukul and Lourith, 2011). In addition, *Staphylococci* are capable of converting branched aliphatic amino acids such

as leucine to highly malodorous short-chain (C4-C5) methyl-branched VFAs, such as isovaleric acid, usually associated to the rancid note of axillary malodor. The main compounds associated with axillary malodor and their odorless precursors are illustrated in Table 2.2.

Table 2.2. Typical compounds associated with axillary malodors
(Adapted from Fredrich et al., 2013).

Chemical class	Odor compound	Odor precursor	Organism
Thiolalcohols	 3-methyl-3-sulfanylhexan-1-ol	 Glycylcysteinyl-S-conjugate	<i>Corynebacterium</i> spp. <i>Staphylococcus</i> spp.
	 3-sulfanylhexan-1-ol		
Medium chain (C6-C10) fatty acids	 3-hydroxy-3-methyl hexanoic acid (3H3MH)	 Glutaminy-conjugate	<i>Corynebacterium</i> spp.
	 3-methyl-2-hexenoic acid (3M2H)		
Short chain (C2-C5) fatty acids	 Isovaleric acid	 Leucine	<i>Staphylococcus</i> spp. <i>Corynebacterium</i> spp.
	 Propionic acid Acetic acid	 Lactic acid Glycerol	Facultative anaerobic <i>Staphylococcus</i> spp. Microaerophilic <i>Propionibacterium</i> spp.
Steroids	 5α-Androst-16-en-3α-ol	 Androsta-5,16-dien-3α-ol	<i>Corynebacterium</i> spp. <i>Micrococcus</i> spp.
	 5α-Androst-16-en-3-one	 Androst-14,6-dien-3-one	

In the 1980s, generation of odoriferous steroids such as androstenol and androstenone by skin bacteria was associated with musk-like and urinous axillary malodors (Labows, 1982; Gower et al., 1994), but it is now postulated that the contribution of these steroids is much less than previously believed (Gordon James et al., 2013). Nowadays, it is considered that the main molecules causing the distinct pungency of underarm odors are thioalcohols and medium chain branched volatile fatty acids (Troccaz et al., 2009). The characteristic body odor associated with these compounds and the detection threshold is presented in Table 2.3.

Table 2.3. Characteristic body odors and their detection thresholds

(Adapted from Kanlayavattanakul and Lourith, 2011).

Odor compound	Organoleptic property	Detection threshold
3-methyl-3-sulfanylhexasan-1-ol	Sweaty	1 ppt
2-methyl-3-sulphanyl butanol	Sweaty	8 ppt
3-hydroxy-3-methyl hexanoic acid (3H3MH)	Spicy	4 ppt
3-methyl-2-hexenoic acid (3M2H)	Pungent, sweaty	14 ppb
Isovaleric acid	Rancid	1 ppm
Androsterol	Musky	6.2 ppb
Androstenol	Urinous	0.2 ppb

The medium chain fatty acids, 3-hydroxy-3-methyl-hexanoic acid (3H3MH) and (*E*)-3-methyl-2-hexenoic acid (3M2H) are the most abundant of these offenders (Natsch et al., 2003; Kanlayavattanakul et al., 2011) and are produced from their non-odorous glutamine conjugate precursors, cj3M2H and cj3H3MH, by the action of N_{α} -acylglutamine aminoacylase from *Corynebacteria spp* commensal to the skin (Natsch et al., 2003; Kanlayavattanakul et al., 2011; Barzantny et al., 2012; Fredrich et al., 2013) (Figure 2.2). In this chapter, we are focusing on the scavenging of these odorless precursors by a selective water compatible MIP.

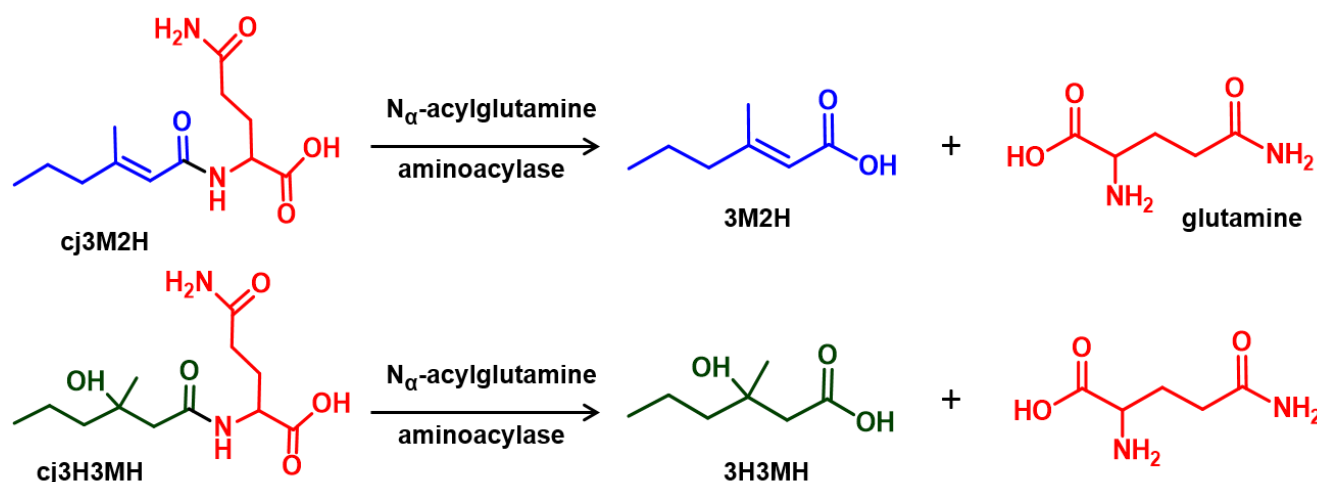


Figure 2.2. Formation of malodorous volatile fatty acids, (*E*)-3-methyl-2-hexenoic acid (3M2H) and 3-hydroxy-3-methyl-hexanoic acid (3H3MH) from their non-odorous glutamine conjugates by *Corynebacteria* spp in axillary sweat.

1.4 Battle against body malodor: The biological effect of treatment agents

In the last decades, concern has been raised regarding the safety of cosmetic products and in particular in underarm cosmetics. The most currently marketed anti-perspirants and deodorants contain respectively aluminum salts and antibacterials, supplemented with odor-covering agents (Preti et al., 2010; Kanlayavattanakul et al., 2011; Natsch, 2013). Antiperspirants are US Food and Drug Administration (FDA) regulated drugs to be used only in the underarm axilla vault and are primarily complexes of aluminum (e.g. aluminum chlorohydrate, aluminum sulfate etc) (Kanlayavattanakul et al., 2011). A wide range of antimicrobials are added to deodorants and antiperspirants to decrease the density of the skin bacterial community. However, the extremely wide use of these products requires alternative solutions with regards to various problems (environmental, respect of skin ecosystem, etc.) (Fredrich et al., 2013; Callewaert et al., 2014).

In this section, we will focus on the active ingredients in deodorants and antiperspirant systems and their risk assessment. In the last years, there has been an increased concern on the use of aluminium salts in personal care products, due to some alleged toxicological risks. Earlier, Anane and Creppy, 2001 have demonstrated that aluminium can induce cell toxicity by oxidative damage, as inferred by the *in vitro* cytotoxicity studies in human skin fibroblasts, using lactate dehydrogenase (LDH) as biomarker. In fact, aluminium salts as active ingredients in antiperspirants, precipitate inside the sweat glands, producing insoluble aluminum hydroxide, which can potentially plug the gland and block the secretion of sweat (Laden and Felger, 1988). In addition, aluminium alters sweating by constricting the dermal duct lumen by direct effect or *via* its anticholinergic action (Burkhart and Burkhart, 2008). A recent study demonstrated the feasibility of cutaneous penetration of aluminium salts from different commercial antiperspirant formulas, in healthy and stripped skin (Pineau et al., 2012). The transdermal uptake of aluminium salts

could suggest their potential effect as skin sensitizers. An allergic reaction was reported in a case study, where a 28-year woman was diagnosed with allergic contact dermatitis, probably induced by the presence of aluminium salts in antiperspirants (Garg et al., 2010).

Furthermore, Exley et al., 2007 demonstrated its association to the increasing occurrence of breast cancer, since a higher content of aluminium was found in the outer breast of breast cancer patients using antiperspirants. It should be noted, though, that there is no evidence relating the regional distribution of aluminium in the breast and the higher incidence of tumours or that the aluminium measured in these breast biopsies originates from an antiperspirant. Given the wide exposure of the human population to antiperspirants, further studies are needed to investigate the longer-term effects of aluminium exposure (Natsch et al., 2015).

The presence of aluminium salts in antiperspirants has also an effect on the commensal bacterial community that should not be compromised as it acts as a protective barrier for the body against harmful pathogens. Callewaert et al., 2014 have reported that the use of antiperspirants shifted considerably the microbial community in the axillary region. Substantially higher community diversity (richness and evenness) was observed on volunteers wearing an antiperspirant. Moreover, aluminum salts induce an enhancement of *Corynebacterium spp* growth to the detriment of *Staphylococcus spp*. This shift leads towards altered odor profile of the axillary region as it favours the growth of the odor-productive bacteria.

Apart from aluminium salts, antiperspirants and deodorants contain a wide range of antimicrobials to control and suppress odor-productive bacteria. Propylene glycol, triclosan, benzalkonium chloride and metal salts are regularly used in these formulations, possessing antimicrobial and antifungal properties (Benohanian, 2001). These ingredients contribute to the decrease of the abundance density of skin microbiota, although complete elimination cannot be obtained. Their stress-inducing effect on the skin commensal bacteria is dependent on the amount of deodorant utilized, the individual sweat rate, sweat content and skin pH. However, it must be mentioned that stable hygiene and cosmetic habits for a long period of time result in stable microbial profile, even when a deodorant/antiperspirant is used. This infers that the bacterial community can adapt to the application of deodorant/antiperspirants (Callewaert et al., 2014).

The extremely wide use of the aforementioned ingredients and their effect as skin sensitizers requires alternative solutions with regard to various problems (environmental, respect of skin ecosystem) (Fredrich et al., 2013). An interesting approach towards safe-to use deodorants was described by Natsch et al., 2013 who focused on the specific biochemical pathways leading to the formation of malodorant molecules. In this respect, they aimed to block the action of the enzyme N_{α} -acylglutamine aminoacylase of *Corynebacteria*, responsible for the cleavage of the glutamine precursors to the odorous volatile fatty acids (Figure 2.2). For this, two different strategies were elaborated; first, carbamates were synthesized as alternative substrates for the enzyme which means that if they are present in excess over the natural

substrate, they will reduce malodor release by competition. The second approach involves the use of phosphonic acid derivatives as enzyme inhibitors. The aforementioned active ingredients were formulated into deodorant systems without classical deodorant principles, applied to the axilla of panellists and their effect on malodor formation was evaluated *in vivo*. Interestingly, the carbamate as alternative substrate reduced malodor formation *in vivo*, in contrast to phosphonic acid-derived inhibitors which exhibited no *in vivo* activity. These promising results, at least in the first case, may lead to safer deodorants ingredients, though at an increased cost.

Herein, we developed an innovative approach for the control of body malodor that does not target the skin microbiota. Our strategy, presented in details in the following section, is based on a multi-target water compatible MIP which was designed to capture the glutamine precursors of malodors before they are converted to the malodorous acids and eventually the acids themselves. Hence, the skin microbiota which helps to protect the body against harmful pathogens would not be disrupted.

I.5 Our strategy: MIPs as scavengers for non-odorous precursors of malodors

As discussed in the previous section, the application of MIPs in cosmetics is limited to the separation and delivery of active compounds. In this project, we focused on the development of imprinting polymers which can function as smart materials in cosmetics. Therefore, we present, for the first time, the use of MIPs as the active ingredient in a cosmetic product, on the example of a new deodorant principle. The idea is to prevent the formation of body odors without disturbing the fragile bacterial equilibrium of the skin. This is achieved by using the MIP as a specific scavenger agent for non-odorous precursors of malodors, thus trapping them from being transformed by bacteria into volatile malodorous compounds (Figure 2.3). The multi-target MIP was developed to capture the glutamine precursors of malodors (cj3H3MH and cj3M2H) (Figure 2.2) before they are converted to the malodorous acids and eventually the acids themselves. As imprinting templates, structural analogues of the glutamine conjugates were employed (Figure 2.4).

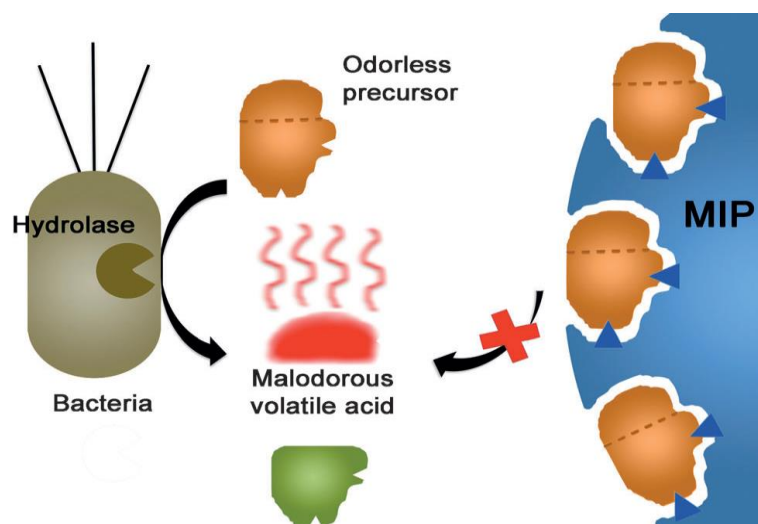


Figure 2.3. Schematic illustration of a MIP as the active ingredient in a cosmetic product to prevent body odor formation. By scavenging the odorless precursor, the MIP prevents its hydrolysis to a volatile malodorous acid by a bacterial enzyme.

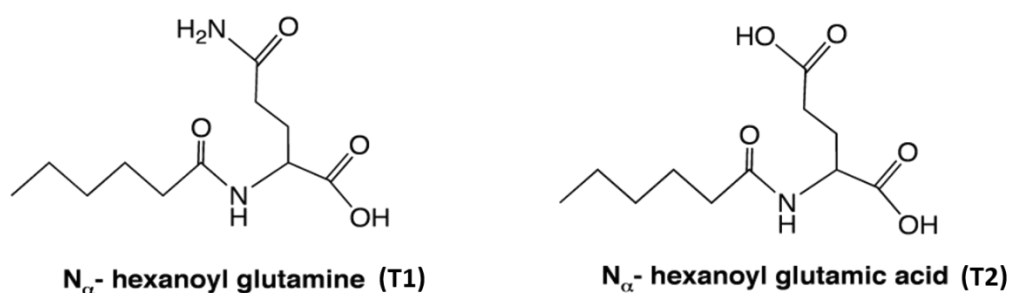


Figure 2.4. Structural analogues used as template molecules in this study.

The main challenge in this work was to be able to use these materials to selectively capture target molecules in an extremely complex and unfavorable environment (mixture of sweat and cosmetic formulation). This is far from obvious despite many efforts in the past years to make MIPs recognize selectively target molecules in an aqueous environment and *a fortiori* in complex matrices (Hall et al., 2005; Urraca et al., 2006; Ma et al., 2013).

Moreover, successful compliance with the requirements for a topical skin application, could render this MIP an interesting alternative to the currently employed active ingredients such as the aluminium salts. In this respect, the biological effect of the designed MIP in terms of epidermal cell viability and effect on the bacteria commensal to the skin will be also discussed in this chapter. This evaluation could be implemented in the future with further experiments, which can facilitate the potential application of this MIP in novel cosmetic products.

II. Results and Discussion

II.1 First attempts toward recognition in sweat

As discussed in the introduction, our aim was to synthesize a specific MIP to trap the non-odorous glutamine conjugates precursors of malodors. A structural analogue of the glutamine conjugates, N_{α} -hexanoyl glutamine (T1) (Figure 2.4) was used as template. Our first polymers were synthesized with the commercially available basic monomers: 4-vinylpyridine (4-VP) and amino ethyl methacrylate (AEM), capable of forming electrostatic interactions with the template T1. For the preparation of MIPs, the use of health compromising solvents was avoided so as to be compatible with dermocosmetic applications. In this respect, EtOH/water (4:1) was chosen as porogen. The MIP prepared with 4-VP as functional monomer demonstrated high and specific binding in EtOH/water (Figure 2.5). The binding was then investigated in a simplified model of human eccrine sweat (artificial sweat), which is a solution containing the major constituents of human sweat, namely urea, lactic acid, albumin and sodium chloride (refer to section III.6 for the detailed composition). Unfortunately, under these conditions no binding was obtained (results not shown).

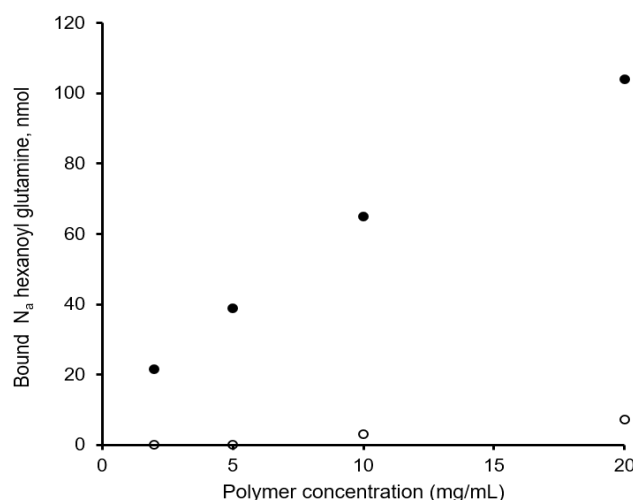


Figure 2.5. Equilibrium binding isotherms for 200 nmol of N_{α} -hexanoyl glutamine on T1/ 4-VP polymers in EtOH: water (4:1). MIP (filled circles) and NIP (empty circles).

To enhance the interaction in artificial sweat, we postulated that placing a second amidine function into the binding site of the amide function of the glutamine conjugates would be beneficial. Therefore, we used the template N_{α} -hexanoyl glutamic acid (T2) which bears 2 carboxylic groups (Figure 2.4). A series of polymers, with different T2/monomer ratios were prepared with T2 and 4-VP, namely T2/4-VP 1 corresponding to a T2:4-VP: EGDMA ratio of 1:2:10, T2/4-VP 2 to a ratio of 1:4:20 and T2/4-VP 3 to a ratio of 1:8:40. Binding experiments performed in the porogen showed that all interactions were specific and the batch with a T2:4-VP: EGDMA ratio of 1:2:10 provided the highest binding (Figure 2.6). However,

just as with T1 as template, no binding was observed in artificial sweat conditions. It seems that the interaction between 4-VP and carboxylates is not strong enough to allow binding in the complex environment of artificial sweat.

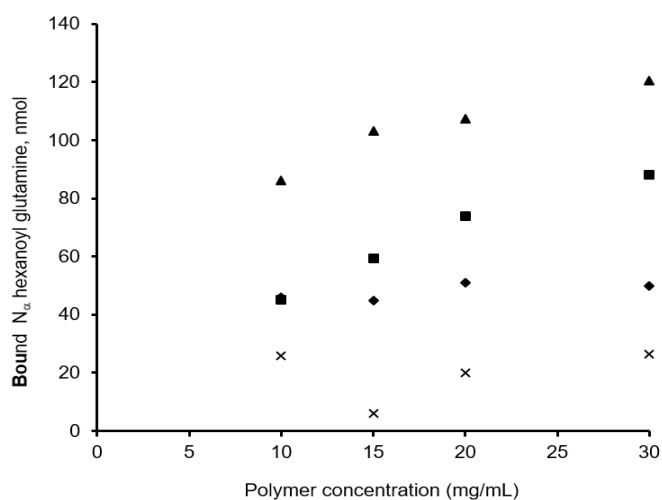


Figure 2.6. Equilibrium binding isotherms for 200 nmol of N_{α} -hexanoyl glutamine on T2-4VP polymers in EtOH: water (4:1). Batch T2/4-VP 1 (rhombuses), batch T2/4-VP 2 (squares), batch T2/4-VP 3 (triangles) and NIP (crosses).

Then, we turned to another commercial basic monomer, namely amino ethyl methacrylate (AEM). Thus, a MIP was synthesized using the latter as the functional monomer and N_{α} -hexanoyl glutamic acid as template. An important amount of non-specific binding was observed in ethanol (Figure 2.7A) while in artificial sweat the MIP showed lower and non-specific binding (Figure 2.7B). Hence, it is clear that none of the typically employed monomers is suitable to achieve binding in the highly complex sample of artificial sweat.

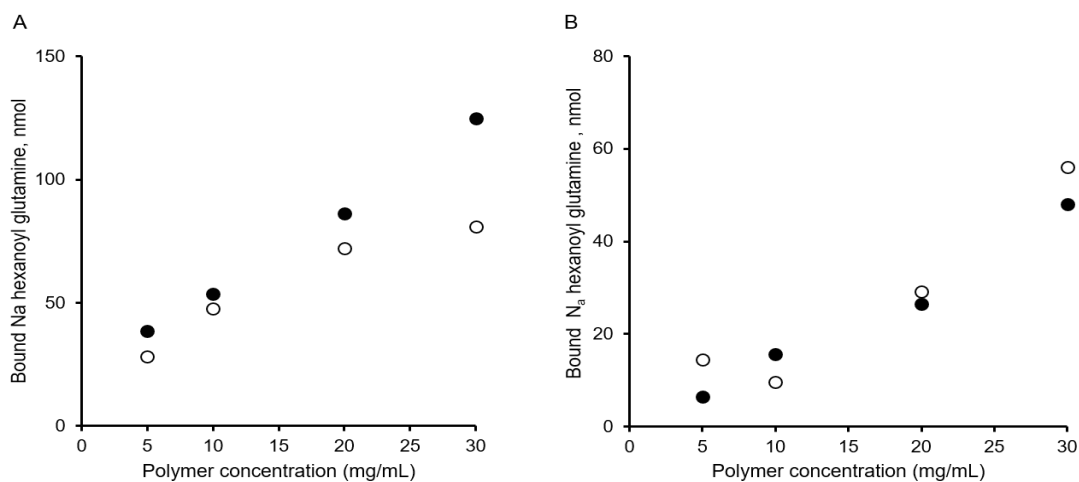


Figure 2.7. Equilibrium binding isotherms for 200 nmol of N_{α} -hexanoyl glutamine for MIP T2-AEM polymers in A) ethanol and B) artificial sweat. MIP (filled circles) and NIP (empty circles).

II.2 Our strategy: MIPs based on a tailor-made amidine monomer

It is evident that for the application targeted here, interactions involving high association constant is essential. Since MIPs prepared with commercial monomers were not performant and specific in artificial sweat, we turned to the synthesis of tailor-made monomer able to provide strong interaction even in the complex environment of human sweat and its artificial model.

Previously, in order to mimic the guanidinium group of arginine in antibodies, known for its strong interaction with carboxylates and phosphates, Wulff and co-workers have synthesized the monomer, *N,N'*-diethyl-(4-vinylphenyl)amidine (Wulff et al., 1997; Wulff and Schönfeld, 1998) which can form stoichiometric non-covalent interaction complexes of $K_a > 10^3 \text{ M}^{-1}$ with various oxyanions like carboxylates, phosphonates and phosphates, in acetonitrile or chloroform (Wulff and Knorr, 2001). Their amidinium-based MIPs could mimic catalytic antibodies by hydrolyzing esters in a mixed buffer/acetonitrile system (Strikovsky et al., 2000). Likewise, MIPs based on urea monomers specially designed for stoichiometric oxyanions targeting, were exploited for their selectivity in mixed organic solvent/buffer systems (Hall et al., 2005; Urraca et al., 2006) but not in 100% aqueous media. For our work, we synthesized an unsubstituted amidine monomer, (4-acrylamidophenyl)(amino)methaniminium acetate (AB) to be able to form a soluble complex in a polar solvent, in our case ethanol/water (Figure 2.8).

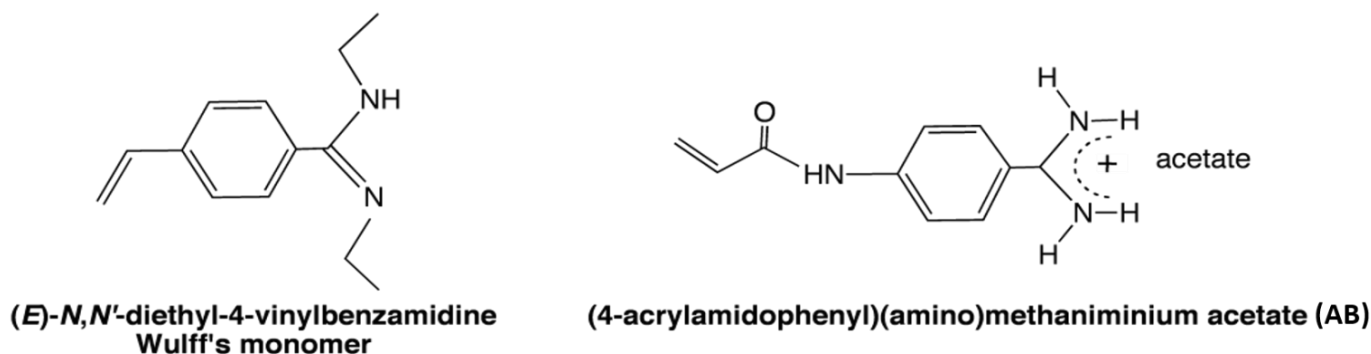


Figure 2.8. Structure of tailor made amidine monomers

The first scavenging MIP based on the tailor-made monomer AB was prepared using N_α -hexanoyl glutamine (Figure 2.4) as template and EGDMA as cross-linker, Perkadox 16 as initiator (compatible with cosmetics and skin care products, unlike most of the commonly-used azo initiators) and ethanol/water (4/1) as solvent. The monomer was synthesized similarly to our previous publication (Beyazit et al., 2014), but as an acetate salt (Figure 2.27 (A, B, C) for ^1H NMR, ^{13}C NMR and mass spectrum), to enable ready exchange with the template carboxylate (Figure 2.9). The stoichiometry between AB and the template was determined by ^1H NMR spectroscopy using the method of continuous variation (Job plot). A 1:1 stoichiometry with a high binding $\beta_{11}=K_{11}$ of $9.4 \times 10^3 \text{ M}^{-1}$ in $\text{CD}_3\text{OD}/\text{D}_2\text{O}$ (4:1) was determined (Figure 2.10), where K_{11} is equal to the association constant (K_a) of the 1:1 complex.

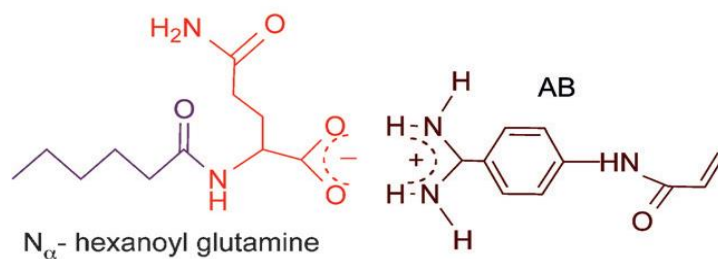


Figure 2.9 Proposed complex formation between the template N_α -hexanoyl glutamine and the monomer AB.

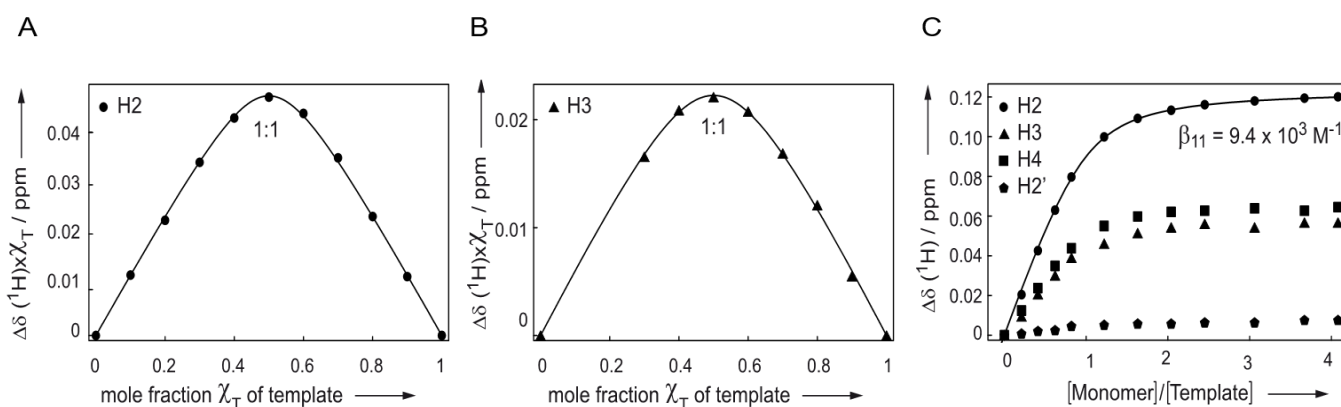


Figure 2.10. ^1H NMR analysis of Job and titration experiments of N_α -hexanoyl glutamine (A, B, C) with AB in $\text{CD}_3\text{OD}/\text{D}_2\text{O}$ (4/1) at 25°C . The chemical shift difference ($\Delta\delta$) of 4 protons (H2, H3, H4 and H2' in Figure S1, Annex 1) close to the interaction sites was measured in the absence and the presence of the monomer. Labile protons could not be exploited for this analysis because of their fast exchange with the solvent, which makes them “invisible”. (A, B) Job plot with non-linear regression analysis (Connors, 1987) show a clear maximum at a mole fraction of 0.5 supporting a 1:1 stoichiometry of the complex monomer-template for the H2 and H3 protons N_α -hexanoyl glutamine. H4 proton could not be followed for the Job due to peak overlap. (C) titration curve with non-linear regression analysis yielding an overall binding constant β_{11} of $9.4 \times 10^3 \text{ M}^{-1}$ for the H2 proton of N_α -hexanoyl glutamine. The non-linear regression analysis of the experimental data has been done using a home-written Mathematica program and a Matlab code written by Pall Thordarson (Thordarson, 2011).

The binding behaviour of the polymers was first investigated in the solvent of synthesis. Equilibrium binding assays showed a high binding capacity and specificity of the MIP towards N_α -hexanoyl glutamine, as evidenced by the quasi-total adsorption of the template by 10 mg of MIP and the higher binding of MIP as compared to the NIP (Figure 2.11). The binding was then investigated in artificial sweat, a solution comprising the major components found in human eccrine sweat, namely, urea, lactic acid, albumin and sodium chloride, as a simplified model (refer to section III.6 for a detailed composition). We observed no

binding, which was attributed to the high sodium chloride concentration, as its suppression from the artificial sweat composition restored binding.

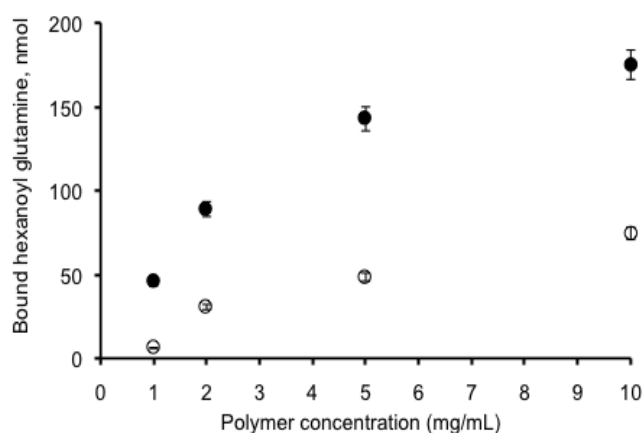


Figure 2.11. Equilibrium binding isotherms for 200 nmol of N_{α} -hexanoyl glutamine in ethanol/water (4/1) for MIP T1-AB (filled circles) and NIP (empty circles), prepared with N_{α} -hexanoyl glutamine as template. Analysis by LC-UV-ELSD. Data are the mean from three independent experiments with four different batches of polymers. The error bars represent standard deviations.

In order to obtain binding in this environment and in the more challenging human sweat medium, we postulated that it would be beneficial to place a second amidinium function into the binding site, able to interact with the amide group of the glutamine conjugates, since this would provide a second strong anchoring point in the binding site. For this, we synthesized another template molecule, N_{α} -hexanoyl glutamic acid (Figure 2.4; see also Figure 2.31 for ^1H NMR, ^{13}C NMR and mass spectrum), which has two free acid groups. Since amidiniums form stronger bonds with carboxylate than with amide groups, this should result in a more stable and favorably pre-organized 1:2 complex of template-AB (Figure 2.12).

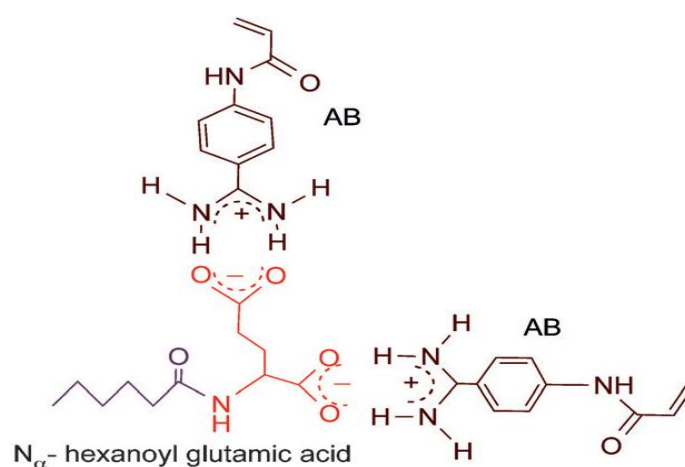


Figure 2.12. Proposed complex formation between the template N_{α} -hexanoyl glutamic acid and the monomer AB.

Our hypothesis was confirmed by ^1H NMR titration and Job plot performed in $\text{CD}_3\text{OD}/\text{D}_2\text{O}$ (4:1), which indeed revealed the coexistence of 1:2 and 1:1 complexes. The analysis of titration experiments supported the Job plot data and provided overall binding constant $\beta_{12} > 10^7 \text{ M}^{-1}$ (Figure 2.13). The link between the overall binding constant and the association constants of the two equilibria is given by the following relationship: $\beta_{12} = K_{11}K_{12}$, where K_{11} and K_{12} represent the association constants of the 1:1 and 1:2 complex, respectively.

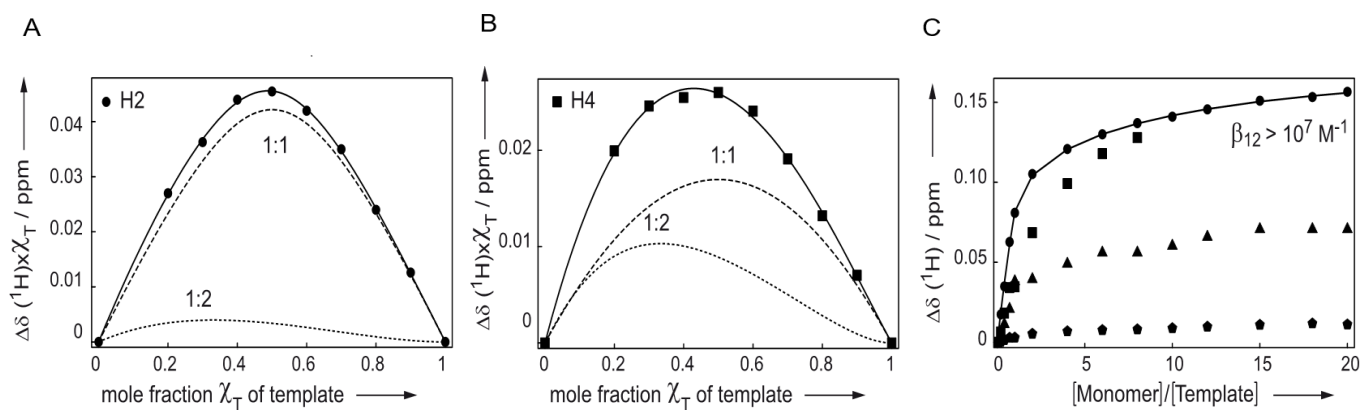


Figure 2.13. ^1H NMR analysis of Job and titration experiments of $N\alpha$ -hexanoyl glutamic acid with AB in $\text{CD}_3\text{OD}/\text{D}_2\text{O}$ (4/1) at 25 °C. The chemical shift difference ($\Delta\delta$) of 4 protons (H2, H3, H4 and H2' in Figure S1, Annex 1) close to the interaction sites was measured in the absence and the presence of the monomer. Labile protons could not be exploited for this analysis because of their fast exchange with the solvent, which makes them “invisible”. (A, B) Job plot with non-linear regression analysis (Connors, 1987) showing a mixture of 1:1 (dashes) and 1:2 (dots) complexes for H2 and H4 protons of $N\alpha$ -hexanoyl glutamic acid. (C) titration curve with non-linear regression analysis of the 1:2 complex corresponding to an overall binding constant (Thordarson, 2011) $\beta_{12} > 10^7 \text{ M}^{-1}$ for the H2 of $N\alpha$ -hexanoyl glutamic acid. Owing to peak overlap, concentration ratios higher than 8 could not be exploited for H4 on the titration curve of $N\alpha$ -hexanoyl glutamic acid. For both template molecules, the protons near the carboxyl group (H2, H3) show the biggest chemical shift difference, whereas the chemical shift difference of the protons further away from the interaction site (H2') is smaller. The non-linear regression analysis of the experimental data has been done using a home-written Mathematica program and a Matlab code written by Pall Thordarson (Thordarson, 2011).

II.3 Binding studies in artificial sweat

We now proceeded to the binding assessment of the MIP templated with $N\alpha$ -hexanoyl glutamic acid in the artificial sweat. Interestingly, the MIP showed high and specific binding in artificial sweat during equilibrium binding studies with 200 nM $N\alpha$ -hexanoyl glutamine and the target glutamine conjugates 100 nM cj3M2H or cj3H3MH (Figure 2.14). This MIP has a diameter of ca. 600 nm, as inferred from the scanning electron microscope image (Figure 2.15) and is suitable for skin applications because their large size prevents their penetration into the skin.

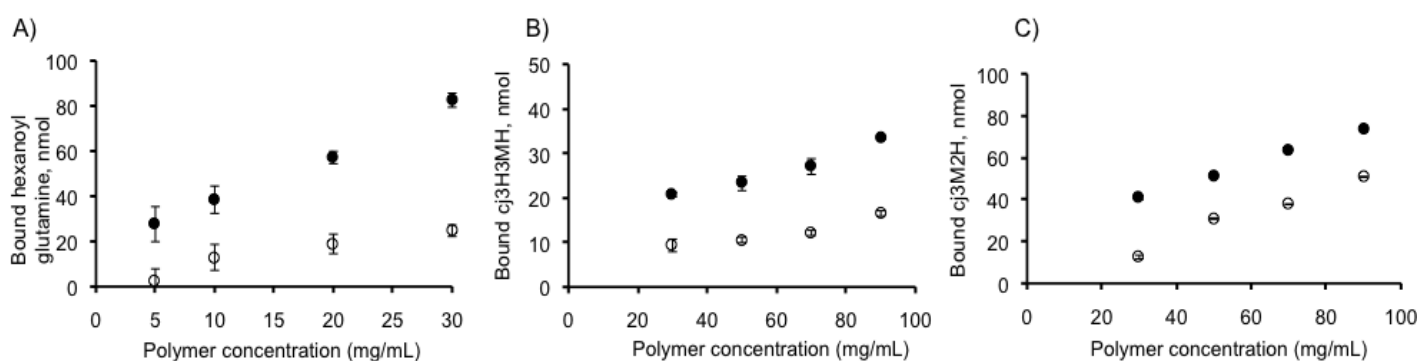


Figure 2.14. Equilibrium binding isotherms in artificial sweat for A) 200 nmol of $N\alpha$ -hexanoyl glutamine; B) 100 nmol of cj3H3MH and C) 100 nmol of cj3M2H, of MIP (filled circles) and NIP (empty circles), prepared with $N\alpha$ -hexanoyl glutamic acid as template. Analysis by LC-UV-ELSD. Data are the mean from two independent experiments. The error bars represent standard deviations.

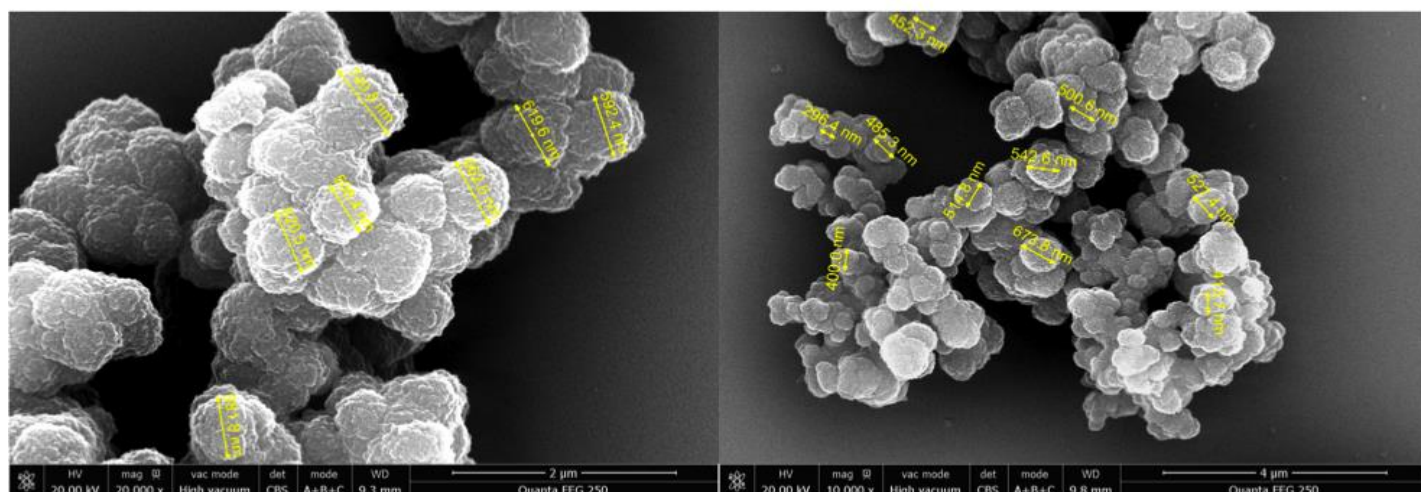


Figure 2.15. SEM images of MIP T2-AB (left) and NIP (right) prepared in methanol.

II.4 Capture of undesirable molecules in human sweat by the T2-AB MIP

Human sweat (pH~6) was collected from the armpit of volunteers prone to develop armpit odors. The volunteers had not used any deodorant products three weeks prior to sweat collection. The sweat was immediately frozen to preserve the composition. It was found to contain 135 ± 6.6 nmol/mL (37 ± 1.8 mg/mL) of cj3H3MH, 16.7 ± 1 nmol/mL (4.3 ± 0.3 mg/mL) of cj3M2H and 2.68 ± 0.14 nmol/mL (391 ± 20 ng/mL) of 3H3MH, as determined by LC-MS/MS (Figure 2.16). These values were deduced from calibration curves in spiked artificial sweat. Though the odorous acids are extremely volatile, the presence of 3H3MH could still be detected with LC-MS/MS, but not 3M2H.

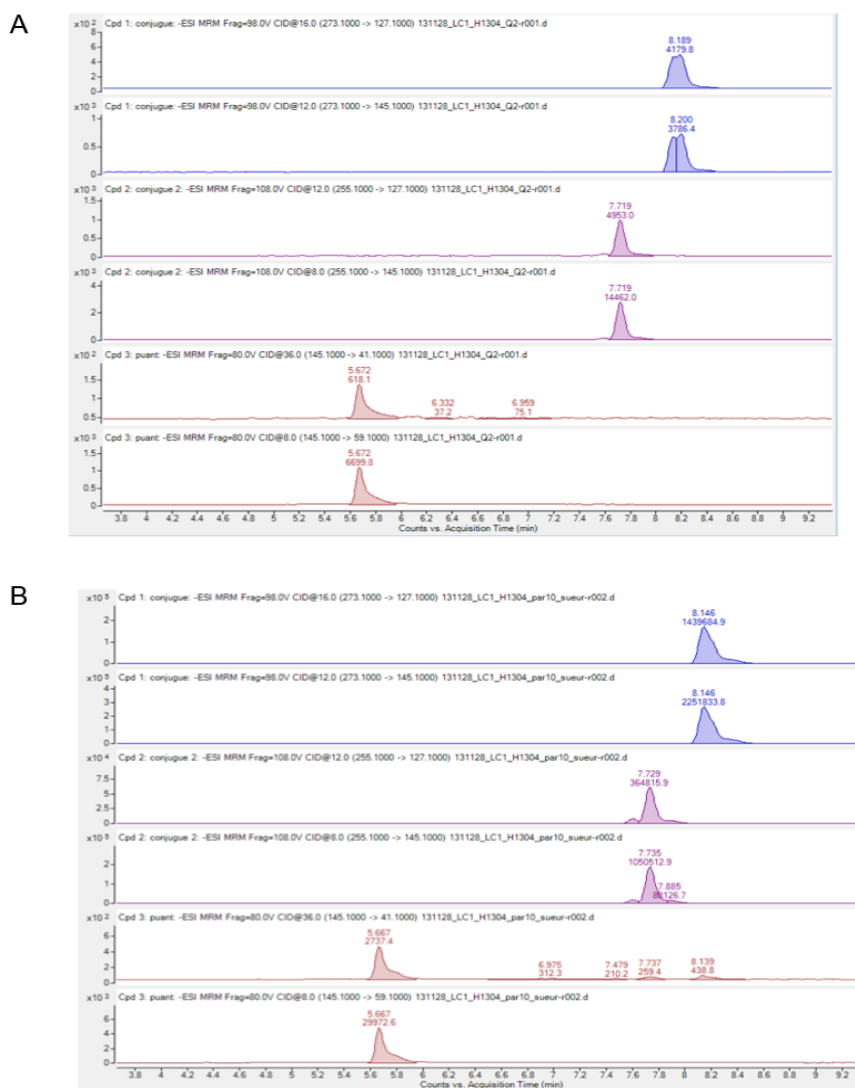


Figure 2.16. Analysis by LC-MS/MS of the glutamine conjugate precursors and the odorous acids in artificial and human sweat. Representative chromatograms of (A) cj3H3MH (blue), cj3M2H (violet) and 3H3MH (red) spiked in artificial sweat and (B) cj3H3MH (blue), cj3M2H (violet) and 3H3MH (red) present in human sweat. Monitoring of cj3H3MH (m/z 273.1 \rightarrow m/z 127.1, m/z 273.1 \rightarrow m/z 145.1) (blue), cj3M2H ($255.1 \rightarrow m/z$ 127.1, m/z 255.1 \rightarrow m/z 145.1) (violet) and 3H3MH (m/z 145.1 \rightarrow m/z 41.1 m/z 145.1 \rightarrow m/z 59.1) (red). 3M2H could not be detected.

To assess the binding performance of the MIP in human sweat, aliquots were incubated overnight with MIP and NIP at 20 °C. Human sweat alone incubated in parallel served as a control. The supernatants were analyzed simultaneously for the presence of cj3H3MH, cj3M2H and the odorant acid 3H3MH. The results showed the MIP was performant in human sweat, as it can capture the two conjugates and 3H3MH to a higher extent than the NIP (Figures 2.17 and 2.18). However, it can be observed that the NIP has some significant non-specific binding. This is not surprising since the interaction between AB and a carboxyl group ($K_a > 10^3 \text{ M}^{-1}$ in DMSO- d_6 with N_α -hexanoyl glutamic acid, as deduced from NMR titration data) is so strong that the randomly distributed amidine groups can also bind to some extent the target molecules non-specifically.

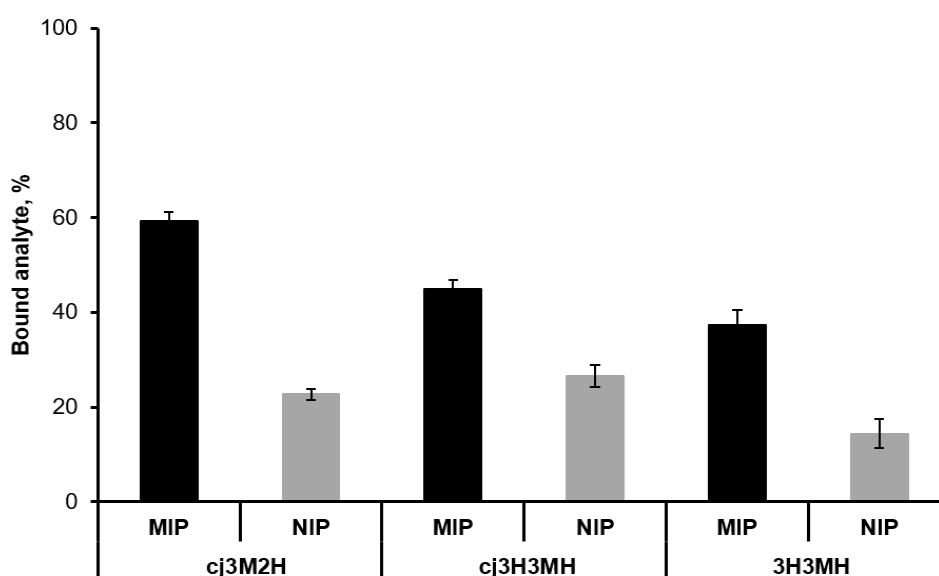


Figure 2.17. Capture of target molecules by 5 mg/mL of MIP and NIP after incubation in human sweat at 20 °C. Human sweat served as blank. Values represent the mean from two independent experiments with three repetitions of LC-MS/MS analyses for each case. The amount of cj3H3MH, cj3M2H and 3H3MH in human sweat was 135, 17 and 3 nmol/mL respectively.

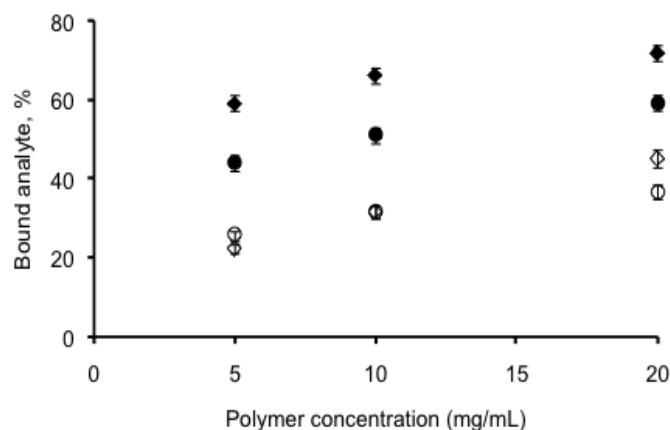


Figure 2.18. Capture at equilibrium of *cj3H3MH* (circles) and *cj3M2H* (rhombus) in human sweat by MIP (filled symbols) and NIP (empty symbols) at 20 °C. Human sweat alone served as control. Analysis by LC-UV-ELSD. Data are the mean from two independent experiments with 3 injections for each point. *cj3H3MH* and *cj3M2H* in human sweat were 135 nmol/mL and 17 nmol/ml, respectively.

The efficiency of the scavenging MIP in human sweat was not an evident task, since human sweat is a very complex sample containing an abundance of compounds (Table 2.1) which could prove detrimental to the recognition properties of the MIP. It contains in particular a large number of carboxylic acids, many of them at concentrations higher than those of our target molecules, for example lactic acid, pantothenic acid, nicotinic acid, and many amino acids. However, despite the presence of numerous constituents with carboxylic acid groups (some in the mM range) such as amino acids, short chain acids and vitamins in human sweat, the MIP selectively captured the target molecules, hence proving the presence of high fidelity imprinted sites.

II.5 Capture in human sweat of *cj3M2H* and *cj3H3MH* by MIP incorporated in a dermocosmetic deodorant formulation.

For real-life application, the MIP needs to function in a deodorant formulation. Thus, equilibrium binding studies were performed, this time at body temperature (37 °C), in the deodorant formulation spiked with either 200 µM of *cj3H3MH* or 100 µM of *cj3M2H*. These values represent upper extremes in terms of concentration of the 2 conjugates in human sweat. Under these conditions, 4 mg of MIP showed high binding capacity as it could capture 89% of *cj3M2H* and 63% of *cj3H3MH* (Figure 2.19). The binding behaviour towards the odorous acid 3H3MH could not be evaluated due to its high volatility at 37 °C.

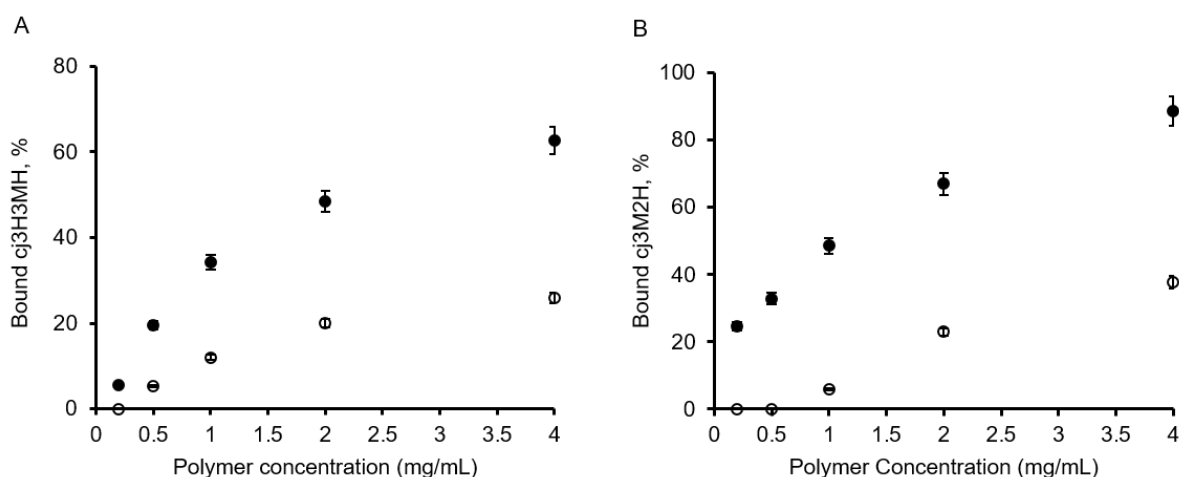


Figure 2.19. Equilibrium binding isotherms of MIP (filled circles) and NIP (empty circles) for spiked A) 200 μM cj3H3MH and B) 100 μM cj3M2H, in a deodorant formulation.

To further simulate the conditions as in a real cosmetic application, the polymers were dispersed in the deodorant formulation and mixed with human sweat in a 1:1 (v/v) ratio. The binding specificity of the two conjugates to the MIP in human sweat seems to be even better when mixed in the deodorant formulation than in sweat alone (Figure 2.20). The lower non-specific binding may be due to the favourable environment created by the lipidic components present in the formulation, or to the higher temperature (37 °C).

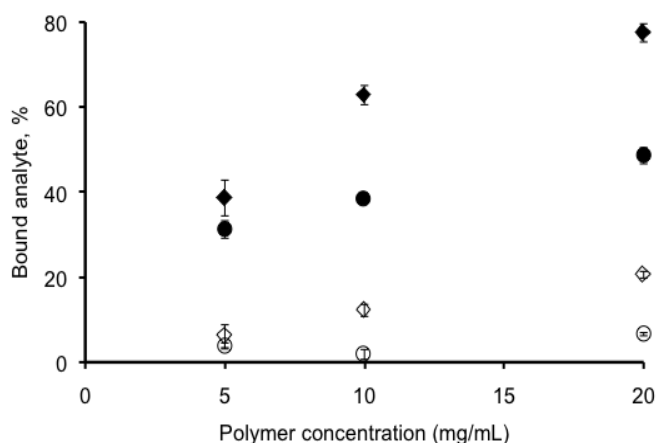


Figure 2.20. Capture of cj3H3MH (circles) and cj3M2H (rhombus) in human sweat by MIP (filled) and NIP (empty) incorporated in a deodorant formulation, at 37 °C. Data are the means from two independent experiments with 3 injections for each point. cj3H3MH and cj3M2H in human sweat were 135 nmol/mL and 17 nmol/mL, respectively.

As an additional proof of specific binding to the imprinted sites of the MIP, a 1:1 mixture of artificial sweat and deodorant formulation was spiked with 200 μM of either cj3H3MH or a short chain carboxylic acid present in human sweat, hexanoic acid. Upon incubation with the polymers, a large difference in binding was observed between MIP and NIP with cj3H3MH, whereas with hexanoic acid, the binding was

lower and virtually the same with MIP and NIP (Figure 2.21), which clearly indicates that the MIP binds specifically the target conjugate in this very complex environment. As expected, the MIP can also bind other COOH containing molecules but via non-specific interactions.

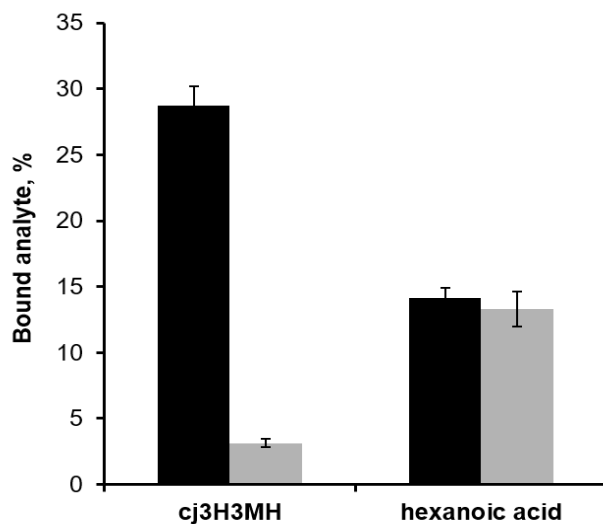


Figure 2.21. Capture of cj3H3MH or hexanoic acid, spiked at 200 μ M, by 10 mg/mL MIP (black) and NIP (grey) in a 1:1 mixture of artificial sweat (16 mM urea, 10 mM lactic acid, 15.2 mM albumin, 30 mM NaCl, pH 5.8) and deodorant formulation at 37 °C. Data are the means from two independent experiments with 3 injections for each point.

In conclusion, we have developed a plastic antibody as the active ingredient of a cosmetic product, on the example of a new deodorant principle to suppress body odors. At the same time, we have demonstrated the feasibility of preparing highly selective molecularly imprinted binding sites for recognition in complex aqueous media, using a polymerizable amidinium monomer which can form stoichiometric interaction with a high binding constant for carboxyl groups. The judicious design of the template resulted in cavities bearing two amidinium functionalities favorably positioned in a precise spatial arrangement so as to selectively capture the precursors of malodorous compounds from human sweat.

II.6 Assessment of HaCaT cell viability in the presence of MIP

In the previous sections, we have illustrated the high potential of the designed MIP as an active ingredient of a cosmetic product on the example of a new deodorant principle. At the same time, one of the main concerns in this work was that the synthesis of MIP should be performed with chemicals that would meet the criteria required by the cosmetic industry regarding topical skin application.

In light of a potential application of this MIP as deodorant principle, we wanted to obtain more information concerning the skin toxicity of the MIP. Herein, the first attempts to assess the effect of the MIP on epidermal cells will be presented. For the evaluation of the *in vitro* toxicity of the MIP, the immortalized keratinocyte cells HaCaT were employed. This cell line was chosen, because the part of the skin that could be potentially exposed to the MIP particles incorporated in a dermocosmetic formulation is the upper sub-layer of the epidermis, the *stratum corneum* composed by cornified keratinocytes (MacNeil, 2007). No other cell line (such as fibroblasts) was employed, since the size of MIP particles does not allow for the disruption of the skin barrier.

The effect of the MIP on the epidermal cells was assessed by the MTT assay, which relies on the measurement of the purple formazan product formed after reduction of the yellow dye 3-(4,5-dimethylthiazol-2-yl)-2,5-diphenyltetrazolium bromide (MTT) in living cells, as illustrated in Figure 2.33. The absorbance of this colored compound at 570 nm can be read by spectrophotometric measurements, which reflect the number of living cells. In this context, the MTT assay allows for the evaluation of the cellular metabolic activity and can contribute to the assessment of the cytotoxic effect of the MIP.

In our case, concentrations of MIP varying from 10 to 500 µg/mL were employed for the MTT test. This wide range of concentrations was chosen so as to be close to the amount used for the binding experiments (refer to section II.4-II.5). Concentrations equal or higher than 1 mg/mL could not be tested, since the MIP precipitated in the microwell, and this precipitation inhibited the correct interpretation of the spectroscopic results. Cell viability was measured after 24 and 48 h incubation of HaCaT cells with the aforementioned concentrations of MIP. The surfactant Triton X at 0.5 % was used as positive control. As shown in Figure 2.22, the MIP particles do not induce cell toxicity for concentrations up to 100 µg/mL, for both incubation periods. At higher concentrations, a small decrease in cell viability was observed, with an 18 % loss of viability at 500 µg/mL. It can be assumed that the decrease in cell viability at higher concentrations of MIP can be caused by the increased stress imposed to the cell by the presence of large aggregated MIP particles.

It is important to note that the increase of incubation time to 48h in the presence of MIP did not have any additional effect on the cell viability. This suggests that the MIP could potentially stay in contact with the skin for longer time without provoking irritation, however more experiments are necessary so as to fully assess the biological effect of MIP as skin sensitizer, involving its application on artificial skin (such as

Episkin) and most importantly clinical studies. Nevertheless, these encouraging results pave the way towards future application of this MIP in deodorant formulations which postulate an anti-odor efficacy for 48h. In this respect, studying further the kinetics of the MIP anti-odor performance would be very useful, to ultimately prove its scavenging efficacy for longer periods.

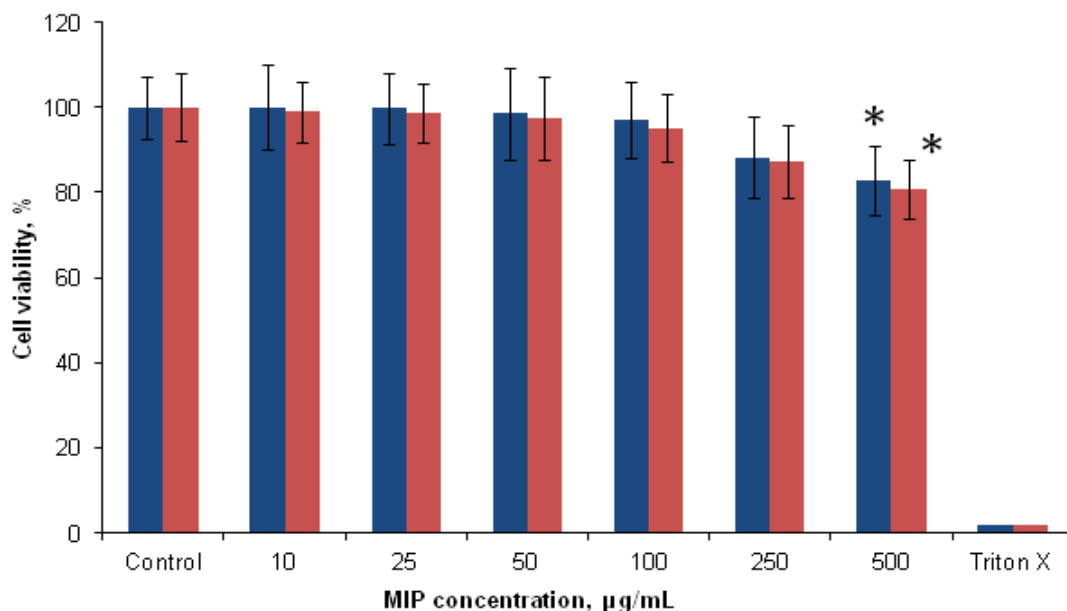


Figure 2.22. Cell viability as determined by MTT assay for HaCaT cells after incubation for 24h (blue) and 48h (red) with MIP particles. Values represent the mean of 5 repetitions in each case. * $P < 0.05$ compared with Control ($n=5$).

We further performed another *in vitro* cytotoxicity test. The cell apoptosis detection kit (Hoechst 33342/PI) was applied under the same experimental conditions as for the MTT test. The membrane-impermeant fluorescent dye propidium iodide (PI), which is excluded from viable cells, was used to evaluate the cytotoxic effect of the MIP on the HaCaT cell line. In dead or cell-membrane damaged cells, PI intercalates between double-stranded DNA and its fluorescence excitation maximum is shifted to the red (535 nm), while its fluorescence emission maximum is shifted to the blue (617 nm). Unfortunately, this imaging-based test was not compatible with materials such as the AB-based MIP particles that exhibit autofluorescence and aggregate easily; thus, the results were not exploitable.

As perspective for future experiments, other cell viability tests could be performed, such as the neutral red uptake which evaluates the cell membrane integrity, or skin inflammation tests based the action of interleukins, as discussed in the Introduction of this chapter. Evidently, the physical properties of the MIP could be further optimized so as to be more suitable for dermocosmetic formulations.

II.7 Effect of MIP on commensal bacteria's growth

Our next step was to demonstrate their effect on the axillary bacteria commensal to the skin. For this reason, we isolated the bacteria in the human sweat sample collected from the axillary region of volunteers and provided by L'Oréal. Our aim is to isolate both *Corynebacteria* and *Staphylococci*, the two dominant genera of axillary bacterial population (Troccaz et al., 2009; Callewaert et al., 2013).

Human sweat sample, which was stored at -20 °C was spread on Luria-Bertani (LB) plates and three bacteria colonies, were observed after 48 h of incubation at 37 °C, as illustrated in Figure 2.23A. We also employed the use of blood agar, an enriched medium (refer to Annex 2 for the detailed composition) adapted for the isolation of more fragile bacteria such as *Corynebacteria*. Two bacteria colonies were observed after 48 h of incubation at 37 °C, (Figure 2.23B). The identification of the bacteria species by simple observation of the colonies cannot be performed.

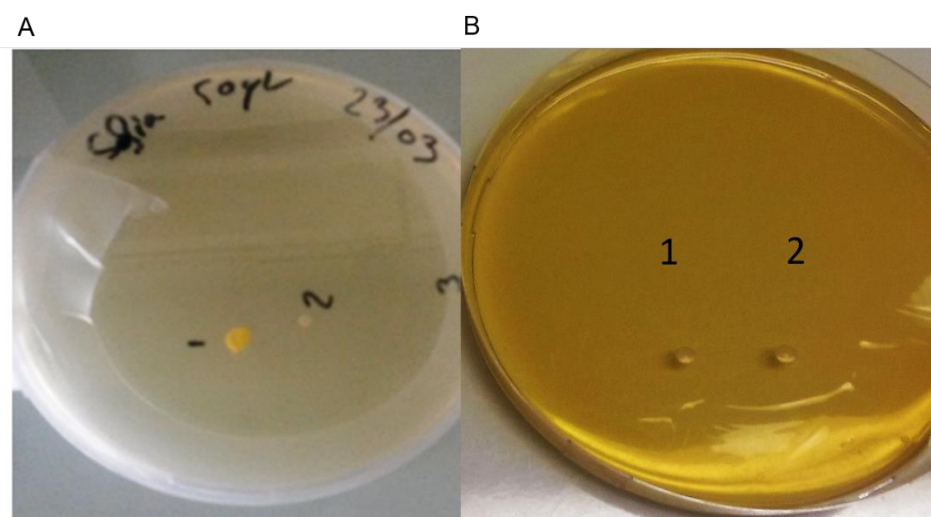


Figure 2.23. Bacterial growth of 50 µL of human sweat after incubation at 37 °C, plated on A) LB and B) Blood agar.

To rapidly identify the bacteria from human sweat, MALDI-TOF mass spectrometry analysis was performed, as described in section III.14. Nowadays, MALDI mass spectrometry has become the method of choice for bacteria identification, since it features short analysis time, high sensitivity, and intact cell measurements, as well as the possibility of automation (Krasny´ et al., 2013). The results of MALDI-TOF analysis showed that the colonies identified belong to 4 bacterial species: *Staphylococcus hominis*, *Staphylococcus epidermidis*, *Corynebacterium Striatum* and *Micrococcus luteus*. In moist areas, such as the human axilla, *Corynebacterium spp.* and *Staphylococcus spp.* dominate the resident flora, which was demonstrated earlier by culture-based approaches (Taylor et al., 2003; Grice et al., 2009). The species identified in the sample of human sweat were employed as a representative model for the evaluation of the effect of the MIP on the bacteria commensal to the skin.

Culture media more enriched in proteins and providing a sufficient carbon source were employed for the experiments described hereafter. The use of such media will enable the growth of all the bacteria (*Corynebacteria* and *Staphylococci*) in the same medium. To examine the bacterial growth rate and to determine the growth curve in the presence of the MIP, *S. epidermidis*, *C. striatum* and *M. luteus* bacteria were grown in 5 mL of liquid Brain Heart Infusion (BHI) medium supplemented with 0.5 mg/mL of MIP. As blank control, samples without the addition of MIP were prepared. Negative control samples corresponding to each bacteria were supplemented with 0.5 mg/mL of silver nitrate. Silver in the form of salts or nanoparticles is a well-known antimicrobial, incorporated into a range of deodorants to suppress the growth of skin resident bacteria associated with body odors (Edwards-Jones, 2009). As shown in Figure 2.24, the incorporation of the MIP in the culture medium did not affect the bacterial growth at any stage of the kinetics. Similar results were obtained for the blank samples and the samples implemented with the MIP in terms of bacterial population number and growth rate. Conversely, no bacterial growth was observed on silver nitrate implemented samples, throughout the experiments for all the bacteria species tested.

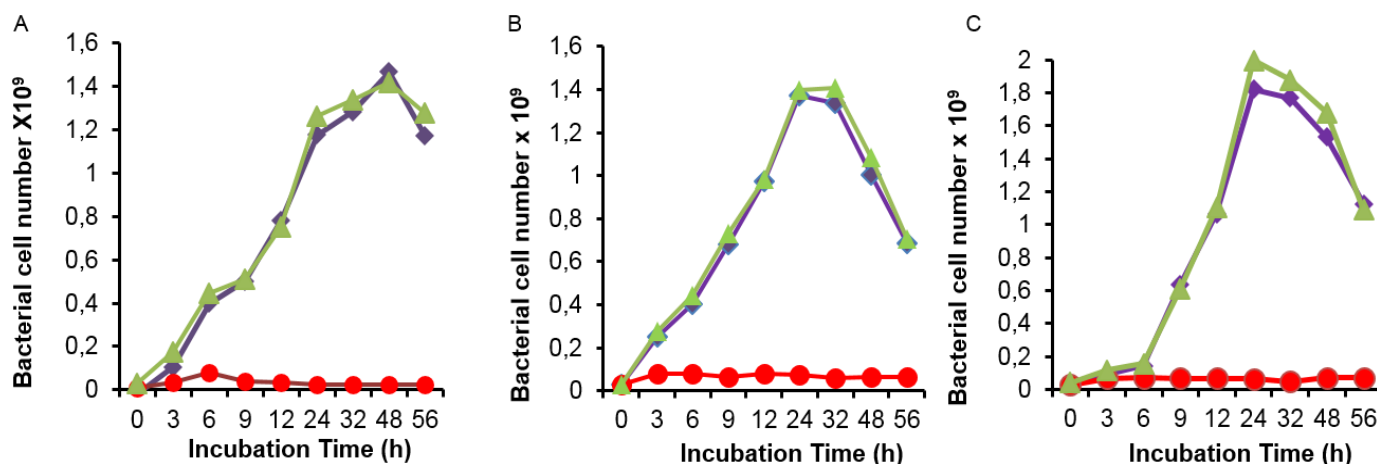


Figure 2.24. Growth curves obtained after incubation of the following bacteria species for a total of 56 hours A) *S. epidermidis*; B) *C. striatum* and C) *M. luteus*. MIP: violet rhombus, Control: green triangle and silver nitrate: red circle. Values represent the mean of two independent experiments.

For the above experiments, the same amount of silver nitrate and MIP was supplemented in the BHI medium. However, the bactericidal effect of silver ions is reported for far lower concentrations of silver ions (Greulich et al., 2012). To verify the effect of silver nitrate at concentration comparable to those reported in literature, the dynamics of bacterial growth for *S. epidermidis* was performed using 100 times lower concentration of silver nitrate, (5 $\mu\text{g/mL}$ prepared from a stock solution of 500 $\mu\text{g/mL}$ in BHI) and similar results were obtained.

Moreover, the effect of the MIP on the bacteria was also investigated in plate cultures (Sondi et al., 2004). As a model, *S. epidermidis* was chosen and cultured on blood agar plates supplemented with 0.5 mg/mL of MIP. The photos taken after 24h of incubation show that the presence of MIP particles at a

concentration of 0.5 mg/mL resulted in a small decrease on the bacteria growth compared to the control samples, as assessed by count of the bacteria colonies (Control= 222 cfu, MIP=168 cfu, Figure 2.25). Interestingly, morphological differences on the bacteria colonies were observed between the treated and non-treated samples. In fact, the colonies appear to have bigger size on the blood agar plate implemented with MIPs compared to the control samples, which may suggest that smaller colonies were merged. It must be noted also that on silver nitrate-implemented sample no bacterial growth was observed (results not shown). Further experiments are necessary to confirm these results.

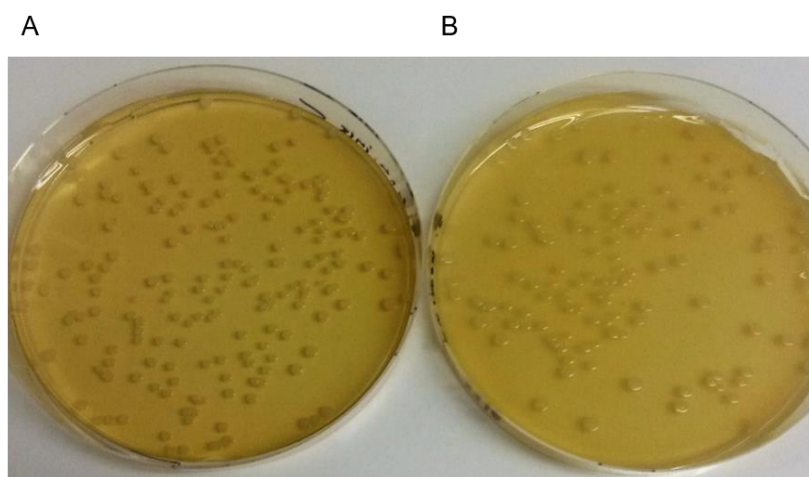


Figure 2.25. Blood agar plates inoculated with *S. epidermidis* A) Control samples; B) Supplemented with MIP at 0.5 mg/mL.

These results, obtained on bacterial cultures *in vitro*, are quite promising, since it appears that the addition of the MIP does not affect the growth of commensal bacteria in liquid culture. Evidently, clinical studies of the MIP incorporated in cosmetic formulations on human subjects are necessary so as to study *in situ* any potential effect on commensal bacteria or shift towards a particular bacteria community, as reported by Callewaert et al., 2014 concerning the use of aluminium salts in antiperspirants. To the best of our knowledge this is the first report suggesting the potential biocompatibility of a MIP, applied as an active ingredient in cosmetics.

III. Experimental

III.1 Materials and methods

HPLC solvents were purchased from Biosolve Chimie (Dieuze, France). Other solvents, bacterial growth media and chemicals were of analytical grade and purchased from VWR International (Fontenay sous Bois, France) or Sigma-Aldrich (St-Quentin Fallavier, France), unless otherwise stated. The odorant acids, 3M2H and 3H3MH were purchased from Interchim (Montlucon, France). Water was purified using a Milli-Q system (Millipore, Molsheim, France).

HaCaT cells were obtained from Cell Lines Service (Eppelheim, Germany). Cell culture flasks (crystal-grade polystyrene), 12 well plates (crystal-grade polystyrene), penicillin/streptomycin, Dulbecco's Modified Eagle Medium (DMEM), phosphate buffered saline (PBS), fetal bovine serum (FBS), 0.25% trypsin/ethylenediaminetetraacetic acid (EDTA) were from Thermo Scientific (Illkirch, France). 3-(4,5-dimethylthiazol-2-yl)-2,5-diphenyl tetrazolium bromide (MTT reagent) was purchased from Sigma-Aldrich (St-Quentin Fallavier, France).

^1H and ^{13}C NMR experiments were performed in $\text{DMSO-}d_6$ on a 400 MHz Bruker spectrometer at 25 °C. Scanning electron microscopy (SEM) imaging was carried out on a Quanta FEG 250 scanning electron microscope (Eindhoven, Netherlands). Polymer particles were sputter coated with gold prior to measurement.

MS-Q-TOF analysis of (4-acrylamidophenyl)(amino)methaniminium acetate, N_α -hexanoyl glutamine and N_α -hexanoyl glutamic acid was performed on an Agilent 6538 Q-TOF mass spectrometer with a dual ESI ion source. The mass spectrometer was operated in positive jet stream ESI mode (range: m/z 50-1100). Nitrogen was used as the dry gas at a flow rate of 12 L/min and a pressure of 30 psi. The nebulizer temperature was set to 300 °C.

HPLC of N_α -hexanoyl glutamine, cj3H3MH and cj3M2H was carried out on an analytical column Agilent Poroshell 120 C18 (4.6 x 50 mm, 2.7 μm) connected to a DIONEX Ultimate 3000 (Thermo Scientific, France) equipped with a diode array detector monitoring at 203 and 235 nm, and an evaporative light scattering detector (ELSD) (380-ELSD, Agilent Technologies, France). The solvent system was A: 0.1% formic acid in water and B: methanol. The gradient program began with 2% B, ramped to 95% B at 10 min, held at 95% for 5 min, returned to 2% B in 0.2 min and was held for 0.8 min. The flow-rate was 1 mL/min. The settings of the ELSD detector were: evaporation temperature 80 °C, nebulization temperature 40 °C and nitrogen flow 1 SLM (standard litre per min). To determine working concentrations, calibration curves were constructed using analyte concentrations varying from 50 to 200 μM which constituted the linear portion of the graphs. All calibration curves gave a coefficient of determination, $R^2 > 0.993$.

LC-MS/MS of cj3H3MH, cj3M2H and 3H3MH was performed on an Agilent 6460 Triple Quadrupole mass spectrometer with an Agilent Jet Stream electrospray ion source. HPLC was carried out on a Kinetex HILIC 2.6 mm (100 Å, 150 x 3 mm, 2.6 mm) column connected to an Agilent Infinity 1290 HPLC. The solvent system was A: 10 mM ammonium acetate in H₂O and B: acetonitrile. The gradient program began and stayed with 98% B for 1.7 min, ramped to 80% B at 12 min, 40% B at 13 min, held at 40% B for 5 min, returned to the initial conditions and kept constant for 10 min. The flow-rate was 0.7 mL/min. The mass spectrometer was operated in negative jet stream ESI mode. Nitrogen was used as nebulizer. The capillary voltage was -4000 V and the ion source gas temperature was 325 °C with a flow-rate of 13 L/min. Jet Stream gas temperature was 400 °C with a flow-rate of 12 L/min. Calibration curves were constructed using analyte concentrations varying from 10 to 2000 ng/mL which constituted the linear portion of the graphs. All calibration curves gave a coefficient of determination, $R^2 > 0.994$.

III.2 Synthesis of templates and functional monomer

- Synthesis of (4-acrylamidophenyl)(amino)methaniminium acetate.

(4-acrylamidophenyl)(amino)methaniminium chloride was first synthesized, as previously described (Beyazit et al., 2014). 34 g (0.25 mol) of sodium acetate trihydrate was dissolved in 200 mL of water and 2 g (9.6 mmole) of 4-aminobenzamidine dihydrochloride was added. (Figure 2.26). The solution was cooled to < 5 °C in an ice bath and 4 mL (49 mmole) of acryloyl chloride was added dropwise. The reaction was left to proceed for 1h. The pH was then adjusted to 4.0 with hydrochloric acid (37%) and precipitation was observed. After filtration, the precipitate was redissolved in 100 mL of water at 40 °C. Hydrochloric acid was again added this time to pH 1.0 and the product was left overnight to crystallize at 4 °C. The crystals were collected by filtration and dried in an oven maintained at 50 °C. The yield of (4-acrylamidophenyl)(amino)methaniminium chloride was 60%. ¹H NMR (400 MHz, DMSO-*d*₆): 10.56 (s, 1H), 8.99 (s, 4H), 7.84 (d, 2H), 7.81 (d, 2H), 6.48 (d, 1H), 6.31 (dd, 1H), 5.82 (s, 1H).

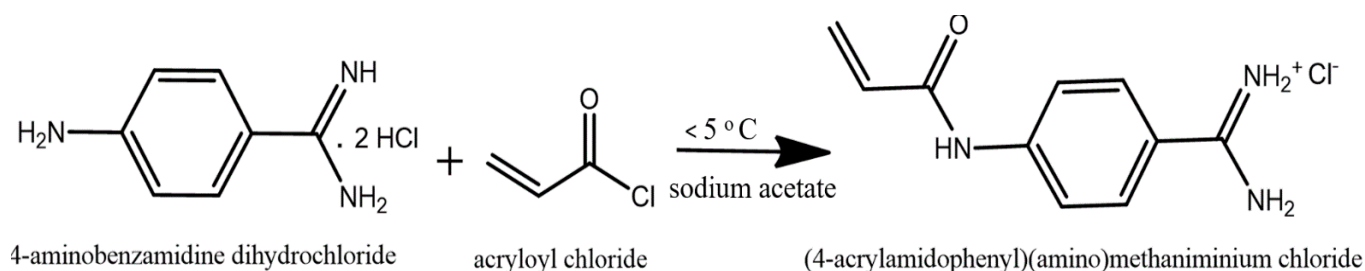


Figure 2.26. Synthesis of (4-acrylamidophenyl)(amino)methaniminium chloride (Beyazit et al., 2014).

For the synthesis of AB, acetate, 1.0 g of (4-acrylamidophenyl)(amino)methaniminium chloride was suspended in 100 mL of saturated sodium acetate solution and stirred overnight. The product was collected by filtration, washed with water to eliminate residual sodium acetate and dried at 50 °C. The yield of (4-acrylamidophenyl)(amino)methaniminium acetate, which we term AB in the text, was 60%.

^1H NMR, ^{13}C NMR and MS spectrum of the compound are shown in Figure 2.27 (A, B, C) and summarize as follows: ^1H NMR (400 MHz, DMSO- d_6): 10.56 (b s, 4H), 7.84 (m, 2H), 7.78 (m, 2H), 6.48 (dd, 1H, 16.9, 10.1 Hz), 6.31 (dd, 1H, 16.9, 1.9 Hz), 5.82 (dd, 1H, 1.9, 10.1 Hz), 1.72 (s, 3H); ^{13}C NMR (100MHz, DMSO- d_6): 175.99 (C1''), 165.1 (C7), 163.7 (C1'), 43.2 (C4), 131.5 (C2'), 128.6 (C2, C6), 128.0 (C3'), 124.2 (C1), 118.9 (C3, C5), 24.8 (C2''); ESI-MS (m/z): $[\text{M}^+]$ 190.10.

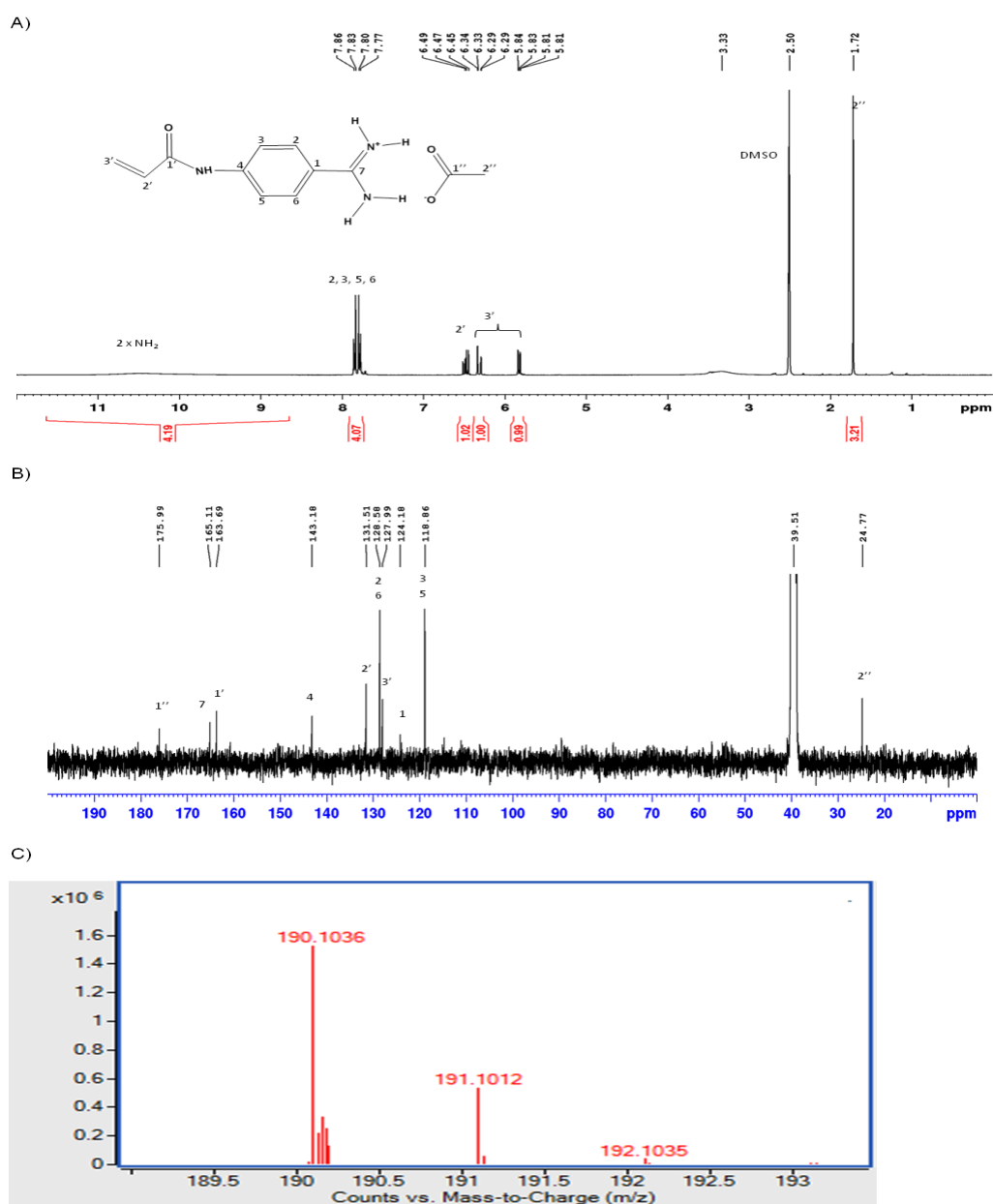


Figure 2.27. A) ^1H NMR; B) ^{13}C NMR in DMSO- d_6 and C) mass spectrum of (4-acrylamidophenyl)(amino)methaniminium acetate; N_α -hexanoyl-L-glutamine.

-Synthesis of N α -hexanoyl-L-glutamine

L-glutamine (34 mmol) and sodium carbonate (102 mmol) were dissolved in 50 mL water in a round-bottom flask. Hexanoyl chloride (34.2 mmol), diluted in 10 mL tetrahydrofuran (THF) was then added slowly under stirring (Figure 2.28) A white precipitate was formed and the reaction left to proceed overnight. The mixture was acidified to pH 1.0 and the organic phase was extracted three times with 50 mL of dichloromethane. After drying with Na₂SO₄ followed by filtration, the solvent was evaporated resulting in a white powder (2.5 g, yield = 35%). Elemental analysis (found): C 53.8%; H 8.24%; N 11.57%; O 26.1%.

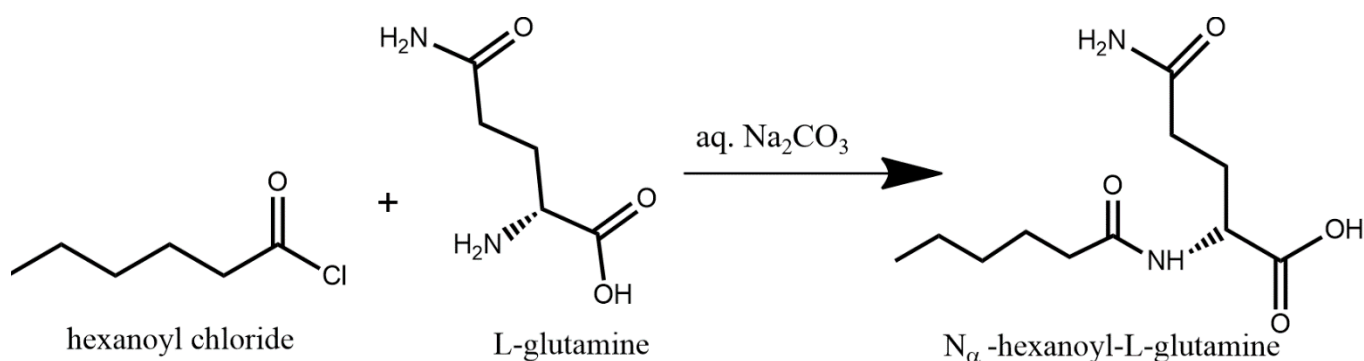


Figure 2.28. Synthesis of N α -hexanoyl-L-glutamine, according to the protocol of L'Oréal.

¹H NMR, ¹³C NMR and MS spectra of the compound are shown in Figure 2.29 (A, B, C) and summarize as follows:

¹H NMR (400 MHz, DMSO-*d*₆): 8.05 (d, 1H, 7.9 Hz), 7.29 (b s, 1H), 6.77 (b s, 1H), 4.14 (m, 1H), 2.10 (m, 4H), 1.92 (m, 1H), 1.73 (m, 1H), 1.49 (m, 2H), 1.25 (m, 4H), 0.90 (t, 3H, 6.9 Hz); ¹³C NMR (100MHz, DMSO-*d*₆) : 173.6 (C1), 173.4 (C5), 172.3 (C1'), 51.5 (C2), 35.0 (C2'), 31.4 (C4), 30.8 (C4'), 26.8 (C3), 24.9 (C3'), 21.9 (C5'), 13.9 (C6'), ESI-MS (m/z): [M+H]⁺ 245.15

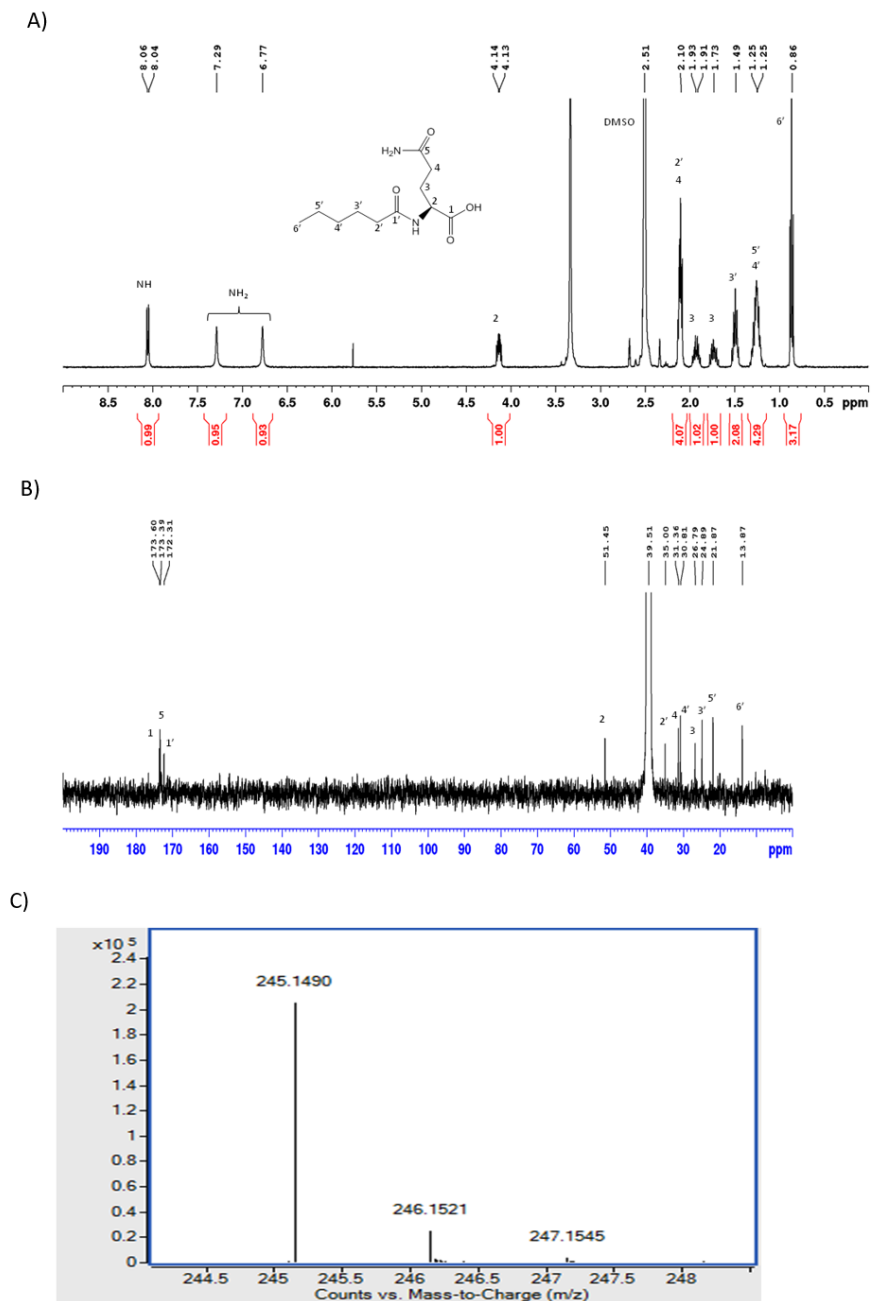


Figure 2.29. A) ^1H NMR; B) ^{13}C NMR in $\text{DMSO-}d_6$ and C) mass spectrum of $N\alpha$ -hexanoyl-L-glutamine.

-Synthesis of N_{α} -hexanoyl-L-glutamic acid

The N_{α} -hexanoyl-L-glutamic acid was synthesized as demonstrated in Figure 2.30. Briefly, L-glutamic acid diethyl ester hydrochloride (0.1 mmol) was dispersed in THF (20 mL). Pyridine (0.2 mmol) was added, followed by dropwise addition of hexanoyl chloride for 5 min. An increase in temperature from 22 °C to 37 °C was noted. The resulting solution was stirred at ambient temperature for 20 h, then filtered. The filtrate was evaporated under reduced pressure to a viscous liquid (2.45 g, yield = 81%). ^1H NMR (400 MHz, $\text{DMSO-}d_6$) confirmed the structure to be diethyl N_{α} -hexanoyl-L-glutamate. This intermediate product (2.45 g) was dissolved in 20 mL ethanol. Sodium hydroxide (1 M, 20 mL) was added and stirred at ambient temperature for 3 days. The pH was lowered to ~ 1.5 with concentrated hydrochloric acid and immediately extracted with ethyl acetate (3 x 20 mL). The organic phases were combined, washed with water (30 mL), dried over sodium sulphate, filtered and the ethyl acetate removed by evaporation under pressure to yield a viscous colorless liquid (1.03 g, yield = 50%). Elemental analysis (found): C 51.5%; H 7.94%; N 10.87%; O 24.92%.

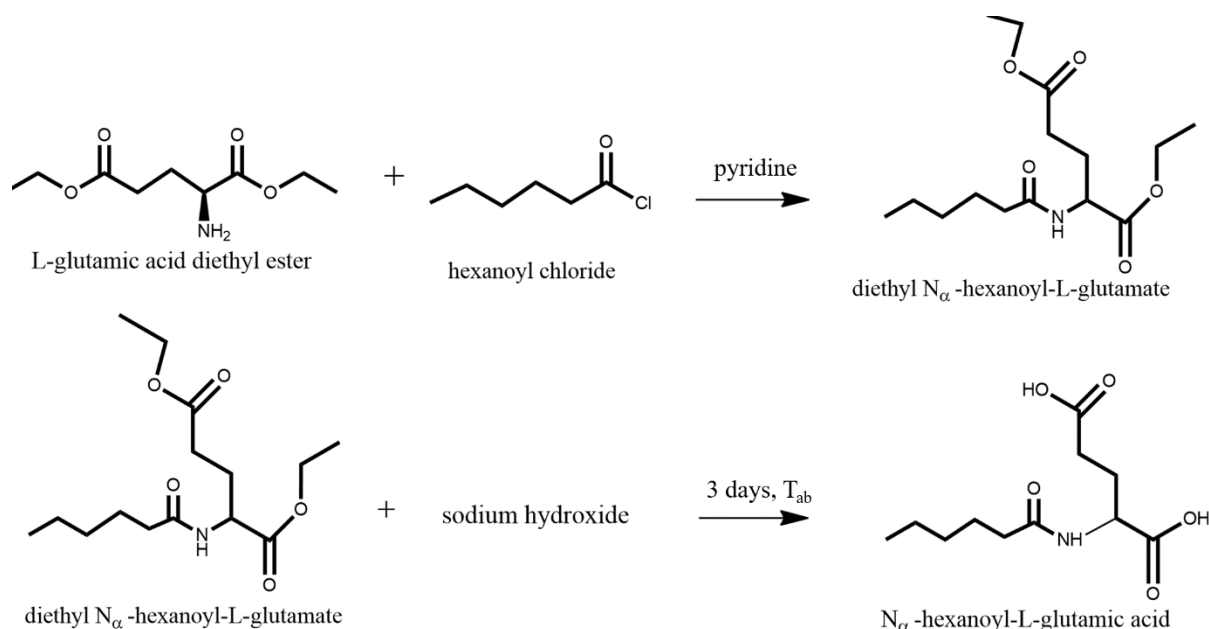


Figure 2.30. Synthesis of N_{α} -hexanoyl-L-glutamic acid, according to the protocol of L'Oréal.

^1H NMR, ^{13}C NMR and MS spectrum of the compound are shown in Figure 2.31 (A, B, C) and summarize as follows: ^1H NMR (400 MHz, $\text{DMSO-}d_6$): 8.05 (d, 1H, 7.9 Hz), 4.19 (m, 1H), 2.29 (m, 2H), 2.10 (m, 2H), 1.95 (m, 1H), 1.75 (m, 1H), 1.50 (m, 2H), 1.25 (m, 4H), 0.90 (t, 3H, 7.2 Hz); ^{13}C NMR (100MHz, $\text{DMSO-}d_6$): 173.7 (C5), 173.5 (C1), 172.4 (C1'), 51.0 (C2), 35.0 (C2'), 30.8 (C4'), 30.1 (C4), 26.3 (C3), 24.9 (C3'), 21.9 (C5'), 13.9 (C6'), ESI-MS (m/z): $[\text{M}+\text{H}]^+246.13$.

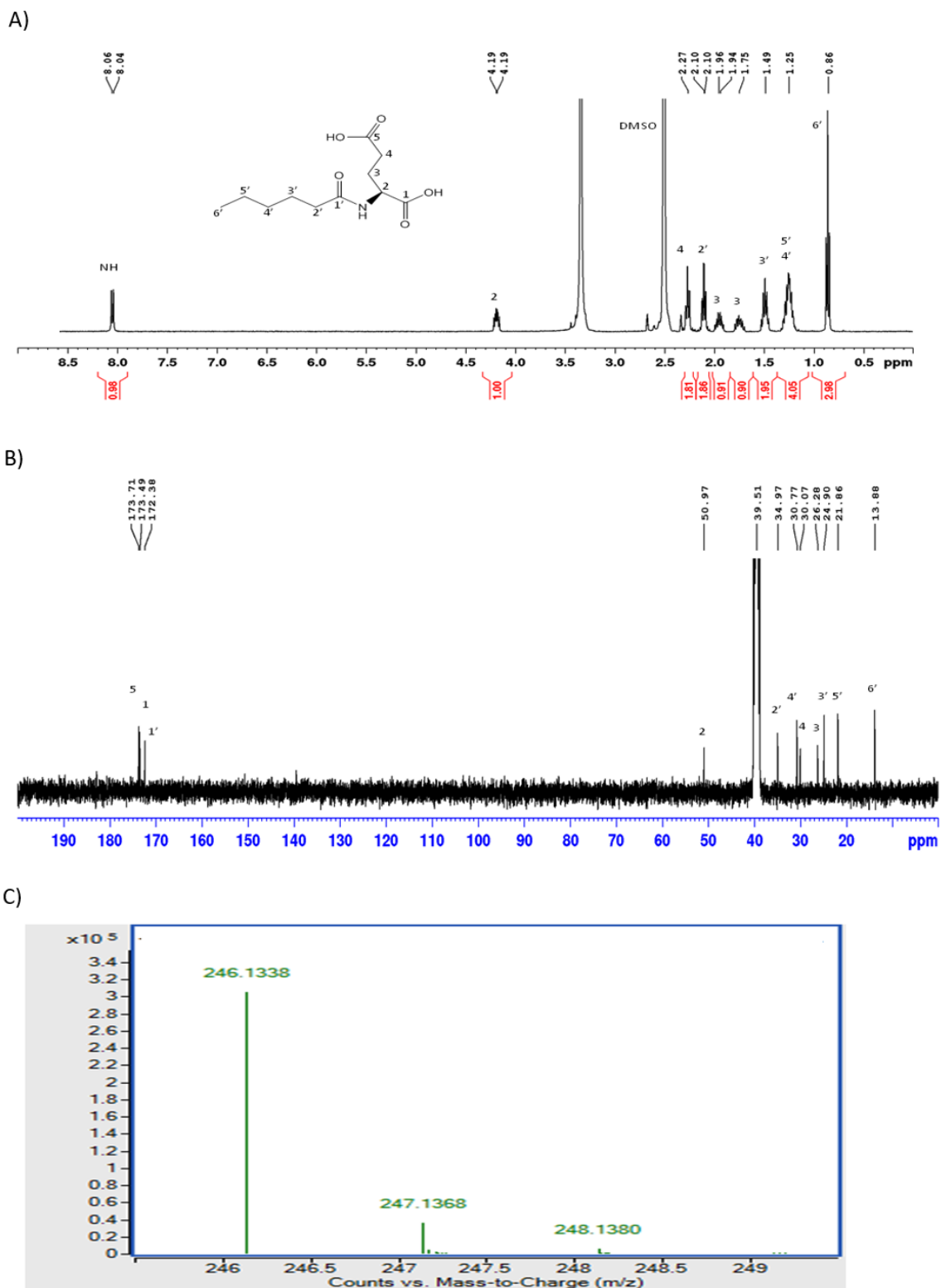


Figure 2.31. A) ^1H NMR; B) ^{13}C NMR in $\text{DMSO-}d_6$ and C) mass spectrum of N_α -hexanoyl-L-glutamic acid.

III.3 NMR studies

The assignment of N_{α} -hexanoyl glutamine and N_{α} -hexanoyl glutamic acid resonances was deduced from COSY spectra (Figure S1, Annex 1)). The stoichiometry and the strength of the AB-template complex were determined by chemical shift analysis using the methods of continuous variation (Job plot) and of titration, respectively. All experiments demonstrate that the free and the template-bound monomer forms are in fast exchange on the NMR timescale in the sense that a single (weighted) averaged chemical shift is observed. NMR studies were first performed in DMSO- d_6 , an aprotic solvent in which both AB and the conjugates are soluble. Later, CD₃OD/D₂O (4/1) was also utilized as solvent for NMR analysis, being the closest to our polymerization solvent. It must be noted that organic and aprotic solvents are typically used for NMR analysis, to enable the study of all protons. In our case both solvent systems were employed so as to better simulate the conditions of MIP polymerization.

Figure 2.32 shows the NMR analysis of the complex formation in DMSO- d_6 at 5 mM for N_{α} -hexanoyl glutamine and at 1 mM for N_{α} -hexanoyl glutamic acid, respectively. The chemical shift difference ($\Delta\delta$), due to complexation, of the alpha proton to the amide nitrogen of the template (H2), was followed as a function of the mole fraction of the template for Job plot and the monomer template ratio for titration experiments. The Job plot supports a 1:1 equilibrium for N_{α} -hexanoyl glutamine:AB and a mixture 1:1 and 1:2 for N_{α} -hexanoyl glutamic acid:AB (Figure (A, C)).

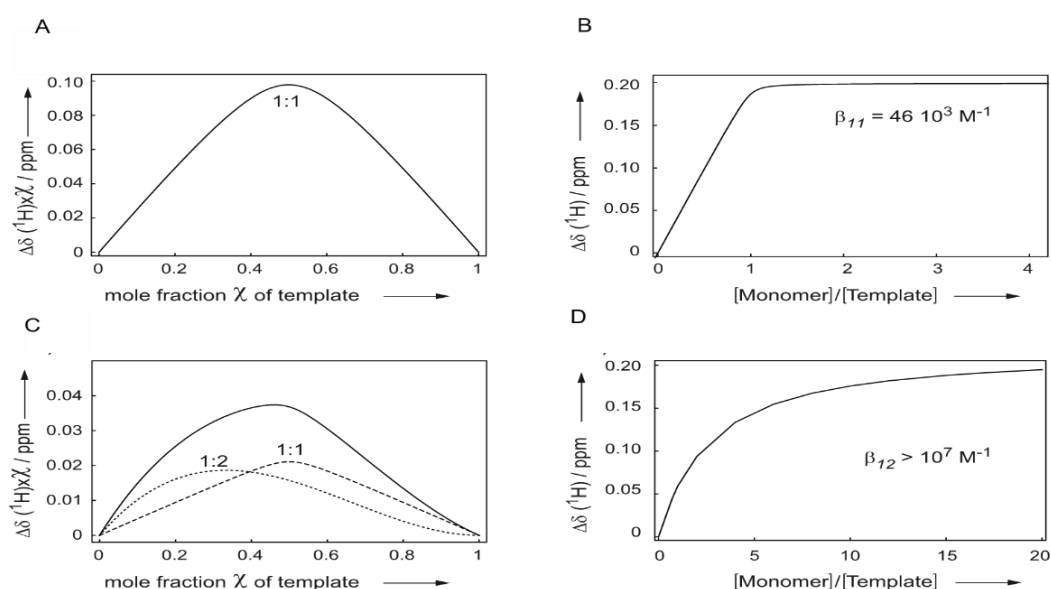


Figure 2.32. ^1H NMR of N_{α} -hexanoyl glutamine (A, B) and N_{α} -hexanoyl glutamic acid (C, D) with AB in DMSO- d_6 at 25 °C. The chemical shift difference ($\Delta\delta$) of the alpha proton to the amide nitrogen of the template molecules was measured in the absence and the presence of the monomer and is represented with filled circles. (A) Job plot and non-linear regression analysis (Connors, 1987) show a clear maximum at a molar fraction of 0.5 supporting a 1:1 stoichiometry of the complex monomer-template and (B) titration

curve and non-linear regression analysis' lead to an overall binding constant (Thordarson, 2011) β_{11} of $46 \times 10^3 \text{ M}^{-1}$ for N_{α} -hexanoyl glutamine. (C) Job plot and non-linear regression analysis showing a mixture of 1:1 (dashes) and 1:2 (dots) complexes and (D) titration curve and non-linear regression analysis of the 1:2 complex corresponding to an overall binding constant $\beta_{12} > 10^7 \text{ M}^{-1}$ for N_{α} -hexanoyl glutamic acid.

Similarly, Figures 2.10 and 2.13 presented in section II.2 show the NMR analysis of the complex formation in $\text{CD}_3\text{OD}/\text{D}_2\text{O}$ (4/1) at 1 mM for N_{α} -hexanoyl glutamine and at 0.5 mM for N_{α} -hexanoyl glutamic acid, respectively. Labile protons could not be exploited for this analysis because of their fast exchange with the solvent, which makes them “invisible”. The chemical shift difference ($\Delta\delta$), due to complexation, of four protons of the template (H2, H3, H4 and H2', see Figure S1, Annex 1), was followed as a function of the monomer to template concentration ratio for titration experiments. The Job plot supports a 1:1 equilibrium for N_{α} -hexanoyl glutamine:AB (Figure 2.10) and a mixture 1:1 and 1:2 for N_{α} -hexanoyl glutamic acid:AB (Figure 2.13). The titration data of H2 proton (full circles) of N_{α} -hexanoyl glutamine were fitted to a 1:1 binding isotherm (full line) by nonlinear regression using the program Mathematica 10.0 and lead to an association constant of $\beta_{11} = K_a = 9.4 \times 10^3 \text{ M}^{-1}$ (Figure 2.10C). Instead, for N_{α} -hexanoyl glutamic acid, a 1:2 binding isotherm had to be used to obtain a good fit, yielding an estimated overall binding constant ($\beta_{12} > 10^7 \text{ M}^{-1}$) (Figure 2.13C). This binding constant is too strong to be accurately measured by NMR. For both template molecules, the protons close to the interaction sites show the biggest chemical shift difference.

For the Job plot in $\text{DMSO}-d_6$, solutions of template and AB, at a constant total molar concentration of 5 mM for N_{α} -hexanoyl glutamine and 1 mM for N_{α} -hexanoyl glutamic acid, were prepared with the template mole fraction, $\chi_T = \frac{[T]}{[T]+[M]}$ varying from 0 to 1 by steps of 0.1.

Similarly, for the Job plot in $\text{CD}_3\text{OD}/\text{D}_2\text{O}$ (4/1), solutions of template and AB, at a constant total mole concentration of 1 mM for N_{α} -hexanoyl glutamine and 0.5 mM for N_{α} -hexanoyl glutamic acid, were prepared with the template mole fraction, $\chi_T = \frac{[T]}{[T]+[M]}$ varying from 0 to 1 by steps of 0.1. The total volume of each sample was 700 μL . For a single equilibrium, the position of the maximum indicates the stoichiometry of the system. Assuming a general reaction for the complex formation, $T_q + M_p \rightarrow C$, where q molecules of template can interact with p molecules of monomer, the equation (1) (Connors, 1987; Renny et al., 2013) is solved symbolically with the program Mathematica and the real solution used for the nonlinear fit of the Job plot data:

$$[C] = \beta_{11}(b\chi_T - q[C])^q(b(1 - \chi_T) - p[C])^p \quad (1)$$

where $[C]$ is the concentration of the complex, β_{11} the association constant, χ_T the template molar fraction and b a constant? The parameters obtained by the fit are b and β_{11} .

Association constants in DMSO- d_6 were determined by titrating an increasing amount of AB into a constant amount of template. Stock solutions of 40 mM AB were prepared and added (from 0 to 4 equivalents for N α -hexanoyl glutamine, and up to 20 equivalents for N α -hexanoyl glutamic acid) to a fixed concentration of template (5 mM for N α -hexanoyl glutamine and 1 mM for N α -hexanoyl glutamic acid).

Similarly, association constants in CD $_3$ OD/D $_2$ O (4/1) were determined by titrating an increasing amount of AB into a constant amount of template. A stock solution of 8 mM AB was prepared and added, from 0 to 4 equivalents, to a fixed 1 mM concentration of N α -hexanoyl glutamine, whereas a 20 mM AB stock solution was added up to 20 equivalents to a fixed concentration of 0.5 mM for N α -hexanoyl glutamic acid. For the same general reaction, the titration equations (2) and (4) were used for an equilibrium 1:1 and 1:2, respectively.

$$\Delta\delta = \delta_0 \frac{[C]}{[T]_0} \quad (2)$$

with δ_0 a constant and $[C]$ solution of the equation (3):

$$[C]^2 - [C] \left([T]_0 + [M]_0 + \frac{1}{\beta_{11}} \right) - [T]_0[M]_0 = 0 \quad (3)$$

where β_{11} is the binding constant, $[T]_0$ and $[M]_0$ total concentrations of the template and monomer, respectively.

$$\Delta\delta = \frac{\delta_{01}K_{11}[M] + \delta_{02}K_{11}K_{12}[M]^2}{1 + K_{11}[M] + K_{11}K_{12}[M]^2} \quad (4)$$

with δ_{01} and δ_{02} constants and $[M]$ solution of the equation (5):

$$K_{11}K_{12}[M]^3 + K_{11}(2K_{12}[T]_0 - K_{12}[M]_0 + 1)[M]^2 + (K_{11}([T]_0 - [M]_0) + 1)[M] - [M]_0 = 0 \quad (5)$$

where K_{11} and K_{12} are the affinity constants for the 1:1 equilibrium and the 1:2 equilibrium, respectively. The overall binding constant is $\beta_{12} = K_{11}K_{12}$ (Connors, 1987). For all Job and titration data presented in this work, the non-linear regression analysis has been done using a home-written Mathematica program and a Matlab code written by Pall Thordarson. (Thordarson, 2011).

III.4 Preparation of molecularly imprinted polymers

The protocol of synthesis of the MIPs prepared with AB as functional monomer is presented below. Typically, 0.2 mmol of N α -hexanoyl glutamine or N α -hexanoyl glutamic acid, 0.2 mmol (with N α -hexanoyl glutamine) or 0.4 mmol of AB, 4 mmol of ethylene glycol dimethacrylate and 0.042 mmol of Bis(*tert*-butylcyclohexyl)peroxydicarbonate (Perkadox 16) were dissolved in 10 mL of ethanol/H₂O (4/1) in a glass vial fitted with an airtight septum. The mixture was purged with nitrogen for 8 min on ice. Polymerization was done overnight at 40 °C in a water bath. The solid gel was then transferred to 50 mL centrifuge tubes and washed under stirring with 2 rounds of methanol/acetic acid (9/1), 2 rounds of methanol/100 mM NH₃ (7/3), 2 rounds of water and 2 rounds of methanol. They were then dried overnight under vacuum. Non-imprinted control polymers (NIPs) were synthesized in the same way but without the addition of the imprinting template.

III.5 Analysis on LC-UV-ELSD of N α -hexanoyl glutamine, cj3M2H and cj3H3MH in ethanol/water (4/1) and artificial sweat.

N α -hexanoyl glutamine, cj3M2H and cj3H3MH were analyzed by HPLC coupled to UV and ELSD detectors. Initially, a spectral scan from 200 to 800 nm was performed to determine the optimum wavelength response for each analyte. Thus, detection was done for cj3M2H at 235 nm, N α -hexanoyl glutamine and cj3H3MH at 203 nm, simultaneously with ELSD. These conditions were applied throughout analyses on HPLC. The injection volume was 10 μ L. Retention times for N α -hexanoyl glutamine, cj3H3MH and cj3M2H were 4.71, 3.53 and 5.04 min, respectively.

III.6 Equilibrium binding studies in ethanol/water and in artificial sweat

Binding studies of N α -hexanoyl glutamine, cj3M2H and cj3H3MH were performed in ethanol/water (4/1) and in artificial sweat composed of urea (0.1% or 16 mM), lactic acid (0.1% or 10 mM), albumin (0.1% or 15.2 mM) and sodium chloride (0.5% or 86 mM), pH 5.8. The imprinted and non-imprinted particles were suspended in either ethanol/water or artificial sweat in a sonicating bath. From this stock suspension, polymer concentrations ranging from 5 to 90 mg/mL were pipetted in separate 1.5 mL polypropylene microcentrifuge tubes and 200 μ M of N α -hexanoyl glutamine or 100 μ M of cj3M2H or cj3H3MH (stock solutions of 2 mM in ethanol) was added. The final volume was adjusted to 0.5 mL with ethanol/water or artificial sweat. The tubes were incubated overnight at ambient temperature on a tube rotator (SB2, Stuart Scientific). They were then centrifuged at 40,000 *g* for 45 min and a 200 μ L aliquot of the supernatant was withdrawn for analysis. The amount of free analyte was quantified by injecting 10 μ L on LC-UV-ELSD.

The amount of analyte bound to the polymers was calculated by subtracting the amount of unbound analyte from the initial amount of analyte added to the mixture.

III.7 Analysis by LC-MS/MS of the conjugates and the odorous acids in human sweat

Since the odorant acids could not be detected by LC-UV-ELSD, LC-MS/MS was employed. This method, as described below, allowed the separation and the quantification of both the odorous acids and their glutamine conjugates simultaneously. 1 mL aliquot of artificial sweat was spiked with the same concentration of cj3H3MH, cj3M2H, 3H3MH and 3M2H, at concentrations from 10 to 2000 ng/mL. The samples were diluted 10-fold with acetonitrile. After centrifugation at 15,000 g for 5 min, 20 μ L of the supernatant was injected and analyzed on LC-MS/MS. Negative electrospray ionization was applied. Spectra were recorded in MRM (multiple reaction monitoring) mode with a dwell time of 50 ms. cj3H3MH, cj3M2H and 3H3MH were well separated on HPLC and were monitored simultaneously, by using transitions m/z 273.1 \rightarrow m/z 127.1 and 145.1, m/z 255.1 \rightarrow m/z 127.1 and 145.1 and m/z 145.1 \rightarrow m/z 41.1 and 59.1 respectively. However, 3M2H (monitoring at m/z 127.1 \rightarrow m/z 45.1 and 83.1) was not detected, even when tested at 10 μ g/mL.

Sweat samples, provided by L'Oréal were aliquoted immediately when received and stored at -20 °C. For quantification in human sweat, 10 μ L aliquots were diluted from 10 to 500-fold with acetonitrile, so as to obtain values responding within the calibration curve and to precipitate the proteins as well. After centrifugation at 15,000 g for 5 min, 20 μ L of the diluted samples were injected on LC-MS/MS and analyzed by monitoring the presence of the two corresponding daughter ions of the analytes. All experiments were done in triplicate.

III.8 Analysis by LC-UV-ELSD of cj3H3MH and cj3M2H in human sweat- Capture of these analytes by MIPs

Since LC-UV-ELSD analysis was as efficient in terms of accuracy as LC-MS/MS, subsequent quantification of the conjugates in human sweat was done on the former equipment, for reasons of simplicity and technical availability. Sweat aliquots stored at -20 °C were thawed when needed and used only once, to eliminate eventual variations caused by microbial degradation. For capture studies, 200 μ L aliquots of human sweat was added to 1, 2 and 4 mg of MIP and NIP, weighed beforehand, in 1.5 mL polypropylene microcentrifuge tubes. The same volume of human sweat alone, acted as blank. The tubes were incubated overnight at ambient temperature on a tube rotator. They were then centrifuged at 40,000 g for 45 min and an 80 μ L aliquot of the supernatant was withdrawn for analysis. The amount of free cj3H3MH and cj3M2H was simultaneously monitored by injecting 10 μ L of the supernatant on LC-UV-

ELSD. The amount of bound cj3H3MH and cj3M2H was calculated by subtracting the amount of unbound analyte from the amount of analyte found in human sweat alone.

III.9 Capture of 3H3MH by MIP in human sweat and quantification by LC-MS/MS

Since 3H3MH could not be detected by LC-UV-ELSD, LC-MS/MS was used. For capture studies, 100 μ L aliquots of human sweat containing either 0.5 mg (i.e. 5 mg/mL) of MIP or NIP or nothing (blank) in 1.5 mL polypropylene microcentrifuge tubes were incubated overnight at ambient temperature on a tube rotator. They were then centrifuged at 40,000 g for 45 min and a 10 μ L aliquot of the supernatant was withdrawn and diluted 10 times with acetonitrile, so as to obtain values responding within the calibration curve and to precipitate the proteins as well. After centrifugation at 15,000 g for 5 min, 20 μ L of the diluted samples were injected on LC-MS/MS and analyzed by monitoring the presence of the two corresponding daughter ions of 3H3MH. All experiments were done in duplicate.

III.10 Preparation of deodorant formulation

A deodorant emulsion was prepared based on a model formulation provided by L'Oreal (Table 2.4). The aqueous phase of the emulsion containing distilled water and pentane-1,2-diol was heated at 75-80 °C, in a water-bath. In parallel, the lipid phase containing the other ingredients was heated at 75-80 °C, under magnetic stirring. Then, the lipid phase was introduced slowly into the aqueous phase at 75-80 °C, under Turax stirring (speed 9500 trs/min). The heating was stopped and the emulsification was allowed to proceed for 20 min. The emulsion was left to cool to 35-40 °C under magnetic stirring and then 2-phenoxyethanol was added. The emulsion was kept at 4 °C until use.

Table 2.4 Composition of the deodorant formula.

Chemicals	Ratio
2-phenoxyethanol	0.5
Polydimethylsiloxane	0.5
Distilled sterilized water	91.75
Pentane-1,2-diol	0.5
Cetylstearyl alcohol	2.5
Cetareth-33	1.25
PPG-15 Stearyl ether	3

III.11 Equilibrium binding studies of the polymers in a deodorant formulation

The imprinted and non-imprinted particles were suspended in the deodorant emulsion formulation in a sonicating bath. From this stock suspension (10 mg/mL), polymer concentrations ranging from 0.2 to 4 mg/mL were pipetted in separate 1.5-mL polypropylene microcentrifuge tubes and 200 μ M cj3H3MH or 100 μ M of cj3M2H (stock solutions of 2 mM in ethanol) was added. The final volume was adjusted to 0.5 mL with the deodorant emulsion. The tubes were incubated overnight at 37 °C on a tube rotator. They were then centrifuged at 40,000 g for 45 min at 37 °C. A very thin lipid layer was formed at the surface; for analysis, a 100 μ L aliquot of the aqueous phase below was carefully withdrawn with a micropipette. The samples were diluted twice with water at 37 °C, in order to avoid blocking of the HPLC column, maintained at 30 °C. The amount of free cj3H3MH and cj3M2H was quantified by injecting 20 μ L on LC-UV-ELSD. Retention times for cj3H3MH and cj3M2H were 3.4 and 5.1 min, respectively. The amount of conjugates bound to the polymers was calculated by subtracting the amount of unbound analyte from the amount of analyte spiked in the formulation.

III.12 Cell culture and count

Human adult low calcium high temperature (HaCaT) cells were cultured in Dulbecco's Eagle Medium (DMEM)-High glucose with 10% Fetal Bovine Serum (FBS) and 1% penicillin/streptomycin medium at 37 °C, 5% CO₂ and 100% humidity. Cells were passaged when confluent using 0.25% trypsin/EDTA in PBS buffer (Panagiotopoulou et al., 2017).

Cell counting was performed using a disposable hemocytometer. Confluent cells were collected and centrifuged for 5 min at 400 g. Then the cell pellet was resuspended in 5 mL of culture medium and the cell suspension was transferred to a 50-mL conical polypropylene centrifuge tube. Subsequently, 15 mL culture medium were added in order to get a final volume of 20 mL. Before the cells get the time to sediment, 500 μ L of the cell suspension was transferred into a polypropylene tube. In another polypropylene tube, 400 μ L of 0.4 % Trypan Blue was pipetted and 100 μ L of the previous cell suspension was added. Afterwards, 100 μ L of the Trypan Blue-treated cells were pipetted into the well of the counting chamber of the hemocytometer. A microscope with a 10x magnification objective was used and the live, unstained cells were counted using a hand tally counter (living cells are impermeable to Trypan Blue). To obtain the number of viable cells/mL in the original cell suspension, the average cell count from each of the sets of the 16 corner squares of the hemocytometer was calculated and then multiplied by 10⁴. This number was further multiplied by 5 to correct for the 1:4 dilution from the Trypan Blue addition.

Using this method, it was deduced that a T75 flask with HaCaT cells at 80-100 % confluency contains 10⁶ cells. This amount was diluted by 100-fold with PBS prior MTT cytotoxicity test.

and 620 nm the reference corresponding to the impurities. Cell viability Cell viability rate was calculated by considering the signal of non-treated cells as the 100% viability and was determined by dividing the absorbance at 570 nm measured for treated cells by that of the non- treated controls.

III.14 Isolation of bacteria from human sweat-Identification by MALDI-TOF/MS

Experiments were performed using Luria-Bertani (LB) broth and agar, Brain Heart Infusion Broth (BHI) and blood agar as culture media (refer to Annex for their detailed composition). These media were prepared according to the manufacturer's instructions, were sterilized prior use at 127 °C for 30 min and were kept in a dark place at ambient temperature until used. As a preliminary test, 10 µL and 50 µL aliquots of human sweat were spread on separate LB plates (a non-inoculated LB plate served as a control). After 3 days of incubation at 37 °C, 3 colonies were obtained with the sample of 50 µL human sweat (Figure 2.23). The same experiment was performed on blood agar plates. These colonies were isolated and amplified in an enriched liquid medium (BHI). After 24 h of incubation at 37 °C bacterial growth was observed.

Identification of bacteria species isolated from human sweat was performed by MALDI-TOF mass spectrometry. Experiments were performed by Benoît Ménard. Preparations of bacterial isolates for MALDI-TOF MS measurement were done by the direct transfer method. Fresh colony material was smeared on a polished steel MSP 96 target (Bruker Daltonik) using a toothpick, overlaid with 1 µL of a saturated α -cyano-4-hydroxy-cinnamic acid (HCCA) matrix solution in 50% acetonitrile-2.5% trifluoroacetic acid (Bruker Daltonik), and air dried at room temperature.

The acquisition and analysis of mass spectra were performed by a Microflex LT mass spectrometer (Bruker Daltonik) using the MALDI Biotyper software package with the reference database version 3.1.2.0 (3,995 database entries) (Bruker Daltonik) and default parameter settings as reported by Schulthess et al., 2013.

The Biotyper software compares each sample mass spectrum to the reference mass spectra in the database, calculates an arbitrary unit score value between 0 and 3 reflecting the similarity between the sample and the reference spectrum, and displays the top 10 matching database records. Scores of ≥ 2.0 were accepted for species assignment and scores of ≥ 1.7 but < 2.0 for identification to the genus level. Scores below 1.7 were considered unreliable. Variations of the cutoff score values were done by reducing the species cutoff values to 1.9, 1.8, and 1.7, and the genus cutoff values to 1.6 and 1.5, followed by reinterpreting the top 10 matching database records.

Based on the aforementioned method, the colonies identified belong to 4 bacterial species: *Staphylococcus hominis*, *Staphylococcus epidermidis*, *Micrococcus luteus* and *Corynebacterium Striatum*.

III.15 Effect of MIP on the growth of skin commensal bacteria

To examine the bacterial growth rate and determine the growth curve in the presence of the MIP, *S. hominis*, *S. epidermidis*, *C. striatum* and *M. luteus* bacteria were grown into 15 mL falcon tubes with 5 mL of liquid BHI medium supplemented with 0.5 mg/mL of MIP. As blank control, samples without the addition of MIP were prepared and as negative control samples corresponding to each bacteria were supplemented with 0.5 mg/mL of silver nitrate. The samples were subsequently inoculated under aseptic conditions. The appropriate volume of inoculum was isolated from the liquid cultures of each species, so as to have 10^6 cells in the 5 mL BHI. All samples prior to the addition of bacteria were sonicated in a water bath for 20 min, so as to achieve a homogenous suspension. Growth rates and bacterial concentrations were determined by measuring optical density (OD) at 600 nm after incubation for 3, 6, 9, 12, 24, 32 and 48 hours. Samples were diluted beforehand so as to obtain absorbance values inferior to 1. The absorbance was measured on a Cary 60 UV-Vis spectrophotometer using BHI medium as blank. The bacterial curves were plotted taking into account that the OD of 1 corresponds to a concentration of 10^9 cells per mL.

The effect of the MIP on the bacteria was also investigated in blood agar plate cultures (for the detailed composition refer to Annex). Approximately 10^5 colony forming units (CFU) of the aforementioned species were cultured on blood agar plates supplemented with 0.5 mg/mL of MIP. Blood agar plates without the addition of MIP, cultured under the same conditions were used as a negative control, while plates supplemented with 0.5 mg/mL silver nitrate served as blank control. The plates were incubated for 24 h at 37 °C and photos of the bacterial colonies were taken.

IV. Conclusions-Perspectives

In conclusion, we have developed a plastic antibody as the active ingredient of a cosmetic product, on the example of a new deodorant principle to suppress body odors. At the same time, we have demonstrated the feasibility of preparing highly selective molecularly imprinted binding sites for recognition in complex aqueous media, using a polymerizable amidinium monomer which can form stoichiometric interaction with a high binding constant for carboxyl groups. The judicious design of the template resulted in cavities bearing two amidinium functionalities favorably positioned in a precise spatial arrangement so as to selectively capture the precursors of malodorous compounds from human sweat.

Furthermore, we have performed some preliminary toxicological studies which revealed a minor biological impact of this MIP to both epidermal cells and bacteria commensal to the skin. This study is a step forward in the understanding and evaluation of the biological effect of MIPs as skin sensitizers. To ultimately prove the MIP's safety with regards its potential application in dermocosmetic applications, more

studies are necessary including inflammation tests with different biomarkers and implementation on artificial skin models such as *Episkin*.

V. References

[A]

Ammala, A., Biodegradable polymers as encapsulation materials for cosmetics and personal care markets. *International Journal of Cosmetic Science* **2013**, 35 (2), 113-124.

Anane, R.; Creppy, E. E., Lipid peroxidation as pathway of aluminium cytotoxicity in human skin fibroblast cultures: Prevention by superoxide dismutase+catalase and vitamins E and C. *Human & Experimental Toxicology* **2001**, 20 (9), 477-481.

[B]

Barzantny, H.; Brune, I.; Tauch, A., Molecular basis of human body odour formation: insights deduced from corynebacterial genome sequences. *International Journal of Cosmetic Science* **2012**, 34 (1), 2-11.

Benohanian, A., Antiperspirants and deodorants. *Clinics in Dermatology* **2001**, 19 (4), 398-405.

Beyazit, S.; Ambrosini, S.; Marchyk, N.; Palo, E.; Kale, V.; Soukka, T.; Tse Sum Bui, B.; Haupt, K., Versatile synthetic strategy for coating upconverting nanoparticles with polymer shells through localized photopolymerization by using the particles as internal light sources. *Angewandte Chemie International Edition* **2014**, 53 (34), 8919-8923.

Brody, H. J., Relevance of cosmeceuticals to the dermatologic surgeon. *Dermatologic Surgery* **2005**, 31, 796-799.

Burkhart, C. G.; Burkhart, C. N., Aluminum alters sweating by constricting the dermal duct lumen. *International Journal of Dermatology* **2008**, 47 (12), 1306-1307.

[C]

Callewaert, C.; Kerckhof, F.-M.; Granitsiotis, M. S.; Van Gele, M.; Van de Wiele, T.; Boon, N., Characterization of Staphylococcus and Corynebacterium Clusters in the Human Axillary Region. *PLOS ONE* **2013**, 8 (8), e70538.

Callewaert, C.; Hutapea, P.; Van de Wiele, T.; Boon, N., Deodorants and antiperspirants affect the axillary bacterial community. *Archives of Dermatological Research* **2014**, 306 (8), 701-710.

Connors, K., Binding Constants, 411 ed. John Wiley & Sons: New York: 1987.

Costello, E. K.; Lauber, C. L.; Hamady, M.; Fierer, N.; Gordon, J. I.; Knight, R., Bacterial community variation in human body habitats across space and time. *Science (New York, N.Y.)* **2009**, 326 (5960), 1694-1697.

[E]

Edwards-Jones, V., *The benefits of silver in hygiene, personal care and healthcare. Letters in Applied Microbiology* **2009**, *49* (2), 147-152.

Exley, C.; Charles, L. M.; Barr, L.; Martin, C.; Polwart, A.; Darbre, P. D., Aluminium in human breast tissue. *Journal of Inorganic Biochemistry* **2007**, *101* (9), 1344-1346.

[F]

FDA. Is It a Cosmetic, a Drug, or Both? (Or Is It Soap?), **2012**, Available at: http://www.fda.gov/Cosmetics/GuidanceRegulation/LawsRegulations/ucm074201.htm#Intended_use, accessed 27 January 2017.

Figueiredo, L.; Erny, G. L.; Santos, L.; Alves, A., Applications of molecularly imprinted polymers to the analysis and removal of personal care products: A review. *Talanta* **2016**, *146*, 754-765.

Fredrich, E.; Barzantny, H.; Brune, I.; Tauch, A., Daily battle against body odor: towards the activity of the axillary microbiota. *Trends in Microbiology* **2013**, *21* (6), 305-312.

[G]

Garg, S. ; Loghdey, S.; Gawkrödger, D. J., Allergic contact dermatitis from aluminium in deodorants. *Contact Dermatitis* **2010**, *62*, 57–58.

Gao, R.; Kong, X.; Su, F.; He, X.; Chen, L.; Zhang, Y., Synthesis and evaluation of molecularly imprinted core-shell carbon nanotubes for the determination of triclosan in environmental water samples. *Journal of Chromatography A* **2010**, *1217* (52), 8095-8102.

Gholivand, M. B.; Shamsipur, M.; Dehdashtian, S.; Rajabi, H. R., Development of a selective and sensitive voltammetric sensor for propylparaben based on a nanosized molecularly imprinted polymer-carbon paste electrode. *Materials Science and Engineering: C* **2014**, *36*, 102-107.

Gower, D., Holland, K.L., Mallet, A.I., Rennie, P.J., Watkins, W.J. Comparison of 16-androstene steroid concentrations in sterile apocrine sweat and axillary secretions: Interconversions of 16-androstenes by the axillary microflora—a mechanism for axillary odour production in man? *The Journal of steroid biochemistry and molecular biology* **1994**, *48* (4), 409-418.

Gordon James, A. G.; Austin, C. J.; Cox, D. S.; Taylor, D.; Calvert, R., Microbiological and biochemical origins of human axillary odour. *FEMS Microbiology Ecology* **2013**, *83* (3), 527-540.

Greaves, A.; Manfre, F.; Haupt, K.; Tse Sum Bui, J. B., Molecularly imprinted polymer for selectively trapping odorous molecules. (L'OREAL), WO 2014/102077 A1, 2014.

Greulich, C.; Braun, D.; Peetsch, A.; Diendorf, J.; Siebers, B.; Epple, M.; Koller, M., The toxic effect of silver ions and silver nanoparticles towards bacteria and human cells occurs in the same concentration range. *RSC Advances* **2012**, *2* (17), 6981-6987.

Grice, E. A.; Kong, H. H.; Conlan, S.; Deming, C. B.; Davis, J.; Young, A. C.; Bouffard, G. G.; Blakesley, R. W.; Murray, P. R.; Green, E. D.; Turner, M. L.; Segre, J. A., Topographical and temporal diversity of the human skin microbiome. *Science* **2009**, 324 (5931), 1190-1192.

[H]

Hall, A. J.; Manesiotis, P.; Emgenbroich, M.; Quaglia, M.; De Lorenzi, E.; Sellergren, B., Urea host monomers for stoichiometric molecular imprinting of oxyanions. *The Journal of Organic Chemistry* **2005**, 70 (5), 1732-1736.

Henry, N.; Favetta, P.; Delépée, R.; Seigneuret, J. M.; Agrofoglio, L. A., Synthesis of a molecularly imprinted polymer to isolate glucosamine from plant extracts by an ionic–non-covalent dual approach. *International Journal of Cosmetic Science* **2015**, 37 (2), 196-206.

Hu, J.; Zeng, F.; Li, P., Methods of manufacturing deodorants, and deodorants resulting thereof. US Patent 2005/0232880.

Hu, J.; Meng, H.; Li, G.; Ibekwe, I. I, A review of stimuli-responsive polymers for smart textile applications. *Smart Materials and Structures* **2012**, 21 (5), 053001.

[J]

Jha, S. K.; Liu, C.; Hayashi, K., Molecular imprinted polyacrylic acids based QCM sensor array for recognition of organic acids in body odor. *Sensors and Actuators B: Chemical* **2014**, 204, 74-87.

[K]

Kanlayavattanukul, M.; Lourith, N., Body malodours and their topical treatment agents. *International Journal of Cosmetic Science* **2011**, 33 (4), 298-311.

Kenawy, E.-R.; Worley, S. D.; Broughton, R., The chemistry and applications of antimicrobial polymers: A state-of-the-art review. *Biomacromolecules* **2007**, 8 (5), 1359-1384.

Krásný, L.; Hynek, R.; Hochel, I., Identification of bacteria using mass spectrometry techniques. *International Journal of Mass Spectrometry* **2013**, 353, 67-79.

Kunath, S.; Panagiotopoulou, M.; Maximilien, J.; Marchyk, N.; Sängler, J.; Haupt, K., Cell and Tissue Imaging with Molecularly Imprinted Polymers as Plastic Antibody Mimics. *Advanced Healthcare Materials* **2015**, 4 (9), 1322-1326.

[L]

Labows, J. N. Perspectives on axillary odor. *Journal of the Society of Cosmetic Chemists in Japan* **1982**, 33 (4), 193-202.

Laden, K.; Felger, C., Antiperspirants and deodorants. *Cosmetic Science and Technology Series*, vol. 7. Marcel Dekker: Ney York: 1988.

Leyden, J.J.; McGinley, K.J.; Hölzle, E.; Labows, J.N.; Kligman, A. M., The microbiology of the human axilla and Its relationship to axillary odor, *Journal of Investigative Dermatology* **1981**, 77 (5), 413-416.

Liu, Y.-Y.; Fan, X.-D., Synthesis and characterization of pH- and temperature-sensitive hydrogel of N-isopropylacrylamide/cyclodextrin based copolymer. *Polymer* **2002**, *43* (18), 4997-5003.

Liu, M.; Li, X.-Y.; Li, J.-J.; Su, X.-M.; Wu, Z.-Y.; Li, P.-F.; Lei, F.-H.; Tan, X.-C.; Shi, Z.-W., Synthesis of magnetic molecularly imprinted polymers for the selective separation and determination of metronidazole in cosmetic samples. *Analytical and Bioanalytical Chemistry* **2015**, *407* (13), 3875-3880.

[M]

Ma, Y.; Pan, G.; Zhang, Y.; Guo, X.; Zhang, H., Narrowly dispersed hydrophilic molecularly imprinted polymer nanoparticles for efficient molecular recognition in real aqueous samples including river water, milk, and bovine Serum. *Angewandte Chemie International Edition* **2013**, *52* (5), 1511-1514.

MacNeil, S., Progress and opportunities for tissue-engineered skin. *Nature* **2007**, *445* (7130), 874-880.

Martin, A.; Saathoff, M.; Kuhn, F.; Max, H.; Terstegen, L.; Natsch, A., A functional ABCC11 allele is essential in the biochemical formation of human axillary odor. *Journal of Investigative Dermatology* **2010**, *130* (2), 529-540.

Mihrianyan, A.; Ferraz, N.; Strømme, M., Current status and future prospects of nanotechnology in cosmetics. *Progress in Materials Science* **2012**, *57* (5), 875-910.

Mu, L.; Sprando, R. L., Application of Nanotechnology in Cosmetics. *Pharmaceutical Research* **2010**, *27* (8), 1746-1749.

[N]

Natsch, A.; Gfeller, H.; Gygax, P.; Schmid, J.; Acuna, G., A specific bacterial aminoacylase cleaves odorant precursors secreted in the human axilla. *Journal of Biological Chemistry* **2003**, *278* (8), 5718-5727.

Natsch, A.; Joubert, C.; Cella, M.; Flachsmann, F.; Geffroy, C., Validation of a malodour-forming enzyme as a target for deodorant actives: in vivo testing of a glutamine conjugate targeting a corynebacterial N α -acyl-glutamine-aminoacylase. *Flavour and Fragrance Journal* **2013**, *28* (4), 262-268.

Natsch, A., What makes us smell: the biochemistry of body odour and the design of new deodorant ingredients. *CHIMIA International Journal for Chemistry* **2015**, *69* (7-8), 414-420.

Netzlaff, F.; Lehr, C. M.; Wertz, P. W.; Schaefer, U. F., The human epidermis models EpiSkin®, SkinEthic® and EpiDerm®: An evaluation of morphology and their suitability for testing phototoxicity, irritancy, corrosivity, and substance transport. *European Journal of Pharmaceutics and Biopharmaceutics* **2005**, *60* (2), 167-178.

[P]

Panagiotopoulou, M.; Kunath, S.; Medina-Rangel, P. X.; Haupt, K.; Tse Sum Bui, B., Fluorescent molecularly imprinted polymers as plastic antibodies for selective labeling and imaging of hyaluronan and sialic acid on fixed and living cells. *Biosensors & bioelectronics* **2017**, *88*, 85-93.

Piérard, G. E.; Elsner, P.; Marks, R.; Masson, P.; Paye, M., EEMCO Guidance for the Efficacy Assessment of Antiperspirants and Deodorants. *Skin Pharmacology and Physiology* **2003**, *16* (5), 324-342.

Pineau, A.; Guillard, O.; Fauconneau, B.; Favreau, F.; Marty, M. H.; Gaudi, A.; Vincent, C.; M.; Marraud, A.; Marty, J.-P., In vitro study of percutaneous absorption of aluminum from antiperspirants through human skin in the Franz™ diffusion cell. *Journal of Inorganic Biochemistry* **2012**, *110*, 21-26.

Preti, G.; Leyden, J. J., Genetic influences on human body odor: from genes to the axillae. *Journal of Investigative Dermatology* **2010**, *130* (2), 344-346.

[R]

Rieger, M. M., Cosmetics. In *Kirk-Othmer Encyclopedia of Chemical Technology*, John Wiley & Sons, Inc.: 2000.

Renny, J. S.; Tomasevich, L. L.; Tallmadge, E. H.; Collum, D. B., Method of continuous variations: applications of job plots to the study of molecular associations in organometallic chemistry. *Angewandte Chemie International Edition* **2013**, *52* (46), 11998-12013.

[S]

Schulthess, B.; Brodner, K.; Bloemberg, G. V.; Zbinden, R.; Bottger, E. C.; Hombach, M., Identification of Gram-positive cocci by use of matrix-assisted laser desorption ionization-time of flight mass spectrometry: comparison of different preparation methods and implementation of a practical algorithm for routine diagnostics. *Journal of clinical microbiology* **2013**, *51* (6), 1834-1840.

Shelley, W. B.; Hurley, H. J., Jr.; Nichols, A. C., Axillary odor; experimental study of the role of bacteria, apocrine sweat, and deodorants. *A.M.A. archives of dermatology and syphilology* **1953**, *68* (4), 430-446.

Shi, S.; Guo, J.; You, Q.; Chen, X.; Zhang, Y., Selective and simultaneous extraction and determination of hydroxybenzoic acids in aqueous solution by magnetic molecularly imprinted polymers. *Chemical Engineering Journal* **2014**, *243*, 485-493.

Shirreffs, S.; Maughan, R., Whole body sweat collection in humans: an improved method with preliminary data on electrolyte content. *Journal of Applied Physiology* **1997**, *82* (1), 336-341.

Sondi, I.; Salopek-Sondi, B., Silver nanoparticles as antimicrobial agent: a case study on *E. coli* as a model for Gram-negative bacteria. *Journal of Colloid and Interface Science* **2004**, *275* (1), 177-182.

Strikovskiy, A. G.; Kasper, D.; Grün, M.; Green, B. S.; Hradil, J.; Wulff, G., Catalytic molecularly imprinted polymers using conventional bulk polymerization or suspension polymerization: Selective hydrolysis of diphenyl carbonate and diphenyl carbamate. *Journal of the American Chemical Society* **2000**, *122* (26), 6295-6296.

[T]

Taylor, D.; Daulby, A.; Grimshaw, S.; James, G.; Mercer, J.; Vaziri, S., Characterization of the microflora of the human axilla. *International Journal of Cosmetic Science* **2003**, *25* (3), 137-145.

Thordarson, P., Determining association constants from titration experiments in supramolecular chemistry. *Chemical Society Reviews* **2011**, *40* (3), 1305-1323.

Troccaz, M.; Borchard, G.; Vuilleumier, C.; Raviot-Derrien, S.; Niclass, Y.; Beccucci, S.; Starkenmann, C., Gender-specific differences between the concentrations of non volatile (R)/(S)-3-Methyl-3-

Sulfanylhexan-1-ol and (R)/(S)-3-hydroxy-3-methyl-hexanoic acid odor precursors in axillary secretions. *Chemical Senses* **2009**, *34* (3), 203-210.

[U]

Urban, J.; Fergus, D. J.; Savage, A. M.; Ehlers, M.; Menninger, H. L.; Dunn, R. R.; Horvath, J. E., The effect of habitual and experimental antiperspirant and deodorant product use on the armpit microbiome. *PeerJ* **2016**, *4*, e1605.

Urraca, J. L.; Hall, A. J.; Moreno-Bondi, M. C.; Sellergren, B., A stoichiometric molecularly imprinted polymer for the class-selective recognition of antibiotics in aqueous media. *Angewandte Chemie International Edition* **2006**, *45* (31), 5158-5161.

[W]

Welss, T.; Basketter, D. A.; Schröder, K. R., In vitro skin irritation: facts and future. State of the art review of mechanisms and models. *Toxicology in Vitro* **2004**, *18* (3), 231-243.

Wendel, V.; Brüggemann, O.; Ptöck, A., Cosmetic preparations based on molecularly imprinted polymers. BASF SE) US2010/ 0048737A1, 2010.

Wulff, G., Gross, T. & Schönfeld, R. Enzyme models based on molecularly imprinted polymers with strong esterase activity. *Angewandte Chemie International Edition* **1997**, *36*, 1962-1964

Wulff, G.; Schönfeld, R., Polymerizable amidines—adhesion mediators and binding sites for molecular imprinting. *Advanced Materials* **1998**, *10* (12), 957-959.

Wulff, G. & Knorr, K. Stoichiometric noncovalent interaction in molecular imprinting. *Bioseparation* **2001**, *10*, 257-276.

• ANNEX 1

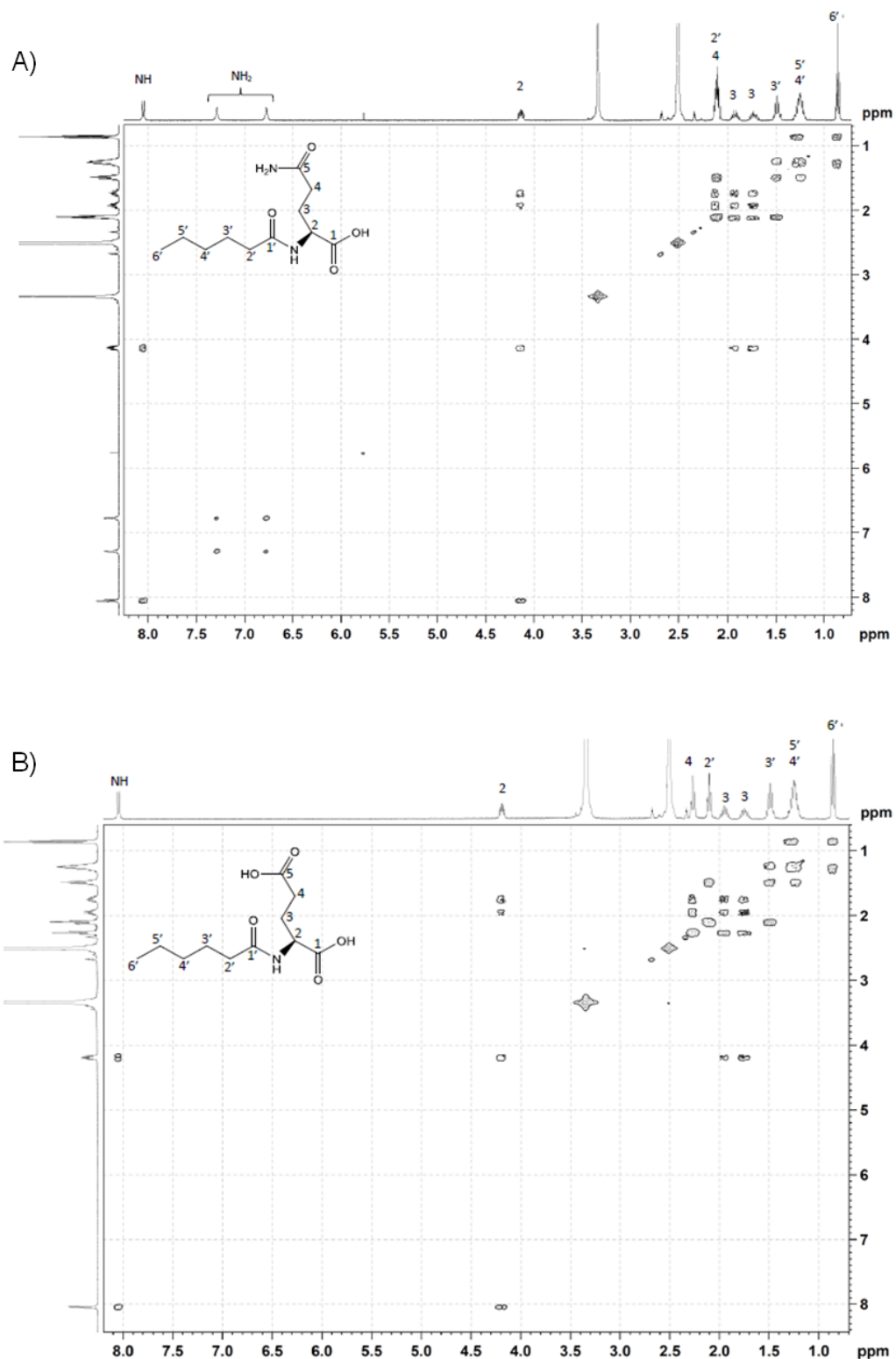


Figure S1. COSY spectra of 5 mM A) $N\alpha$ -hexanoyl glutamine and B) $N\alpha$ -hexanoyl glutamic acid, in $DMSO-d_6$.

ANNEX 2

Culture media

Luria-Bertani (LB) broth

- 10 g/L tryptone
- 10 g/L NaCl
- 5 g/L yeast extract

Luria-Bertani (LB) agar plates

The same composition as LB broth with 20 g/L agar added

Brain heart infusion (BHI)

- 5 g/L beef heart (infusion from 250 g)
- 12.5 g/L calf brains (infusion from 200 g)
- 2.5 g/L disodium hydrogen phosphate
- 2 g/L D (+)- glucose
- 10 g/L peptone
- 5 g/L NaCl

Blood agar base

- 10 g/L beef heart (infusion from 250 g)
- 10 g/L tryptose
- 5 g/L NaCl
- 15 g/L agar

Chapter 3

MIPs for food technology- selective extraction of the antioxidant betanin from beetroot extract



I. Introduction

I.1 MIPs as selective sorbents in food technology

Interest in developing more efficient and selective methods for clean-up and preconcentration of natural-sourced pigments is continuously growing. This is primarily linked to the explosion of the natural food colorant market since some synthetic pigments have been suggested to be involved in child hyperactivity (McCan et al., 2007; Nigg et al., 2012) and are negatively perceived by the consumers. Moreover, most plant pigments exhibit antioxidant properties which render them highly attractive for applications in the pharmaceutical, cosmetic and nutraceutical areas. For instance, dietary antioxidant pigments such as fat-soluble carotenoids, chlorophylls and curcuminoids and water-soluble anthocyanins have been widely studied for their potential to prevent diseases associated to aging as well as to reduce the risk of cardiovascular disease and cancers (Surh, 2003).

Typically, the industrial use of these natural compounds requires extensive and sometimes tedious purification from their natural sources. Currently used extraction and purification protocols often involve long processing, possible degradation of the natural compounds or use of non-environmental friendly organic solvents. Thus, there is a trend to develop more economic, biocompatible, facile methods for the clean-up of bioactive compounds, paving the way for their wide application not only in food industry but to other application areas as well.

In this chapter, we aimed to demonstrate the great potential of MIPs as selective sorbents for the purification of natural compounds and as an interesting alternative to the currently used non-selective polymeric adsorbents. For this reason, we developed a single step purification method based on molecularly imprinted polymers for the selective clean-up of betanin, a natural pigment found in beetroots. As discussed, in chapter 1, MIPs can be an extremely attractive choice as selective capture materials with applications in analytical separations, due to their molecular recognition properties, combined with their high stability, mechanical robustness, low cost and easy synthesis (Haupt et al., 2012; Whitcombe et al., 2014). Advantageously, the use of MIPs as affinity sorbents allows not only the pre-concentration of target analytes, but also the elimination of matrix components in complex samples (Tse Sum Bui and Haupt, 2010; Turiel and Martin-Esteban, 2010; Kecili et al., 2014). Featuring high selectivity, MIPs have been extensively used as sorbents in SPE (namely MISPE) for the extraction of compounds from a large variety of matrices including food (Ali et al., 2010; Giovannoli et al., 2014) and of bioactive compounds with antioxidant properties such as curcuminoids and quercetin from vegetal samples (Castro Lopez et al., 2012; Wulandari et al., 2015).

I.2 Betanin: An important bioactive natural pigment

In this work, we focus on betanin, a water-soluble pigment belonging to betalains, a class of highly bioavailable natural pigments (Tesoriere et al., 2005; Frank et al., 2005; Livrea and Tesoriere, 2012) with interesting biological activities (Moreno et al., 2012; Esatbeyoglu et al., 2015; Gandia-Herreo et al., 2016). Betalains replace the anthocyanins in a small number of taxonomically related plant families including yellow cactus pears (*Opuntia* spp.) (Stintzing et al., 2002), grain or leafy amaranth (*Amaranthus* sp.) (Cai et al., 2005), *Rivina humilis* L. berries (Khan et al., 2015) and Swiss chard petioles (Kugler et al., 2004), amongst others. They are classified into two groups according to their color: red/purple betacyanins and yellow betaxanthins (Figure 3.1 A).

The major commercially exploited betalain crop is red beetroot (*Beta vulgaris* L.). Table beetroot, as well as sugar beetroot, constitutes an important crop for the region of Picardy where this thesis was performed. Beetroot extract has been approved by the Food and Drug Administration (FDA) and the European Union, as a natural red-violet coloring agent (E162) and is used worldwide for coloring food, beverages, cosmetics and drugs (FDA, 2009; EFSA, 2015). Typical food commodities colored with betalains include dairy products, fruit fillings for bakery products, relishes, various instant products, confectionery, meat substitutes and sausages. Beet concentrates have been particularly suitable for use in foods like yoghurts, drinks, ice cream, hard candies, salad dressings, cake mixes, finished meat products and meat substitutes, gelatin desserts, powdered drink mixes, etc. but use is limited because of the stability properties (Neelwarne and Halagur 2012). Beetroot extract is used also by the pharmaceutical industry as a coloring agent in drug formulations, in both solid and liquid forms (Pai and D’Mello, 2004).

Beetroot extract sold on the market contains a number of different pigments but the predominant colouring principle consists of a number of betacyanins (red) of which betanin accounts for 75–95% and its C15-epimer, isobetanin 15–45% (EFSA, 2015). Vulgaxanthin I (25–70%) and vulgaxanthin II (5–15%) are the major pigments in the betaxanthin (yellow) fraction, which includes as well as several degradation products of betalains (light brown-yellow). The betalains’ content and composition are strongly dependent on beetroot cultivar, farming and storage conditions (Kujala et al., 2002).

Structurally, betalains are immonium derivatives of betalamic acid (Figure 3.1). Due to glycosylation and acylation betalains exhibit a huge structural diversity Betaxanthins (Latin: beta = beet; Greek: xanthos = yellow) are condensation products of betalamic acid and amino acids or amines. On the other hand, condensation products of betalamic acid and *cyclo*-Dopa [*cyclo*- 3-(3,4-dihydroxyphenylalanine)] are commonly referred to as betacyanins due to their deep violet color (Greek: kyaneos = blue). This extra conjugation shifts the absorption maximum from 480 nm (yellow, betaxanthins) to about 540 nm (violet, betacyanins) (Strack et al., 2003) 5Figure 3.1B).

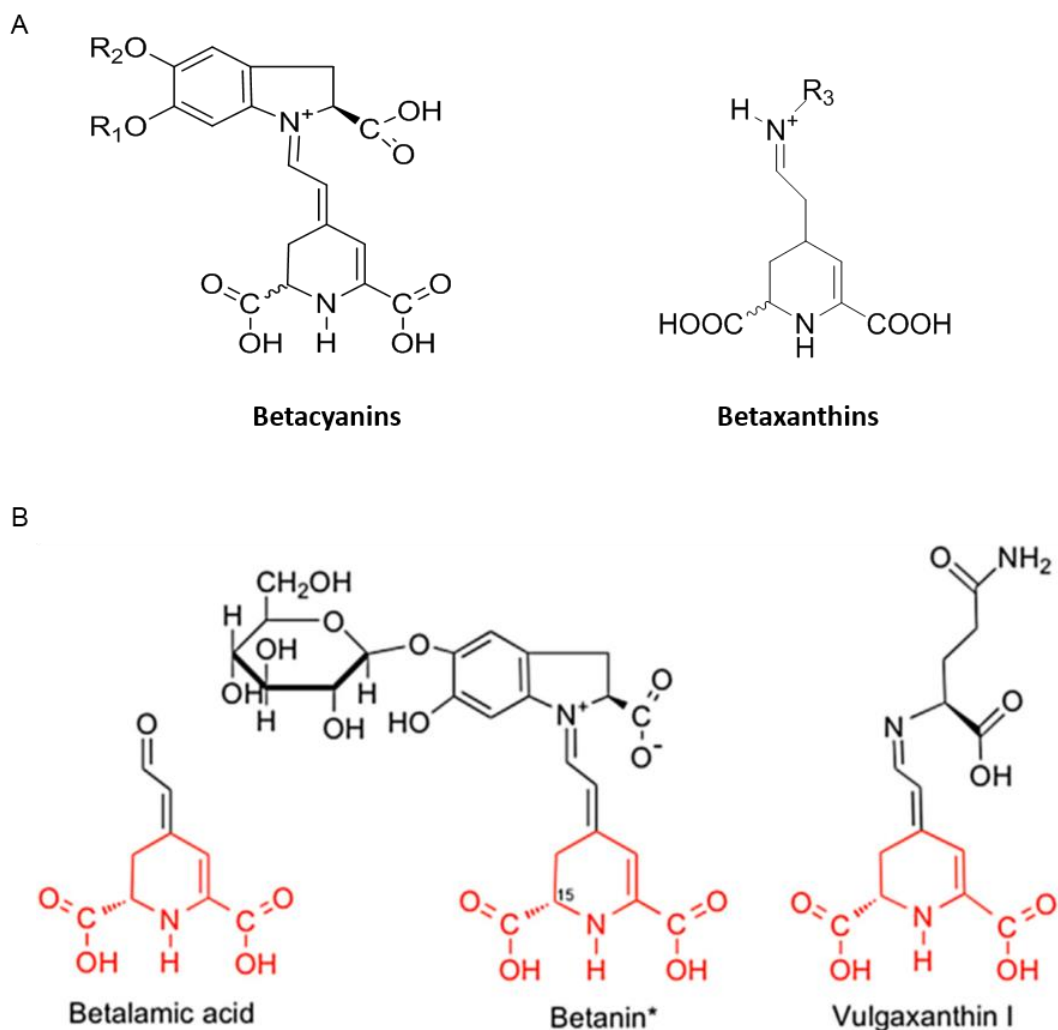


Figure 3.1. A) Generic structure of betacyanins and betaxanthins; B) Chemical structures of betanin and vulgaxanthin I, highlighted in red the betalamic acid common backbone.

Recently, potential health benefits of betalains and betalain-rich foods (e.g. red beet, *Opuntia* sp.) have been discussed. Particular research is focused on betanin, as the major pigment in red beets and presumably the most bioactive (Livrea and Tesoriere, 2012). It is important to note that betanin and other betacyanins feature high bioavailability which conditions its health-promoting properties. In fact, very low amounts of unmetabolized betanin/isobetanin (0.28 to 0.9%) of the administered dose was recovered in human urine after consumption of red beet juice (Kanner et al., 2001; Frank et al., 2005), this in addition to a high intestinal transport (Tesoriere et al., 2013) are consistent with a high bioavailability.

Besides their colorant properties, betanin and other betacyanins exert significant antioxidant activity, protecting against oxidative stress both *in vitro* and *in vivo* (Kanner et al., 2001; Tesoriere et al., 2009). For instance, *ex vivo* experiments showed that betanin acts as a lipoperoxyl radical-scavenger better than β -carotene in a copper-oxidized low density lipoprotein (LDL) model. Furthermore, recent studies with multiple cancer cell lines have demonstrated a high chemopreventive potential that finds *in vitro* support in

a strong antiradical and antioxidant activity. Specifically, it has been shown that red beet coloring agent E162 reduced significantly the incidence of skin, lung, liver, colon and esophagus tumors in various animal models (Lechner et al., 2010) and in human pancreatic, breast and prostate cancer cell lines (Kapadia et al., 2013). Beyond their cancer preventive role, the antitumoral activity of beetroot extracts highly concentrated in betanin has been demonstrated *in vitro* on several human cancer cell lines (Reddy et al., 2005; Sreekanth et al., 2007).

Recently, our group has shown that a purified dried beetroot extract containing 80% of betanin/isobetanin in a ratio 0.6/0.4 (20% impurities attributed to proteins) selectively inhibits cancer cell proliferation and viability (Figure 3.2) (Nowacki et al., 2015). For the assessment of the biological effect of betanin extract both cancer (B16F10, MCF-7, MDA-MB-231, HT-29) and normal (HUVEC, MRC-5) were tested in 2D and 3D cultures. Figure 3.2 shows that betanin and isobetanin treatment significantly decreased the proliferation of B16F10 melanoma and MCF-7 breast cancer cells on both surfaces. Conversely, the effect on the normal endothelial cells HUVEC was less pronounced, while MRC-5 diploid cells are not sensitive at all. This study clearly indicates the potential therapeutic effect of betanin/isobetanin extract for the treatment of cancer and paves the way for further applications in clinical studies.

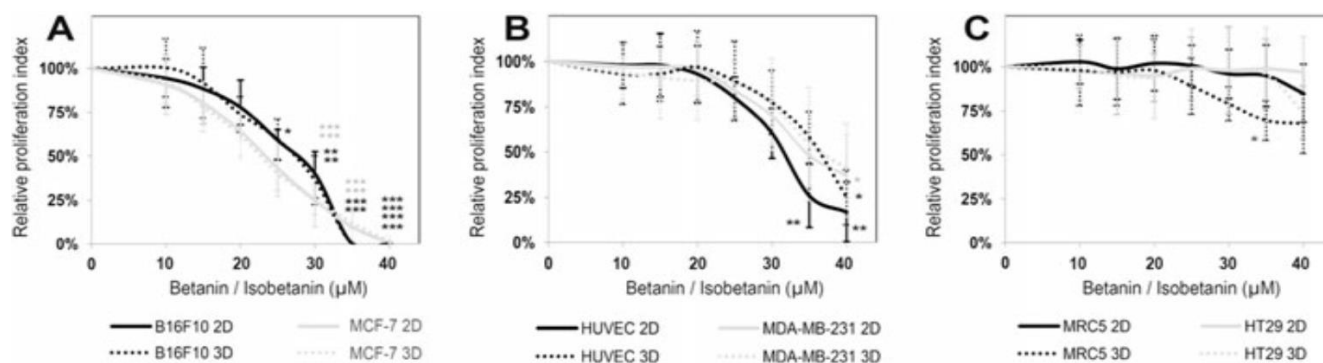


Figure 3.2. Effect of betanin /isobetanin. concentrate on cell proliferation Relative proliferation index of cancer and non-tumorigenic cells treated with betanin /isobetanin. Results are means \pm SD of three experiments each performed in triplicate. Asterisks indicate significant differences in cell proliferation index of treated and control cells (Dunn test). Reproduced from Nowacki et al., 2015.

For all the above reasons, betanin appears to be a very promising bioactive colorant that can find diverse applications in food technology and in therapeutics due to its high antioxidant and chemopreventive potential. In the following chapter, we will focus on methods to obtain highly pure betanin, in an effort to facilitate and expand its applications.

I.3 Existing protocols for the extraction and purification of betanin

Authorized betanin sold on the market is obtained by isolation from red beet. Efficient extraction and purification methods should maximize betalain recovery with minimal amount of adjuncts and minimal degradation or alteration of its natural state.

Extraction is conventionally performed in water/alcoholic solutions, due to the hydrophilic nature of betanin (Delgado-Vargas et al., 2000). Furthermore, novel processing techniques such as power ultrasound, high-pressure processing, pulsed electric field, dielectric heating (microwave) and supercritical fluid processing techniques can be employed for extraction of betalains from plant matrices (Tiwari and Cullen, 2012; Cardoso-Ugarte et al., 2014). These processes can also be used as a pre-treatment or in combination with environment friendly and safe organic solvents to enhance extraction efficiency. It is worth noting that the stability of betanin poses a great challenge during extraction as variations in temperature (exceeding 50 °C), water activity, oxygen, light and pH (stable between pH 3 to 7) may cause significant degradation (Figure 3.3) (Herbach et al., 2006; Azeredo et al., 2009).

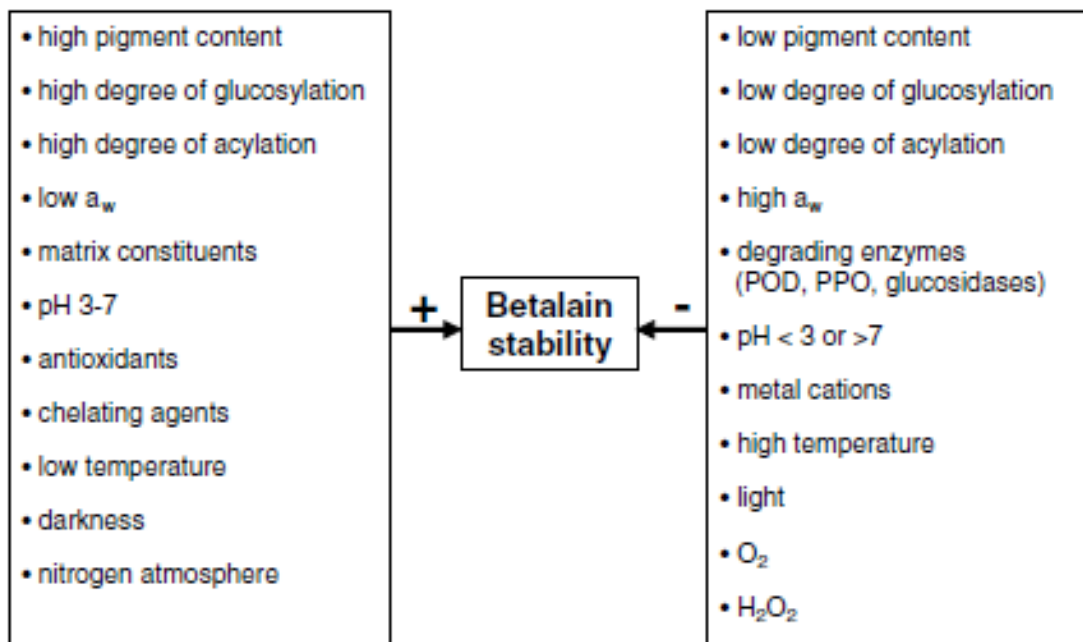


Figure 3.3. Factors influencing the chemical stability of betalains. Reproduced from Herbach et al., 2006.

After extraction, purification is typically carried out by conventional column chromatography such as normal and reversed phase silica (Rudrappa et al., 2004), ion-exchange (Gonçalves, et al., 2012), gel permeation (Schliemann et al., 1996; Kanner et al., 2001; Gonçalves, et al., 2012) and polymeric resins (Rudrappa et al., 2004; Reddy et al., 2005; Nowacki et al., 2015), very often followed by a (semi)-preparatory reversed phase HPLC (Kanner et al., 2001). However, these methods suffer from a number of disadvantages, such as long processing time, use of non-environmentally friendly organic solvents like methanol and acetonitrile, betanin degradation during processing or salt introduction in the case of the ion-

exchange elution step (Gonçalves, et al., 2012). Thus, the potential use of betanin as a bioactive compound on an industrial scale requires alternative solutions for the efficient clean-up from its natural source.

I.4 Our strategy

In this work, we first evaluated the purification degree which could be obtained using commercially available resins. We employed a new operating sequence based on an ion-exchange resin which was subsequently coupled to an adsorption resin for desalination in order to maximize the purity degree of the betanin/isobetanin concentrate, as described in Section II.1. Nevertheless, some issues need further optimization such as the large amount of solvent and resin required and the need for desalination after the use of the ion-exchange resin.

In this respect, we postulated that the use of MIPs as selective sorbents could be an interesting alternative to traditional purification protocols, since their specific recognition properties could improve importantly the performance of the purification method. Thus, we developed a fast and economic procedure based on molecularly imprinted solid-phase extraction (MISPE) for the selective clean-up of betanin and its stereoisomer isobetanin from beetroot extracts.

Several issues had to be addressed for the preparation of a performant water compatible MIP. The main challenge is to achieve selective recognition in beetroot extract. In fact, beetroot constitutes quite a complex matrix and is mainly composed of carbohydrates, sugars, proteins, vitamins, amino acids and minerals (Neelwarne and Halagur, 2012), which can interfere with the molecular recognition of betanin (Table 3.1). Moreover, betanin itself cannot be used as template for MIP preparation due to its low stability in general and under polymerization conditions (presence of free radicals) in particular. To circumvent this problem we employed a structurally relevant dummy template, a strategy commonly used to avoid template bleeding during analysis (Tse Sum Bui and Haupt, 2010). To the best of our knowledge, this is the first published report of a MIP for the purification of betanin/isobetanin from beetroots.

Table 3.1. Nutrients found in red beet tubers (Adapted from Neelwarne and Halagur, 2012).

Nutrients	Beet tubers
Water (g)	87.58
Energy (kcal)	43
Protein (g)	1.61
Total fat (g)	0.17
Carbohydrate (g)	9.56
Sugars (g)	6.76
Fiber (g)	2.8

II. Results-Discussion

II.1 Extraction-Purification with commercial resins

In the first part of this chapter, we focus on the purification of betalains from beetroot extract, using column chromatography with commercially available adsorbents. Hence, we developed and optimized a two-step purification process which involves the subsequent purification by an ion exchange and hydrophobic resin. We postulated that the combination of both resins could contribute to the improvement of the purity degree of the obtained pigments.

II.1.1. Optimization of the extraction conditions

The extraction of pigments from betalain-containing matrices such as beetroot tubers was performed by maceration of the root in solvent. Due to their hydrophilic properties betalains can be water-extracted, although, in most cases, the use of methanol or ethanol solutions (20–80%) is required to limit the co-extraction of carbohydrates (Delgado-Vargas et al., 2000). The protocol of extraction was previously optimized in our laboratory by Dr. Laetitia Nowacki for her PhD thesis (Nowacki, 2014) and was repeated and reproduced during my thesis. A summary of the results is presented in Figure 3.4. Based on the screening of different ratios of ethanol and water as extraction media tested for the quantification of pigments as well as proteins and sugars using, we concluded that a high percentage of ethanol, equal or up to 80%, in the extraction solvent should be used to obtain the maximum concentration of pigments and as

well as the minimum of co-extracted proteins and carbohydrates in the macerate. Thus, the ratio ethanol/H₂O (4:1 v/v) was used for the following extractions. The final extraction protocol is presented in Figure 3.5 and in Section III.2.

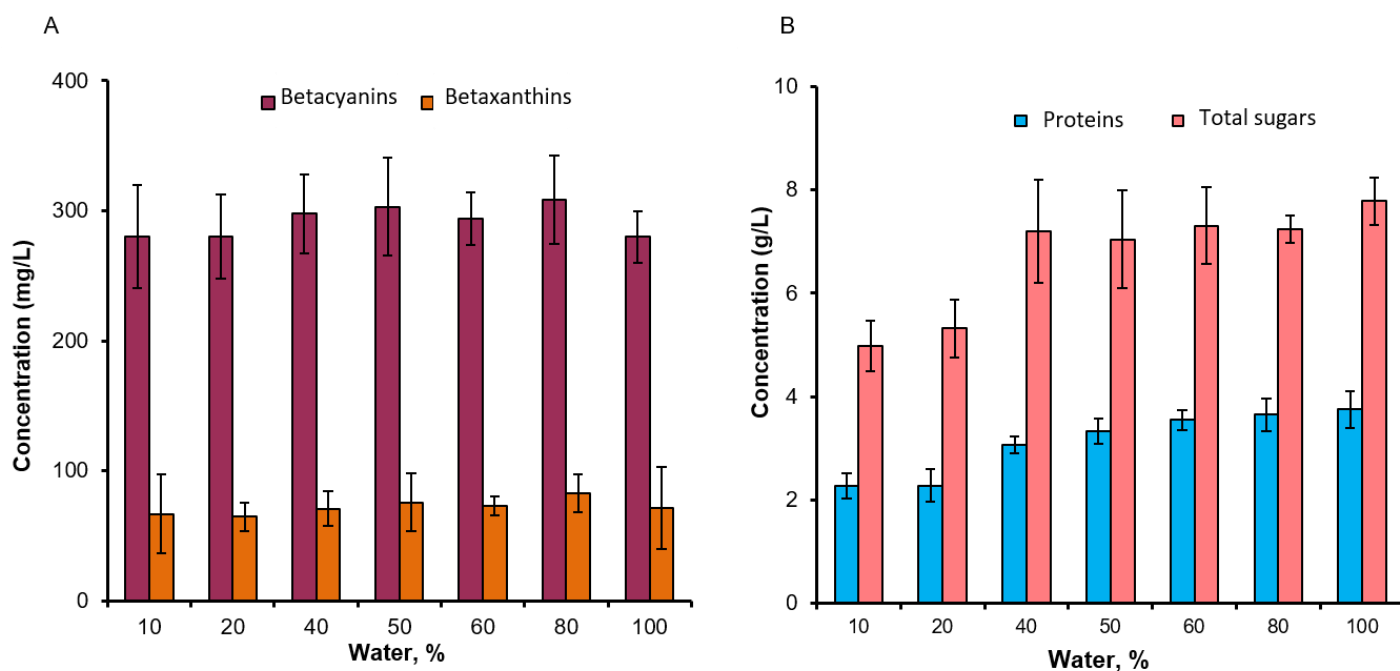


Figure 3.4. Variations of concentrations related to the percentage of water in the extraction solvent for A) betacyanins and betaxanthines; B) Proteins (based on the protocol of Lowry, 1951) and sugars (based on the protocol of Dubois, 1956).

II.1.2. Elaboration of the purification process

For the purification of betalains and specifically betanin/isobetanin, a column chromatography protocol based on commercial resins was developed and optimized. The choice of the resins utilized was based on the reported examples in the literature for betalains (refer also to Section I.3) and other phenolic compounds such as anthocyanins (Chandrasekhar et al., 2012). In fact, most applications for the removal of phenolic compounds are based on hydrophobic resins or ion exchange resins (Kammerer et al., 2011; Soto et al.; 2011). The binding to apolar resins is based on relatively weak interactions between the hydrophobic adsorbent matrix and the non-polar phenolic compounds through van der Waals forces. On the other hand, the principle of ion exchange resins is based on their functional anionic or cationic groups interacting with ionic compounds of the solute or through hydrophobic interactions of the polymeric resin matrix with apolar components.

In this work, an acrylic ion exchange resin (Amberlite FPA98) coupled to a hydrophobic resin based on styrene and divinylbenzene (Amberlite XAD16) were utilized, as illustrated in Table 3.6, Section III.4.1 Preliminary studies were performed to determine the bed volume (BV) required, the capacity of each resin

and the experimental conditions for the flow-through, washing and elution steps (Table 3.2). It easy to conclude that the ion exchange resin has superior adsorption capacity compared to the hydrophobic resin; In fact, the XAD16 resin was saturated rather quickly, even though larger BV was used and an additional dilution by 3-fold was applied. This suggests that larger BV of resin are necessary so as to avoid pigment loss, which also entails the increased consumption of organic solvents.

Table 3.2. A summary of the preliminary studies performed on single columns of XAD16 and FPA98 resins.

Resins	Bed Volume (mL)	Concentration of pigments (mg/L)	Break-through Volume	Volume of eluant (mL)
FPA98 <i>betacyanins</i> <i>betaxanthins</i>	10	220 170	>9 BV 7 BV	NaCl, 8% 5-6 BV
XAD16 <i>betacyanins</i> <i>betaxanthins</i>	30	53 44	1 BV 0.5 BV	MeOH ~2 BV

Taken into account the results obtained from the preliminary studies, we moved further to the application of our concept, which combines the advantages of both resins. The experimental procedure presented in this thesis constituted an optimized protocol to ensure maximal enrichment in betalains (specifically in betanin/isobetanin) and at the same time successfully remove an important amount of matrix materials. The process of resins' coupling is shown in Figure 3.5 and described in details as follows.

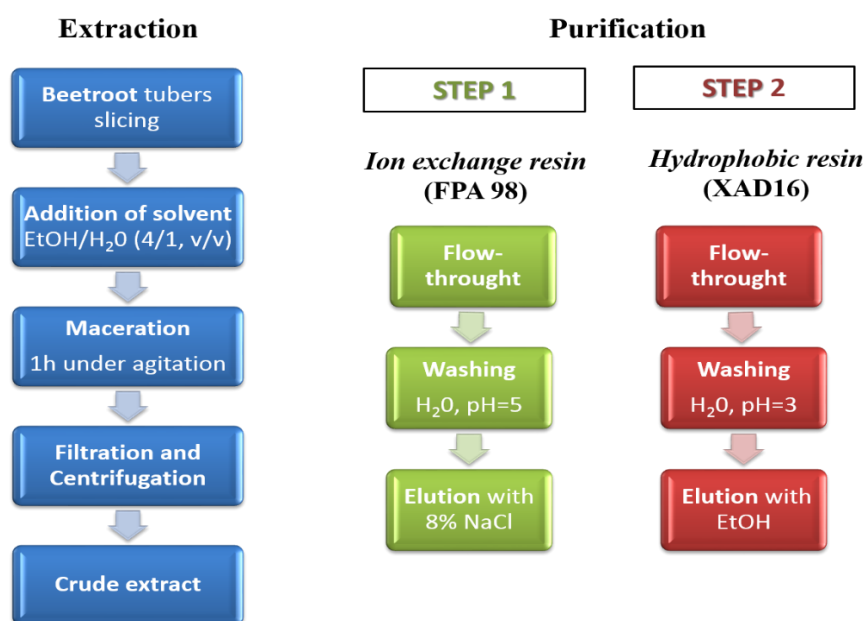


Figure 3.5. Organogram of extraction and purification processes.

- **First Step: Purification by the Amberlite FPA 98 resin**

Prior purification on the resin FPA 98, the beetroot extract was equilibrated to pH 5. Our previous experiments have shown that the performance of the ion exchange resin is improved with the increase of pH, taking into that the ionic form of betacyanins is pH-dependent (Frank et al., 2005). The optimum pH range observed for the performance of the resins was between 5 and 7, so pH 5 was chosen, to ensure maximum pigment stability. To avoid elution and further loss of non-retained betalains during the flow-through step, 10 times higher volume of resin compared to the preliminary capacity studies was utilized (refer to table 3.2). Specifically, 100 mL of resin were used for 150 mL of beetroot extract, with initial concentration of betacyanins and betaxanthins in solution of 230 mg/L and 240 mg/L respectively, as determined by UV-Vis spectroscopy. After the flow-through, rinsing was performed with water pH=5 (at least 3 BV) to remove non retained impurities. Betalains were eluted from the ion exchange column with 8 % NaCl solution, so as to modify the ion exchange force of the resin. A single fraction was collected with total volume of 250 mL, pH=5 with final concentration of both betacyanins and betaxanthins in solution at 230 mg/L.

- **Second Step: Purification by the Amberlite XAD 16 resin**

To enable the coupling of the two types of resins, the performance of XAD16 resin was first evaluated in high NaCl conditions. Given that the eluent used for the purification in FPA 98 is 8% NaCl, the eluted beetroot extract is highly charged in salt. For this, purification was performed on a 30 mL XAD16 column using 8% NaCl charged extract, which was prior eluted from the resin FPA 98. The performance of the XAD16 resin in the presence of 8% NaCl was compared with our previously obtained results in the absence of salt and no difference could be found in terms of adsorption capacity. This suggests that the presence of salt does not interfere with the mechanism of adsorption renders and feasible our proposed setup.

Following optimization, a volume of 1.2 L of resin Amberlite XAD16 was packed to achieve successful desalination and to enable treatment of high amount of beetroot extract. The sample of 250 mL eluted from the FPA 98 resin, equilibrated to pH 3, was passed through the column. This pH was chosen as a compromising solution, to enable good absorption of betalains, while avoiding pigment degradation (refer to section I.3). Subsequently the adsorbent was rinsed with water pH=3 (at least 3 L) to ensure that all the NaCl remaining in the fraction acquired from step 1 was removed. Then, elution was performed with 2 L of methanol. The fraction containing the higher concentration of betaxanthins was eluted first during the rinsing with water and elution steps (Figure 3.6). Then fraction with vivid red-violet color corresponding to betacyanins was collected (600mL). In this way, desalination and further enrichment in betanin/isobetanin was achieved. The concentration of betacyanins and betaxanthins in solution in the final sample was 950 mg/L and 570 mg/L respectively.

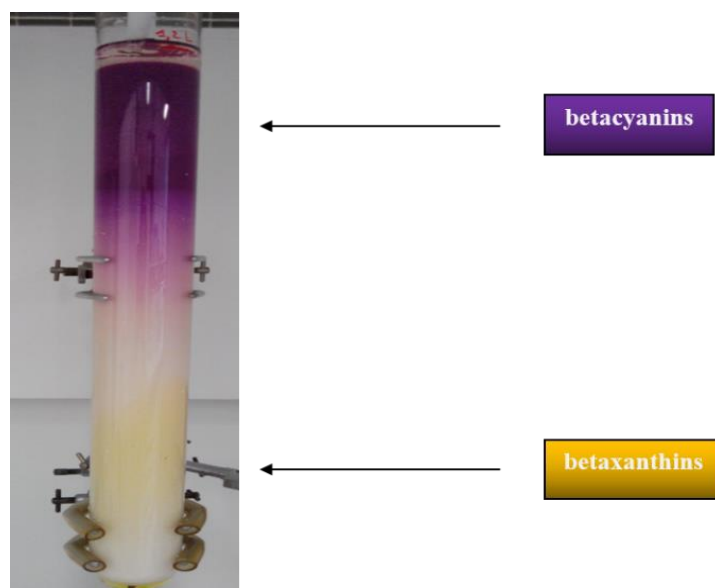


Figure 3.6. Profile of pigments' color in the column packed with the resin XAD 16 during rinsing with water.

II.1.3. Purification results

The concentration of betalains (betacyanins and betaxanthins), sugars and proteins was quantified at each step with UV-Vis spectrometry. The values obtained were presented in Table 3.3. In the first step of purification (FPA 98 column) only 15% loss of pigments was observed. Conversely, loss of pigments is more important on the XAD16 resin, with 33% and 60% loss for betacyanins and betaxanthins respectively. This effect can be expected due to the large amount of solvent used for washing.

Table 3.3. Concentration and total weight of betalains in the beetroot extract at each step of purification

	Before FPA 98	After FPA98	After XAD16
Volume (mL)	300	250	40
Weight (mg)			
betacyanins	69	57.5	38
betaxanthins	72	60	22.8
Concentration (mg/mL)			
betacyanins	0.23	0.23	0.95
betaxanthins	0.24	0.24	0.57

Interestingly, an important amount of matrix materials was eluted after purification. In fact, a total 70 % of proteins were removed while it appears that sugars were almost totally eliminated (Figure 3.7).

This suggests a significant enrichment in pigments, which was confirmed by the increased purity degree of betacyanins and betaxanthins in the processed beetroot extract (Table 3.4). More specifically, a 44-fold and 24-fold enrichment in betacyanins and betaxanthins respectively was achieved after purification, compared to the crude beetroot extract, whose purity degree is very low (<0.5 %).

Table 3.4. %_w of purity degree of pigments in the crude and purified beetroot extract.

% _w purity	Crude extract	Purified extract (after XAD16)	Purified Extract (after FPA98 + XAD16)
Betacyanins	0.41	12.8	17.8
Betaxanthins	0.46	8.3	11.1

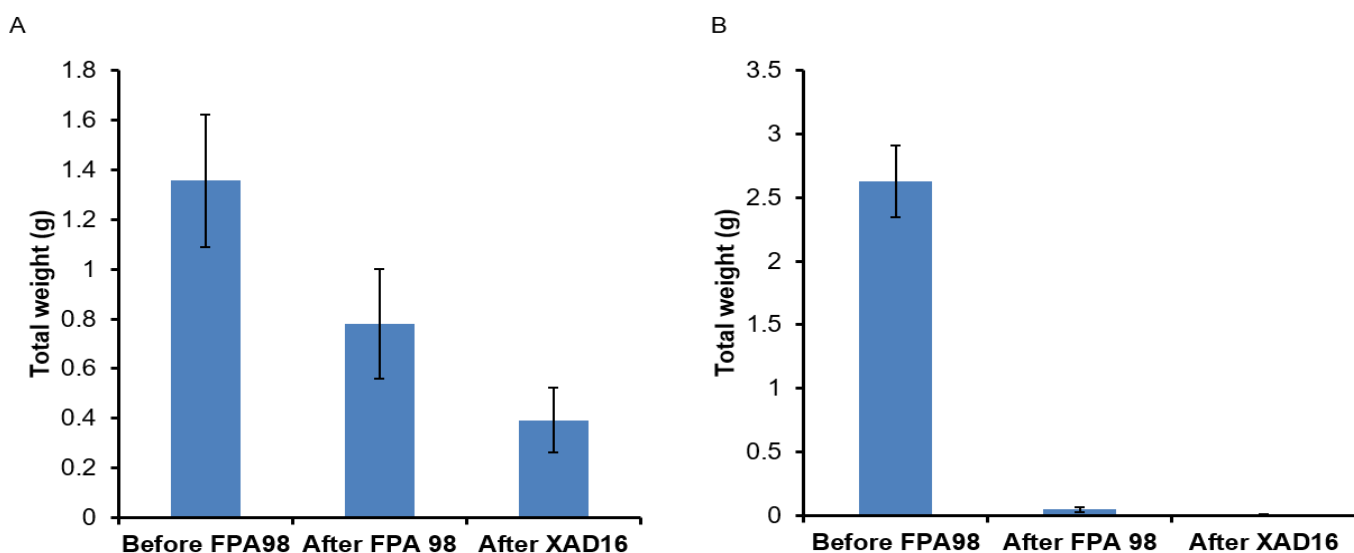


Figure 3.7. Concentration of A) proteins and B) total sugars (right) in the beetroot extract corresponding to each purification step.

To ultimately prove that the coupling of the two resins is a more efficient method of purification in terms of purity and yield than the single column methods usually performed (Stintzing, 2002), a purification process was performed using only the XAD 16 in the same bed volume (1.2 L). All other parameters were kept constant, to enable the direct comparison between experiments. The percentage of purity degree of betalains was calculated after lyophilisation of samples for both the unprocessed and purified beetroot extract, namely 12.8 % for betacyanins and 8.25 % for betaxanthins (Table 3.5). It is easy to conclude that the coupling of two resins is a more efficient method compared to a single step purification with XAD16 resin.

To conclude for this part, we developed a two-step purification method for the clean-up of betalains and specifically of betanin/isobetanin. We observed that by employing this protocol, betanin and isobetanin could be obtained in an elevated purity degree compared to a single-step purification. As reported in the literature, anion exchange resins are highly performant but the amount of salt in the purified fractions results in high conductance and limits further applications (Gonçalves et al., 2012). Hence, the subsequent use of a hydrophobic resin successful removed the salt and increased to purity degree of the final sample. However, further research is needed to develop highly efficient water compatible materials that require minimal amount of solvents and can improve and accelerate the purification process of natural compounds. The following part hopes to enlighten more this interesting subject.

II.2 Purification with MIP sorbents

After having evaluated and optimized the performance of commercial resins for the purification of betalains, we now focused on betanin/isobetanin clean-up using a selective MIP sorbent. We postulated that the selective molecular recognition properties of the imprinted material would facilitate the enrichment in betanin/isobetanin. The extraction protocol utilized in this study was applied under identical conditions for the purification with commercial resins (described in Section III.2)

It must be noted that, recently and in parallel with our work, the company *Biotage* has developed a water compatible MIP resin (RENSA PY) that enables the fractionation of betalains after flash chromatography. This resin bears surface functionality containing both hydrophobic and pyridine moieties and betanin is expected to be retained predominantly through electrostatic interactions. Further discussion concerning the RENS A PY MIP will be provided later on.

II.2.1. Synthesis and evaluation of the binding characteristics of MIPs in batch mode

i) Choice of template

As discussed in the introduction, the challenge in this work is to design a performant MIP that is biocompatible and can efficiently recognize the target molecule betanin/isobetanin. Since betanin could not be employed as template due to its instability at high temperatures employed during polymerization, a dummy template was used for the MIP synthesis. The choice of the appropriate structural analogue of betanin was not an easy task, considering the unique chemical structure of the target molecules. Unfortunately, betalamic acid (Figure 3.8), the structural element of all betalains, though structurally more closely related to the target analytes, could not be used as it is not commercially available. Furthermore, its chemical synthesis is a tedious multistep procedure that gives very low yields and various degradation products and thus a stable product can be obtained only through derivatization (Cabanés et al., 2014).

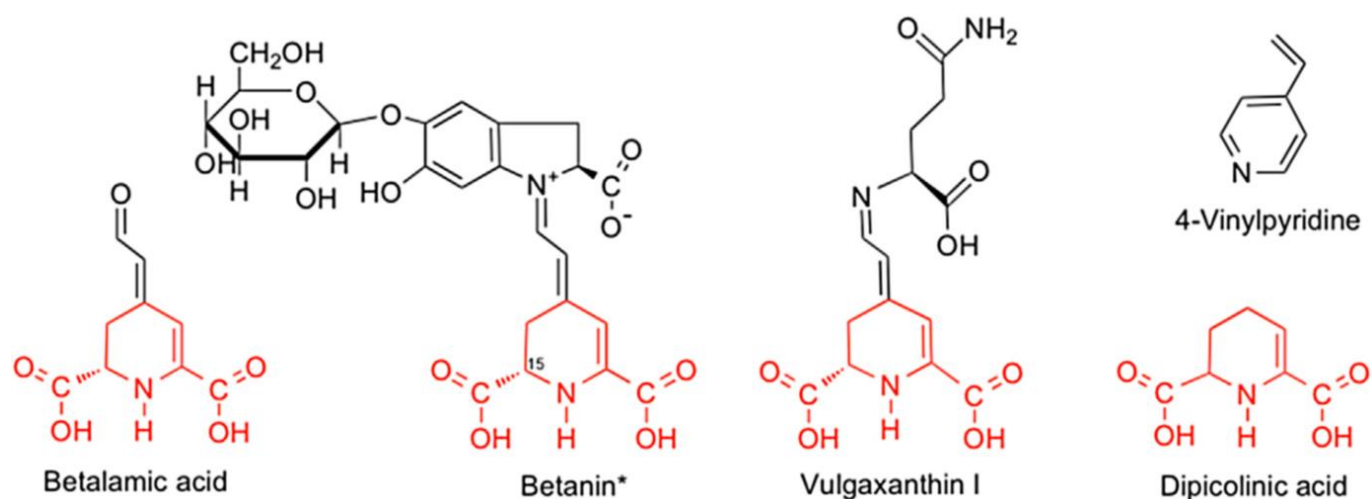


Figure 3.8. Chemical structures of compounds described in this study.

Thus, we tried to identify molecules that bear common structural moieties with the target molecules and that are chemically stable during polymerization. Possible candidates considered were the aromatic acids, chelidamic and dipicolinic acid. Dipicolinic acid (pyridine-2,6-dicarboxylic acid) (Figure 3.8) has some structural similarity with betanin/isobetanin, is commercially available and cheap; therefore, was selected as template for the preparation of our MIP. DPA is also a biomarker of bacterial endospores. The description of MIPs as sensing materials for this molecule, in the assessment of sterility of medical instruments and for problems related to food spoilage and bioterrorism, have already been described in the literature. The different MIPs were prepared using metal-chelating monomers synthesized in-house (Gultekin et al., 2010), were of unknown water-compatibility (Kim et al., 2012) or were synthesized using a sol-gel approach at a high temperature (Smith et al., 2011). In their recent study, Gultekin and co-workers proposed a thiol ligand-capping method with methacrylamidocysteine attached to gold-silver nanoclusters, with reconstructed surface shell based on MIPs as recognition elements for DPA (Gultekin et al., 2010). This approach seems rather complicated for the application targeted here, where MIPs should be featured as a low-cost and easy to tailor alternatives of the conventional purification sorbents and meet the criteria for an agrifood application as well.

ii) Preparation of MIPs

As our MIP had to be highly specific and selective under mild and aqueous conditions, we used one of our protocols previously employed for MIP synthesis of 2, 4-dichlorophenoxyacetic acid (2, 4-D) (Haupt et al., 1998), which like DPA, possesses an aromatic ring and an acidic group. Thus, the MIP was prepared by free radical polymerization using 4-VP as functional monomer, EGDMA as cross-linker in a ratio template: monomer: crosslinker of 1:4:20, Vazo 52 as initiator and methanol/water (4/1) as solvent. The

yield of polymerization was ~70%. We also prepared MIPs *via* the sol-gel approach using as co-monomer an organically modified organosilane monomer that possesses a phenyl group to enhance hydrophobic and π - π interactions in aqueous conditions (Lordel et al., 2010). As discussed in Chapter 1, sol-gel MIPs are *de facto* water compatible and can be an interesting alternative to the organic MIPs. A summary of the synthesized imprinted materials is presented in Table 3.5.

Table 3.5. Imprinted polymers prepared for this study

Polymer	Template	Functional Monomers	Cross-linker	Initiator	Solvent	
MIP DPA-4-VP	DPA 0.1mmol	4-VP 0.4 mmol	EGDMA 2 mmol	ABDV 0.022 mmol	MeOH/H ₂ O (4/1, v/v) 4 mL	
Sol gel MIP	DPA 0.5 mmol	APTES 0.5 mmol	PETMOS 0.5 mmol	TEOS 5 mmol	HCl 0.1M 1 mL	EtOH/H ₂ O (4/1, v/v) 4 mL

iii) Evaluation of the binding characteristics of the imprinted materials

A luminescence method was applied for the detection and quantification of DPA. It has been reported that DPA can be assayed by measuring the luminescence of its chelate with a lanthanide ion (Hindle et al., 1999). The lanthanide complexes have been used as labels in biological and chemical applications due to their unique properties such as high quantum yield, large Stokes shift, long decay time, and narrow emission bands. Since intrinsically luminescence of the lanthanides ions is weak, emission from their excited state must be sensitized by energy transfer from suitable UV-absorbing chelating ligands, such as DPA (Zdunek et al., 2013). For this study the reporter lanthanide Eu^{3+} was used, giving a soluble complex in aqueous solutions, since it is less susceptible to solvent quenching and intensely luminescent. The interaction of DPA with Eu^{3+} leads to a large Stokes shift with an intense red emission at 615 nm corresponding to a ${}^5\text{D}_0 \leftrightarrow {}^7\text{F}_2$ electronic transition of the template for an excitation wavelength of 280 nm (Smith et al., 2011). The linearity was verified by a calibration curve of the complex in water (Section III.5.2, Figure 3.20).

The binding behavior of both the organic and sol-gel polymers towards DPA was investigated in the solvent of synthesis and in water. For the MIP 4-VP equilibrium binding assays in both methanol/water (Figure 3.9A) and water (Figure 3.9B) showed that the MIP is very specific for DPA as no or negligible binding was observed with the non-imprinted polymer (NIP), respectively. A synergistic combination of electrostatic and π - π stacking interactions between the basic and aromatic monomer 4-VP and DPA might be the driving force, allowing strong complex formation in a polar environment (O'Mahony et al., 2005). The binding capacity of the MIP for DPA was determined by plotting a graph of B (bound) versus F (free) (Figure 3.9C). The data, fitted to a Langmuir model, showed a dissociation constant (K_d) of 3.2×10^{-4} M

and a maximum binding capacity (B_{max}) of 9.3 nmol/mg of MIP. These values are similar to those reported for MIP (DPA) prepared using in-house functional monomers (Gultekin et al., 2010).

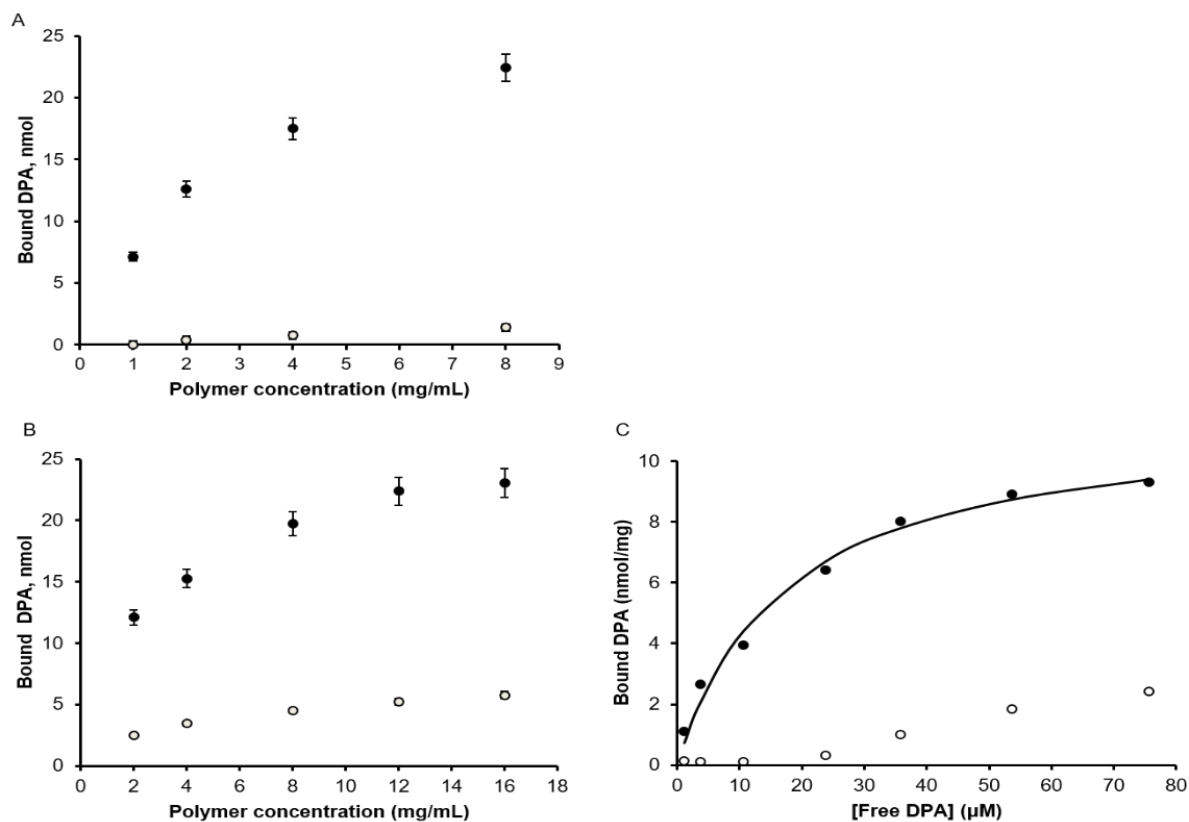


Figure 3.9. A) Equilibrium binding isotherms of MIP (filled circles) and NIP (empty circles) for spiked 25 μM in MeOH/water (4/1). Data are the mean from three independent experiments with three different batches of polymers; B) Equilibrium binding isotherms of MIP (filled circles) and NIP (empty circles) for spiked 25 μM in water. Data are the mean from three independent experiments with three different batches of polymers; C) Binding capacity of MIP and NIP (8 mg) in 1 mL of water. The concentration of DPA was varied from 10 μM to 150 μM . Data are the mean of two independent experiments.

Conversely to the organic polymers, both sol-gel MIP and NIP showed high binding, as illustrated in Figure 3.10A and 3.10B, respectively. Unfortunately, the high capacity of the sol gel MIP is completely compromised by the significant non-specific binding to the NIP. It is interesting to point out that for this experiment, lower concentrations of polymers were employed compared to the organic MIPs, since at the same concentration range both MIP and NIP bound the total amount of DPA added. The increased amount of non-specific binding is often a problem in bulk sol-gel imprinting and further studies are necessary to address this matter (Lofgreen and Ozin 2014). Novel formats that result in ordered mesoporous sol gel polymers could be proved beneficial for the improvement of the MIP specificity (Casado et al., 2017).

Considering the pronounced specificity of organic MIPs for DPA in water, the MIP synthesized with 4-VP as chosen for further studies.

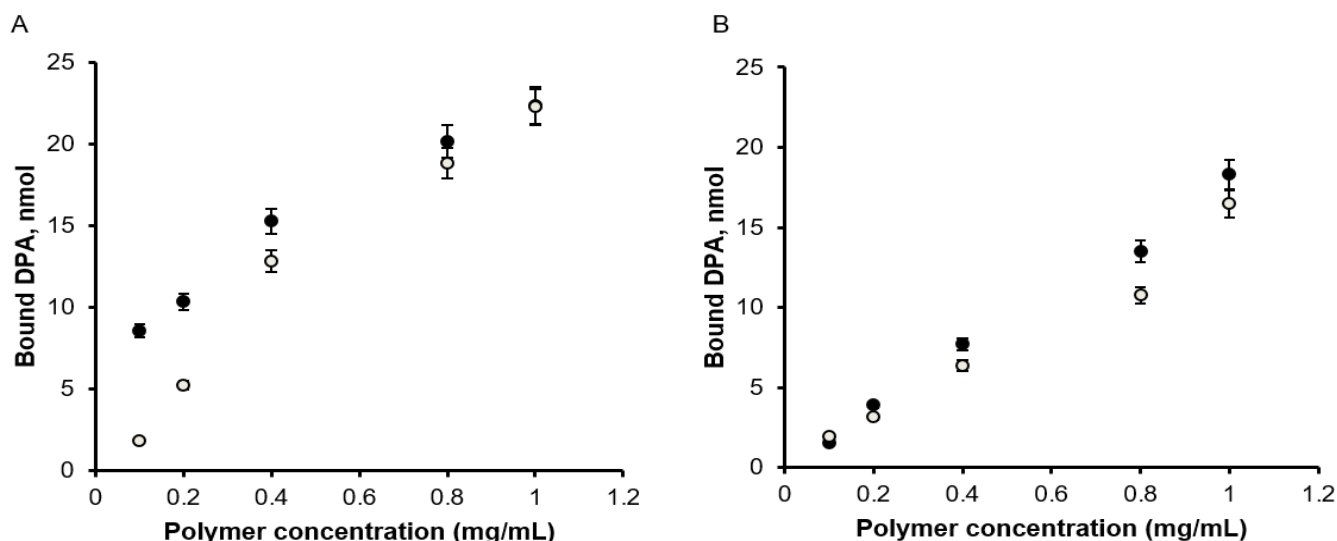


Figure 3.10. Equilibrium binding isotherms of sol-gel MIP (filled circles) and NIP (empty circles) for spiked 25 μM in A) ethanol and B) water. Data are the mean from three independent experiments.

iv) Evaluation of monomer-template interaction

It is very interesting that this 4-VP based MIP works perfectly in water, as both high and specific binding towards DPA is obtained. This is rather remarkable, considering the sometimes complicated approaches, employed in order to enhance the water compatibility of MIPs (for more details refer to Chapter 1, Section I.5). In order to rationalize the design of our MIP protocol, we considered necessary to study in details the interaction between DPA and 4-VP.

Thus, to better comprehend the nature and strength of interactions between DPA and 4-VP, nuclear magnetic resonance (NMR) and isothermal titration calorimetry (ITC) experiments were performed. NMR and ITC are powerful techniques that can characterize monomer-template interactions. While NMR can provide the thermodynamics of an interaction if titration experiments are performed at different temperatures. ITC has the particular advantage to give access directly in one experiment at constant temperature to all thermodynamics parameters of the interaction (Freyer et al., 2008). This method has been mainly used to characterize protein–ligand interactions in aqueous buffers with binding constants between 100 and 10^8 M^{-1} and it is rarely used for association between small molecules because these interactions are often weak (Gue et al., 2008). In the field of MIPs, very few studies report the use of ITC as tool for evaluation of binding interactions. For instance, ITC was employed to study the interaction between MIP implemented with DNA aptamers, as composite materials for the recognition of adenosine (Zhang and Liu, 2016), or for the rational design of MIPs towards the pesticide cinchonidine (Fish et al., 2005). The study of Gue et al., 2008 is also very interesting, as he focused on the evaluation of low-affinity binding interactions, such as obtained from the association of small molecules, traditionally involved in MIP synthesis.

For our study, in collaboration with Dr. Luminita Duma, CNRS Researcher in our group, we developed a protocol for the assessment of the interaction of DPA with 4-VP, which is described in section III.5.6. The low affinity of the DPA/4-VP interaction and the use of methanol/water (4/1) as a solvent made the task challenging. Moreover, given the use of an acid in the ITC titration experiment, we had to adapt the experimental conditions by adding the 4-VP to a constant concentration of DPA such as to avoid significant variations of pH.

Figure 3.11A depicts the raw ITC data recorded for the titration of 4-VP into DPA in methanol/water (4/1). Since there is not enough information in the titration data to fit all the parameters (n , stoichiometry; K_a , association constant; ΔH , enthalpy of interaction), the stoichiometry cannot be accurately extracted from the ITC data and has been obtained by other means. ^{13}C NMR Job plot experiments (Annex, Figure S1) in methanol/water (4/1) yielded to a stoichiometry of 1. The dilution-corrected and integrated ITC data are shown in Figure 3.11B together with the fitted curve using a one-site binding model with a fixed $n = 1$ stoichiometry. The parameters resulting from the non-linear regression fit of the ITC titration curve confirm the existence of an interaction between 4-VP and DPA in methanol/water (4/1) with an association constant K_a of 340 M^{-1} (consistent with affinity obtained by NMR titration shown in Annex, Figure S1) and the following thermodynamic parameters: $\Delta H = -8.14 \text{ kcal/mol}$, $T\Delta S = -4.69 \text{ kcal/mol}$. The binding of 4-VP to DPA is driven by favorable enthalpic changes with an unfavorable entropic contribution. The favorable binding enthalpy is associated with the formation of hydrogen bonds and van der Waals contacts whereas the unfavorable binding entropy may be induced by conformational changes and/or hydrophobic effect (Velazquez-Campoy et al., 2004; Zeng et al., 2012). These results are also supported by molecular modelling results (Annex, Figure S2) which show the the complex structure is stabilized by hydrogen bonds between the carboxyl groups of DPA and the nitrogen of 4-VP. To the best of our knowledge this is the first time that the study of DPA binding interaction with a functional monomer has been performed, so a comparison with any relevant bibliographical data cannot be provided.

These results suggest that the interaction between DPA and 4-VP is not characterized by a high affinity, however other phenomena such as hydrophobic effect and ion-pairing may contribute as driving forces for affinity and specificity in water (O'Mahony et al., 2005).

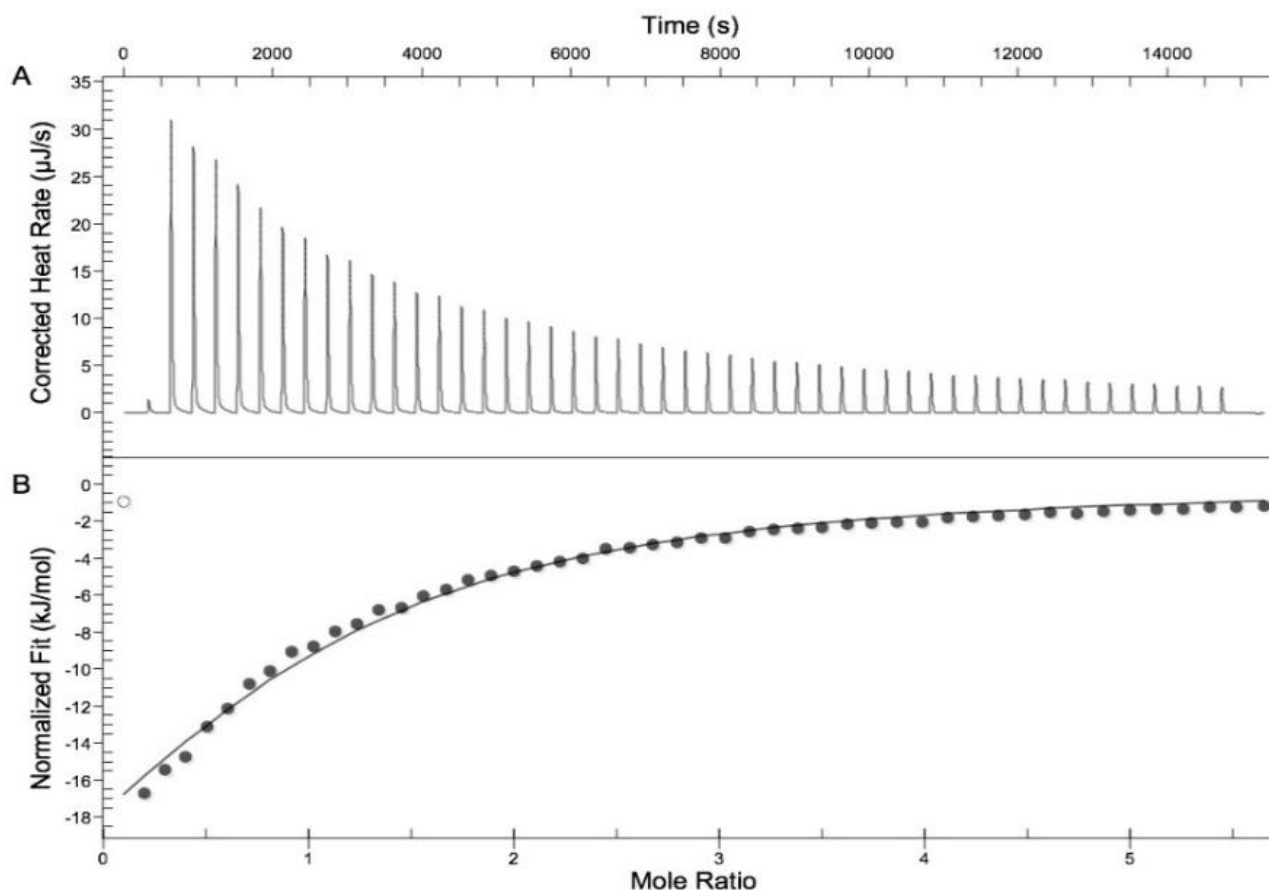


Figure 3.11. ITC data and binding analysis of 4-VP/DPA interaction in methanol/water (4/1) at 25 °C. A) Raw data from the titration of 50 mM of 4-VP added into 3 mM of DPA. Upward peaks indicate an exothermic reaction; B) Integrated areas under each peak are represented against the molar ratio of titrant to titrate and fitted with a non-linear single-site model. The first point (empty circle) was not included in the data analysis.

v) Binding studies with betanin: isobetanin in batch mode

Since the MIP with 4-VP was very efficient in specifically capturing DPA in aqueous conditions, the next step was to evaluate its recognition properties for betanin/isobetanin extracted from beetroots as described in Section III.2. Thus, binding studies were performed with diluted beetroot juice (corresponding to 10 μg/mL of betanin/isobetanin, measured spectrophotometrically as described in Section III.3). Figure 3.12 indicates that the MIP can bind the target analytes to a higher extent than the NIP. Some amount of non-specific binding is observed in batch experiments, but this would not be a problem for the MISPE, as illustrated in the next section. Thus, we decided to further in the study of MISPE for the clean-up of betanin/isobetanin in crude beetroot juice.

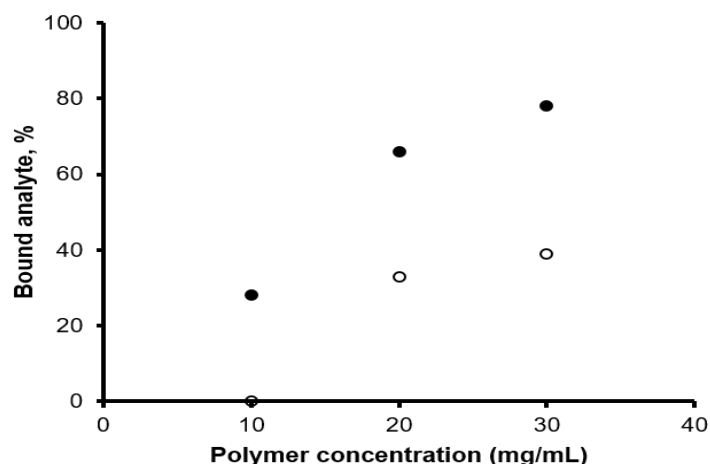


Figure 3.12. Equilibrium binding isotherms of MIP (filled circles) and NIP (empty circles) for 10 µg/mL of betanin/isobetanin in beetroot extract after 2 h incubation at 25 °C. The betanin/isobetanin content was measured spectrophotometrically at 538 and 600 nm, as described in Section III.3.

II.2.2. Solid phase extraction of betanin/isobetanin from crude beetroot extract

Firstly, the MIP was packed into a column and its binding capacity for betanin/isobetanin was determined. Increasing volumes (by step of 0.5 mL) of a diluted beetroot extract containing a constant amount of betanin/isobetanin (10 µg/mL) were percolated on 60 mg of MIP packed in an SPE cartridge. Each flow-through fraction was collected and analyzed for betanin/isobetanin content (Figure 3.13A). Thus, a maximum loaded volume of 2 mL of diluted beetroot extract, corresponding to a maximum pigment loss of 5% (Figure 3.13B), was selected to further study the extraction behaviour of betanin/isobetanin on the MIP sorbent.

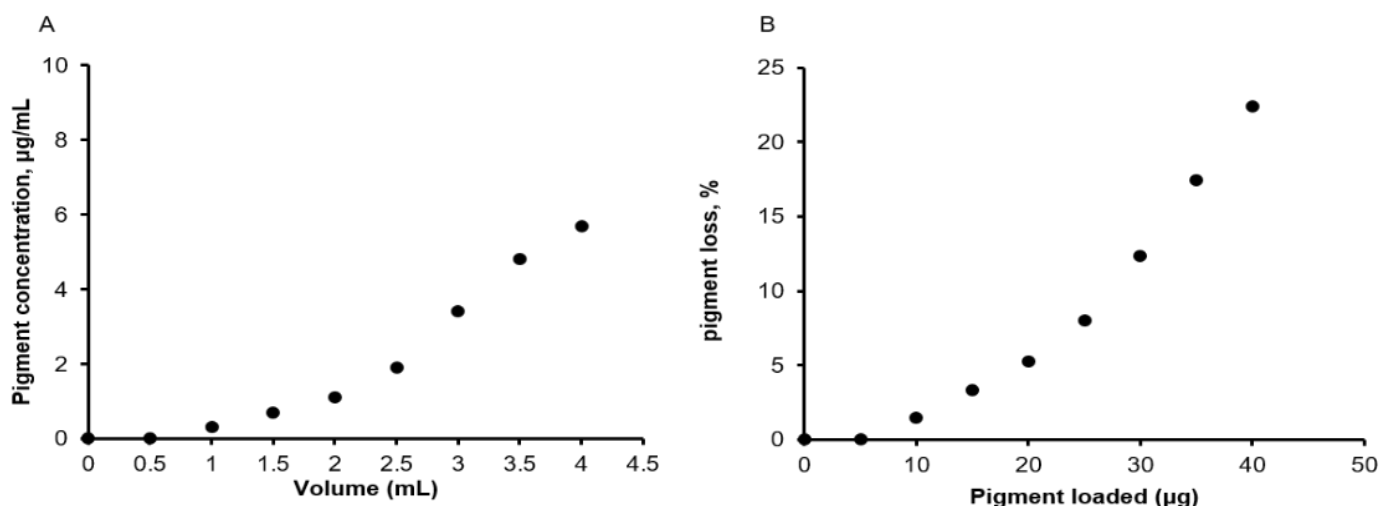


Figure 3.13. A) Evolution of betanin/isobetanin concentration throughout the collection of 0.5 mL fractions during percolation of beetroot extract on the MIP sorbent; B) Corresponding graph with percentage of flow-through of pigment vs loaded pigment.

Therefore, 60 mg of MIP and NIP were packed in separate SPE cartridges and the conditions of loading, washing and elution were optimized. 2 mL of diluted beetroot was loaded on the columns. The target analytes (red-violet) as well as the betaxanthins (yellow) were retained by the MIP during the loading as compared to the NIP where all the coloured pigments passed through the column without retention. Then, a washing step with 4 mL of water (by fractions of 1 mL) was applied to eliminate the non-retained compounds. During the passage of the first 2 mL washings with water, the yellow betaxanthins were washed out of the column, whereas the red-violet betacyanins did not move even after the passage of an additional 2 mL of water. Further washings with water did not affect the retention of the red pigments. Figure 3.14A shows that the total pigment loss on the MIP does not exceed 20 ± 5 % while on the NIP, there is a loss of 95 ± 0.5 % during these two steps.

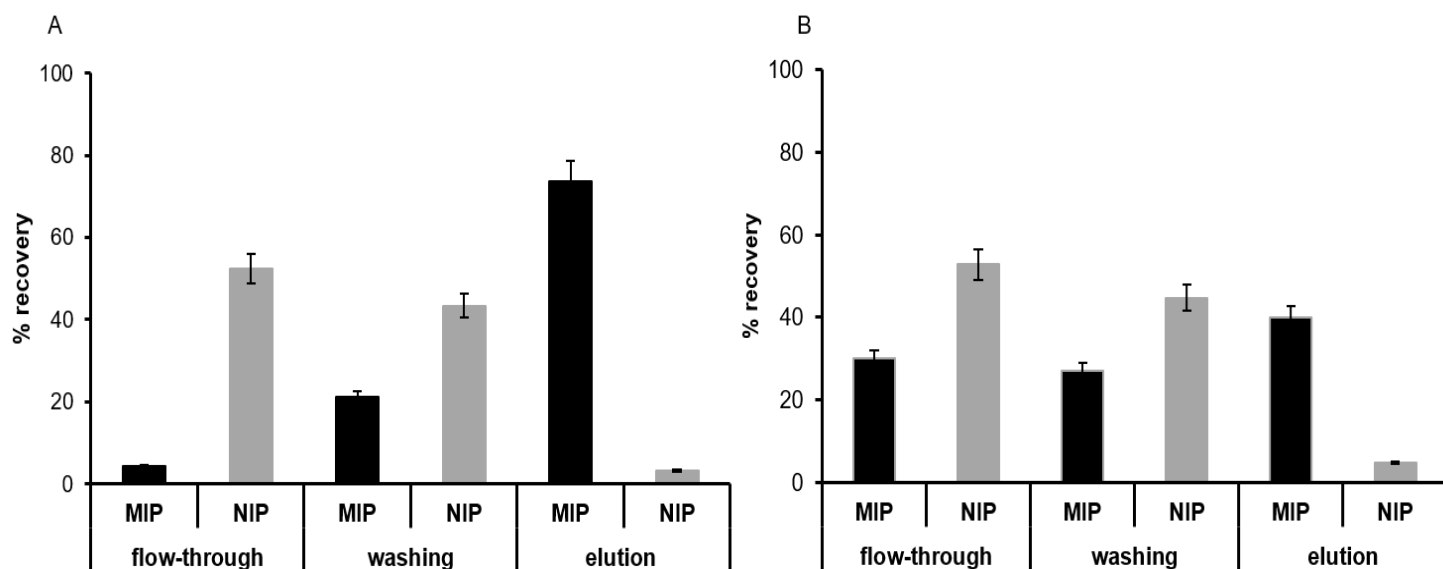


Figure 3.14. Extraction recoveries of A) betanin/isobetanin and B) betaxanthins obtained on 60 mg of polymers. Conditioning with 4 mL of water; loading of 2 mL diluted beetroot extract (betanin/isobetanin and betaxanthins 10 $\mu\text{g}/\text{mL}$); washing with 4 mL water; elution with 4 mL ethanol/acetic acid (1/1). Data represent the mean of five independent experiments, with 2 different batches of polymers.

Afterwards, the elution step was optimized taking into account the low stability of the target molecules at pH values lower than 2 and higher than 8 (Azeredo, 2009). To that aim, different elution solvent compositions were tested, namely ethanol, methanol, methanol (or ethanol)/acetic acid and methanol (or ethanol)/trifluoroacetic acid at different ratios so as to have different pHs. The best recovery was achieved using ethanol/acetic acid (1/1), pH 3.0. 4 mL of eluent was applied to ensure maximal recovery of the target molecules. Under these conditions, the extraction recovery for betanin/isobetanin was 80 ± 5 % for the MIP and 5 ± 0.5 % for the NIP (Figure 3.14), indicating a highly specific retention of the target analytes by the MIP sorbent. As expected, our MIP could not differentiate between betanin and

isobetanin as these molecules differ only by the configuration of the C15 chiral center. One should remember that betanin and isobetanin exist in monoanionic form with deprotonated C2 and C15 carboxylic groups at pH ~3 (Frank et al., 2005). This pH-driven mechanism of retention was also observed for the purification of betalains on the RENSA PY resins of *Biotage*. In the latter case, retention on the surface pyridine moieties of RENSA PY occurred at pH <6. We can assume that since our MIP is prepared using a pyridine monomer as well, similar retention mechanism may exist.

As mentioned before, in this part of the work we focus on the purification of betanin/isobetanin. Nevertheless, it is interesting to point out the differences of the extraction recoveries between betanin/isobetanin and betaxanthins. Under the same experimental conditions, the MIP showed significantly lower recoveries for betaxanthins at the elution step compared to betanin/isobetanin (Figure 3.14B). The fact that initially both betaxanthins and betacyanins were retained on the MIP and not at all on the NIP indicates that high-fidelity imprinted sites were present. As the two betalains have a similar structural backbone as DPA (Figure 3.1), the initial retention of both is expected. However, at the end of percolation and during the washing steps almost 60% of betaxanthins were eluted, as opposed to 25% for betanin/isobetanin. This can probably be explained due to the difference in polarity between the two betalains; the yellow pigments being more polar were more easily eluted (Gonçalves et al., 2012).

II.2.3. HPLC-ESI-MS/MS analysis of betanin samples

The crude and purified extracts were then subjected to RP-HPLC analysis coupled with UV-Vis (204, 477 and 538 nm) and electrospray mass spectrometry in positive ion mode for the identification of individual components. As shown in Figure 3.15B, betanin ($t_R = 12.3$ min, $[M+H]^+ = 551$), isobetanin ($t_R = 14.6$ min, $[M+H]^+ = 551$) and a negligible peak (1% with respect to the areas of betanin/isobetanin) corresponding to vulgaxanthin I ($t_R \sim 4.1$ min, $[M+H]^+ = 340.12$) were present in the purified sample at both 477 nm (detection of betacyanins and betaxanthins) and 204 nm (detection of all pigments and impurities) (Kujala et al., 2002; Gonçalves et al., 2012; Nowacki et al., 2015).

Sugars, mainly saccharose as identified by ESI-MS/MS and vulgaxanthin I, the major pigment of betaxanthins, (Figure 3.15A), that were present before passing through the MIP column, were removed by the MIP. A commercial betanin sample, sold by Sigma-Aldrich as a beetroot extract diluted in dextrin, was also analyzed and both vulgaxanthin I and sugars were detected (Figure 3.15C).

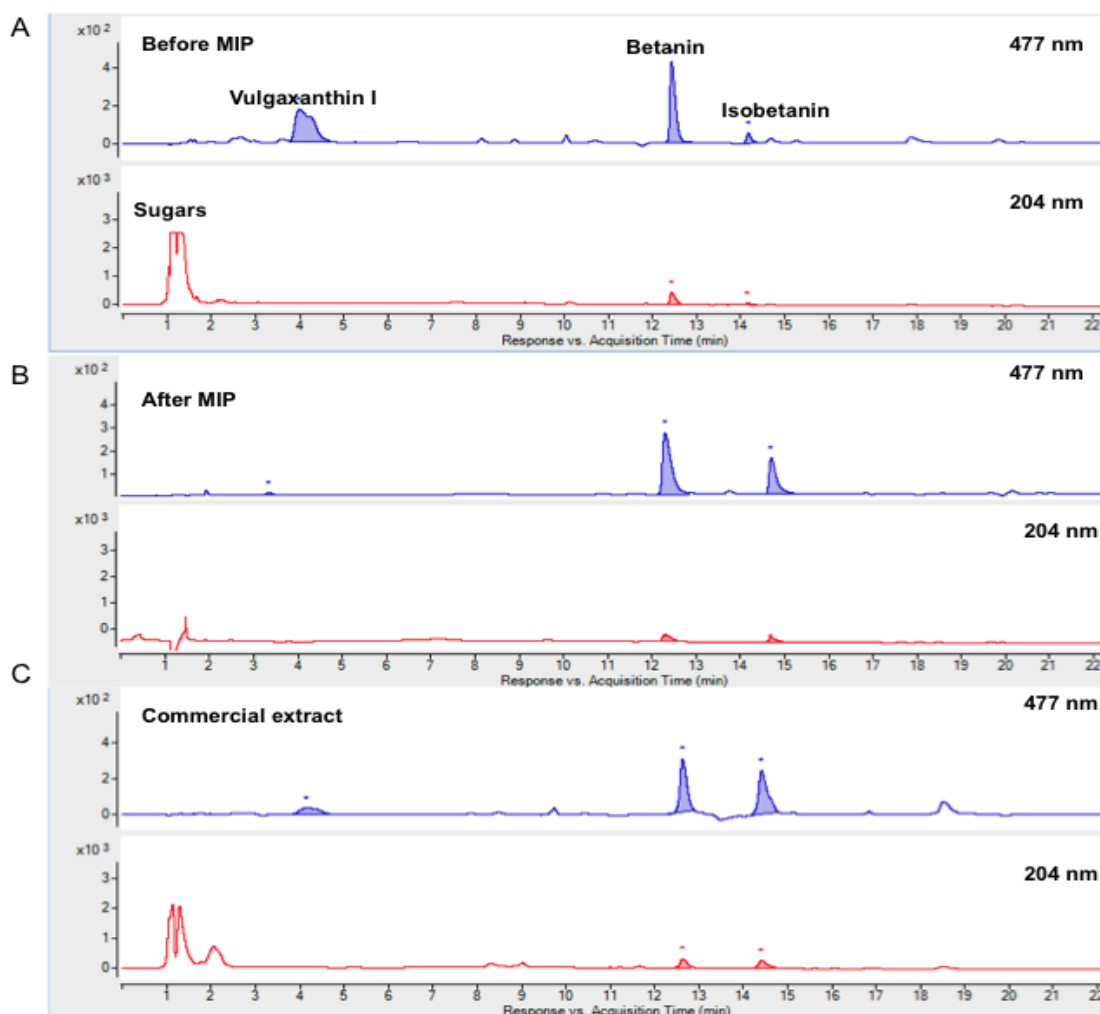


Figure 3.15. Representative chromatograms of diluted beetroot extract (A) before and (B) after extraction on MIP and (C) commercial betanin in dextrin. Retention times were attributed by mass spectrometry analysis: sugars (mainly saccharose m/z $[M+Na]^+ = 365.1054$, $t_R \sim 1.3$ min); vulgaxanthin I (m/z $[M-NH_3]^+ = 323.08$, $t_R = \sim 4.1$ min); betanin (m/z $[M+H]^+ = 551.1497$, $t_R = 12.3$ min) and isobetanin (m/z $[M+H]^+ = 551.1497$, $t_R = 14.6$ min).

Confirmation that the molecules were betanin, isobetanin and vulgaxanthin I was obtained by tandem mass spectroscopy (Figure 3.16A). The mass spectrum shows the daughter ion produced by fragmentation of the parent ion of m/z of 551.1 assigned to betanin or isobetanin. The fragment ion at the mass charge (m/z) of 389.09 indicated that this ion is obtained by glucose loss and corresponds to the protonated aglycone ion, $[\text{betanidin} + H]^+$ or $[\text{isobetanidin} + H]^+$ (Castellanos-Santiago and Yahia, 2008). The structures between betanin and isobetanin cannot be distinguished by MS/MS, as they differ only by the absolute configuration of the C15 chiral center but betanin is slightly more polar, so is less retained as compared to isobetanin on the RP column (Gonçalves et al., 2012; Račkauskienė et al., 2015). Concerning vulgaxanthin I, the fragment ion at the mass charge (m/z) of 323.08 corresponds to the daughter ion $[M-$

NH_3^+ produced by fragmentation of the parent ion of m/z 340.12, assigned to vulgaxanthin I (Figure 3.16B). The other fragment ions are characteristic of vulgaxanthin I (Gonçalves et al., 2012).

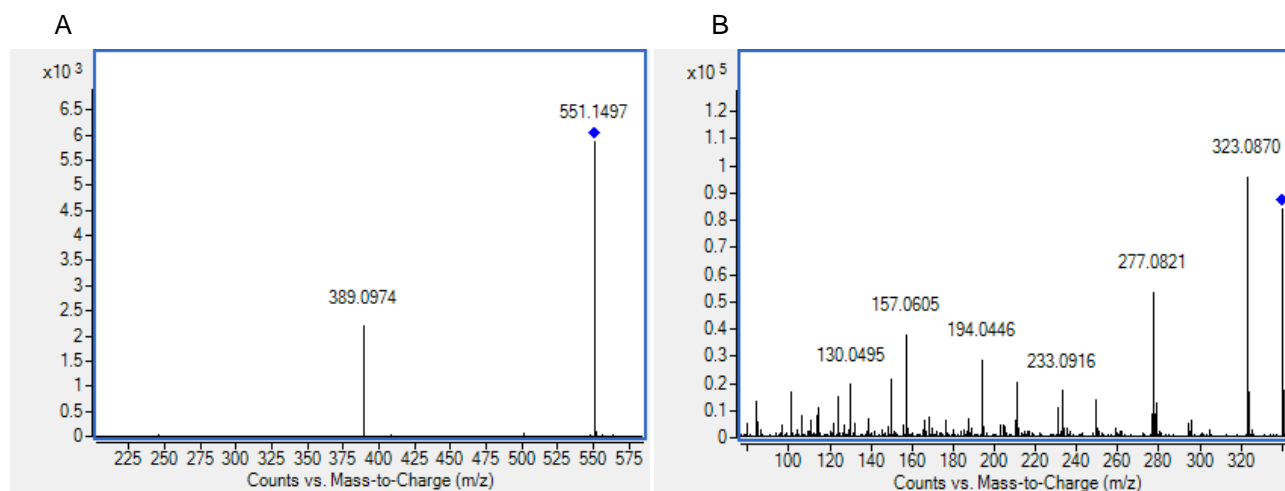


Figure 3.16. Positive electrospray tandem mass spectrum of A) betanin or isobetanin and B) vulgaxanthin I. The daughter ion of m/z 389.09 corresponding to protonated aglycone is obtained by fragmentation of the parent ion of m/z 551.1 of betanin or isobetanin. The daughter ion of m/z 323.08 corresponding to $[\text{M}-\text{NH}_3]^+$ obtained by fragmentation of the parent ion of m/z 340.12 of vulgaxanthin I.

The HPLC profile of the betanin and isobetanin pigments was also monitored at 538 nm, where they exhibit optimum wavelength response (Von Elbe, 2001; Nowacki et al., 2015) (Figure 3.17). Based on the peak area values, the betanin/isobetanin ratios of the beetroot extract before and after MIP purification as well as in commercial betanin was calculated and found to be 10.3 ± 0.2 , 2.2 ± 0.1 and 1.0 ± 0.1 respectively. The amount of betanin is higher than isobetanin in the crude extract as compared to the purified extract which contains 69% of betanin and 31% of isobetanin, and is equivalent in the commercial betanin extract. This is not surprising as betanin isomerizes readily to isobetanin during extraction and storage (Gonçalves et al., 2012). The betanin/isobetanin ratio of the purified extract is similar to the one obtained previously in our group using 1 L of Amberlite XAD-16 column followed by semi-preparative RP-HPLC (Nowacki et al., 2015) thus the MIP could behave as an interesting alternative, in terms of rapidity and economy, to the latter method.

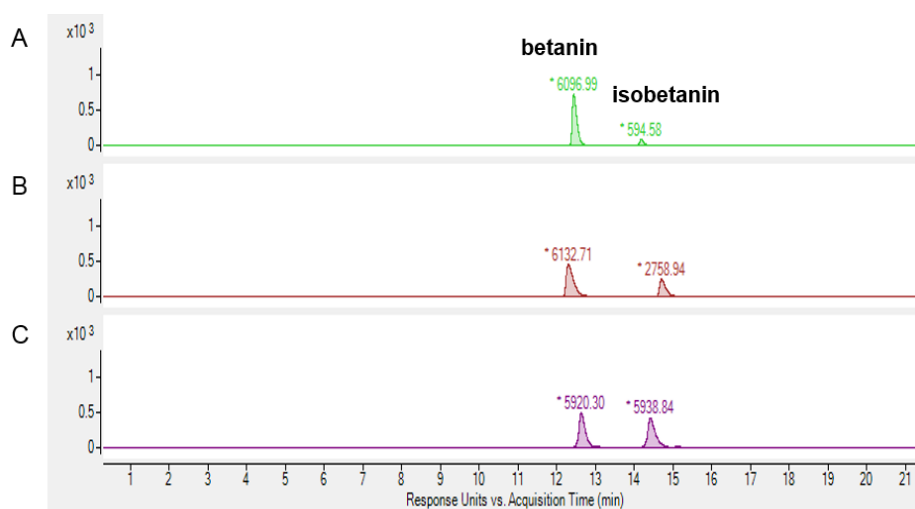


Figure 3.17. Representative chromatograms of A) Crude beetroot extract before MIP; B) Purified sample after MIP and C) Commercial betanin. The identification of peaks was performed by ESI-MS/MS in positive mode: betanin ($m/z [M+H]^+ = 551.1507$, $t_R = 12.3$), isobetanin ($m/z [M+H]^+ = 551.1507$, $t_R = 14.6$ min). Detection with UV at 538 nm.

It should be noted that significant discrepancies are reported in the literature between the chromatographic and spectrophotometric data for the quantitative analysis of betalains in processed beetroot juice (Von Elbe, 2005; Gonçalves et al., 2012). In fact, other colored compounds and degradation derivatives such as neobetainin (Wybraniek, 2005; Nemzer et al., 2011) may contribute to a bathochromic shift in the absorption spectra of the eluted beetroot extract. Thus, it can be assumed that the actual amount of betaxanthins in the eluted sample, as determined by UV-Vis spectroscopy can be overestimated. Owing to the reported discrepancies between the analytical methods, HPLC analysis is currently the preferred method for the straightforward quantification and identification of betalains (Delgado- Vargas et al., 2000). In our case, concrete evidence of the elimination of vulgaxanthin I, the major betaxanthin was confirmed by LC-MS/MS, as illustrated in Figure 3.15.

II.2.4. Elimination of impurities in the purified sample

Proteins and carbohydrates are the most abundant constituents in crude beetroot extract (Neelwarne and Halagur, 2012). Therefore, the total carbohydrate and protein quantification before and after the MIP column was determined according to the method of Dubois et al., 1956 and Lowry et al., 1951 respectively. The amount of proteins present in the injected beetroot extract and the purified fraction was $340 \pm 30 \mu\text{g}$ and $72 \pm 5 \mu\text{g}$ respectively; this means that 21% of the original proteins was co-eluted with the betanin/isobetanin (Figure 3.18). For the sugars, there was $731 \pm 60 \mu\text{g}$ present in the crude extract and none in the purified sample as the absorbance measured was lower than the limit of detection (LOD) of the

calibration curve (Section III.3, Figure 3.19A), indicating that they have been totally eliminated on the MIP column.

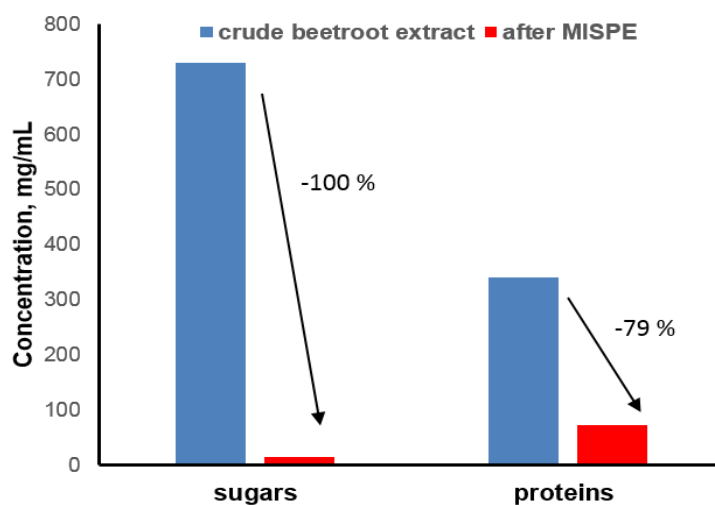


Figure 3.18. Concentration of sugars and proteins before and after purification by the MIP, indicating the percentage of the matrix materials eliminated by the purification process.

II.2.5. Determination of degree of purity-comparison with commercially available resins

The efficiency of MISPE method for the betanin purification was finally evaluated by determining its degree of purity in the final product. The lyophilized purified extract contained 32 %_w of betanin and isobetanin. This indicates a strong enrichment of beetroot extract by these pigments, taking into account that the crude extract contains only 0.1%_w of betanin and its isomer. This single-column purification method appears to be very competitive, since the purity degree of the beetroot extracts industrially produced are always found to be very low (<1.2 %) (Nowacki et al., 2015).

At this point, the purification efficiency of the developed MIP was also compared to a conventional non-selective adsorbent (Amberlite® XAD16) widely used in the literature for betanin purification from vegetal sources (Stintzing, 2002; Reddy et al., 2005; Khan et al., 2012). It should be noted that a direct comparison of the two methods cannot be performed with confidence, since the experimental conditions applied in each case are very different. Nevertheless, the MISPE purification method appears to be more advantageous, owing to an additional enrichment by almost a three-fold, observed for betanin and isobetanin, compared to the traditional method. Definitely, the difference is less pronounced when we compare the purity degree obtained by MISPE with the optimized two-step coupling method presented in section I. However, one must bear in mind that the coupling set-up requires the use of large amount of organic solvent (MeOH) for the elution. On the other hand, with the synthesis described in this paper, 300 mg of MIP was obtained allowing 50 purifications of a total of 1 mg of betanin/isobetanin, using only environmentally friendly solvents.

All together, these results demonstrate for the first time the efficiency of MIPs as selective sorbents for the purification of betanin from its complex natural source, with potential applications for the clean-up of beetroot extract on a semi-industrial scale. Further experiments are necessary to assess the performance of the MISPE on a larger scale.

III. Experimental

III.1 Chemicals

All chemicals and solvents were of analytical grade and purchased from VWR International (Fontenay sous Bois, France) and Sigma-Aldrich (St-Quentin Fallavier, France), unless mentioned otherwise. LC-MS solvents were purchased from Biosolve chimie (Dieuze, France). The inhibitor, hydroquinone (100 ppm) in 4-vinylpyridine (4-VP, 95%) was removed by vacuum distillation. Ethylene glycol dimethacrylate (EGDMA) was used as received. Azo-bis-dimethylvaleronitrile (ABDV) was from DuPont Chemicals (Wilmington, USA). The polymeric resins Amberlite XAD 16 and FPA 98 were purchased from Sigma-Aldrich and were activated before use, as described in section III.4.1. Folin Ciocalteu phenol reagent 2N was diluted 2-fold in water prior to use. Water was deionized (resistivity higher than $18.2 \text{ M}\Omega\cdot\text{cm}^{-1}$) and filtered using a Milli-Q plus unit (Millipore, Molsheim, France).

III.2 Extraction of pigments from beetroots

Fresh red beetroots were purchased from a local market in Compiègne, France. Unpeeled beetroots were finely grated and mixed with ethanol: water (4:1) for extraction of pigments, under continuous mechanical stirring for 30 min in the dark. Typically, 300 mL of solvent was used per 100 g of beetroot. The mixture was centrifuged at 15000 g for 15 min and the supernatant was removed to be re-centrifuged once again. The new supernatant was then filtered using a cellulose filter (2 μm , Whatman). Ethanol was evaporated under reduced pressure and the resulting crude extract was filtered through a hydrophilic polypropylene membrane (0.2 μm , Pall Corporation). The crude extract was stored at $-20 \text{ }^\circ\text{C}$ and diluted to the required concentration with Milli-Q water just prior use.

III.3 Characterization of beetroot extract

Quantifications of betacyanins (betanin/isobetanin), betaxanthins, protein and total carbohydrate contents were recorded on a Cary 60 UV-Visible spectrophotometer (Agilent technologies) at 20 °C.

-Betanin/isobetanin quantification: The concentration of pigments in all samples was evaluated spectrophotometrically using the multi-component method described by J. H. von Elbe, 2001. Briefly, the absorbance values of the samples (diluted if necessary) are measured at 477, 538 nm (a) and 600 nm (c) in a 1-cm path glass cuvette; these will be used to calculate the betanin/isobetanin and betaxanthins concentration and to correct for small amounts of impurity, respectively. The corrected light absorbance of betanin/isobetanin (x) is calculated as $x = 1.095(a-c)$ and of betaxanthins (y) as $y = b-z-x/3.1$ with $z = a-x$, representing the absorbance of colored impurities at 600nm. The concentration of betacyanins (calculated in terms of betanin) and betaxanthins (calculated in terms of vulgaxanthin I) is obtained using an absorptivity value ($A_{1\%}$) 538 nm of 1120 for betanin and ($A_{1\%}$) 477 nm of 750 for vulgaxanthin I and applying the dilution factor. $A_{1\%}$ is the extinction coefficient representing a 1% solution (1.0 g/100 mL).

-Total carbohydrate quantification: Carbohydrate content was determined according to the DuBois method (Dubois et al., 1956). Briefly, 500 μ L of sample (diluted 10-fold with water) was added into 10 mL glass vials containing 500 μ L of 5% phenol solution (99%) in water. Then, 2 mL of concentrated sulfuric acid (98%) was added to the solution. After vortexing, the samples were kept for 30 min at 90 °C and then cooled down to 20 °C. The absorbance was recorded at 492 nm and compared to a calibration curve constructed using glucose as a standard with concentrations varying from 10 μ g/mL to 100 μ g/mL (Figure 3.19A).

-Protein quantification: Protein quantification was performed according to the Lowry method (Lowry et al., 1951). Briefly, 500 μ L volume of sample was pipetted in 10 mL glass tubes, then 2.5 mL of reagent containing CuSO_4 and 250 μ L of Folin Ciocalteu phenol reagent solution diluted to 1 N, were added. After agitation, the samples were incubated for 30 min in the dark. The absorbance was measured at 750 nm. A calibration curve was constructed using bovine serum albumin (BSA) in water as standard with concentrations varying from 50 to 500 μ g/mL (Figure 3.19B).

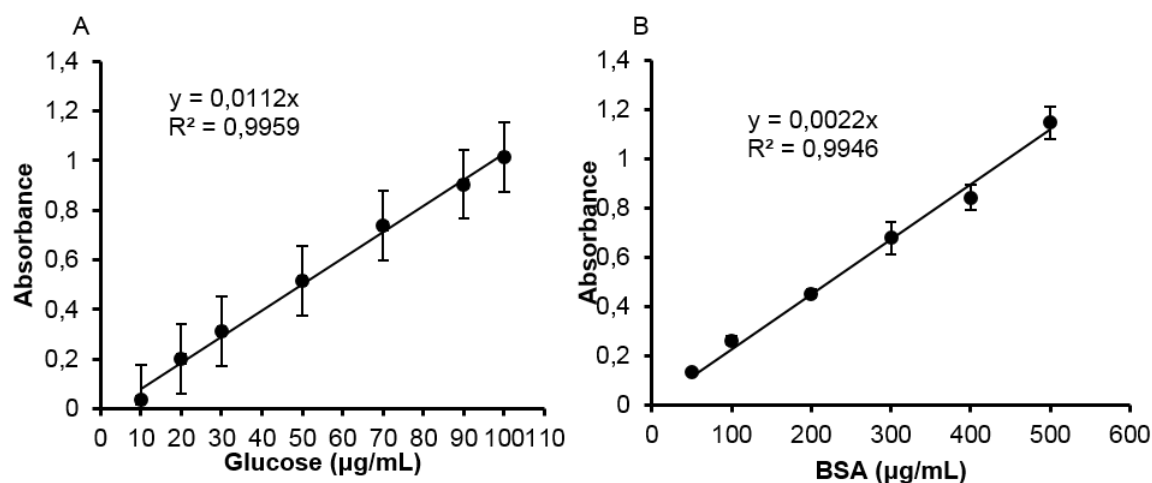


Figure 3.19. Calibration curves of A) Glucose as a standard for the quantification of carbohydrates at 492 nm by the Dubois method; B) BSA as a standard for the quantification of proteins at 750 nm by the Lowry method. Data represent the mean of three independent experiments.

III.4 Purification with commercial resins

III.4.1. Preparation-activation of the resins

For this study, two adsorbent resins were utilized, as summarized in Table 3.6. The ion-exchange resin Amberlite FPA 98 was equilibrated for two days in a 10-fold volume of water, pH 5. Then, the resin was packed in a glass column of appropriate bed volume (10 mL for FPA 98 and 1.2 L for XAD16). The term bed volume (BV) describes the volume of resin packed in the column, which is equal to 1 m³ solution/m³ resins. The adsorption resin Amberlite XAD 16 was activated as follows: after equilibration in water for one day and then packed in a glass column. 1 BV of resins was activated (or regenerated) with 5 BV of NaOH 2%, 5 BV of H₂O, 5 BV of HCl 0.5%, and 5 BV of H₂O, pH 3. The pH of the beetroot extract used for purification on ion exchange and adsorption resins was fixed at 5 and 3 respectively. After each use, the resin XAD16 was regenerated following the steps of first 4 steps of resin preparation, while the FPA 98 was regenerated using an 8% NaCl solution in water at a 10-fold of volume. Resins could be stored at a 20% ethanol solution in water and could be reused up to 10 times.

Table 3.6. Commercial Amberlite resins used in this study.

Resins	Material	Polarity/Adsorption mode	Pores diameter (nm)	Total exchange capacity
Amberlite XAD 16	Styrene, divinylbenzene	Hydrophobic	250-300	-
Amberlite FPA 98	Highly cross-linked acrylic structure	Strong ion-exchange	-	0.8 eq./L (Cl ⁻ form)

III.4.2. Protocol of purification - Determination of the degree of purity

The protocol of purification by the coupling of two resins was described in the section I.1.2; since its optimization constitutes the main objective of the purification studies with commercially available resins. The purity degree of the crude and purified beetroot samples was calculated as follows: The samples were lyophilized and afterwards weighed with precision. In parallel the predicted weight of pigments was calculated from the concentration of pigments obtained by UV-Vis spectroscopy. The percentage of purity degree was calculated using the following expression:

$$\%_m = (\text{mg of pigments calculated} / \text{mg of product weighted}) * 100$$

III.5 Purification with MIPs

III.5.1. Preparation of the imprinting materials

i) Organic MIPs

Typically, 0.1 mmol of DPA, 0.4 mmol of 4-VP, 2 mmol of EGDMA and 0.022 mmol of Vazo 52 were dissolved in 4 mL of methanol/water (4/1) in a glass vial fitted with an airtight septum. The mixture was then purged with nitrogen for 5 min. Polymerization was done overnight in a water bath at 40 °C. A soft polymeric gel was obtained. The polymers were then transferred to 50 mL centrifuge tubes and washed under agitation with 2 rounds of methanol/acetic acid (9/1), 2 rounds of NH₃ 100 mM/methanol (7/3), 2 rounds of water and 2 rounds of methanol. They were then dried overnight under vacuum. Non-imprinted polymers (NIPs) were synthesized in the same way but without the addition of the imprinting template. The formulation of the synthesized MIP is presented in the following table.

To assess the amount of functional monomer 4-VP necessary for successful molecular recognition, another MIP based on this protocol was synthesized using 1:1 ratio of template to functional monomer instead of 1:4.

Table 3.7. Formulation of the MIP DPA-VPY used in this study

Polymer	Template	Functional Monomers	Cross-linker	Initiator	Solvent
MIP DPA-4-VP	DPA 0.1mmol	4-VP 0.4 mmol	EGDMA 2 mmol	ABDV 0.022 mmol	MeOH/H ₂ O (4/1, v/v) 4 mL

ii) Sol- gel MIPs

First, the functional monomers 3 (aminopropyl) triethoxysilane (APTES) and pyridyl ethyl trimethoxysilane (PETMOS) and the template were incubated for 30 min in the polymerization solvent consisted of 4 mL EtOH and 1 mL H₂O in a 20 mL glass vials. After prepolymerization, the cross-linker

tetraethyl orthosilicate (TEOS) and the catalyst HCl were added. The vial was capped and the mixture was incubated at 60 °C under magnetic stirring for 3 days. The polymers were dried overnight in an oven maintained at 100 °C. They were ground manually with a mortar and pestle, transferred to 2-mL microcentrifuge tubes and milled with 2.8 mm ceramic beads and 1 mL of MeOH in a Precellys 24 homogenizer. The polymers were then transferred to 50 mL centrifuge tubes and washed under agitation at 60 °C with 3 rounds of MeOH/0.1 M HCl, 3 rounds of MeOH/0.1 M NH₄OH and rinsed with two rounds of water and two rounds of MeOH. They were then dried overnight under vacuum. Non-imprinted polymers (NIS) were synthesized in the same way but without the addition of the template. The formulation of the synthesized MIS is presented in the following table.

Table 3.8. Formulation of MIS used in this study

Polymer	Template	Functional Monomers		Cross-linker	Catalyst	Solvent
MIS DPA	DPA 0.5 mmol	APTES 0.5 mmol	PETMOS 0.5 mmol	TEOS 5 mmol	HCl 0.1M 1 mL	EtOH/H ₂ O (4/1, v/v) 4 mL

III.5.2. Quantification of dipicolinic acid

DPA was quantified by measuring the luminescence of its chelate with europium ions. Stock solutions of 2.5 mM DPA and 10 mM europium chloride were prepared in ethanol. The DPA stock was diluted 10-fold with water to construct a calibration curve (12.5 - 125 µM); 50 to 500 µL of DPA was added to 100 µL of EuCl₃ in 1.5 mL-polypropylene microcentrifuge tubes in the dark, which was completed by water to a volume of 1 mL (Figure 3.20). The samples were placed in a quartz cuvette for recording of their luminescence emission at 615 nm using an excitation wavelength of 280 nm, slit 3 nm. All fluorescence measurements were performed on a Fluorolog-3 fluorescence spectrophotometer (Horiba Jobin Yvon, Longjumeau, France) at 20 °C.

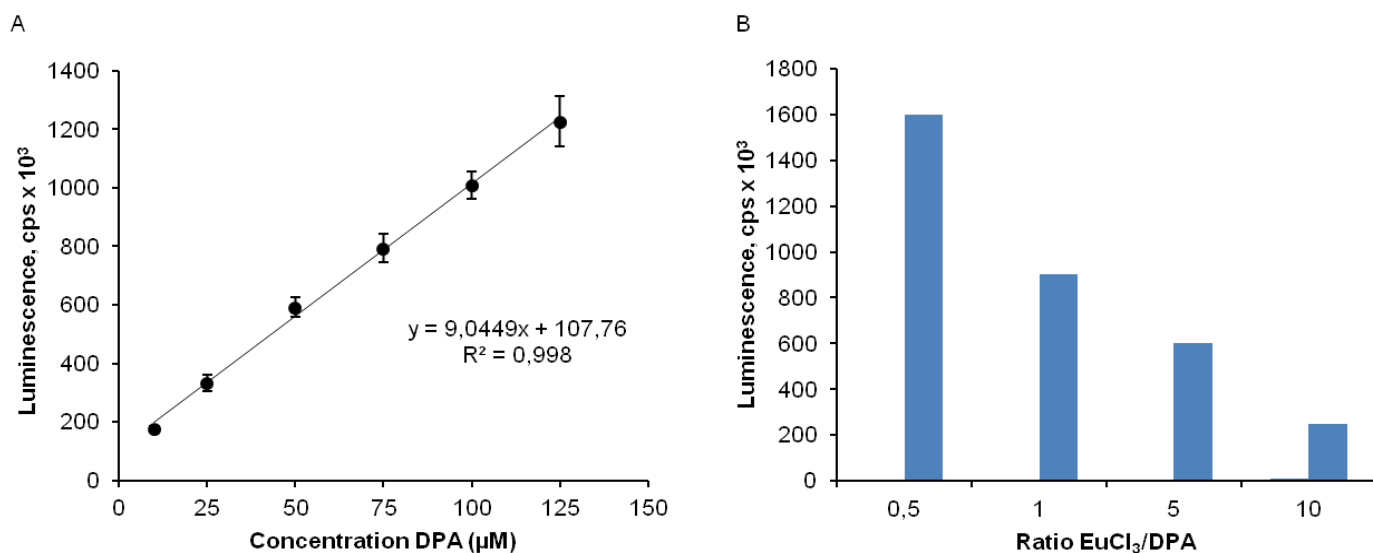


Figure 3.20. A) Calibration curve of the complex Eu^{3+} -DPA in water ($\lambda_{ex} = 280 \text{ nm}$, $\lambda_{em} = 615 \text{ nm}$, slit = 3 nm). $[\text{Eu}^{3+}] = 1 \text{ mM}$. Data represent the mean of three independent experiments; B) Titration of the complex Eu^{3+} -DPA in water ($\lambda_{exc} = 280 \text{ nm}$, $\lambda_{em} = 615 \text{ nm}$, slit = 3 nm).

III.5.3. Equilibrium binding assays

i) Organic MIPs

The imprinted and non-imprinted particles (20 or 40 mg/mL) were suspended in methanol/water or water in a sonicating bath. From this stock suspension, polymer concentrations ranging from 0.5 to 16 mg/mL were pipetted in separate 1.5 mL-polypropylene microcentrifuge tubes and 25 µM of DPA (stock solution of 2.5 mM in ethanol) was added. The final volume was adjusted to 1 mL with solvent. The samples were incubated overnight at ambient temperature on a tube rotator (SB2, Stuart Scientific). They were then centrifuged at 40000 g for 45 min and a 700 µL aliquot of the supernatant was withdrawn for analysis. 70 µL of EuCl_3 (stock solution of 10 mM in ethanol, stored in the dark at $-20 \text{ }^\circ\text{C}$) was subsequently added to each sample. The samples were placed in a quartz cuvette for recording of their luminescence. The amount of DPA bound to the polymers was calculated by subtracting the amount of unbound DPA from the initial amount of DPA added.

For capacity studies, a fixed amount of polymers at 8 mg/mL was used and the concentration of DPA varied from 12.5 to 150 µM (stock solution of DPA 2.5 mM, diluted 10 fold with water to 250 µM). The imprinted and non-imprinted particles (40 mg/mL) were suspended in water in a sonicating bath and a 200 µL aliquot was pipetted in separate 1.5 mL-polypropylene microcentrifuge tubes. The appropriate amount of DPA (50 to 600 µL) was added to each sample. The final volume was adjusted to 1 mL with water. The samples were incubated overnight at ambient temperature on a tube rotator. They were then centrifuged at 40000 g

for 45 min and a 700 μL aliquot of the supernatant was withdrawn for analysis. 70 μL of 10 mM of EuCl_3 was subsequently added to each sample and the luminescence measured.

In order to have an idea of whether betalains are recognized by the MIP, binding experiments were done with diluted beetroot extract. 30 mg of MIP or NIP were weighed in 1.5 mL polypropylene microcentrifuge tubes. 1 mL of diluted beetroot extract (concentration of betanin/isobetanin 10 $\mu\text{g}/\text{mL}$ and betaxanthins 13 $\mu\text{g}/\text{mL}$, measured spectrophotometrically, as described in Section II.3) was added and incubated for 2 h at 20 $^\circ\text{C}$. They were then centrifuged at 40000 g for 45 min and a 700 μL aliquot of the supernatant was withdrawn for analysis. The absorbance was recorded at 477, 538 and 600 nm, as described by Von Elbe, 2001. The amount of pigments bound to the polymers was calculated by subtracting the amount of unbound analyte from the initial amount of analyte.

ii) **Sol- gel MIPs**

The binding behavior of the two batches of sol gel polymers was tested first in ethanol and then in water, under the aforementioned conditions applied for the organic polymers. Equilibrium binding studies were also performed at lower polymer concentrations ranging from 0.1 to 1 mg/ mL (stock suspension of 2 mg/mL in the corresponding solvent). Binding and release studies of pigments were carried out with 1 mL of diluted beetroot extract, using 30 to 100 mg of polymers, as described above.

III.5.4. Evaluation of imprinted materials by SPE

The capacity of the 4- VP MIP for betanin/isobetanin was determined as follows: 60 mg of MIP was slurry packed in a 1 mL disposable cartridge equipped with 10 μm porous polyethylene frits (Sigma-Aldrich, France). After conditioning with 4 mL water, increasing volume of diluted beetroot extract (betanin/isobetanin 10 $\mu\text{g}/\text{mL}$), by fraction of 0.5 mL, was loaded. The flow-through was collected by fractions of 0.5 mL in separate tubes. The amount of betanin/isobetanin was determined in each fraction by UV-Vis measurements.

For betanin/isobetanin extraction, typically, 60 mg of MIP and NIP were slurry packed in separate 1 mL disposable cartridges. The cartridges were placed in a Waters SPE 12-vial vacuum manifold connected to a vacuum pump (PC3001 Vario^{pro}, Vaccuobrand, France). After conditioning the polymers with 4 mL of water, 2 mL of diluted beetroot extract (10 $\mu\text{g}/\text{mL}$ of betanin/isobetanin), was loaded. The cartridges were subsequently washed with water (4 mL) to remove the unretained compounds. Betanin/isobetanin was eluted with 4 mL of ethanol/acetic acid (100 %) (1/1). All eluted fractions were pooled and immediately lyophilized to remove ethanol and acetic acid, so as to avoid pigment degradation. The lyophilized sample

was then dissolved in 1 mL of water and together with the pooled flow-through and washing fractions, were analyzed by spectrophotometry at 538 and 600 nm to determine the betanin/isobetanin amount and the extraction recovery. The columns were regenerated with 10 mL of a solution of HCl (37%) in methanol, pH 2.0.

III.5.5. HPLC-ESI-MS/MS analysis

LC-MS/MS was employed for the identification of individual components contained in the beetroot extract. The HPLC system (Infinity 1290, Agilent Technologies, France) was equipped with a diode array detector coupled to a Q-TOF micro hybrid quadrupole time of flight mass spectrometer (Agilent 6538, Agilent Technologies, France). HPLC analyses were performed on a Thermo Scientific Hypersyl C18 reversed phase (RP) column (150 x 2.1 mm, 3 μ m, 100 Å). The mobile phase consisted of water + 0.1% formic acid (eluent A) and acetonitrile (eluent B). The gradient program began with 0% B, ramped to 13% B at 21 min, held at 13% for 4 min, increased to 100% B at 30 min and was kept constant at 100% B until 35 min. The flow rate was set at 0.4 mL/min. Detection was monitored at 204, 280, 477 and 538 nm. Diluted beetroot juice, the purified sample from the MIP column and a commercially available betanin extract in dextrin were prepared so as to obtain a concentration of betanin/isobetanin 10 μ g/mL (spectrophotometrically), for analysis. This amount corresponds to a weighed amount of 50 mg of the commercial extract in 1 mL water. The injection volume was 10 μ L for the purified extract and for the others, the volume was adjusted so as to obtain a similar area to the betanin area in the purified extract, for strict comparison. Under these conditions, the retention times for vulgaxanthin I, betanin and isobetanin were ~ 4.1 min, 12.3 and 14.6 min respectively. Positive ion electrospray (ESI) mass spectra were acquired by scan mode in the range m/z 100 to m/z 1200 at electrospray voltage of 3800 V and fragmentor voltage of 140 V. Nitrogen was used as the dry gas at a flow rate of 12.0 L/min and a pressure of 45.0 psi. The nebulizer temperature was set to 350 °C.

Betanin/isobetanin and vulgaxanthin I structural identities were confirmed by tandem mass spectrometry using a collision energy of 15 eV and 20 eV respectively.

III.5.6. Isothermal Titration Calorimetry (ITC) studies

ITC measurements were performed at 25 °C on a TA Instruments low volume Nano ITC. The microcalorimeter employs a reference and a sample cell both in 24K Gold with a fixed 190 μ L and a 50 μ L syringe. The syringe needle is equipped with a flattened, twisted paddle at the tip to ensure continuous mixing of the solutions in the sample cell rotating at 300 rpm. Prior to each measurement, each solution was degassed for 15 minutes to remove air bubbles. For all the experiments the reference cell was filled

with methanol/water (4/1). Before the first injection, the instrument required 7200 s to equilibrate, which seems to be specific to the methanol/water mixture, whereas 300 s were sufficient after each injection. Duplicate titrations were carried out by consecutive 1.01 μL injections of 50 mM 4-VP into the sample cell filled with 3 mM DPA. 48 injections in total were performed. A dilution experiment was performed by consecutive injections of 1.01 μL aliquots of 50 mM 4-VP into the sample cell filled with methanol/water (4/1). The heat of dilution of 4-VP in methanol/water was subtracted from the titration data. Representative titration curves were fitted to a single-site binding model to extract the affinity constant (K_a) and enthalpy change (ΔH). The pH of the DPA free and in complex with 4-VP varied from 3.3 to 4.5 indicating a small contribution to the interaction coming from an acid-base equilibrium.

III.5.7. Nuclear Magnetic Resonance (NMR) studies

The stoichiometry and the strength of the interaction between DPA and 4-VP have also been determined by NMR using the method of continuous variation (Job plot) (Renny, 2013) and titration (Connors, 1987; Thordarson, 2011). In all experiments, the free and the template-bound monomer forms are in fast exchange on the NMR timescale in the sense that a single (weighted) averaged chemical shift is observed. The chemical shift difference ($\Delta\delta$), due to complexation, of the carboxyl of the template (Figure 1 in Annex) was followed at 25°C (using CD_3OD as standard) as a function of mole fraction of the template in the Job plot and as a function of the monomer/template concentration for titration experiments, respectively. The carboxyl resonance was selected because it showed the greatest chemical shift difference among all carbons and is close to the potential binding site. For the Job plot, solutions of DPA and 4-VP, at a constant total concentration of 10 mM were prepared with the template mole fraction, $\chi_T = \frac{[T]}{[T]+[M]}$, varying from 0 to 1 by steps of 0.1. The total volume of each sample was 700 μL . Association constants were determined by titrating an increasing amount of 4-VP into DPA kept constant at 10 mM concentration. Stock solutions of 80 mM 4-VP and 20 mM DPA were prepared and different volumes of the monomer (up to 4 equivalents) were added to 350 μL of 10 mM concentration of template. For an equilibrium 1:1, the overall binding constant is $\beta_{11} = K_a$ where K_a is the association constant. For all the data presented in this work (Job and titration experiments), the non-linear regression analysis was done using a home-written Mathematica program.

III.5.8. Computational studies

Molecular modelling has been undertaken to get information about the nature of potential interactions between the template molecule, DPA, and the functional monomer, 4-VP. Spartan software was used to obtain the energy minimized conformation of DPA in combination with 4-VP, the functional monomer

exploited in the polymer synthesis of the present work. For the monomer/template (4-VP/DPA) system, a semi-empirical calculation of the equilibrium geometry has been done with the AM1 force field in water.

IV. Conclusions - Perspectives

In this chapter, we have showed the utility of water compatible MIPs as selective absorbents for the purification of natural compounds. We developed a rapid, eco-friendly and single-step MISPE method for the clean-up of betanin/isobetanin from crude beetroot extract. This method is very economic as the column could be easily regenerated allowing a reuse of the MIP for up to 10 times without significant loss of its binding capacity and specificity. Importantly, no organic solvents or salt were introduced during processing as opposed to the purification step using ion exchange resins described in Section II.1. The MISPE procedures were fully optimized allowing the almost complete removal of matrix components such as sugars and proteins, resulting in high extraction recovery of betanin/isobetanin in a single step. Moreover, the whole extraction procedure was performed in environmentally friendly solvents with either ethanol or water. Our MISPE method is very promising for the future development of well-formulated beetroot extract with specified betanin/isobetanin content, ready for food or medicinal use. This method can probably be extended to extract vulgaxanthin I, a source of yellow natural pigments from yellow beet which is scarcely investigated. These results pave the way to a wide-scale use of betanin-enriched beetroot extract with antioxidant and anticancer properties for applications in the food, biomedical and cosmetics areas. More experiments could be performed to enable the scale-up of this MISPE method for the purification of large amounts of beetroot juice, as in the case of the RENSA PY resin of *Biotage*.

V. References

[A]

Ali, W. H.; Derrien, D.; Alix, F.; Pérollier, C.; Lépine, O.; Bayouhd, S.; Chapuis-Hugon, F.; Pichon, V., Solid-phase extraction using molecularly imprinted polymers for selective extraction of a mycotoxin in cereals. *Journal of Chromatography A* **2010**, *1217* (43), 6668-6673.

Azeredo, H. M. C., Betalains: properties, sources, applications, and stability – a review. *International Journal of Food Science & Technology* **2009**, *44* (12), 2365-2376.

[C]

Cabanes, J.; Gandía-Herrero, F.; Escribano, J.; García-Carmona, F.; Jiménez-Atiénzar, M., One-step synthesis of betalains using a novel betalamic acid derivatized support. *Journal of Agricultural and Food Chemistry* **2014**, *62* (17), 3776-3782.

Casado, N., Pérez-Quintanilla, D., Morante-Zarcelero, S., Sierra, I., Current development and applications of ordered mesoporous silicas and other sol-gel silica-based materials in food sample preparation for xenobiotics analysis. *Trends in Analytical Chemistry* **2017**, *88*, 167–184.

Castellanos-Santiago, E.; Yahia, E. M., Identification and quantification of betalains from the fruits of 10 mexican prickly pear cultivars by High-Performance Liquid Chromatography and Electrospray Ionization Mass Spectrometry. *Journal of Agricultural and Food Chemistry* **2008**, *56* (14), 5758-5764.

Castro López, M. d. M.; Cela Pérez, M. C.; Dopico García, M. S.; López Vilariño, J. M.; González Rodríguez, M. V.; Barral Losada, L. F., Preparation, evaluation and characterization of quercetin-molecularly imprinted polymer for preconcentration and clean-up of catechins. *Analytica Chimica Acta* **2012**, *721* (0), 68-78.

Cardoso-Ugarte, G. A.; Sosa-Morales, M. E.; Ballard, T.; Liceaga, A.; San Martín-González, M. F., Microwave-assisted extraction of betalains from red beet (*Beta vulgaris*). *LWT - Food Science and Technology* **2014**, *59* (1), 276-282.

Chandrasekhar, J.; Madhusudhan, M. C.; Raghavarao, K.S.M.S., Extraction of anthocyanins from red cabbage and purification using adsorption, *Food and Bioproducts Processing*, **2012**, *90* (4), 615-623.

Connors K. A., In *Binding constants. The measurement of complex stability*, John Wiley & Sons, Inc.: 1987.

[D]

Delgado-Vargas, F.; Jiménez, A. R.; Paredes-López, O., Natural pigments: Carotenoids, anthocyanins, and betalains — Characteristics, biosynthesis, processing, and stability. *Critical Reviews in Food Science and Nutrition* **2000**, *40* (3), 173-289.

DuBois, M.; Gilles, K. A.; Hamilton, J. K.; Rebers, P. A.; Smith, F., Colorimetric method for determination of sugars and related substances. *Analytical Chemistry* **1956**, *28* (3), 350-356.

[E]

Esatbeyoglu, T.; Wagner, A. E.; Schini-Kerth, V. B.; Rimbach, G., Betanin—A food colorant with biological activity. *Molecular Nutrition & Food Research* **2015**, *59* (1), 36-47.

EFSA ANS Panel (EFSA Panel on Food Additives and Nutrient Sources added to Food), 2015. Scientific Opinion on the re-evaluation of beetroot red (E 162) as a food additive. *EFSA Journal* **13** (2015) 4318-4373. doi:10.2903/j.efsa.2015.4318 Available online: www.efsa.europa.eu/efsajournal

[F]

FDA (US Food and Drug Administration), 2009. Code of Federal Regulations. Title 21. Volume 1. Cite: 21CFR73.260. Sec. 73.260 Vegetable juice. Revised as of April 1, 2009

Fish, W. P.; Ferreira, J.; Sheardy, R. D.; Snow, N. H.; O'Brien, T. P., Rational design of an imprinted polymer: Maximizing selectivity by optimizing the monomer–template ratio for a cinchonidine MIP, prior to polymerization, using microcalorimetry. *Journal of Liquid Chromatography & Related Technologies* **2005**, *28* (1), 1-15.

Frank, T.; Stintzing, F. C.; Carle, R.; Bitsch, I.; Quaas, D.; Straß, G.; Bitsch, R.; Netzel, M., Urinary pharmacokinetics of betalains following consumption of red beet juice in healthy humans. *Pharmacological Research* **2005**, *52* (4), 290-297.

[G]

Gandía-Herrero, F.; Escribano, J.; García-Carmona, F., Purification and antiradical properties of the structural unit of betalains. *Journal of Natural Products* **2012**, *75* (6), 1030-1036.

Gandía-Herrero, F.; Escribano, J.; García-Carmona, F., Biological activities of plant pigments betalains. *Critical reviews in food science and nutrition* **2016**, *56* (6), 937-945.

Gonçalves, L. C. P.; Trassi, M. A. d. S.; Lopes, N. B.; Dörr, F. A.; Santos, M. T. d.; Baader, W. J.; Oliveira Jr, V. X.; Bastos, E. L., A comparative study of the purification of betanin. *Food Chemistry* **2012**, *131* (1), 231-238.

Gué, A.-M.; Lattes, A.; Laurent, E.; Mauzac, M.; Mingotaud, A.-F., Characterization of recognition sites for diethyl 4-nitrobenzylphosphonate, an organophosphate pesticide analogue. *Analytica Chimica Acta* **2008**, *614* (1), 63-70.

Gültekin, A.; Ersöz, A.; Sarıözlü, N. Y.; Denizli, A.; Say, R., Nanosensors having dipicolinic acid imprinted nanoshell for *Bacillus cereus* spores detection. *Journal of Nanoparticle Research* **2010**, *12* (6), 2069-2079.

[H]

Haupt, K.; Dzgoev, A.; Mosbach, K., Assay system for the herbicide 2, 4-dichlorophenoxyacetic acid using a molecularly imprinted polymer as an artificial recognition element. *Analytical Chemistry* **1998**, *70* (3), 628-631.

Hindle, A.A.; Hall, E.A.H., Dipicolinic acid (DPA) assay revisited and appraised for spore detection. *Analyst* **1999**, *124*, 1599-1604.

[K]

Kammerer, J.; Boschet, J.; Kammerer, D. R.; Carle, R., Enrichment and fractionation of major apple flavonoids, phenolic acids and dihydrochalcones using anion exchange resins. *LWT - Food Science and Technology* **2011**, *44* (4), 1079-1087.

Kanner, J.; Harel, S.; Granit, R., Betalains, a new class of dietary cationized antioxidants. *Journal of Agricultural and Food Chemistry* **2001**, *49* (11), 5178-5185.

Kapadia Govind, J.; Rao, G. S.; Ramachandran, C.; Iida, A.; Suzuki, N.; Tokuda, H., Synergistic cytotoxicity of red beetroot (*Beta vulgaris* L.) extract with doxorubicin in human pancreatic, breast and prostate cancer cell lines *Journal of Complementary and Integrative Medicine* **2013**; *10*, 113-122.

Kecili, R.; Billing, J.; Nivhede, D.; Sellergren, B.; Rees, A.; Yilmaz, E., Fast identification of selective resins for removal of genotoxic aminopyridine impurities via screening of molecularly imprinted polymer libraries *Journal of Chromatography A* **2014**, *1339*, 65-72.

Kim, H.; Kim, Y.; Chang, J. Y., Preparation of a molecularly imprinted polymer containing europium(III) ions for luminescent sensing. *Journal of Polymer Science Part A: Polymer Chemistry* **2012**, *50* (23), 4990-4994.

Khan, M. I.; Harsha, P. S. C. S.; Chauhan, A. S.; Vijayendra, S. V. N.; Asha, M. R.; Giridhar, P., Betalains rich *Rivina humilis* L. berry extract as natural colorant in product (fruit spread and RTS beverage) development. *Journal of Food Science and Technology* **2015**, *52* (3), 1808-1813.

Kugler, F.; Stintzing, C.; Carle, R., Identification of betalains from petioles of differently colored swiss chard (*Beta vulgaris* L. ssp. *cicla* [L.] alef. Cv. bright lights) by High-Performance Liquid Chromatography–Electrospray Ionization Mass Spectrometry, *Journal of Agricultural and Food Chemistry* **2004**, *52* (10), 2975-2981.

Kujala, T. S.; Vienola, M. S.; Klika, K. D.; Lojonen, J. M.; Pihlaja, K., Betalain and phenolic compositions of four beetroot (*Beta vulgaris*) cultivars. *European Food Research and Technology* **2002**, *214* (6), 505-510.

[L]

Lechner, J. F.; Wang, L.-S.; Rocha, C. M.; Larue, B.; Henry, C.; McIntyre, C. M.; Riedl, K. M.; Schwartz, S. J.; Stoner, G. D., Drinking water with red beetroot food color antagonizes esophageal carcinogenesis in N-Nitrosomethylbenzylamine-treated rats. *Journal of Medicinal Food* **2010**, *13* (3), 733-739.

Livrea, M. A.; Tesoriere, L., Lipoperoxyl radical scavenging and antioxidative effects of red beet pigments. In B. Neelwarne (Ed.) *Red Beet Biotechnology: Food and Pharmaceutical Applications*, Springer, New York, **2012**, pp 105-124.

Lofgreen, J. E.; Ozin, G. A., Controlling morphology and porosity to improve performance of molecularly imprinted sol-gel silica. *Chemical Society Reviews* **2014**, *43* (3), 911-933.

Lowry, O. H.; Rosebrough, N. J.; Farr, A. L.; Randall, R. J., Protein measurement with the Folin phenol reagent. *Journal of biological Chemistry* **1951**, *193* (1), 265-275.

[M]

McCann, D.; Barrett, A.; Cooper, A.; Crumpler, D.; Dalen, L.; Grimshaw, K.; Kitchin, E.; Lok, K.; Porteous, L.; Prince, E.; Sonuga-Barke, E.; Warner, J. O.; Stevenson, J., Food additives and hyperactive behaviour in 3-year-old and 8/9-year-old children in the community: a randomised, double-blinded, placebo-controlled trial. *The Lancet* **2007**, *370* (9598), 1560-1567.

Moreno, D. A.; García-Viguera, C.; Gil, J. I.; Gil-Izquierdo, A., Betalains in the era of global agri-food science, technology and nutritional health. *Phytochemistry Reviews* **2008**, *7* (2), 261-280.

[N]

Neelwarne, B.; Halagur, S.B., Red Beet: An Overview, in: B. Neelwarne (Ed.), Red Beet Biotechnology: Food and Pharmaceutical Applications, Springer, New York, **2012**, pp. 1-43.

Nemzer, B., Pietrzkowski, Z., Spórna, A., Stalica, P.W., Thresher, W., Michałowski, T., Wybraniec, S., Betalainic and nutritional profiles of pigment-enriched red beet root (*Beta vulgaris* L.) dried extracts. *Food Chemistry* **2011**, *127*, 42–53.

Nigg, J. T.; Lewis, K.; Edinger, T.; Falk, M., Meta-analysis of attention-deficit/hyperactivity disorder or attention-deficit/hyperactivity disorder symptoms, Restriction Diet, and Synthetic Food Color Additives. *Journal of the American Academy of Child & Adolescent Psychiatry* **2012**, *51* (1), 86-97.

Nowacki, L. Étude des effets antiprolifératifs de la bétanine extraite de betterave sur cellules cancéreuses humaines et de son mode d'action au niveau des membranes cellulaires. 2014.

Nowacki, L.; Vigneron, P.; Rotellini, L.; Cazzola, H.; Merlier, F.; Prost, E.; Ralanairina, R.; Gadonna, J.-P.; Rossi, C.; Vayssade, M., Betanin-enriched red beetroot (*Beta vulgaris* L.) extract induces apoptosis and autophagic cell death in MCF-7 Cells. *Phytotherapy Research* **2015**, *29* (12), 1964-1973.

[O]

O'Mahony, J.; Molinelli, A.; Nolan, K.; Smyth, M. R.; Mizaikoff, B., Towards the rational development of molecularly imprinted polymers: ¹H NMR studies on hydrophobicity and ion-pair interactions as driving forces for selectivity. *Biosensors and Bioelectronics* **2005**, *20* (9), 1884-1893.

[P]

Pai, S., and Mello P.D., Stability evaluation of beetroot colour in various pharmaceutical matrices. *Indian Journal of Pharmaceutical Sciences* **2004**, *66*, 696-699.

[R]

Račkauskienė, I.; Pukalskas, A.; Venskutonis, P. R.; Fiore, A.; Troise, A. D.; Fogliano, V., Effects of beetroot (*Beta vulgaris*) preparations on the Maillard reaction products in milk and meat-protein model systems. *Food Research International* **2015**, *70*, 31-39.

Reddy, M. K.; Alexander-Lindo, R. L.; Nair, M. G., Relative inhibition of lipid peroxidation, cyclooxygenase enzymes, and human tumor cell proliferation by natural food colors. *Journal of Agricultural and Food Chemistry* **2005**, *53* (23), 9268-9273.

Renny, J. S.; Tomasevich, L. L.; Tallmadge, E. H.; Collum, D. B. Method of continuous variations: applications of Job plots to the study of molecular associations in organometallic chemistry. *Journal of Angewandte Chemie International Edition* **2013**, 52, 11998-12013.

Rudrappa, T.; Neelwarne, B.; Aswathanarayana, R. G., In situ and ex situ adsorption and recovery of betalains from hairy root cultures of *Beta vulgaris*. *Biotechnology Progress* **2004**, 20 (3), 777-785.

[S]

Schliemann, W.; Joy, R. W.; Komamine, A.; Metzger, J. W.; Nimtz, M.; Wray, V.; Strack, D., Betacyanins from plants and cell cultures of *Phytolacca americana*. *Phytochemistry* **1996**, 42 (4), 1039-1046.

Smith, C. B.; Anderson, J. E.; Edwards, J. D.; Kam, K. C., In situ surface-etched bacterial spore detection using dipicolinic acid–europium–silica nanoparticle bioreporters. *Applied Spectroscopy* **2011**, 65 (8), 866-875.

Soto, M. L.; Moure, A.; Domínguez, H.; Parajó, J. C., Recovery, concentration and purification of phenolic compounds by adsorption: A review. *Journal of Food Engineering* **2011**, 105 (1), 1-27.

Sreekanth, D.; Arunasree, M. K.; Roy, K. R.; Chandramohan Reddy, T.; Reddy, G. V.; Reddanna, P., Betanin a betacyanin pigment purified from fruits of *Opuntia ficus-indica* induces apoptosis in human chronic myeloid leukemia Cell line-K562. *Phytomedicine* **2007**, 14 (11), 739-746.

Stintzing, F. C.; Schieber, A.; Carle, R., Identification of betalains from yellow beet (*Beta vulgaris* L.) and cactus pear [*Opuntia ficus-indica* (L.) Mill.] by High-Performance Liquid Chromatography –Electrospray Ionization Mass Spectrometry. *Journal of Agricultural and Food Chemistry* **2002**, 50 (8), 2302-2307.

Surh, Y.-J., Cancer chemoprevention with dietary phytochemicals. *Nature Reviews Cancer* **2003**, 3 (10), 768-780.

[T]

Tesoriere, L.; Gentile, C.; Angileri, F.; Attanzio, A.; Tutone, M.; Allegra, M.; Livrea, M. A., Trans-epithelial transport of the betalain pigments indicaxanthin and betanin across Caco-2 cell monolayers and influence of food matrix. *European Journal of Nutrition* **2013**, 52 (3), 1077-1087.

Thordarson, P., Determining association constants from titration experiments in supramolecular chemistry. *Chemical Society Reviews* **2011**, 40, 1305-1323.

Tiwari, B. K.; Cullen, P. J., Extraction of Red Beet Pigments. In B. Neelwarne (Ed.) *Red Beet Biotechnology: Food and Pharmaceutical Applications*, Springer, New York, **2012**, pp 373-391.

Tse Sum Bui, B.; Haupt, K., Molecularly imprinted polymers: synthetic receptors in bioanalysis. *Analytical and Bioanalytical Chemistry* **2010**, 398 (6), 2481-2492.

Turiel, E.; Martín-Esteban, A., Molecularly imprinted polymers for sample preparation: A review. *Analytica Chimica Acta* **2010**, 668 (2), 87-99.

[V]

Velázquez-Campoy, A.; Ohtaka, H.; Nezami, A.; Muzammil, S.; Freire, E., Isothermal titration calorimetry. In *Current Protocols in Cell Biology*, John Wiley & Sons, Inc.: 2001.
Von Elbe, J., Betalains, *Current Protocols in Food Analytical Chemistry*. **2001**.

[W]

Whitcombe, M.J.; Kirsch, N.; Nicholls, I.A., Molecular imprinting science and technology: a survey of the literature for the years 2004-2011, *Journal of Molecular Recognition* **2014**, *27*, 297-401.

Wulandari, M.; Urraca, J.; Descalzo, A.; Amran, M. B.; Moreno-Bondi, M., Molecularly imprinted polymers for cleanup and selective extraction of curcuminoids in medicinal herbal extracts. *Analytical and Bioanalytical Chemistry* **2015**, *407* (3), 803-812.

Wybraniec, S, Formation of decarboxylated betacyanins in heated purified betacyanin fractions from red beet root (*Beta vulgaris* L.) monitored by LC-MS/MS. *Journal of Agricultural and Food Chemistry* **2005**, *53*(9): 3483–3487.

[Z]

Zdunek, J.; Benito-Peña, E.; Linares, A.; Falcimaigne-Cordin, A.; Orellana, G.; Haupt, K.; Moreno-Bondi, M. C., Surface-imprinted nanofilaments for europium-amplified luminescent detection of fluoroquinolone antibiotics. *Chemistry – A European Journal* **2013**, *19* (31), 10209-10216.

Zeng, Z.; Patel, J.; Lee, S.-H.; McCallum, M.; Tyagi, A.; Yan, M.; Shea, K. J., Synthetic polymer nanoparticle–polysaccharide interactions: A systematic study. *Journal of the American Chemical Society* **2012**, *134* (5), 2681-2690.

Zhang, Y.-L.; Zhang, Z.-Y., Low-affinity binding determined by titration calorimetry using a high-affinity coupling ligand: A thermodynamic study of ligand binding to protein tyrosine phosphatase 1B. *Analytical Biochemistry* **1998**, *261* (2), 139-148.

Zhang, Z.; Liu, J., Molecularly imprinted polymers with DNA aptamer fragments as macromonomers. *ACS Applied Materials & Interfaces* **2016**, *8* (10), 6371-6378.

ANNEX

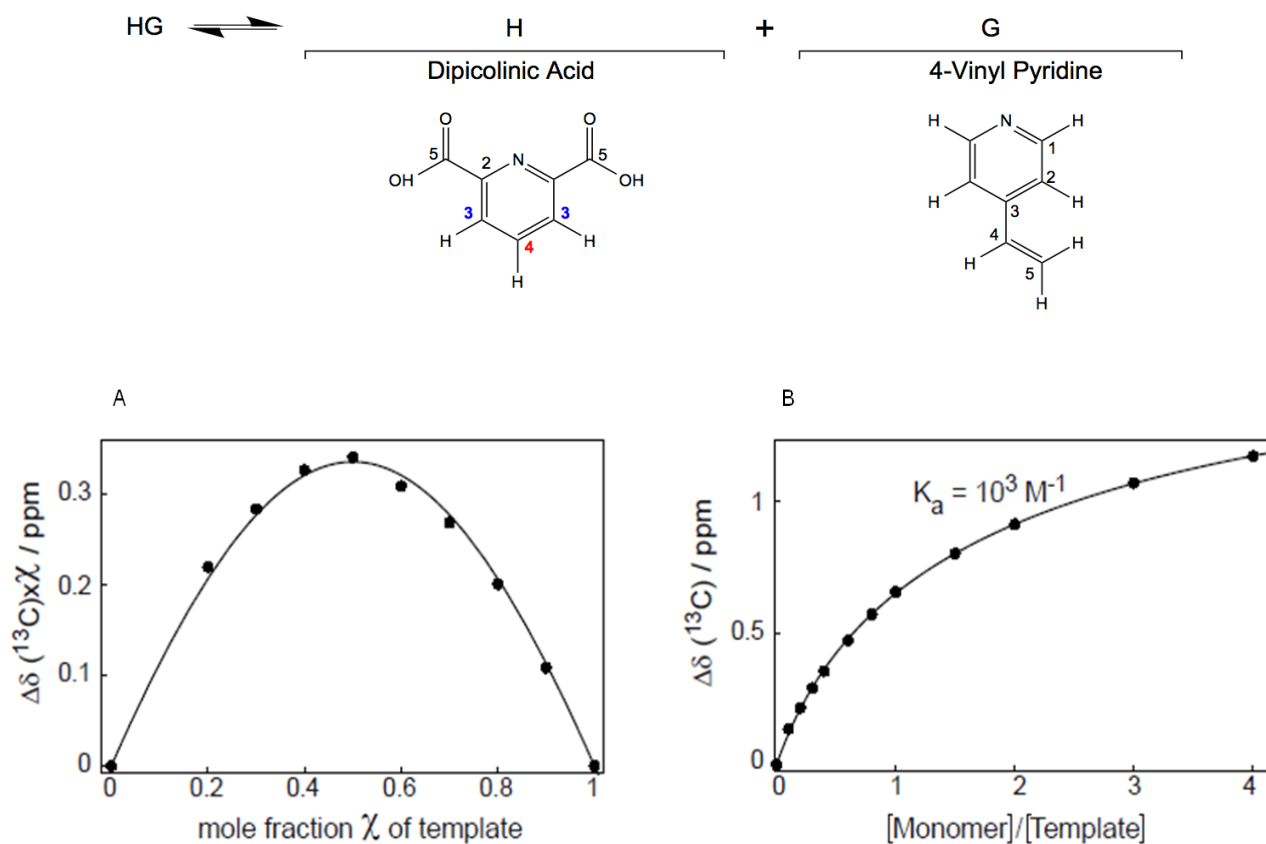


Figure S1. ^{13}C NMR studies in MeOD/ D_2O for the carboxyl carbon of DPA. A) Job plot and non-linear regression with 1:1 equilibrium equation for the complex DPA/4-VP; B) Titration data and non-linear regression with 1:1 equation, $K_a = 10^3 \text{ M}^{-1}$.

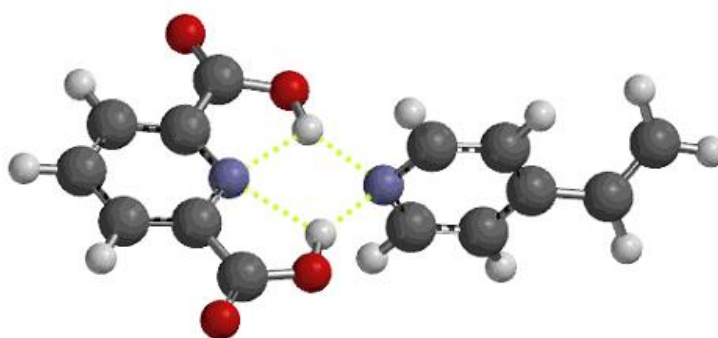


Figure S2. The minimized equilibrium configuration of DPA/4-VP complex obtained in water by molecular modelling with the semi-empirical method AM1 using the software Spartan. This simulation an equilibrium 1:1 for the complex DPA/4-VP. Red balls correspond to oxygens, dark gray to carbons, gray to hydrogens and blue to nitrogens. The dashed green lines correspond to hydrogen bonds.

General Conclusions and Perspectives

In this Ph.D. thesis, we demonstrated, through two examples, the great potential of molecularly imprinted polymers as selective receptors in “real world” applications.

In the first part of the thesis, we developed a multitarget MIP as an active principle for suppressing body odors. To fight malodors, most currently marketed antiperspirants and deodorants contain, respectively aluminum salts and unspecific antibacterials, supplemented with odor-covering agents. None of these two solutions is ideal as the former blocks the natural flow of sweat and the latter kills the skin bacteria, which is a natural barrier to harmful pathogens. In order to preserve the fragile skin microbiota, we synthesized a MIP and applied it as a specific scavenger agent to trap non-odorous precursors of malodors, thus preventing them from being transformed by bacteria into volatile malodorous compounds. The main challenge was to design a MIP that could efficiently capture the target molecules in an extremely complex and unfavorable environment (mixture of sweat and cosmetic formulation). Our first attempts, where the MIP was prepared with commercial monomers were not successful, as no binding was observed in the artificial model of human sweat. Therefore, we realized that for the application targeted here, interactions involving high association constants were essential. Hence, we synthesized an unsubstituted amidine monomer, (4-acrylamidophenyl) (amino) methaniminium acetate (AB), which can form a stoichiometric interaction with a high binding constant for carboxyl groups. In a dermocosmetic formulation, the MIP could capture selectively the precursors of malodorous compounds, amidst a multitude of other molecules present in human sweat.

Further work could be dedicated to improve the MIP's binding capacity and morphological characteristics so as to facilitate the implementation in various types of dermocosmetic formulations. This could be achieved by further optimization of the protocol of synthesis, or by adjusting it towards the synthesis of xerogel. Furthermore, the synthesized amidinium-based monomer would also find utility for the preparation of MIPs for a wide range of carboxylate, phosphate, phosphonate and possibly sulfate-based biological molecules. The resulting polymers would constitute a novel generation of MIPs with improved selectivities in complex aqueous environments. They could find applications as active principles in other cosmetic products and more generally in areas dealing with highly complex environments, where selective recognition is required like in sensing, bioanalysis, medical treatment and proteomic applications.

Preliminary studies on the biological effect of the designed MIP were performed, in terms of epidermal cell viability and effect on the bacteria commensal to the skin. Our results revealed a minor effect of this MIP on epidermal HaCaT cells, as inferred by the MTT cytotoxicity test. Moreover, addition of the MIP in liquid culture of skin commensal bacteria *Corynebacteria spp.* and *Staphylococcus epidermidis* did not affect the growth rate. This study is a step forward in the understanding and evaluation of the biological effect of MIPs as skin sensitizers, but there is room for improvement. To ultimately prove the MIP's safety

with regards to its potential application in dermocosmetic applications, more studies are necessary including inflammation tests with different biomarkers such as cytokines and implementation on artificial skin models such as *Episkin*.

In the second part of the thesis, a water compatible MIP was synthesized as selective sorbent for the clean-up of betanin and its stereoisomer isobetanin. Betanin is a natural pigment derived from red beets, with important biological activities. This bioactive molecule, currently used as food colorant, was hardly explored in the past and only recently, its antiproliferative properties against cancer cells *in vitro* and *in vivo* have been reported. The isolation of large amounts of betanin is problematic due to its instability to extreme pH and temperature conditions. Typically, purification is carried out by conventional column chromatography such as normal and reversed phase silica, ion-exchange and hydrophobic resins which suffer from a number of disadvantages. Hence, we postulated that the use of MIPs as selective sorbents could be an interesting alternative to traditional purification protocols, since their specific recognition properties could improve importantly the performance of the purification. Thus, we report for the first time a MISPE for the purification of betanin and isobetanin from crude beetroot extract. Our MIP was imprinted with dipicolinic acid, a structural analogue of the chromophore group of betanin, and could specifically recognize the target molecule in batch studied. When packed on a SPE column, the MIP sorbent could selectively retain betanin and isobetanin, allowing at the same time the removal of matrix components such as sugars and proteins. In conclusion, our MISPE method is very promising for the future development of well-formulated highly concentrated betanin/isobetanin mixtures ready for food or medicinal use.

To further extend our studies, the purification efficiency of the developed MIP was also compared to a conventional non-selective adsorbent (Amberlite® XAD16) widely used in the literature for betanin purification from vegetal sources. The results showed a 2-fold increase of the purification degree with respect to the XAD16 protocol. In the future, more experiments will be necessary to fully scale-up the procedure and enable a direct comparison with the commercial resins. Moreover, this method can probably be extended to extract vulgaxanthin I, a source of yellow natural pigments from yellow beet which is scarcely investigated. As further perspectives, the binding capacity of the MIP could be also optimized, by using for instance, a template molecule which has a closer structural similarity to betanin.

To conclude, this PhD thesis has allowed us to better understand the significant advantages of MIPs as tailor-made synthetic receptors, with emphasis on recognition in complex environments. The field of molecular imprinting has been developed remarkably since the pioneering studies of Wulff and Mosbach, owing to the intensive research performed in the last years. Extensive efforts towards the optimization of synthetic protocols and the rational design of MIPs have allowed to circumvent some of the issues related to MIP synthesis such as low affinity and selectivity in complex environments as well as the successful targeting of biomacromolecules. Hence, it is evident that MIPs can be more than an alternative to antibodies, being more versatile, robust and cost-effective.

Nowadays, MIPs feature outstanding recognition properties in complex samples and can be applicable to a wide range of biotechnological areas, from bioimaging and biosensors to drug delivery and therapeutics. Combination of MIPs with other recognition materials such as aptamers or sensing probes such as up-converting particles or quantum dots can further enlarge their application range. Some of the recent milestone examples of MIPs applied in real-world applications were discussed in this thesis, including MIPs for ocular therapeutics, diagnostics and cancer treatment. It is our hope that the recent advances in MIP technology will contribute to their commercialization on an industrial scale.

Annex: Achievements

Publications

Nestora, S.; Merlier, F.; Beyazit, S.; Prost, E.; Duma, L.; Baril, B.; Greaves, A.; Haupt, K.; Tse Sum Bui, B., Plastic antibodies for cosmetics: Molecularly imprinted polymers scavenge precursors of malodors. *Angewandte Chemie International Edition* **2016**, *55*, 6252-6256.

Nestora, S.; Merlier, F.; Prost, E.; Haupt, K.; Rossi, C.; Tse Sum Bui, B., Solid-phase extraction of betanin and isobetanin from beetroot extracts using a dipicolinic acid molecularly imprinted polymer. *Journal of Chromatography A* **2016**, *1465*, 47-54.

Panagiotopoulou, M., Beyazit, S., **Nestora, S.**, Haupt, K., Tse Sum Bui, B. Initiator-free synthesis of molecularly imprinted polymers by polymerization of self-initiated monomers. *Polymer* **2015**, *66*, 43-51.

Oral communications

Nestora S., Merlier F., Prost E., Haupt K., Rossi C., Tse Sum Bui B. (2016)
Development of a selective molecularly imprinted sorbent for the purification of betanin from beetroots
18th World Conference on Food Science and Technology, August 21-25, Dublin, Irelande.

Nestora S., Rossi C., Merlier F., Haupt K., Tse Sum Bui B. (2015)
Molecularly imprinted polymers as selective receptors for the treatment of complex samples”
SAMOSS ITN -3st Summer School and International meeting, October 11-18, Dead Sea, Israel.

Nestora S., Rossi C., Merlier F., Haupt K., Tse Sum Bui B. (2015)
Molecularly imprinted polymers as selective receptors for the treatment of complex samples
Graduate student symposium on molecular imprinting, August 27 -29, Kent, UK.

Nestora S., Merlier F., Haupt K., Tse Sum Bui B. (2015)
Molecularly imprinted polymers as anti-odor materials in cosmetics
EMRS 2015 Spring Meeting, May 11-15, Lille, France.

Nestora S., Rossi C., Haupt K., Tse Sum Bui B (2014)
Molecularly imprinted polymers for the purification, detection, stabilization and vectorization of antioxidants derived from plants
SAMOSS ITN -1st Summer School, July 21-25, Madrid, Spain.

Poster presentations at conferences

Nestora S., Haupt K., Tse Sum Bui B., Greaves A. (2016)
Molecularly imprinted polymers as anti-odor materials in cosmetics
4th International Conference on Cosmetics “COSM’innov 2016”, May 23-25, Orleans, France.

Nestora S., Merlier F., Bartkowski M., Li B., Greaves A., Haupt K., Tse Sum Bui B. (2014)
Molecularly imprinted polymers as anti-odor materials in cosmetology
8th International Conference on Molecularly Imprinted Polymers “MIP 2014”, September 18-21,
Zhenjiang, China.

Illustration in magazines and emissions

The work presented in Chapter 2 and published in 2016 was illustrated by the following magazines and journals (amongst others):

- **Chemistry World**, 11/05/16: <https://www.chemistryworld.com/news/plastic-antibodies-in-deodorant-to-fight-body-odour/1010242.article>
- **CNRS INSB**, 11/05/16: <http://www.cnrs.fr/insb/recherche/parutions/articles2016/k-haupt.html>
- **Scientific American**, 11/05/16: <https://www.scientificamerican.com/article/plastic-antibodies-in-deodorant-attack-your-smelly-molecules/>
- **CoffiScience**, 12 /06/16: <https://www.coeffiscience.ca/actualites/science-et-chimie-verte/anglais-anticorps-plastiques-dans-le-deodorant-pour-combattre-les-odeurs-corporelles>
- **Le Figaro**, 16/06/16 : <http://sante.lefigaro.fr/actualite/2016/06/16/25105-nano-billes-plastique-pour-pieger-vos-mauvaises-odeurs>
- **Courrier Picard**, 04/07/16 : <http://www.courrier-picard.fr/region/compiegne-un-neo-deo-imagine-par-des-chercheurs-ia190b0n809862>
- **France Inter**, 09/09/16 : <https://www.franceinter.fr/emissions/futur-proche/futur-proche-09-septembre-2016>
- **Le parisien**, 30/10/16: <http://www.leparisien.fr/compiegne-60200/pour-votre-sante-ce-chercheur-de-compiegne-cree-le-deodorant-du-futur-30-10-2016-6269547.php>
-

It was also the subject of the following radio and television emissions respectively:

- **La matinale d' Europe 1**, 15 /06 /16: <http://www.europe1.fr/emissions/innovation/les-deodorants-du-futur-2772707>
- **Le magazine de la santé- France 5**, 20/09/16: <http://www.allodocteurs.fr/emissions/le-magazine-de-la-sante/>

Other activities

Teaching activity

2014-2015: 64 hours of laboratory supervision: 30h organic chemistry (TP CM13), 24h chromatography (TP BL01), 10h sensory and texture analysis of food (BT09).

2015-2016: 64 hours of laboratory supervision: 24h organic chemistry (TP CM13), 24h histology (TP BL01), 16h sensory and texture analysis of food (BT09).

*« Un savant dans son laboratoire n'est pas seulement un technicien :
c'est aussi un enfant placé devant des phénomènes naturels
qui l'impressionnent comme des contes de fées.
Nous devons avoir un moyen pour communiquer ce sentiment à l'extérieur,
nous ne devons pas laisser croire que tout progrès scientifique
se réduit à des machines et des engrenages. »*

Marie Curie

